Determination of the stable isotope fractionation ($\delta^{18}O$ and $\delta^{13}C$) during precipitation of speleothem calcite: Novel cave analogue laboratory experiments

Dissertation

zur Erlangung des akademischen Grades

„Doktor der Naturwissenschaften“

im Promotionsfach Geologie/Paläontologie

Am Fachbereich 09 für Chemie, Pharmazie und Geowissenschaften

der Johannes Gutenberg-Universität Mainz

vorgelegt von

Maximilian Hansen

geb. in Frankfurt am Main

Mainz 2017

Dekanin:

1. Berichterstatter:

2. Berichterstatter:

Tag der mündlichen Prüfung: 06.07.2017

Eidesstattliche Erklärung

Hiermit versichere ich die vorliegende Arbeit selbständig und nur unter Verwendung der angegebenen Hilfsmittel verfasst zu haben. Ich habe oder hatte die hier vorgelegte Dissertationsarbeit nicht als Prüfungsarbeit für eine staatliche oder andere wissenschaftliche Prüfung eingereicht. Ich hatte weder die jetzt als Dissertation vorgelegte Arbeit noch Teile davon bei einer anderen Fakultät bzw. einem anderen Fachbereich als Dissertation eingereicht.

_____

(Maximilian Hansen)
Mainz, 15. Mai 2017

Zusammenfassung

Speläotheme sind einzigartige Paläoklimaarchive, welche meist kontinuierliche stabile Isotopenproxys ($\delta^{18}O$ und $\delta^{13}C$) aus allen Teilen der Welt liefern. Eine quantitative Interpretation dieser Isotopensignale zur Rekonstruktion des Klimas der Vergangenheit und/oder Änderungen der Umweltbedingungen ist bisher schwierig. Verschiedenste Prozesse, welche sich in der Atmosphäre, dem Boden, dem Epikarst und in der Höhle abspielen können diese Signale beeinflussen und verfälschen. Besonders die zugrundeliegenden Fraktionierungsprozesse, wie die stabilen Isotopensignale in den Kalzit des Speläothems eingebaut werden, sind im Detail noch nicht genau verstanden und werden teils kontrovers diskutiert. Um die gängigen Fraktionierungsmodelle zu untersuchen, wurden im Rahmen dieser Arbeit Experimente entwickelt und unter vollständig kontrollierten, höhlenanalogen Bedingungen durchgeführt. Diese simulieren alle Prozesse, die während der Bildung von Speläothemen auftreten können. Die experimentellen Aufbauten befinden sich in einer Klimabox, welche es ermöglicht alle Umgebungsbedingungen, wie die Temperatur, relative Luftfeuchtigkeit, den pCO_2 sowie die Isotope des CO_2 zu kontrollieren und analog zu einem natürlichen System einzustellen. Mit den Ergebnissen dieser Arbeit ist es *erstmals* möglich die zeitliche Entwicklung aller chemischen Parameter (pH-Wert, Abscheidungsrate, Übersättigung in Bezug auf Kalziumkarbonat) und die $\delta^{13}C$ und $\delta^{18}O$ Isotopie des anorganisch gelösten Kohlenstoffs (DIC) als auch des direkt abgeschiedenen $CaCO_3$ zu *gleicher* Zeit zu bestimmen. Dies ermöglicht eine direkte Bestimmung der Isotopenfraktionierung aller beteiligten Spezies im System (CO_2, DIC, $CaCO_3$ und H_2O) in Abhängigkeit der experimentellen Parameter (z.B., Temperatur und pCO_2).

Ein Prozess, welcher potentiell Einfluss auf das Isotopensignal einer Kalzit abscheidenden Lösung haben kann, ist der Isotopenaustausch zwischen dem Lösungsfilm auf der Oberfläche eines Speläothems und dem gasförmigen CO_2 der (Höhlen-) Atmosphäre. Zur Quantifizierung dieses Prozesses wurde in einer ersten Studie eine Theorie entwickelt, welche den Isotopenaustausch zwischen dünnen Lösungsfilmen mit gasförmigem CO_2 beschreibt. Um die Theorie zu überprüfen, wurden Experimente durchgeführt, in welchen $NaHCO_3$–Lösungsfilme zweier Konzentrationen CO_2-haltigen Atmosphären bei einer festen Temperatur von 20 °C ausgesetzt wurden. Die experimentellen Ergebnisse können gut mit der vorher entwickelten Theorie erklärt werden.

In einer Folgestudie wurden die Austauschprozesse für Kohlenstoffisotope weitergehend untersucht. In einer Reihe neuer Experimente wurde eine größere Spannweite an $NaHCO_3$-Konzentrationen verwendet, sowie mehrere Temperaturen und dünnere Filmdicken. Die

Lösungen wurden Atmosphären mit deutlich niedrigerem pCO_2 ausgesetzt. Zusätzlich wurde ein alternatives, zweites Modell, ein vollständiges Diffusions-Reaktions-Modell entwickelt, um die Zeitkonstanten für den Kohlenstoffisotopenaustausch zu berechnen. Das Modell kann durch die experimentell beobachteten Werte gut erklärt werden und legt nahe, dass sich der Isotopenaustausch möglicherweise früher auswirken kann als nach dem Modell der ersten Studie zu erwarten war.

In einer weiteren Art von Experimenten wurde die zeitliche Entwicklung einer $CaCO_3$ abscheidenden Lösung untersucht, indem alle Prozesse, welche einen potentiellen Einfluss auf die Isotopenzusammensetzung des (Speläothem-)Kalzits haben könnten, imitiert wurden. Während der Experimente wurden dünne Filme verschieden konzentrierter $CaCO_3$-Lösungen auf geneigten Marmor- oder gesandstrahlten Borosilikatglasplatten zum Fließen gebracht. Nach verschiedenen Fließstrecken, und damit Aufenthaltszeiten auf den Platten, wurde die Isotope ($\delta^{18}O$ und $\delta^{13}C$) des DIC und des direkt ausgefällten $CaCO_3$ untersucht. Zusätzlich wurden für jede Fließstrecke pH-Wert und elektrische Leitfähigkeit bestimmt. In den $\delta^{13}C$-Werten wurde eine starke negative Fraktionierung zwischen $CaCO_3$ und DIC beobachtet, welche einen „kinetischen“ oder Ungleichgewichtsfraktionierungsprozess nahelegt. Die initiale Fraktionierung in den $\delta^{18}O$ Werten zwischen Kalzit und Wasser ist in guter Übereinstimmung zu zuvor beobachteten Werten aus natürlichen Systemen. Dies zeigt, dass in der Klimabox, natürliche (Höhlen-)Systeme realistisch simuliert werden können. Mit zunehmender Aufenthaltszeit auf den Platten steigen die Isotopenwerte des ausgefällten Kalzits sukzessive an, welcher dann im Vergleich zum Wasser der Lösung deutliche Unterschiede zu typischen Gleichgewichtsfraktionierungsfaktoren aufweist. Die Fraktionierungen für $\delta^{13}C$ und $\delta^{18}O$ scheinen zudem an die Abscheidungsraten gekoppelt zu sein, sie zeigen stärkere Fraktionierungen für größere Abscheidungsraten. Die zeitliche Entwicklung der $\delta^{18}O$ und $\delta^{13}C$ Werte sowohl für das den DIC, als auch für das direkt ausgefällt $CaCO_3$ können mit einem Rayleigh-Fraktionierungsmodell erklärt werden.

All diese Ergebnisse zeigen, dass das Potential des im Rahmen dieser Arbeit entwickelten experimentellen Aufbaus für zukünftige Studien sehr groß ist. So werden die Proben dieser Arbeit derzeit noch auf ihre „Clumped isotope“ Zusammensetzung untersucht, was in dieser zeitlichen Auflösung bisher nicht möglich war. Mit dem vorhandenen Aufbau ließe sich nahezu jeder beliebige Proxy (z.B. der Einbau Spurenelemente in Speläotheme) unter sehr genau kontrollierten Bedingungen untersuchen.

Abstract

Speleothems are unique paleoclimate archives, often providing continuous long term stable isotope records from all parts of the world. Quantitative interpretation of these isotope records in terms of past climate and/or environmental variability remains challenging, because various processes occurring in the atmosphere, the soil, the epikarst and inside the cave, may obscure these climate signals. In particular, the basic fractionation processes which influence the incorporation of stable isotope signals into speleothems are not fully understood yet and are still a matter of controversial discussion in the speleothem community. In the framework of this thesis experiments were developed and conducted in order to test the most established fractionation models. The experiments were performed under completely controlled, cave analogue conditions aiming to simulate all processes occurring during the formation of speleothems. The different experimental setups are placed inside a climate box, which enables to control all surrounding conditions, such as temperature, relative humidity and pCO_2 as well as isotope composition of the CO_2 and adjust them to natural conditions. For the *first* time it is possible to observe the temporal evolution of all chemical parameters (pH, precipitation rate, supersaturation with respect to calcite) and the isotope composition of the DIC, as well as of the directly precipitated $CaCO_3$ at the *same* time. This enables to directly investigate the stable isotope fractionation of all involved species in the system (CO_2, DIC, $CaCO_3$ and H_2O) as a function of the experimental parameters (e.g., temperature and pCO_2).

One process, which potentially obscures the isotope signal of a calcite precipitating solution, is the isotope exchange between the thin solution film on top of a speleothem and the gaseous CO_2 of the (cave) atmosphere. In order to quantify this process in a first study a theory was developed, describing the isotope exchange between thin solution films and gaseous CO_2. To test this experiments were conducted exposing $NaHCO_3$-solution films of two concentrations to CO_2 containing atmospheres at a temperature of 20 °C. The experimental results can be well explained by the previously derived theory.

In a second study the carbon isotope exchange processes was further investigated by performing new experiments closer to natural conditions at a wider range of $NaHCO_3$-concentrations and temperatures, as well as significantly lower pCO_2 and with film thicknesses in the range of natural observations. Additionally, a complete diffusion-reaction model was introduced to calculate the time constants for the carbon isotope exchange. The model explains the experimentally observed values very well and suggests that carbon isotope exchange might get significant at an earlier stage than expected by the model of the first study.

In a second type of experiments, the temporal evolution of a $CaCO_3$ precipitating solution was investigated by closely mimicking all processes potentially affecting the isotope composition of (speleothem) calcite. During the experiments, thin solution films of $CaCO_3$-solutions of different concentrations were caused to flow down inclined marble or sand blasted borosilicate glass plates. After different distances of flow and, thus, residence times the stable isotope composition ($\delta^{13}C$ and $\delta^{18}O$) of the dissolved inorganic carbon and the directly precipitated $CaCO_3$ were analyzed. Additionally, the pH and electrical conductivity values were determined. For the $\delta^{13}C$ values, a strong negative fractionation between $CaCO_3$ and DIC was observed, indicating "kinetic" or disequilibrium isotope fractionation. The initial fractionation of $\delta^{18}O$ between calcite and water corresponds well to previously reported values from natural systems, proving that the climate box closely simulates a natural (cave) system. With increasing residence time on the plates, however, the calcite progressively shows increasing $\delta^{18}O$ and $\delta^{13}C$ values, away from previously reported values. The fractionation for both $\delta^{13}C$ and $\delta^{18}O$-values additionally seems to depend on precipitation rate, showing stronger fractionations for higher precipitation rates. The temporal evolution of $\delta^{18}O$ and $\delta^{13}C$ values for both, the DIC and the $CaCO_3$ experiments, can be well explained using a Rayleigh distillation model.

All these results show, that there is great potential for future work with the experimental setup which was developed within this thesis. Currently samples from the precipitation experiments are analyzed for their clumped isotope composition, which has not been possible at this resolution for speleothem analogue generated samples so far. In principle almost every relevant climate proxy used in speleothem science could be investigated using the here presented setup under very well constrained conditions (e.g., incorporation of trace elements or isotope).

Acknowledgements

Table of Contents

List of Figures

List of Tables

Chapter 1: Introduction

Over the last decades, speleothems have become well established important paleoclimate archives. They potentially provide information about various environmental and climate conditions from all parts of the world (e.g., Fairchild and Baker, 2012) and can be dated very accurately using U-series disequilibrium methods (Richards and Dorale, 2003; Scholz and Hoffmann, 2008). The combination with the most commonly used paleoclimate proxies, the stable oxygen and carbon isotopes ($\delta^{18}O$ and $\delta^{13}C$), enable to generate high resolution, often continuous, long term paleoclimate records (e.g., Asmerom et al., 2010; Bar-Matthews et al., 2003; Boch et al., 2011; Cheng et al., 2016; Cruz et al., 2005; Fleitmann et al., 2004). Many speleothem isotope records are based on the interpretation of $\delta^{18}O$ values, which provide information on past precipitation (e.g., Bar-Matthews et al., 2003; Cheng et al., 2016), temperature (e.g., Mangini et al., 2005), water vapor source and atmospheric circulation (e.g., Cruz et al., 2005; Wassenburg et al., 2016). The $\delta^{13}C$ values also have great potential for paleoclimate reconstruction, especially for sub orbital paleoclimate change, such as rapid changes in vegetation (Genty et al., 2003; Hellstrom and McCulloch, 2000; Mischel et al., 2016), temperature changes on annual timescales (Scholz et al., 2012) or even monthly resolved rainfall patterns (Breecker, 2017). However, the stable isotope signals in speleothems depend on a complex interplay of various processes occurring in the atmosphere, the soil, the epikarst and inside the cave, which potentially obscure the isotope signal until speleothem calcite is deposited. Therefore, the interpretation of $\delta^{18}O$ and $\delta^{13}C$ records in terms of past climate and environmental variability (i.e., amount of meteoric precipitation and temperature) remains challenging.

This thesis aims to closely resemble all natural processes potentially influencing the stable isotope signals in the laboratory and to test the established theoretical models (e.g., Dreybrodt, 2008; Dreybrodt and Scholz, 2011; Scholz et al., 2009). Therefore, novel laboratory experiments were developed to investigate the temporal evolution of stable isotope signals during precipitation of $CaCO_3$ from a thin film of solution, as on the surface of speleothems. The experimental setup is placed inside a climate box in which all influencing parameters, such as relative humidity, temperature, pCO_2 and isotope composition of the CO_2, can be controlled and adjusted to cave analogues conditions. The box is sealed during the experiments and is equipped with rubber gloves which allow to adjust the experimental setup, to take samples and to conduct in situ measurements without contaminating the climate box atmosphere. Small amounts of solution can be transferred out of and into the system via an air lock, the “sewer port”, without biasing the artificial cave atmosphere by laboratory air.

The experiments presented in this study allow to quantify stable isotope fractionation between all involved species in the system, the DIC, the directly precipitated $CaCO_3$, the water and the CO_2 of the atmosphere as a function of the experimental parameters such as supersaturation with respect to calcite, temperature and (cave) air pCO_2. This is the first study, which enables to determine isotope fractionation between *all* involved species in the system ($CO_{2,aq}$, $CO_{2,g}$, HCO_3^-, H_2O and $CaCO_3$) at the *same time*. Without a detailed understanding of these basic mechanisms controlling the stable isotope fractionation quantitative reconstruction of past climate will not be possible.

One process, which could potentially influence the stable isotope signals in speleothems, is the isotope exchange (for both $\delta^{13}C$ and $\delta^{18}O$) between the dissolved inorganic carbon (DIC) and the gaseous CO_2 of the (cave) atmosphere. This is investigated in Manuscript I (Chapter 3). To quantify this phenomenon a theory was derived and experiments were conducted at room temperature (ca. 20 °C). During the experiments $NaHCO_3$-solutions of 10 and 5 mmol/l with different film thicknesses (between 0.13 mm and 2 mm) were exposed to CO_2 containing atmospheres with pCO_2 of 500, 12,500 and 25,000 ppmV. The CO_2 of the atmosphere had a defined isotope composition that differed significantly from that of the solution (Chapter 3 Dreybrodt et al., 2016). The experimentally observed time constants for isotope exchange are in well agreement to the previously derived theory.

Isotope exchange is again investigated in Manuscript II (Chapter 4). Therefore new experiments were conducted at conditions closer to a natural system by carefully investigating the carbon isotope exchange between thin solution films, as they occur on the surface of speleothems (ca. 0.1 mm in thickness) and the CO_2 of the atmosphere. During the experiments thin films of a flowing $NaHCO_3$-solutions with a wider range of concentrations than in Manuscript I (1, 2, 5 and 10 mmol/l) were exposed to atmospheres containing 1000 and 3000 ppmV CO_2 of known isotope composition at three temperatures (10, 20 and 30 °C). Additionally, an alternative, complete diffusion-reaction-model for carbon isotope exchange is introduced, providing time constants for carbon isotope exchange under cave conditions. The experimentally observed temporal evolution of $\delta^{13}C$ values can be well described by the new model (Chapter 4, Hansen et al., in press). The experimental data and the new model suggest, that isotope exchange might get significant earlier than expected in Manuscript I, especially for concentrations closer to natural environments.

Of great interest for the interpretation of speleothem isotope records are the basic mechanisms during precipitation of speleothem calcite and the corresponding stable isotope fractionation factors. Therefore, experiments were developed to investigate the temporal

evolution of $\delta^{13}C$ and $\delta^{18}O$ values for both the DIC and the directly precipitated $CaCO_3$ from a thin film of a laminar flowing $CaCO_3$-solution (2, 3 and 5 mmol/l) on a marble or borosilicate glass plate (Manuscripts III and IV; Chapters 5 and 6). This enables to investigate the stable isotope fractionation between DIC, $CaCO_3$ and H_2O as a function of the experimental conditions, such as supersaturation with respect to calcite, pCO_2 (1000 and 3000 ppmV) and temperature (10, 20 and 30 °C), and to compare the results to state of the art (cave) isotope fractionation models. The results show that isotope fractionation seems to be strongly dependent on the precipitation rate, and the temporal evolution of isotope values can be well explained using a classical Rayleigh distillation model. Furthermore, a strong negative isotope fractionation is observed for the $\delta^{13}C$ values between $CaCO_3$ and the DIC. With increasing distance of flow and, thus, decreasing supersaturation the fractionation becomes smaller approaching typical isotope equilibrium values (Manuscript III, Chapter 5). Negative fractionation is commonly associated with 'kinetic' isotope fractionation processes (e.g., Mook and De Vries, 2000; Sharp, 2007). The $\delta^{18}O$ values show a similar dependence on the precipitation rate. The initial isotope fractionation for $\delta^{18}O$ between $CaCO_3$ and water (i.e., at the beginning of the plates) corresponds well to observations from in situ farmed calcites in natural cave systems (e.g., Johnston et al., 2013; Tremaine et al., 2011). However, with increasing residence time on the plates substantial deviations from the initial fractionation factors are observed (Manuscript IV; Chapter 6).

Chapter 2: Basics

2.1 Speleothem growth

Speleothems grow in isolated environments of caves, potentially providing environmental and climatic information over the duration of hundreds of thousands of years. Prerequisite for the formation of caves, and thus for the formation of all kinds of speleothems, is a carbonate host rock and the availability of water. In principle, meteoric precipitation which falls above a cave system, seeps through the soil where the pCO_2 is orders of magnitude higher than in the atmosphere (up to a few percent vs. ca. 450 ppmV) due to root respiration and microbial activity (Fairchild and Baker, 2012). This leads to the formation of carbonic acid and, consequently, relatively low pH values of the seeping water:

$$CO_2(g) + H_2O \Leftrightarrow H_2O + CO_2(aq) \Leftrightarrow H_2CO_3. \quad (2.1)$$

Note, that the total DIC at low pH is mainly provided by dissolved CO_2(aq), whereas the proportion of carbonic acid (H_2CO_3) is about 600 times smaller (e.g., Appelo and Postma, 2004).

If this solution subsequently seeps further down into the carbonate host rock through fissures and joints, $CaCO_3$ is dissolved:

$$CO_2 + H_2O + CaCO_3 \Leftrightarrow Ca^{2+} + 2\ HCO_3^-. \quad (2.2)$$

During dissolution, every $CaCO_3$ molecule consumes one molecule of CO_2. Depending on the availability of CO_2 and, thus, on the pH value of the solution, this reaction is reversible. As a consequence, the distribution of the different species is directly related to the pCO_2 and the pH of the solution. These reactions are controlled by a series of fast and slow reactions, controlled by a complex interplay of diffusion and/or different reaction constants (for details see e.g., Dreybrodt, 1988; Dreybrodt et al., 1997; Zeebe and Wolf-Gladrow, 2001).

Afterwards, the solution may reach a cavity or a cave system, where the pCO_2 is, in general, orders of magnitude lower than in the soil and epikarst. If the water then drips down to the top of a stalagmite, a thin layer of solution is formed (about 0.1 mm in thickness). Due to the gradient between the pCO_2 of the solution and the pCO_2 of the (cave) atmosphere, the excess CO_2 degasses in the range of a few seconds (Hansen et al., 2013). As a consequence, the pH of the solution increases to values of about 8. The most abundant carbon species of the DIC is then provided by HCO_3^- (about 95 %), the solution reaches supersaturation with respect to calcite and eventually $CaCO_3$ is precipitated (e.g., Dreybrodt et al., 1997). This results in the growth of speleothems. When the solution flows down the flanks of a stalagmite, $CaCO_3$ is precipitated in thin layers (e.g., Mühlinghaus et al., 2007; Romanov et al., 2008a). A schematic overview on the processes in a natural karst and cave system is given in Figure 2.1.

The rate for precipitation of $CaCO_3$, F [mmol/cm^{2}s], has been described by Plummer et al. (1978):

$$F = k_1 * [H^+]_s + k_2 *[H_2CO_3]_s + k_3 - k_4 * [Ca^{2+}]_s * [HCO_3^-], \quad (2.3)$$

where k_1, k_2, k_3 are temperature dependent rate constants for dissolution and k_4 is the rate constant for precipitation of $CaCO_3$, which also depends on the pCO_2 of the solution. The brackets denote the concentrations of the individual molecules at the calcite surface. The precipitation term is dominant as long as the solution is supersaturated with respect to calcite. When F approaches 0, the system is in chemical equilibrium. Each $CaCO_3$ molecule precipitating to the carbonate surface produces one molecule of CO_2 (Eq. 2.2), which is then almost instantaneously released

into the atmosphere by molecular diffusion. This involves the relatively slow conversion of H_2CO_3 into CO_2 and H_2O (Fig. 2.2). Consequently, the precipitation rate is additionally limited by the conversion of HCO_3^- into CO_2. For the precipitation of speleothem calcite from a thin film of solution, the precipitation rate has been derived by combining all three processes (Buhmann and Dreybrodt, 1985a; Dreybrodt et al., 1997):

$$F = \kappa * ([Ca^{2+}] - [Ca^{2+}]_{eq}) \; [mol*cm^{-2}*s^{-1}] \tag{2.4}$$

$$\kappa = (0.52 + 0.04*T + 0.004*T^2) * 10^{-5} \; cm/s, \tag{2.5}$$

$[Ca^{2+}]$ is the Ca^{2+} concentration at time t, $[Ca^{2+}]_{eq}$ the equilibrium concentration, which depends on cave pCO_2, T is the temperature in °C and κ is a rate constant. For common ranges of film thicknesses in caves, κ is independent from the film thickness and only depends on temperature (Baker et al., 1998; Romanov et al., 2008a).

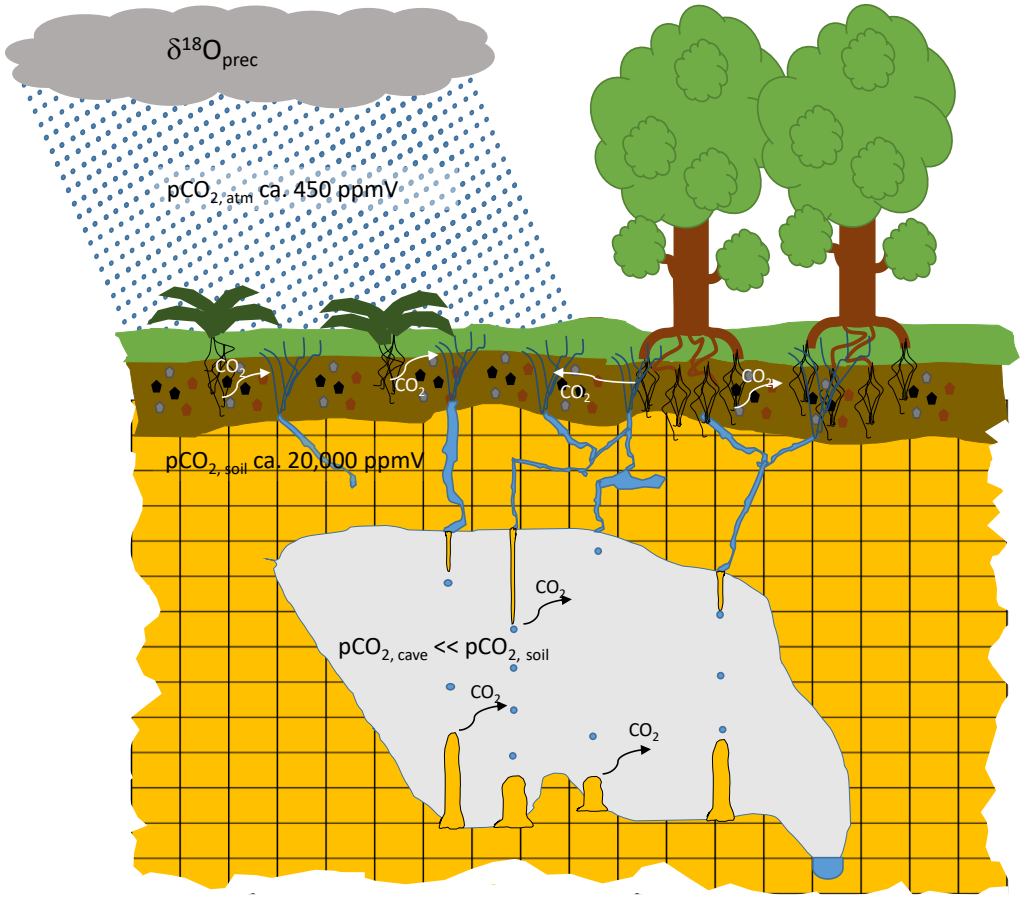

Fig. 2.1: Schematic cross section of a cave system, with all steps involved until speleothem calcite is deposited: meteoric precipitation, formation of carbonic acid due to uptake of CO_2, dissolution of $CaCO_3$ host rock, degassing and formation of speleothems inside the cave.

As a result, supersaturation with respect to calcite decreases exponentially with a characteristic time constant τ_{pr} (Dreybrodt, 1988), and the temporal evolution of the [Ca^{2+}] and [HCO_3^-] concentration can be written as (Buhmann and Dreybrodt, 1985a):

$$[Ca^{2+}](t) = \left([Ca^{2+}]_0 - [Ca^{2+}]_{eq}\right)\left(exp^{\left(-t/\tau_{pr}\right)}\right) + [Ca^{2+}]_{eq} \quad (2.6)$$

$$\tau_{pr} = {}^{d}/_{\kappa} \ , \quad (2.7)$$

where d is the film thickness and [Ca^{2+}] the concentration at time t, $t = 0$ and chemical equilibrium, respectively.

2.2 Stable isotope fractionation in the (speleothem) carbonate system

2.2.1 Theoretical background in stable isotope geochemistry

The behavior of the heavy and the light isotopes of a specific element in terms of their chemical and physical properties are slightly different. This is caused by small differences in the mass of the atomic nuclei of the different isotopes. Thereby the heavier isotope is defined by higher binding energies and generally a lower mobility. This results in a faster responsiveness of the light isotope of an element than the heavier ones in a chemical reaction. This leads to an isotope effect, commonly referred to isotope fractionation, expressed by a fractionation factor α. These effects are in general small, thus, isotope effects are often expressed by the fractionation, ε, which is defined as the deviation of α from 1 in permil (for further details see e.g., Mook and De Vries, 2000):

$$\varepsilon_{B/A} = \alpha_{B/A} - 1 = \frac{R_B}{R_A} - 1 \ (* 10^3‰), \quad (2.8)$$

where R denotes the isotope ratio before and after physical or chemical transition (phases A and B), respectively.

There are three basic types of isotope fractionation: equilibrium, disequilibrium and kinetic fractionation. An equilibrium process is defined as a (isotope) flux between two different reservoirs, which is equal in both directions with a corresponding equilibrium fractionation factor. On the contrary, kinetic isotope fractionation is a one dimensional, irreversible process. In a natural system, isotope fractionation can neither be characterized by kinetic nor complete equilibrium fractionation. Thus, the fractionation is more likely to be a combination of both

processes and is often referred to disequilibrium fractionation. In the speleothem literature, the term 'kinetic fractionation' has been frequently used to describe a deviation of the isotope value expected under conditions of isotope equilibrium. For the carbon isotopes this has been associated with rapid degassing of CO_2 (e.g., Hendy, 1971; Mickler et al., 2006). However, strictly speaking, the term 'kinetic fractionation' is misleading, because it is used to describe a one dimensional, rate dependent, irreversible process resulting in strong and negative isotope fractionation (e.g., Mook and De Vries, 2000; Sharp, 2007).

There are a number of stable isotope fractionation factors available for both $\delta^{13}C$ and $\delta^{18}O$. Mostly, they were determined in laboratory experiments by precipitating synthetic $CaCO_3$ from a bulk solution and measuring all species in the system (DIC, $CaCO_3$, $CO_2(g)$, H_2O) as a function of temperature and/or precipitation rate under controlled conditions. For carbon isotopes, the most commonly reported values are those for $^{13}\varepsilon_{CaCO3/HCO3-}$ and $^{13}\varepsilon_{CO2(aq)/HCO3-}$ (e.g., Emrich et al., 1970; McCrea, 1950; Mook et al., 1974; Romanek et al., 1992; Vogel et al., 1970). For the interface between calcite and water ($^{18}\alpha_{CaCO3/H20}$) they are evaluated using the same method (e.g., Friedman and O'Neil, 1977; Kim and O'Neil, 1997; McCrea, 1950; O'Neil et al., 1969). Beck et al. (2005) determined fractionation factors for $^{18}\alpha_{HCO3-/H2O}$ and $^{18}\alpha_{CO2/H2O}$ by performing equilibration experiments for the carbonate system with $NaHCO_3$ solutions at different pH values and temperature.

However, for the interpretation of speleothem stable isotope signals, these fractionation factors are not be completely applicable because the chemical and physical behavior in thin solution films, as they occur on the surface of speleothems, are considerably different from those in a larger body of solution. In larger solution bodies, diffusion is the rate limiting step for chemical reactions, whereas diffusion is very fast in thin solution layers (e.g., Hansen et al., 2013). Furthermore, the previously postulated 'equilibrium' fractionation factors, especially for $\delta^{18}O$, were recently questioned and suggested to depend on additional controls, such as pH (Watkins et al., 2014; Zeebe et al., 1999a), precipitation rate (Dietzel et al., 2009; Watkins et al., 2014) or the reaction kinetics (Watkins et al., 2013). This in agreement to observations from cave determined fractionation factors by measuring in situ farmed (cave) calcite and the $\delta^{18}O$ values of the corresponding drip water. For instance, Johnston et al. (2013) and Tremaine et al. (2011) observed higher $^{18}\alpha_{calcite\text{-}water}$ values than predicted for isotope equilibrium by Kim and O'Neil (1997). Coplen (2007) reported even higher values for $^{18}\alpha_{CaCO3\text{-}H2O}$ by measuring water and calcite from a slowly growing calcite vain in Devils Hole, Nevada. All these findings are very important in terms of paleoclimate reconstruction from speleothem calcite and urge to carefully reassess the mechanisms behind stable isotope fractionation in speleothems.

2.2.2 Modelling stable isotope fractionation in speleothems

Besides the numerous fractionation factors from the literature, there are different approaches available aiming to model the temporal evolution of $\delta^{18}O$ and $\delta^{13}C$ of speleothem calcite, which is still a matter of controversial discussion in the speleothem community. In particular, whether speleothem $CaCO_3$ is precipitated under "kinetic" or equilibrium conditions is still a matter of debate. In a pioneering theoretical study, Hendy (1971) suggested that progressive enrichment of both $\delta^{13}C$ and $\delta^{18}O$ values as well as a positive correlation between $\delta^{13}C$ and $\delta^{18}O$ values along an individual growth layer is an indicator for disequilibrium isotope fractionation. In the following years, this "Hendy test" has been widely applied to test speleothem samples for the suitability of paleoclimate reconstruction (e.g., Moreno et al., 2010; Williams et al., 2005). However, the applicability of this test has recently been questioned, since it does not account for initial disequilibrium conditions (e.g., Day and Henderson, 2011; Dorale and Liu, 2009; Mühlinghaus et al., 2009).

When $CaCO_3$ is precipitated to the calcite surface of a stalagmite, Ca^{2+} and HCO_3^- ions are progressively removed from the solution with a characteristic time constant τ_{pr} (Eq. 2.6). As a consequence, the solution progressively "looses" C and O atoms into different sinks ($CaCO_3$, H_2O, CO_2; see Eq. 2.2). This chemical process is accompanied by isotope fractionation, whereupon each sink has its own fractionation factor. Thus, the isotope composition of the DIC reservoir and the $CaCO_3$ progressively changes with increasing (precipitation) time. A schematic overview of the involved chemical and physical processes in a thin solution layer on top of a speleothem as well as the different isotope fractionation factors is shown in Figure 2.2.

In the last decade, a number of theoretical studies were published, aiming to describe more quantitatively isotope fractionation in speleothems. There are mainly two different approaches: On the one hand a 'kinetic' fractionation model (Dreybrodt, 2008) and on the other hand a Rayleigh distillation model (Scholz et al., 2009). Using a Rayleigh distillation model as in Scholz et al. (2009) has often been applied to describe isotope fractionation process during precipitation of $CaCO_3$(e.g., Bar-Matthews et al., 1996; Mickler et al., 2004; Mook and De Vries, 2000; Romanov et al., 2008b; Salomons and Mook, 1986). This is reasonable, since the removal of a substance from a reservoir accompanied by isotope fractionation is a classic case of a Rayleigh fractionation process and widely applied in isotope geochemistry (e.g., Mook and De Vries, 2000).

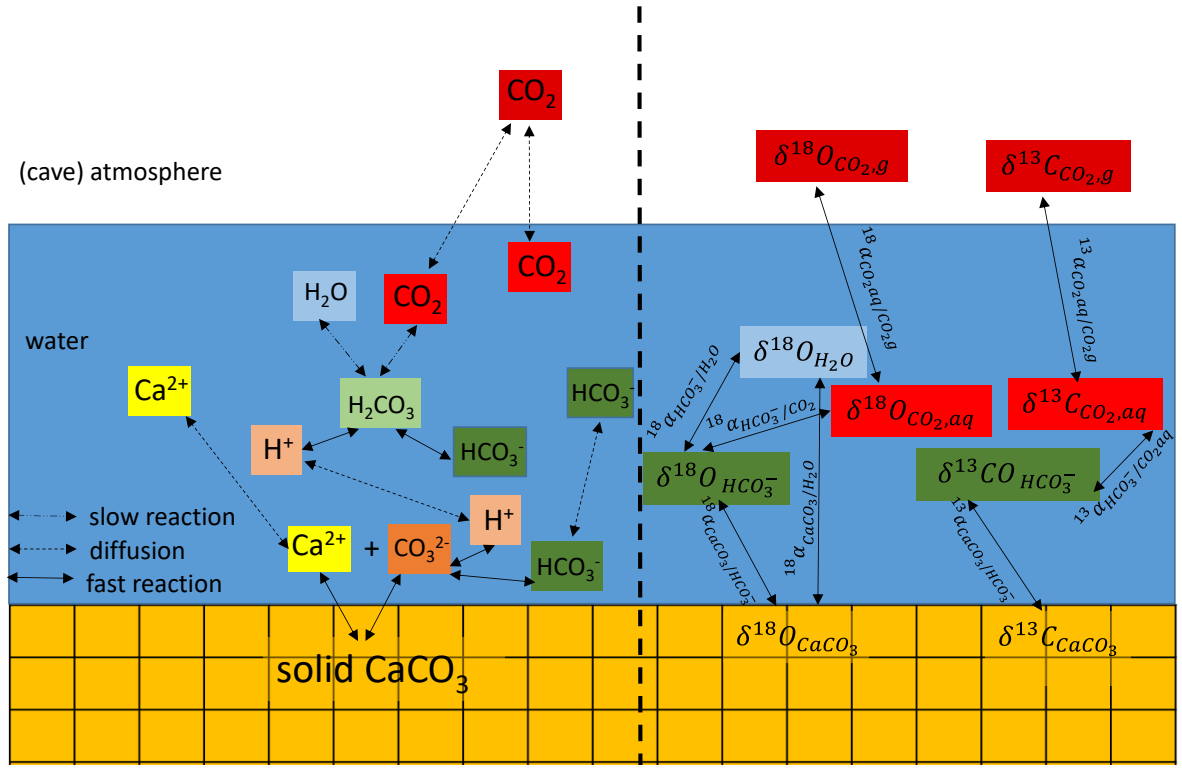

Fig. 2.2: Schematic overview over the processes in a thin layer of calcite precipitating solution on top of a speleothem. In the left part the physical and chemical processes between the different dissolved species and the water are summarized. Note the different timescales for the chemical reactions and the diffusion, indicated by different arrow lines. The right hand side compiles the 'flux' of isotopes and the corresponding fractionation factors for both, $\delta^{18}O$ and $\delta^{13}C$ in the system. Note, that the fractionation between CO_3^{2-} and $CaCO_3$ is neglected here, because at common pH in (cave-) solutions the CO_3^{2-} portion is very small (modified after Dreybrodt 2009 and Scholz et al. 2009).

In an alternative approach, Dreybrodt (2008) proposed a 'kinetic' fractionation model, which is based on the reasonable assumption that the heavy and the light isotopes are precipitated independently from each other, and consequently have slightly different rates and time constants for precipitation. Furthermore, a 'kinetic constant', γ, was introduced, which determines the $\delta^{18}O$ and $\delta^{13}C$ value of the DIC in equilibrium and is dependent on processes at the calcite surface. However, strictly speaking the term 'kinetic' model is misleading, because (i) equilibrium fractionation factors are used and (ii) a 'kinetic' fractionation process is commonly defined as a one way, irreversible, process (e.g., Mook and De Vries, 2000; Sharp, 2007). Further details can be found in Dreybrodt (2008) and Dreybrodt and Scholz (2011). Note, that γ has not been confirmed by experiments yet. In a recent study this approach has been extended by taking the isotope

exchange between the DIC and the gaseous CO_2 of the (cave) atmosphere into account (Dreybrodt and Romanov, 2016).

Interestingly both models (Dreybrodt, 2008; vs. Scholz et al., 2009) show a similar temporal evolution of isotope values until about 75 % of the initial [Ca^{2+}] has been precipitated to the stalagmite surface. Note that both models use equilibrium fractionation factors. In principle, if kinetic fractionation factors are used, a Rayleigh fractionation can be used to describe isotope fractionation in speleothems. A more detailed discussion on the differences between the 'kinetic' model and Rayleigh fractionation can be found in Dreybrodt (2016). However, neither the Rayleigh model nor the 'kinetic' model could be confirmed by experiments yet.

2.3 Previous experimental work

The mechanisms behind isotope fractionation have also been investigated in several laboratory experiments with synthetic carbonates. One of the first experimental studies was presented by Fantidis and Ehalt (1970), who performed experiments in a glass tube by precipitating $CaCO_3$ from a Ca^{2+}-HCO_3^- solution under laboratory atmosphere. They observed considerable deviations from expected equilibrium values for the fractionation between water and calcite as well as larger enrichments for $\delta^{18}O$ and $\delta^{13}C$ as expected for isotope equilibrium. However, a direct comparison of their results to a natural environment remains difficult because they were not able to avoid evaporation from their solution films due to lower relative humidity than in a natural environment. Furthermore, they had no precise control on temperature and pCO_2. Nevertheless, they were able to reproduce 'kinetic' isotope effects, which they also observed in natural stalagmites.

More recently, Wiedner at al. (2008) and Polag at al. (2010) performed experiments under better constrained conditions in a refrigerator. For their experiments, a $NaHCO_3$ and a $CaCl_2$ solution were pumped into a glass channel where they were mixed and then flew down on a glass fiber mat acting as crystallization substrate. During the experiments, they controlled relative humidity, temperature and pCO_2 of the atmosphere (which was kept at 0 ppmV). Additionally, they calculated the saturation state of the solutions at the moment of mixing. They observed an enrichment in both $\delta^{18}O$ and $\delta^{13}C$ values of the precipitated calcite with increasing distance of flow. Unfortunately, they did not perform direct measurements of the isotope composition of the water, but estimated the $\delta^{18}O_{H2O}$ values from the measurements of the isotope composition of the

HCO_3^-. Thus, the determination of a temperature dependent fractionation factor between calcite and water remained impossible.

In a different approach, Day and Henderson (2011) more closely mimicked cave conditions by imitating the dissolving epikarst section and the cave environment using two different reaction vessels in which they controlled temperature and pCO_2. In these vessels, dissolution and precipitation of $CaCO_3$ were controlled via the ambient pCO_2 of the experimental atmosphere. In their precipitation flask, they placed inclined glass plates seeded with crystallization nuclei, on which they dripped the $CaCO_2$-CO_{2-} solution at different temperatures and drip rates. They observed a temperature dependent fractionation for $^{18}\alpha_{calcite\text{-}water}$ which better corresponds to naturally observed values (e.g., Coplen, 2007; Johnston et al., 2013; Tremaine et al., 2011) than to typical 'equilibrium' fractionation factors (e.g., Kim and O'Neil, 1997; O'Neil et al., 1969). Additionally, they observed increasing $\delta^{18}O$ values with increasing distance from the impinging point of their drips.

All these laboratory experiments provided very important information and improved the understanding on the controls of stable isotope values in a speleothem record. However, all these studies were only able to provide information about the temporal evolution of the stable isotopes of the precipitated calcite as a function of temperature and/or drip rate. They had no control on the experiment once it was started and, direct investigations of the temporal evolution of the solution, such as pH values, $[Ca^{2+}]$ concentration and the isotope composition of the DIC were not possible. Thus, direct determination of isotope fractionation factors between all participating species, DIC, $CaCO_3$ and H_2O were not possible. It is particularly important to understand all basic mechanisms under which speleothem $CaCO_3$ is precipitated for the understanding of past climate records from speleothems. This is particularly important in terms of quantitative reconstruction of past temperature as well as meteoric precipitation source and amount, which has been impossible so far.

The experiments presented in the framework of this thesis aim to more closely resemble a natural cave system and to simulate all potential processes affecting the $\delta^{13}C$ and $\delta^{18}O$ values during precipitation of $CaCO_3$ from a flowing thin layer of solution as on the surface of a speleothem. For the first time, the temporal evolution of the stable isotope values of both the DIC and the precipitated $CaCO_3$ as well as pH and the precipitation rates of calcite are directly investigated. This significantly improves all previous experiments and enables to study isotope fractionation between all different species in the carbonate system (i.e., HCO_3^-, CO_2, $CaCO_3$ and H_2O) and to compare the results to theoretical model predictions.

2.4 References

Appelo, C.A.J., Postma, D. (2004) *Geochemistry, groundwater and pollution*. CRC press.

Asmerom, Y., Polyak, V.J., Burns, S.J. (2010) Variable winter moisture in the southwestern United States linked to rapid glacial climate shifts. *Nature Geosci* **3**, 114-117.

Baker, A., Genty, D., Dreybrodt, W., Barnes, W.L., Mockler, N.J., Grapes, J. (1998) Testing Theoretically Predicted Stalagmite Growth Rate with Recent Annually Laminated Samples: Implications for Past Stalagmite Deposition. *Geochimica et Cosmochimica Acta* **62**, 393-404.

Bar-Matthews, M., Ayalon, A., Gilmour, M., Matthews, A., Hawkesworth, C.J. (2003) Sea–land oxygen isotopic relationships from planktonic foraminifera and speleothems in the Eastern Mediterranean region and their implication for paleorainfall during interglacial intervals. *Geochimica et Cosmochimica Acta* **67**, 3181-3199.

Bar-Matthews, M., Ayalon, A., Matthews, A., Sass, E., Halicz, L. (1996) Carbon and oxygen isotope study of the active water-carbonate system in a karstic Mediterranean cave: Implications for paleoclimate research in semiarid regions. *Geochimica et Cosmochimica Acta* **60**, 337-347.

Beck, W.C., Grossman, E.L., Morse, J.W. (2005) Experimental studies of oxygen isotope fractionation in the carbonic acid system at 15°, 25°, and 40°C. *Geochimica et Cosmochimica Acta* **69**, 3493-3503.

Boch, R., Cheng, H., Spötl, C., Edwards, R., Wang, X., Häuselmann, P., 2011. NALPS: a precisely dated European climate record 120–60 ka, Clim. Past, **7**, 1247–1259.

Breecker, D.O. (2017) Atmospheric pCO2 control on speleothem stable carbon isotope compositions. *Earth and Planetary Science Letters* **458**, 58-68.

Buhmann, D., Dreybrodt, W. (1985) The kinetics of calcite dissolution and precipitation in geologically relevant situations of karst areas: 1. Open system. *Chemical Geology* **48**, 189-211.

Cheng, H., Edwards, R.L., Sinha, A., Spötl, C., Yi, L., Chen, S., Kelly, M., Kathayat, G., Wang, X., Li, X., Kong, X., Wang, Y., Ning, Y., Zhang, H. (2016) The Asian monsoon over the past 640,000 years and ice age terminations. *Nature* **534**, 640-646.

Coplen, T.B. (2007) Calibration of the calcite–water oxygen-isotope geothermometer at Devils Hole, Nevada, a natural laboratory. *Geochimica et Cosmochimica Acta* **71**, 3948-3957.

Cruz, F.W., Burns, S.J., Karmann, I., Sharp, W.D., Vuille, M., Cardoso, A.O., Ferrari, J.A., Silva Dias, P.L., Viana, O. (2005) Insolation-driven changes in atmospheric circulation over the past 116,000 years in subtropical Brazil. *Nature* **434**, 63-66.

Day, C.C., Henderson, G.M. (2011) Oxygen isotopes in calcite grown under cave-analogue conditions. *Geochimica et Cosmochimica Acta* **75**, 3956-3972.

Dietzel, M., Tang, J., Leis, A., Köhler, S.J. (2009) Oxygen isotopic fractionation during inorganic calcite precipitation — Effects of temperature, precipitation rate and pH. *Chemical Geology* **268**, 107-115.

Dorale, J.A., Liu, Z. (2009) Limitations of Hendy test criteria in judging the paleoclimatic suitability of speleothems and the need for replication. *Journal of Cave and Karst Studies* **71**, 73-80.

Dreybrodt, W. (1988) *Processes in Karst Systems*. Series in Physical Environment, Vol. **4**, Springer, Heidelberg.

Dreybrodt, W. (2008) Evolution of the isotopic composition of carbon and oxygen in a calcite precipitating $H_2O–CO_2–CaCO_3$ solution and the related isotopic composition of calcite in stalagmites. *Geochimica et Cosmochimica Acta* **72**, 4712-4724.

Dreybrodt, W. (2009) Physik von Stalagmiten. Physik Journal **8** Nr. 2, 25-30.

Dreybrodt, W. (2016) Problems in using the approach of Rayleigh distillation to interpret the ^{13}C and ^{18}O isotope compositions in stalagmite calcite. *Acta Carsologica* **45**.

Dreybrodt, W., Eisenlohr, L., Madry, B., Ringer, S. (1997) Precipitation kinetics of calcite in the system $CaCO_3$-H_2O-$C0_2$: The conversion to CO_2 by the slow process $H^+ + HCO_3^- \rightarrow CO_2 + H_2O$ as a rate limiting step. *Geochimica et Cosmochimica Acta* **61**, 3897-3904.

Dreybrodt, W., Hansen, M., Scholz, D. (2016) Processes affecting the stable isotope composition of calcite during precipitation on the surface of stalagmites: Laboratory experiments investigating the isotope exchange between DIC in the solution layer on top of a speleothem and the CO_2 of the cave atmosphere. *Geochimica et Cosmochimica Acta* **174**, 247-262.

Dreybrodt, W., Romanov, D. (2016) The evolution of ^{13}C and ^{18}O isotope composition of DIC in a calcite depositing film of water with isotope exchange between the DIC and a CO_2 containing atmosphere, and simultaneous evaporation of the water. Implication to climate proxies from stalagmites: A theoretical model. *Geochimica et Cosmochimica Acta* **195**, 323-338.

Dreybrodt, W., Scholz, D. (2011) Climatic dependence of stable carbon and oxygen isotope signals recorded in speleothems: From soil water to speleothem calcite. *Geochimica et Cosmochimica Acta* **75**, 734-752.

Emrich, K., Ehhalt, D.H., Vogel, J.C. (1970) Carbon isotope fractionation during the precipitation of calcium carbonate. *Earth and Planetary Science Letters* **8**, 363-371.

Fairchild, I.J., Baker, A. (2012) *Speleothem science: from process to past environments*. John Wiley & Sons.

Fantidis, J., Ehhalt, D.H. (1970) Variations of the carbon and oxygen isotopic composition in stalagmites and stalactites: Evidence of non-equilibrium isotopic fractionation. *Earth and Planetary Science Letters* **10**, 136-144.

Fleitmann, D., Burns, S.J., Neff, U., Mudelsee, M., Mangini, A., Matter, A. (2004) Palaeoclimatic interpretation of high-resolution oxygen isotope profiles derived from annually laminated speleothems from Southern Oman. *Quaternary Science Reviews* **23**, 935-945.

Friedman, I., O'Neil, J.R., 1977. Data of geochemistry: Compilation of stable isotope fractionation factors of geochemical interest, Survey professional paper **440** KK. US Government Printing Office, Washington.

Genty, D., Blamart, D., Ouahdi, R., Gilmour, M., Baker, A., Jouzel, J., Van-Exter, S. (2003) Precise dating of Dansgaard-Oeschger climate oscillations in western Europe from stalagmite data. *Nature* **421**, 833-837.

Hansen, M., Dreybrodt, W., Scholz, D. (2013) Chemical evolution of dissolved inorganic carbon species flowing in thin water films and its implications for (rapid) degassing of CO_2 during speleothem growth. *Geochimica et Cosmochimica Acta* **107**, 242-251.

Hansen, M., Scholz, D., Froeschmann, M.-L., Schöne, B.R., Spötl, C. (in press) Carbon isotope exchange between gaseous CO_2 and thin solution films: Artificial cave experiments and a complete diffusion-reaction model. Geochimica et Cosmochimica Acta.

Hellstrom, J.C., McCulloch, M.T. (2000) Multi-proxy constraints on the climatic significance of trace element records from a New Zealand speleothem. *Earth and Planetary Science Letters* **179**, 287-297.

Hendy, C.H. (1971) The isotopic geochemistry of speleothems—I. The calculation of the effects of different modes of formation on the isotopic composition of speleothems and their applicability as palaeoclimatic indicators. *Geochimica et Cosmochimica Acta* **35**, 801-824.

Johnston, V.E., Borsato, A., Spötl, C., Frisia, S., Miorandi, R. (2013) Stable isotopes in caves over altitudinal gradients: fractionation behaviour and inferences for speleothem sensitivity to climate change. *Clim. Past* **9**, 99-118.

Kim, S.-T., O'Neil, J.R. (1997) Equilibrium and nonequilibrium oxygen isotope effects in synthetic carbonates. *Geochimica et Cosmochimica Acta* **61**, 3461-3475.

Mangini, A., Spötl, C., Verdes, P. (2005) Reconstruction of temperature in the Central Alps during the past 2000 yr from a $\delta^{18}O$ stalagmite record. *Earth and Planetary Science Letters* **235**, 741-751.

McCrea, J.M. (1950) On the isotopic chemistry of carbonates and a paleotemperature scale. *The Journal of Chemical Physics* **18**, 849-857.

Mickler, P.J., Banner, J.L., Stern, L., Asmerom, Y., Edwards, R.L., Ito, E. (2004) Stable isotope variations in modern tropical speleothems: Evaluating equilibrium vs. kinetic isotope effects 1. *Geochimica et Cosmochimica Acta* **68**, 4381-4393.

Mickler, P.J., Stern, L.A., Banner, J.L. (2006) Large kinetic isotope effects in modern speleothems. *Geological Society of America Bulletin* **118**, 65-81.

Mischel, S.A., Scholz, D., Spötl, C., Jochum, K.P., Schröder-Ritzrau, A., Fiedler, S. (2016) Holocene climate variability in Central Germany and a potential link to the polar North Atlantic: A replicated record from three coeval speleothems. *The Holocene*.

Mook, W.G., Bommerson, J.C., Staverman, W.H. (1974) Carbon isotope fractionation between dissolved bicarbonate and gaseous carbon dioxide. *Earth and Planetary Science Letters* **22**, 169-176.

Mook, W.G., De Vries, J. (2000) Volume I: Introduction: Theory, Methods, Review. *Environmental Isotopes in the Hydrological Cycle—Principles and Applications, International Hydrological Programme (IHP-V), Technical Documents in Hydrology (IAEA/UNESCO) No* **39**, 75-76.

Moreno, A., Stoll, H., Jiménez-Sánchez, M., Cacho, I., Valero-Garcés, B., Ito, E., Edwards, R.L. (2010) A speleothem record of glacial (25–11.6 kyr BP) rapid climatic changes from northern Iberian Peninsula. *Global and Planetary Change* **71**, 218-231.

Mühlinghaus, C., Scholz, D., Mangini, A. (2007) Modelling stalagmite growth and $\delta^{13}C$ as a function of drip interval and temperature. *Geochimica et Cosmochimica Acta* **71**, 2780-2790.

Mühlinghaus, C., Scholz, D., Mangini, A. (2009) Modelling fractionation of stable isotopes in stalagmites. *Geochimica et Cosmochimica Acta* **73**, 7275-7289.

O'Neil, J.R., Clayton, R.N., Mayeda, T.K. (1969) Oxygen isotope fractionation in divalent metal carbonates. *The Journal of Chemical Physics* **51**, 5547-5558.

Plummer, L., Wigley, T., Parkhurst, D. (1978) The kinetics of calcite dissolution in CO_2-water systems at 5 degrees to 60 degrees C and 0.0 to 1.0 atm CO_2. *American Journal of Science* **278**, 179-216.

Polag, D., Scholz, D., Mühlinghaus, C., Spötl, C., Schröder-Ritzrau, A., Segl, M., Mangini, A. (2010) Stable isotope fractionation in speleothems: Laboratory experiments. *Chemical Geology* **279**, 31-39.

Richards, D.A., Dorale, J.A. (2003) Uranium-series chronology and environmental applications of speleothems. *Reviews in Mineralogy and Geochemistry* **52**, 407-460.

Romanek, C.S., Grossman, E.L., Morse, J.W. (1992) Carbon isotopic fractionation in synthetic aragonite and calcite: Effects of temperature and precipitation rate. *Geochimica et Cosmochimica Acta* **56**, 419-430.

Romanov, D., Kaufmann, G., Dreybrodt, W. (2008a) Modeling stalagmite growth by first principles of chemistry and physics of calcite precipitation. *Geochimica et Cosmochimica Acta* **72**, 423-437.

Romanov, D., Kaufmann, G., Dreybrodt, W. (2008b) $\delta^{13}C$ profiles along growth layers of stalagmites: Comparing theoretical and experimental results. *Geochimica et Cosmochimica Acta* **72**, 438-448.

Salomons, W., Mook, W. (1986) Isotope geochemistry of carbonates in the weathering zone. *Handbook of environmental isotope geochemistry* 2, 239-269.

Scholz, D., Frisia, S., Borsato, A., Spötl, C., Fohlmeister, J., Mudelsee, M., Miorandi, R., Mangini, A. (2012) Holocene climate variability in north-eastern Italy: potential influence of the NAO and solar activity recorded by speleothem data. *Clim. Past* **8**, 1367-1383.

Scholz, D., Mühlinghaus, C., Mangini, A. (2009) Modelling $\delta^{13}C$ and $\delta^{18}O$ in the solution layer on stalagmite surfaces. *Geochimica et Cosmochimica Acta* **73**, 2592-2602.

Scholz, D., Hoffmann, D. (2008) $^{230}Th/U$-dating of fossil corals and speleothems. *Eiszeitalter und Gegenwart* **57**, 52-76.

Sharp, Z. (2007) *Principles of stable isotope geochemistry*. Pearson Education Upper Saddle River, NJ.

Tremaine, D.M., Froelich, P.N., Wang, Y. (2011) Speleothem calcite farmed in situ: Modern calibration of $\delta^{18}O$ and $\delta^{13}C$ paleoclimate proxies in a continuously-monitored natural cave system. *Geochimica et Cosmochimica Acta* **75**, 4929-4950.

Vogel, J.C., Grootes, P.M., Mook, W.G. (1970) Isotopic fractionation between gaseous and dissolved carbon dioxide. *Zeitschrift für Physik* **230**, 225-238.

Wassenburg, J.A., Dietrich, S., Fietzke, J., Fohlmeister, J., Jochum, K.P., Scholz, D., Richter, D.K., Sabaoui, A., Spotl, C., Lohmann, G., Andreae, M.O., Immenhauser, A. (2016) Reorganization of the North Atlantic Oscillation during early Holocene deglaciation. *Nature Geosci* advance online publication.

Watkins, J.M., Hunt, J.D., Ryerson, F.J., DePaolo, D.J. (2014) The influence of temperature, pH, and growth rate on the $\delta^{18}O$ composition of inorganically precipitated calcite. *Earth and Planetary Science Letters* **404**, 332-343.

Watkins, J.M., Nielsen, L.C., Ryerson, F.J., DePaolo, D.J. (2013) The influence of kinetics on the oxygen isotope composition of calcium carbonate. *Earth and Planetary Science Letters* **375**, 349-360.

Wiedner, E., Scholz, D., Mangini, A., Polag, D., Mühlinghaus, C., Segl, M. (2008) Investigation of the stable isotope fractionation in speleothems with laboratory experiments. *Quaternary International* **187**, 15-24.

Williams, P.W., King, D.N.T., Zhao, J.X., Collerson, K.D. (2005) Late Pleistocene to Holocene composite speleothem ^{18}O and ^{13}C chronologies from South Island, New Zealand—did a global Younger Dryas really exist? *Earth and Planetary Science Letters* **230**, 301-317.

Zeebe, R.E., Bijma, J., Wolf-Gladrow, D.A. (1999) A diffusion-reaction model of carbon isotope fractionation in foraminifera. *Marine Chemistry* **64**, 1499-227.

Zeebe, R.E., Wolf-Gladrow, D. (2001) *CO_2 in Seawater: Equilibrium, Kinetics, Isotopes*. Amsterdam: Elsevier Science, B.V. 346 pp.

Chapter 3: Manuscript I

Processes affecting the stable isotope composition of calcite during precipitation on the surface of stalagmites: Laboratory experiments investigating the isotope exchange between DIC in the solution layer on top of a speleothem and the CO_2 of the cave atmosphere

Wolfgang Dreybrodt[1] , Maximilian Hansen[2], Denis Scholz[2]

Published in Geochimica et Cosmochimica Acta.

[1]Faculty of Physics and Electrical Engineering, University of Bremen, Germany

[2]Institute for Geosciences, University of Mainz, Germany

Dreybrodt, W., M. Hansen, and D. Scholz, Processes affecting the stable isotope composition of calcite during precipitation on the surface of stalagmites: Laboratory experiments investigating the isotope exchange between DIC in the solution layer on top of a speleothem and the CO_2 of the cave atmosphere. Geochimica et Cosmochimica Acta, 2016. **174**: p. 247-262.

Abstract

We present a theoretical derivation of the exchange time, τ_{ex}, needed to establish isotopic equilibrium between atmospheric CO_2 in a cave and HCO_3^- dissolved in a thin water film covering the surface of a speleothem. The result is $\tau_{ex} = \tau_{red}^{ex} \cdot [HCO_3^-] / (K_H \cdot p_{CO_2}^{cave})$, where τ_{red}^{ex} depends on the depth, a, of the water film and on temperature. $[HCO_3^-]$ is the concentration of bicarbonate, $p_{CO_2}^{cave}$ the partial pressure of CO_2, and K_H is Henry's constant. To test the theory we prepared stagnant or flowing thin films of a $NaHCO_3$ solution and exposed them at 20°C to an CO_2 containing atmosphere of p_{CO2} 500, 12,500, or 25,000 ppmV and defined isotope composition. The $\delta^{13}C$ and $\delta^{18}O$ values of the DIC in the solution were measured as a function of the exposure time. For stagnant films with depths between 0.06 to 0.2 cm the $\delta^{13}C$ values exhibit an exponential approach towards isotope equilibrium with the atmospheric CO_2 with exchange time, τ_{ex}. The $\delta^{18}O$ values first evolve towards isotopic equilibrium with atmospheric CO_2, reach a minimum value and then drift away from the isotopic equilibrium with atmospheric CO_2 approaching a steady state caused by isotopic exchange of oxygen with water. The experimental findings are in satisfactory agreement with the theoretical predictions.

To further investigate isotope evolution in cave analogue conditions, a water film containing 5 mmol/L of $NaHCO_3$ with a depth of 0.013 cm flowing down an inclined borosilicate glass plate was exposed to an atmosphere with $p_{CO2} = 500$ ppmV at a temperature of 20°C. The $\delta^{13}C$ and $\delta^{18}O$ values were measured as a function of flow (exposure) time, t. The isotope compositions in the DIC of the water film decrease linear in time by $\delta_{DIC}(t) = \delta_{DIC}(0) - (\delta_{DIC}(0) - \delta_{DIC}(\infty)) \cdot t/\tau_{ex}$ where $\delta_{DIC}(0)$ is the initial isotope composition of dissolved inorganic carbon (DIC) in the water film and $\delta_{DIC}(\infty)$ its final value. From these data an exchange time τ_{ex} of ca. 7000 s was obtained, in satisfactory agreement with the theoretical predictions. The exchange times can be calculated by $\tau_{ex} = \tau_{red}^{ex} \cdot [HCO_3^-] / (K_H \cdot p_{CO_2}^{cave})$, where τ_{red}^{ex} is given by the theory as function of temperature and the depth, (a), of the water film. This way it is possible to obtain exchange times for various conditions of stalagmite growth as they occur in caves.

3.1 Introduction

Speleothems occur in many climate zones of the Earth and can be dated with high accuracy and precision by U-series disequilibrium methods (e.g., Richards and Dorale, 2003; Scholz and Hoffmann, 2008). The most widely applied climate proxies in speleothems are the $\delta^{13}C$ and $\delta^{18}O$ values, which can be measured at high temporal resolution providing long-term climate records. However, the interpretation of these records in terms of past climate variability (temperature and meteoric precipitation) is difficult, because complex processes occurring in the soil, the epikarst, and during the flow of the water down to the cave may influence the stable isotope composition (Dreybrodt and Scholz, 2011). Finally, isotope fractionation processes occurring on the speleothem surface during precipitation of calcite may cause variations in both $\delta^{13}C$ and $\delta^{18}O$ (Deininger et al., 2012; Dreybrodt, 2008; Dreybrodt and Deininger, 2014; Dreybrodt and Scholz, 2011; Mickler et al., 2004; Riechelmann et al., 2013; Scholz et al., 2009). All these processes may obscure climatic signals potentially contained in the stable isotope records, rendering quantitative reconstruction of past temperature and/or precipitation changes questionable.

One process, often overlooked in the literature is carbon and oxygen isotope exchange between the CO_2 of the cave atmosphere and the dissolved inorganic carbon (DIC) in the water film from which calcite is precipitated to the speleothem. In ventilated caves, both the p_{CO2} and the $\delta^{13}C$ value of the CO_2 of the cave atmosphere may show large variations (Spötl, 2005) (Baldini et al., 2008) (Cowan et al., 2013) (Mandić et al., 2013). In general, the $\delta^{13}C$ value of the cave CO_2 is a mixture of atmospheric CO_2, which has a $\delta^{13}C$ value of ca. -8 ‰, and CO_2 produced by decomposition of organic matter in the soil or in the deeper epikarst from where it is transferred to the cave (Kowalczk and Froelich, 2010). The latter has a $\delta^{13}C$ value of approximately -22 ‰. Consequently, the $\delta^{13}C$ value of the cave atmosphere, $\delta^{13}C_{cave}$, may vary between these two extreme values (Scholz et al., 2009). Recently, Frisia et al. (2011) hypothesized that "… this opens the possibility to use the $\delta^{13}C$ of cave calcite, in favorable conditions, as a proxy of cave air p_{CO2} and C isotope composition (Baskaran and Krishnamurthy, 1993)". They continued that "a thorough understanding of the evolution of $\delta^{13}C$ in karst systems thus becomes critically important to develop and validate inverse models which allow the reconstruction of past climate-related parameters or atmospheric changes from $\delta^{13}C$ data of stalagmites".

Carbon isotope exchange between the DIC in the solution layer on the speleothem surface and the CO_2^{cave} of the cave atmosphere establishes isotopic equilibrium between the aqueous CO_2 in the solution and the gaseous CO_2^{cave} of the cave atmosphere. The corresponding isotope shift between the initial state and the final state in the DIC is $\delta_f^{13}CO_2^{film} - \delta_i^{13}CO_2^{film}$, where $\delta_i^{13}CO_2^{film}$ is

the initial δ-value of the aqueous CO_2 dissolved in the water film, and $\delta_f^{13}CO_2^{film}$ is the final δ- value. For $\delta^{13}C$ the value $\delta_i^{13}CO_2^{film}$ can be up to about -15 ‰. However, these variations will only be imprinted into speleothem calcite if they occur during precipitation of calcite from the actual water film (i.e., during the time interval, τ_{pr}, characteristic for the exponential decline of calcite deposition rates). Therefore, the isotope exchange time, τ_{ex}, characterizing the temporal approach towards isotope equilibrium between the CO_2 in the cave atmosphere and the DIC in the water film, is of utmost importance. If the drip interval, $T_{drip} << \tau_{ex}$, changes in the stable isotope values of the cave air will not be visible in the stable isotope signals of the speleothem. In contrast, for $\tau_{ex} << T_{drip}$, the isotope value of the DIC and, consequently, the calcite precipitated will reflect an influence of isotope exchange with the cave atmosphere. Similar arguments hold for oxygen, but in addition one has also to consider exchange between DIC and the water of the film.

A first theoretical attempt to estimate τ_{ex} was reported by Dreybrodt and Scholz (2011). Although their approach includes some correct ideas, the coupling between diffusion of CO_2 from the cave atmosphere into the water film and its conversion into HCO_3^- was not appropriately described. Their exchange time is $\tau_{ex} = \tau_{red}^{ex} \cdot [HCO_3^-] / (K_H \cdot p_{CO_2}^{cave})$, where τ_{red}^{ex} is formally defined as reduced exchange time, depending only on transport mechanisms. However, Dreybrodt and Scholz (2011) only considered transport by molecular diffusion and did not take into account the chemical conversion of CO_2 into HCO_3^- correctly. Therefore their reduced exchange time τ_{red}^{ex} is incorrect, whereas the dependence of τ_{ex} on $[HCO_3^-] / (K_H \cdot p_{CO_2}^{cave})$ is true. Accidentally numerically reasonable values of τ_{ex} for special cave conditions have been reported (Deininger et al., 2012), by using the equation from Dreybrodt and Scholz (2011).

In this paper we will derive the correct expression for τ_{red}^{ex}. This also explains the errors in the prior work.

We present a new derivation of the reduced exchange time, τ_{red}^{ex}, taking into account both, molecular diffusion and conversion of CO_2 into HCO_3-. We find for typically thin water films on the surface of speleothems with depth, a ≤ 0.02 cm, that the reduced exchange time is almost independent of (a) and close to, $\tau_{red}^{ex} = 1/k$, where k is the rate constant of the reaction $CO_2 + H_2O \leftrightarrow HCO_3^- + H^+$.

We present laboratory experiments to determine the temporal evolution of the $\delta^{13}C$ and $\delta^{18}O$ values of a $NaHCO_3$ solution exposed as a thin layer with film depth ranging from 0.01 cm to 0.2 cm to a CO_2-containing atmosphere. We observe an exponential decay of $\delta^{13}C_{DIC}$ value towards

an equilibrium value. The time constant of this decay is in reasonable agreement with the theoretical predictions.

3.2 Theoretical background

After the water has entered the cave from the fissures of the rock, a thin layer of depth, (a), either flowing at the ceiling, the cave wall or on the surface of a stalactite or stalagmite is established. It contains the following species of molecules: aqueous $^{12}CO_2$ with initial concentration $^{12}c_i$ and aqueous $^{13}CO_2$ with initial concentration $^{13}c_i$ and bicarbonate, HCO_3^-, with initial concentrations $^{12}h_i$ and $^{13}h_i$ for the two isotopic species, respectively. For cave waters pH is generally about 8 and carbonate ions can be neglected. Charge balance then requires $[Ca^{2+}] = 2(^{12}h_i + ^{13}h_i)$. In this initial state all species in the water are in chemical and isotopic equilibrium with each other.

3.2.1 Relation between the change of the δ-value and the change of isotope concentrations during exchange reactions.

This solution, after it has entered the cave, is exposed to the cave atmosphere containing CO_2 with partial pressures $p^{12}CO_2$ and $p^{13}CO_2$ for the two isotopes, which generally are not in isotope equilibrium with the aqueous CO_2 in the water layer with the initial concentrations $^{12}c_i$ and $^{13}c_i$, respectively and the bicarbonate with concentrations $^{12}h_i + ^{13}h_i$. Outgassing of CO_2 establishes chemical equilibrium between the gaseous CO_2 in the cave atmosphere and the aqueous CO_2 in the water film within several ten seconds (Dreybrodt and Scholz, 2011).

Henry's law requires that the concentrations of the aqueous CO_2 at the surface of the water film at (x= 0), are given by

$$^{12}c(x=0) = K_H^{12} \cdot p_{CO2}^{12} \text{ and } ^{13}c(x=0) = K_H^{13} \cdot p_{CO2}^{13} \qquad (3.1)$$

where K_H is Henry's constant for the respective isotope.

If $^{12}c_i < ^{12}c(x=0)$, a flux CO_2 from the cave atmosphere enters the water film by molecular diffusion. CO_2 leaves the water if $^{12}c_i > ^{12}c(x=0)$. The same is true for the heavy isotope. The deviation of the CO_2 concentrations, ^{12}c and ^{13}c, in the water film from their initial values $^{12}c_i$ and $^{13}c_i$, in equilibrium with the initial bicarbonate concentration $^{12}h_i$ and $^{13}h_i$, drives the isotope composition of HCO_3^- to a new isotope equilibrium with concentrations $^{12}h_f$ and $^{13}h_f$ by the reaction $CO_2 + H_2O \leftrightarrow HCO_3^- + H^+$.

For pH values between 7.5 and 9, as they are common in karst water, HCO_3^- is the dominant species with abundance of about 95% and CO_3^{2-} can be neglected. Furthermore in carbonate solutions charge balance requires $[Ca^{2+}] = 2(^{12}h + ^{13}h)$ for calcium and $[Na^{2+}] = (^{12}h + ^{13}h)$ for a

sodium carbonate solution as used in our experiments. Since in our experiments precipitation does not occur, $[Na^{2+}]$ is constant in time its derivative in time is $d[Na^{2+}]/dt = d(^{12}h + ^{13}h)/dt = 0$, from which follows $d^{12}h/dt = -\, d^{13}h/dt$. Therefore if a heavy bicarbonate ion enters into the solution by the reaction $CO_2+H_2O \leftrightarrow HCO_3^-+H^+$ a light bicarbonate ion has to leave it by the corresponding backward reaction or vice versa. From this follows that $^{12}h_f - {}^{12}h_i = -(^{13}h_f - {}^{13}h_i)$ for the final isotopic equilibrium. This is generally true for all processes of isotope exchange. In any case, the isotope composition changes only when a rare isotope (abundant isotope) enters in the solution and an abundant (rare) one leaves it.

In the following we calculate the change of the δ-value of bicarbonate $\delta H^{13}CO_3^-$ from the definition of δ. Note that we use the δ-value as a small number, not in the ‰-notation. To obtain the ‰-value one has to multiply our δ-notation by a factor of 1000.

The relation between δ and the concentrations is given by the definition of δ

$$\delta_f - \delta_i = \left(\frac{R_f}{R_s} - 1\right) - \left(\frac{R_i}{R_s} - 1\right) = \frac{R_f}{R_s} - \frac{R_i}{R_s} = \left(\frac{R_f}{R_i} - 1\right)\frac{R_i}{R_s} = \left[\left(\frac{^{13}h_f}{^{13}h_i}\right)\left(\frac{^{12}h_i}{^{12}h_f}\right) - 1\right]\frac{R_i}{R_s} \qquad (3.2)$$

R_i is the initial isotope ratio in the solution, R_f the final one, and R_s is that of a standard.
Using $^{12}h_f - {}^{12}h_i = -(^{13}h_f - {}^{13}h_i) = \Delta h$ and inserting $^{12}h_f = {}^{12}h_i + \Delta h$ and $^{13}h_f = {}^{13}h_i - \Delta h$ one obtains

$$\delta_f - \delta_i = = \left[\left(\frac{^{13}h_i + \Delta h}{^{13}h_i}\right)\left(\frac{^{12}h_i}{^{12}h_i - \Delta h}\right) - 1\right]\frac{R_i}{R_s} = \left[\left(1 + \frac{\Delta h}{^{13}h_i}\right) \Big/ \left(1 - \frac{\Delta h}{^{12}h_i}\right) - 1\right]\frac{R_i}{R_s} \qquad (3.3)$$

With $\Delta h/{}^{13}h_i << 1$ and $\Delta h/{}^{12}h_i << 1$ and neglecting terms in $(\Delta h)^2$ one gets

$$\delta_f - \delta_i = \left[\left(1 + \frac{\Delta h}{^{13}h_i}\right)\left(1 + \frac{\Delta h}{^{12}h_i}\right) - 1\right]\frac{R_i}{R_s} = \left(\frac{\Delta h}{^{13}h_i} + \frac{\Delta h}{^{12}h_i}\right)\frac{R_i}{R_s} \qquad (3.4)$$

with $R_i \cong R_s$ and $^{13}h_i/{}^{12}h_i = R_i \cong 0.01$ we get

$$\delta_f - \delta_i = \left(\frac{\Delta h}{^{13}h_i} + \frac{\Delta h}{^{12}h_i}\right) \cong \frac{\Delta h}{^{13}h_i} \qquad (3.6)$$

Note that the change in δ is dominated by the change of concentration of the rare isotope.
If the concentrations $^{13}h_f$ and $^{13}h_i$ change in time such that isotope equilibrium is maintained this relation is also valid as $\delta(t_f) - \delta(t_i)$ for all times t_f and t_i during the process of exchange.

3.2.2 Evolution of isotope concentrations in time.

We now turn to the evolution of the concentrations in time. The purpose of this section is to find the exchange time, τ_{ex}, which gives the time scale needed until the DIC comes to isotope equilibrium with the CO_2 in the surrounding atmosphere. As we will find, the approach to isotope equilibrium

is exponential with $\delta(t)- \delta_{eq} = (\delta_i-\delta_{eq})\exp(-t/\tau_{ex})$, where δ_i is the initial value and δ_{eq} is the final value in isotope equilibrium. In this case after the time $3\cdot t_{ex}$ the system has reached $\delta(3\cdot\tau_{ex}) - \delta_{eq} = 0.05(\delta_i-\delta_{eq})$, in other words, 95% of the initial distance to equilibrium have been passed.

Since, as stated above, $d^{12}h/dt = - d^{13}h/dt$, it is sufficient to consider only one isotope with concentration, c, representative for both and omit the index ^{12} or ^{13} in the notations. At the surface of the water film, $x = 0$, the concentration of CO_2 is given by Henry's law , $c(x=0) = K_H \cdot p_{CO2}$. At the water rock interface ($x = a$) flux of carbon is excluded and $\partial c(a,t)/\partial x = 0$.

We assume that at time t=0 the concentration of aqueous CO_2 , c_i , is locally constant in the water film and in isotope and chemical equilibrium with the initial bicarbonate concentration, h_i. The final concentrations, c_f, of aqueous CO_2 and h_f of bicarbonate, when the new isotope equilibrium with the CO_2 in the cave air has been established are locally constant within the film. p_{CO2} in the cave and its isotope composition can be regarded as constant in time, due to its huge reservoir. Therefore $c_f = K_H/pCO_2^{cave}$. The total amount of carbon (for each isotope), which can be absorbed (or released) from the water film is $C^{tot} = V(c_f-c_i) + V(h_f-h_i)$, where V is the volume of the film. C^{tot} can be regarded as a reservoir, which must be filled to attain isotope equilibrium.

In a first step we assume that C^{tot} is infinitely large. Later on, this will be relaxed. The evolution of the concentration c(x,t) of aqueous CO_2 is described by the reaction-diffusion equation

$$D\frac{\partial^2 c}{\partial x^2} - k(c - c_i) = \frac{\partial c}{\partial t} \qquad (3.6)$$

with boundary conditions $c(x=0) = K_H \cdot p_{CO2}$ and $\partial c(a,t)/\partial x = 0$.

D is the coefficient of molecular diffusion and k is the rate constant of the reaction $CO_2+H_2O \leftrightarrow HCO_3^-+H^+$.

To solve Eqn. (3.6) we define, $c'=c-c_i$, and rewrite Eqn. (3.6) as

$$D\frac{\partial^2 c'}{\partial x^2} - kc' = \frac{\partial c'}{\partial t}, \qquad (3.7)$$

The solution of this equation can be found by Danckwert's method and is given in Crank (1979). The temporal evolution of the flux, F, of CO_2 into the water film, derived from this solution contains a transient part, which decays exponentially with time constant, t_{trans}:

$$t_{trans} = \frac{1}{\frac{\pi^2 D}{4a^2} + k} \qquad (3.8)$$

This transient part describes the temporal build-up of the CO_2-concentration profile in the water film, which attains a steady state independent on time after $t > 3\ t_{trans}$. As a consequence

also the flux, F, of CO_2 into the water film decays to a constant value independent of time when the steady state is reached. Since Danckwert's steady state solution of the flux is a complicated infinite numerical series, we prefer to derive an equivalent steady state solution by setting $\partial c'/\partial t = 0$ in eqn. (3.7).

$$D\frac{\partial^2 c'}{\partial x^2} = k \cdot c' \tag{3.9}$$

The solution of this differential equation is reported by Bird et al. (1960), and the flux, F of CO_2 from the cave atmosphere into the water, is given by the expression:

$$F = \frac{D}{a} \cdot (c_f - c_i) \cdot \sqrt{\frac{ka^2}{D}} \cdot \tanh\left(\sqrt{\frac{ka^2}{D}}\right) \tag{3.10}$$

Note that we have assumed that the reaction term kc' is constant in time. In other words, there must be an infinite reservoir C^{tot} which can absorb the resulting HCO_3^-. This implies that DIC never reaches isotope equilibrium. If the reservoir C^{tot} is finite, however, the flux must become zero when the reservoir is full. If the flux, F, is low, such that ($[HCO_3^-](t)$ - $[HCO_3^-]_f$) changes only slightly during a time span of length t_{trans} we can approximate the temporal dependence of $F = F(t)$ by a quasi steady-state solution.

$$F(t) = \frac{D}{a} \cdot (c_f - c(t)) \cdot \sqrt{\frac{ka^2}{D}} \cdot \tanh\left(\sqrt{\frac{ka^2}{D}}\right) \tag{3.11}$$

$c(t)$ is the average CO_2 concentration, which drives the flux. It changes slowly in time such that during a time span, t_{trans}, $c_f - c(t)$ varies only by a few percent. When c(t) has reached the value c_f isotope equilibrium is established and the flux F becomes zero.

Mass balance requires

$$\frac{d[HCO_3^-](t)}{dt} = \frac{dh^{av}}{dt} = \frac{F(t) \cdot A}{V} = \frac{D}{a^2} \cdot \sqrt{\frac{ka^2}{D}} \cdot \tanh\left(\sqrt{\frac{ka^2}{D}}\right) \cdot \left([CO_2]_f - [CO_2](t)\right) \tag{3.12}$$

where h^{av} is the spatial average, $[HCO_3^-]$ and $[CO_2]$ are average concentrations. A is the surface area of the water film and V its volume. For plane water films $V/A = a$, the film depth.

Now we turn to the evolution of ^{13}C. In isotope equilibrium the shift $\delta(t)$-δ_i of aqueous CO_2 after time t must be equal to that of bicarbonate. See eqn. 3.4. Therefore from

$$[H^{13}CO_3^-](t) - [H^{13}CO_3^-]_f = (\delta(t) - \delta_f) \cdot [H^{13}CO_3^-]_i \quad \text{and} \quad [^{13}CO_2](t) - [^{13}CO_2]_f = (\delta(t) - \delta_f) \cdot [^{13}CO_2]_i \tag{3.13}$$

one finds

$$[^{13}CO_2](t)-[^{13}CO_2]_f=\left([H^{13}CO_3^-](t)-[H^{13}CO_3^-]_f\right)\cdot\frac{[^{13}CO_2]_i}{[H^{13}CO_3^-]_i}\cong\left([H^{13}CO_3^-](t)-[H^{13}CO_3^-]_f\right)\cdot\frac{[CO_2]_i}{[HCO_3^-]_i} \quad (3.14)$$

Inserting eqn. 3.14 into eqn. 3.12 one gets

$$\frac{d[H^{13}CO_3^-](t)}{dt}=\frac{F(t)\cdot A}{V}=-\frac{D}{a^2}\cdot\sqrt{\frac{ka^2}{D}}\cdot\tanh\left(\sqrt{\frac{ka^2}{D}}\right)\cdot\left([H^{13}CO_3^-](t)-[H^{13}CO_3^-]_f\right)\cdot\frac{[CO_2^{aq}]}{[HCO_3^-]}\cdot \quad (3.15)$$

This equation describes the exponential evolution of the dissolved $[H^{13}CO_3^-](t)$ to isotopic equilibrium with the cave atmosphere with exchange time constant, τ_{ex}: $[H^{13}CO_3^-](t)=\left([H^{13}CO_3^-]_i-[H^{13}CO_3^-]_f\right)\exp(-t/\tau_{ex})+[H^{13}CO_3^-]_f$ with

$$\tau_{ex}=\frac{\frac{a^2}{D}\cdot\frac{[HCO_3^-]}{[CO_2^{aq}]}}{\sqrt{\frac{ka^2}{D}}\tanh\left(\sqrt{\frac{ka^2}{D}}\right)}=\frac{\frac{a^2}{D}}{\sqrt{\frac{ka^2}{D}}\tanh\left(\sqrt{\frac{ka^2}{D}}\right)}\cdot\frac{[HCO_3^-]}{[K_H\cdot p_{CO_2^{cave}}]}=\tau_{red}^{ex}\cdot\frac{[HCO_3^-]}{[K_H\cdot p_{CO_2^{cave}}]}=\tau_{red}^{ex}\cdot\frac{[HCO_3^-]}{[CO_2]} \quad (3.16)$$

This approximation is valid for $\tau_{ex} > 0.1\ t_{trans}$ to warrant quasi-steady state conditions. In this equation we also define the reduced exchange time, τ_{red}^{ex}. This time depends only on the parameters k, D, and a, determining transport and is used for better representing the experimental results in Fig.3.1.

This mathematically complex result can be also understood by the following plausibility argument: To establish isotope equilibrium the reservoir C^{tot} of $H^{13}CO_3^-$ given by $(\delta_f-\delta_i)^{13}h_i\cdot V$ must be filled. The time needed to fill this reservoir with $^{13}CO_2$ from the cave atmosphere is given by

$$T_{fill}=(\delta_f-\delta_i)[H^{13}CO_3^-]_i\cdot V/^{13}\overline{F}\cdot A, \quad (3.17)$$

where $^{13}\overline{F}$ is an average value for the flux between the maximum ($^{13}F=^{13}F_i$) and minimum (F=0, at equilibrium) values. ^{13}F can be approximated by $^{13}\overline{F}=^{13}F/2$. Inserting $^{13}\overline{F}$, gives $T_{fill}=2\tau_{ex}$. Note that T_{fill} is the time required to fill the empty reservoir $(\delta_f-\delta_i)^{13}h_i\cdot V$, which is an approximation to the exchange time, τ_{ex}, as derived from eqn. (3.16).

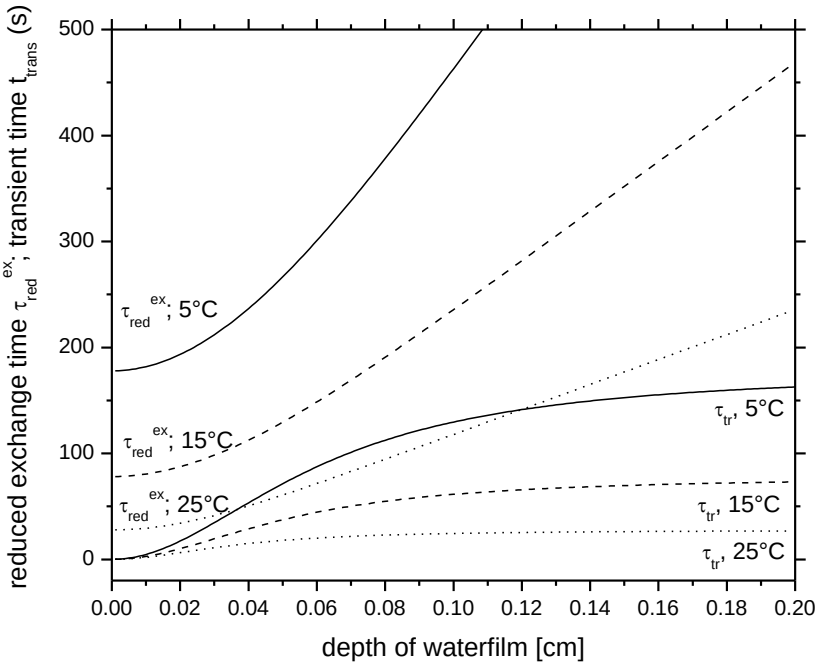

Fig. 3.1: Theoretical reduced exchange time, τ_{red}^{ex}, in dependence on the film thickness, a, for various temperatures. See eqn.16. The exchange time, τ_{ex}, is related to τ_{red}^{ex} by $\tau_{ex} = \tau_{red}^{ex} \cdot [HCO_3^-] / (K_H \cdot p_{CO_2}^{cave})$. The transient time, ttrans, needed to establish a quasi steady state is also shown. See eqn.3.8.

All results are also valid for the oxygen isotope. However, in addition to exchange with the oxygen isotopes of the cave atmosphere an entirely different mechanism causes exchange of oxygen isotopes with those of the water. This will be discussed later.

In the following, we provide numbers for a = 0.02 cm. For 25°C, $\tau_{ex}^{red} = 33$ s, for 15 °C, $\tau_{ex}^{red} = 87$ s, and for 5°C, $\tau_{ex}^{red} = 193$ s. The corresponding exchange times, τ_{ex}, for $p_{CO2}^{cave} = 1 \cdot 10^{-3}$ atm and [DIC] = 2.5 mmol/l are $\tau_{ex}^{25} = 3300$ s at 25°C, $\tau_{ex}^{15} = 8700$ s at 15°C, and $\tau_{ex}^{5} = 19{,}300$ s at 5°C. Isotope exchange between the cave atmosphere and the DIC of the solution will only have a significant effect on the isotopic composition of the precipitated speleothem calcite if the exchange time, τ_{ex}, is in the range of the precipitation time, τ_{pr}. For a = 0.02 cm, the corresponding values for τ_{pr} are $\tau_{pr}^{25} = 640$ s, $\tau_{pr}^{15} = 1000$ s, and $\tau_{pr}^{5} = 2500$ s (Dreybrodt and Scholz,

2011). For a = 0.01 cm, the values of τ_{pr} are lower by a factor of 2. In all cases, τ_{pr} is lower than the corresponding τ_{ex} by one order of magnitude ($\tau_{pr} / \tau_{ex} \approx 0.1$).

3.3 Experimental Methods

The basic idea of all experiments is to create a thin layer of a carbonate solution (pH = 7-8) with a defined depth, a, and known $\delta^{13}C$ and $\delta^{18}O$ values of the DIC. This film is exposed to an atmosphere containing CO_2 with a specific p_{CO2} and stable isotope values ($\delta^{13}C$ = -43.8 ‰ and $\delta^{18}O$=-30.21 ‰), which are not in isotopic equilibrium with the DIC. In a $CaCO_3$-H_2O-CO_2 solution, progressive precipitation of calcite will increase both the $\delta^{13}C$ and the $\delta^{18}O$ values of the DIC (Dreybrodt, 2008) (Scholz et al., 2009) (Dreybrodt and Scholz, 2011). In order to avoid this effect, we use a solution of $NaHCO_3$ in pure water. After a specific exposure time, the solution is removed from the atmosphere, and the DIC is completely precipitated as $SrCO_3$. Using various exposure times enables us to determine the dependence of the $\delta^{13}C$ and $\delta^{18}O$ values of the DIC on the exposure time, to monitor the temporal evolution of the $\delta^{13}C$ and $\delta^{18}O$ values and, thus, to determine the exchange times, τ_{ex}.

In the first type of experiments we use an atmosphere surrounding the water film with a p_{CO2} higher than the p_{CO2} in equilibrium with the CO_2-concentration in the water. This is not the case in caves where generally the p_{CO2} in the calcite precipitating water film is higher than that of the cave atmosphere. This is simulated in the second type of experiments.

Immediately after the solution is exposed to the atmosphere, equilibration, either by out gassing of CO_2 from the water, as in caves, or by uptake of CO_2 as in the first type of experiments takes place. In any case chemical equilibrium between atmospheric CO_2 and the aqueous CO_2 in the water is established within several ten seconds. Thereafter, to attain chemical equilibrium between HCO_3^- and aqueous CO_2 needs about 100 seconds more (Dreybrodt, 2012) (Dreybrodt, 2011).

After chemical equilibrium between DIC and the CO_2 in the atmosphere has been reached, we have disequilibrium between the isotope composition of the CO_2 in the atmosphere and the DIC, independent of the pathway, how this disequilibrium has been reached. Therefore both types of experiments start with identical initial conditions and are therefore suitable to explore the dynamics of isotope exchange.

3.3.1 Preparation of solutions

Solutions of $NaHCO_3$ in MQ water were prepared by dissolving analytic grade $NaHCO_3$. The stable isotope values of the $NaHCO_3$ are $\delta^{13}C = -5.99$ ‰ and $\delta^{18}O = -9.98$ ‰ vs. VPDB. We used concentrations of $NaHCO_3$ of 5 and 10 mmol/l. The pH of the initial solution was 8.44. After the solution had been exposed to an CO_2 atmosphere ($\delta^{13}C = -45.8$ ‰; $\delta^{18}O = -30.2$ ‰) with a p_{CO2} =500 ppmV, 12,500 ppmV and 25,000 ppmV, respectively, the pH decreased to a final value between 8.4 down to 6.9 for the high p_{CO2} values, reflecting the diffusion of CO_2 into the solution. Thus, the pH values during the experiment are in the range of karst waters. The pCO_2 of the surrounding atmosphere in most experiments, however, is much higher than in cave environments. This is necessary because otherwise the exchange times would become too long for experimental observation. Since the purpose of the experiments is to validate the theory, the deviation from cave environments is not of concern.

3.3.2 Experimental set-up.

In order to establish a thin water film of depth, a, we completely covered the bottom of a sand-blasted borosilicate glass petri dish with a defined volume of $NaHCO_3$-solution. The minimum depth, which could be established, was, a = 0.05 cm. For lower film thickness, the film was not stable and broke into several parts due to surface tension. The petri dish was then put into an exsiccator, which contained water to establish a relative humidity of 100 %. Fig. 3.2 shows a sketch of the experimental set-up. The exsiccator had an inlet for CO_2. The CO_2 concentration was monitored during the experiment using a Vaisala® CO_2-sensor GMP 222 (up to 5000 ppmV) and GMP 221 for the percent-range. Prior to the experiment, the exsiccator was evacuated and flushed with pure N_2 or Ar. Then, the Petri dish containing the thin film of solution was transferred into the open exsiccator by hand. Therefore contamination of the pure gas atmosphere in the exsiccator by CO_2 from the laboratory could not be avoided completely. Then the exsiccator was closed. To provide a desired p_{CO2} a defined volume of CO_2-gas with $\delta^{13}CO_2 = -43.8$ ‰ and $\delta^{18}CO_2 = -30.21$‰ was introduced by a syringe. Pumping the piston several times resulted in a homogenous distribution of CO_2 inside the exsiccator. To establish an even thickness and a horizontal position of the water film, the exsiccator was located on an adjustable tripod. After defined exposure time, the exsiccator was opened and the solution was instantaneously precipitated as $SrCO_3$ (see section 3.3). A photo of the setup is shown in the supplementary information (Supplementary 3.1).

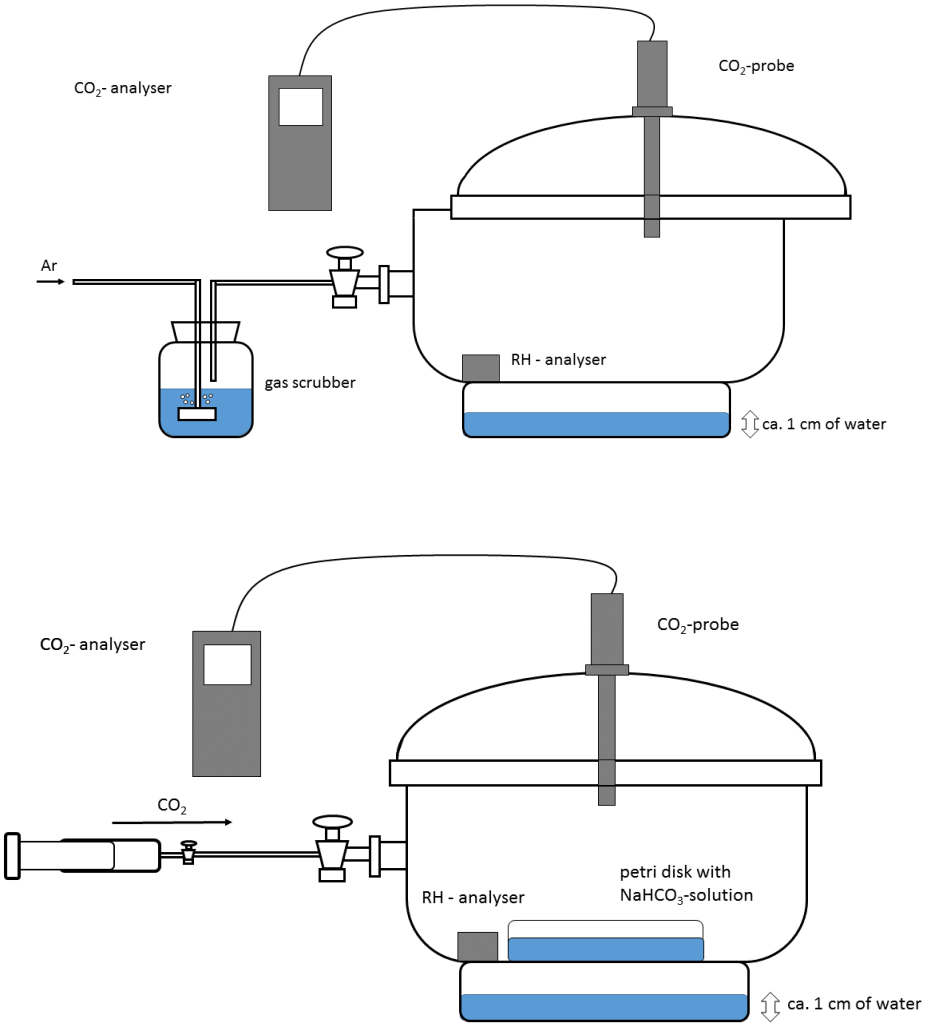

Fig. 3.2: Sketch showing the experimental set up. The upper panel shows the filling of the exsiccator with Ar. The lower panel shows the introduction of CO_2 using a syringe.

In a second type of experiment, we used a large box with a volume of 500 L, which allows adjusting all parameters, such as relative humidity rH, pCO_2, and temperature, to cave-analogue conditions and controlling them during the experiment. The box is equipped with gloves allowing to perform experiments when the box is closed. For film thicknesses between 0.6 mm and 2 mm, we used petri dishes as described for the experiments conducted in the exsiccator. A photo of the box is presented in the supplementary information (Supplementary 3.2).

Prior to each experiment, the box was flushed with N_2 until a minimum pCO_2 value of 50 ppmV had been reached. Subsequently, the water films in the petri dish were established. The pCO_2 in the box was adjusted by introducing a defined amount of CO_2 into the system. This way the pressure in the exsiccator might increased slightly but was equalisated by the syringe we used

to inject the CO_2, corrections for this are not necessary. After different exposure times, t, the solution was transferred into a Luer-Lock® syringe, which was then closed by a Luer-Lock® buckler to avoid degassing or isotope exchange. Finally, the sample was removed from the box through a sewer port for precipitation of the DIC (see section 3.3.3).

In a third type of experiments, we used the box with the same conditions as described above. Instead of the petri dishes, the box contained an inclined, sand-blasted borosilicate glass plate. The $NaHCO_3$-solution was pumped onto the glass plate by a peristaltic pump resulting in a thin film of water with a thickness of about 0.01 cm flowing down the plate in laminar flow as described by Hansen et al. (2013). After different distances of flow and, thus, residence times on the glass plate, the solution was collected, removed from the box, and the DIC was precipitated as $SrCO_3$ (see section 3.3.3). All experiments were performed at 20°C using a pCO_2 of 500 ppmV or 25,000 ppmV.

3.3.3 Precipitation of DIC as $SrCO_3$

For stable isotope analysis, the DIC was precipitated as $SrCO_3$. We use a 50 ml Luer-Lock® syringe with a metal ring and a small hole above the 50 ml mark. The syringe was filled with Ar to avoid contamination with atmospheric CO_2 and then closed with a Luer-Lock® buckler. Subsequently, the solution with DIC was transferred through the hole into the syringe. By adding a solution of 1 N NaOH and 1.5 N $SrCl_2$ into the syringe, the pH of the DIC solution was driven to high values (up to pH ≈ 12) resulting in immediate precipitation of the DIC as $SrCO_3$ (Beck et al., 2005). The hole was then immediately closed by adjusting the piston to avoid isotope exchange with atmospheric CO_2. In order to warrant the homogeneity of the precipitate, the solution was shaked and then filtered through a Merck Millipore polycarbonate filter with a pore size of 0.2 µm. Afterwards, the precipitate was rinsed with methanol until a neutral pH was reached. Subsequently, the filter was transferred into an exsiccator, which was then evacuated in order to dry the precipitate and avoid isotope exchange with atmospheric CO_2. For stable isotope analysis, a small amount (~100 µg) of the precipitate was scratched off the filter using a spatula. From each filter, two samples were analyzed in order to test for the homogeneity of the precipitates.

3.3.4 Stable isotope analysis

Stable isotope analysis of water samples was determined at the University of Innsbruck by equilibration with carbon dioxide using an on-line, continuous-flow system (Gasbench II) linked to a ThermoFisher DELTA^{plus}XL mass spectrometer. Calibration of the mass spectrometer was accomplished using VSMOW, GISP, and SLAP standards. The 1σ analytical error on the $\delta^{18}O$ values is 0.08 ‰.

Stable isotope analysis of $SrCO_3$ samples was performed at the Institute for Geosciences, University of Mainz, Germany, using a Thermo Finnigan MAT 253 continuous flow-isotope ratio mass spectrometer coupled to a GasBench II, as described by Schöne et al., 2005. The sample weights ranged from 27 to 125 µg. The obtained $\delta^{18}O$-values were not corrected for the oxygen-isotope acid fractionation factor of $SrCO_3$ because this is practically identical to that of $CaCO_3$ (Kim et al., 2015). Furthermore using the calcite acid fractionation factor may cause a constant offset from the true values for all samples investigated. Since the interpretation of the data is based on differences of δ values the conclusions remain correct irrespective of the acid fractionation factor employed.

3.3.5 Reproducibility and homogeneity of the precipitation methods

In order to test the precision, reproducibility and homogeneity of our precipitation method, we used a 3 mmol/l calcium carbonate solution, supersaturated with respect to calcite (pH ≈ 8.19). The solution was prepared as described by Hansen et al. (2013) by dissolving $CaCO_3$ in pure MQ-water by sparging with CO_2. After the $CaCO_3$ was completely dissolved and the solution was clear, it was stored for four days at pH ≈ 6.5 to establish isotope equilibrium between the dissolved carbon species. Subsequently, the solution was degassed of CO_2 by sparging with pure Ar gas, and the pH value was monitored until supersaturation was reached at (pH ≈ 8.19) after several minutes. This way a solution of DIC, consisting by 95% of HCO_3^-, with defined isotope composition was obtained. The isotope composition of this solution turned out to be stable for more than 1hour.

Five aliquots of the solution with volume of 5 ml each were sampled immediately and precipitated as $SrCO_3$ as described in section 3.3.3. Subsequently, we scratched off samples from each filter for stable isotope analysis. One filter was emptied completely resulting in 14 sub-samples. From the other four filters, two sub-samples were analysed.

The data for the completely sampled filter show an average $\delta^{13}C$ value of -31.8 ‰ with a standard deviation of 0.13 ‰. The average $\delta^{18}O$ value is -8.8 ± 0.07 ‰ (1σ sd). Thus, the

precipitate is distributed homogeneously on the filters. The four other precipitates show an average $\delta^{13}C$ value of -31.78 $\pm$ 0.25 ‰ and a mean $\delta^{18}O$ value of -8.91 $\pm$ 0.11 ‰. Averaging all measurements results in $\delta^{13}C$ = -31.78 $\pm$ 0.22 ‰ and $\delta^{18}O$ = -8.88 $\pm$ 0.12 ‰. The reproducibility of our precipitation method is, thus, 0.1‰ and 0.25‰ for $\delta^{18}O$ and $\delta^{13}C$, respectively. All isotope values of the reproducibility experiment are given in Table 3.2.

To test whether the δ-values of the solution samples may be affected during storage in air-tight, closed Luer-Lock® syringes, five samples from a $CaCO_3$ solution were taken in syringes, stored in the climate box at 20°C and a pCO_2 of 1000 ppmV, and precipitated as $SrCO_3$ after 15, 30, 45 and 60 min, respectively. The results show that the isotope signal is stable over 60 min. At t=0, the $\delta^{13}C$ value is –33.0 $\pm$ 0.1 ‰, and the $\delta^{18}O$ value is –8.6 $\pm$ 0.03 ‰. After 60 min, we observed a $\delta^{13}C$ value of -32.6 $\pm$ 0.1 ‰ and a $\delta^{18}O$ value of -8.82 $\pm$ 0.02 ‰. The mean values of all measurements are $\delta^{13}C$ = - 32.5 $\pm$ 0.6 ‰ and $\delta^{18}O$ = -8.7 $\pm$ 0.1 ‰. In summary, the storage in the Luer-Lock® syringes only introduces small errors and consequently allows storing the solution without degassing of CO_2 or further exchange with the box-atmosphere until precipitation. The results of the stable isotope measurements are given in Table 3.3.

3.4 Experimental Results

Fig. 3.3 illustrates the time dependence of $\delta^{13}C$ value for the experiments in the ecsiccator. The experimental parameters are provided in the corresponding panels. All experiments were performed at a temperature of 20 $\pm$ 1°C. At the beginning of the experiments, the $\delta^{13}C$ value of the DIC was close to the $\delta^{13}C$ value of the solid $NaHCO_3$ (-6 ‰). This is reasonable since these samples were only very shortly exposed to the CO_2 atmosphere. Nevertheless, the corresponding $\delta^{13}C$ values were slightly lower by about 1 ‰ than those of the $NaHCO_3$ reflecting the effect of carbon isotope exchange with the CO_2, which has a substantially more negative $\delta^{13}C$ value (-43.8 ‰). Due to progressive isotope exchange with the CO_2, the $\delta^{13}C$ value of the DIC dropped exponentially to a final value, which remained constant for over up to 3000 min, the longest exposure time used in our experiments. Fig. 3.4 depicts the temporal evolution of the $\delta^{18}O$ values of the DIC for the experiments shown in Fig. 3.3. Similar as for the evolution of the $\delta^{13}C$ values, the $\delta^{18}O$ values first decrease as $\delta^{13}C$. Then, however, after a minimum $\delta^{18}O$ value has been reached, the $\delta^{18}O$ values slowly increase.

3.5 Discussion

3.5.1 Carbon isotope exchange

We fitted all experimental data according to

$$\delta^{13}C_{DIC}(t) = (\delta^{13}C^{0}_{DIC} - \delta^{13}C^{eq}_{DIC})\exp(-t/\tau_{ex}) + \delta^{13}C^{eq}_{DIC}, \qquad (3.18)$$

which allows to determine the exchange times, τ_{ex}. The values obtained for the different experimental parameters are given in the corresponding figures (Figs. 3.3a-d) and in Table 2.1. To compare the experimental exchange times with the theoretically predicted values, we used the relation $\tau^{ex}_{red} = \tau_{ex} \cdot K_H \cdot p^{cave}_{CO2} / [HCO_3^-]$ to obtain the reduced exchange times, τ^{ex}_{red}, from the experimentally obtained exchange times τ_{ex}. Fig. 3.5 shows the theoretically predicted value of τ^{ex}_{red} as a function of the film thickness, a, for a temperature of 20°C. The experiment conducted using a flowing water film of 0.013 cm depth agrees well with the theoretical predictions. The experimental data are generally in satisfactorily agreement with the theoretically predicted values if we assume an experimental uncertainty of ca. 20 % resulting from errors in p_{CO2}, temperature, and film thickness. This shows that our theory represents a reliable prediction of the exchange times.

When isotope exchange is completed, isotopic equilibrium between the different dissolved carbon species is established. In order to calculate the $\delta^{13}C$ value of the DIC in equilibrium, a mass balance is required. We used PHREEQC (Parkhurst and Apello, 1999) to calculate the species distribution in the exposed solution for each experiment. For carbon isotopes, two sources of carbon exist in the system, $NaHCO_3$ and CO_2. The biggest reservoir for carbon isotopes in the system (for both the experiments conducted in the exsiccator and the climate box) is the (gaseous) CO_2 (>99.9%). Thus the system converges to isotope equilibrium with gaseous CO_2. When the solution is exposed to the CO_2 atmosphere, the pH-value of the $NaHCO_3$ drops from ≈ 8.2 to ≈ 7.0 resulting in a change of the species distribution. For 5 mmol/l $NaHCO_3$, 20°C and a p_{CO2} of 25,000 ppmV, the distribution of carbon species, calculated using PHREEQC, is 83.2 % for the bicarbonate (HCO_3^-) and 16.8 % for aqueous CO_2. Using the $\delta^{13}C$ values of the original substances and the corresponding fractionation factors, one can calculate the expected isotope compositions for the equilibrium.

For carbon isotopes, we have the following reservoirs in the system: gaseous CO_2, aqueous CO_2 and dissolved bicarbonate. At the pH of our experiments CO_3^{2-} can be neglected. The mass balance then is:

$$\delta^{13}C_{(DIC,eq)} = X_{CO2aq}\cdot\delta^{13}C_{CO2aq(eq)} + X_{HCO3^-}\cdot\delta^{13}C_{HCO3^-(eq)} = X_{CO2aq}\cdot(\delta^{13}C_{CO2g} - \varepsilon_{CO2g/CO2aq}) + X_{HCO3^-} \cdot(\delta^{13}C_{CO2g} - \varepsilon_{HCO3^-/CO2g}), \quad (3.19)$$

where X_{CO2aq} is the molar fraction of the dissolved CO_2 in the water film, X_{HCO3^-} is the molar fraction of the dissolved bicarbonate, and the ε_i's are the corresponding fractionation factors between gaseous CO_2 and the dissolved carbon species. With the initial isotope value for the gaseous CO_2 (-46.77 $\pm$ 0.43 ‰), $\varepsilon_{CO2g/CO2aq}$ = - 1.08 ‰ (Vogel et al., 1970) and $\varepsilon_{HCO3^-/CO2g}$ = - 8.46 ‰ (Mook et al., 1974), the expected equilibrium value is -38.66 ‰.

The experiments conducted in the exsiccator show an offset of ca. 5 ‰ between the experimental and the expected equilibrium values. This might be due to a systematic experimental error occurring when the petri dish is taken out of the open exsiccator by hand. After chemical equilibration, the solution is in equilibrium with a high p_{CO2} (25,000 and 12,500 ppmV, respectively), whereas the p_{CO2} of the laboratory atmosphere is substantially lower (800 ppmV). Thus, CO_2 will rapidly degas from the solution when the petri dish is removed from the exsiccator and transferred into the syringe for precipitation as $SrCO_3$. For thin films of water, degassing of CO_2 occurs within seconds (Hansen et al., 2013). Consequently, although this experimental step only takes a few seconds, degassing of CO_2 will occur affecting the content of CO_2 in the solution and, thus, the $\delta^{13}C$ value of the DIC. In our second setup (i.e., the climate box), both degassing of CO_2 and contamination from the laboratory atmosphere can be avoided. This is confirmed by the experimentally determined $\delta^{13}C$ values, which are in satisfactory agreement with the expected equilibrium values within $\pm$ 1‰. It should be stressed, however, that the aim of our experiments is to determine exchange times by measuring differences of δ-values. Therefore these deviations are not of concern.

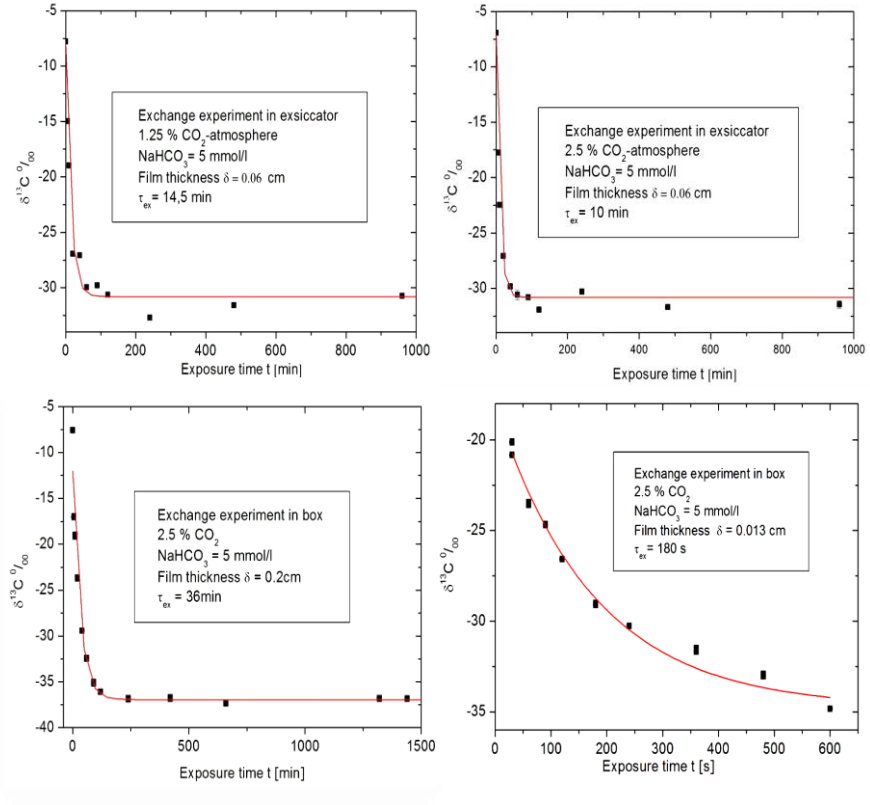

Fig.3.3: Temporal evolution of the $\delta^{13}C$ values (VPDB) of the DIC after exposing the solution to a CO_2 atmosphere. The concentration of [$NaHCO_3$] was 5 mmol/l for all experiments. The red lines show fits to the data using the program Origin in order to estimate the exchange time, τ_{ex} (see text for details).

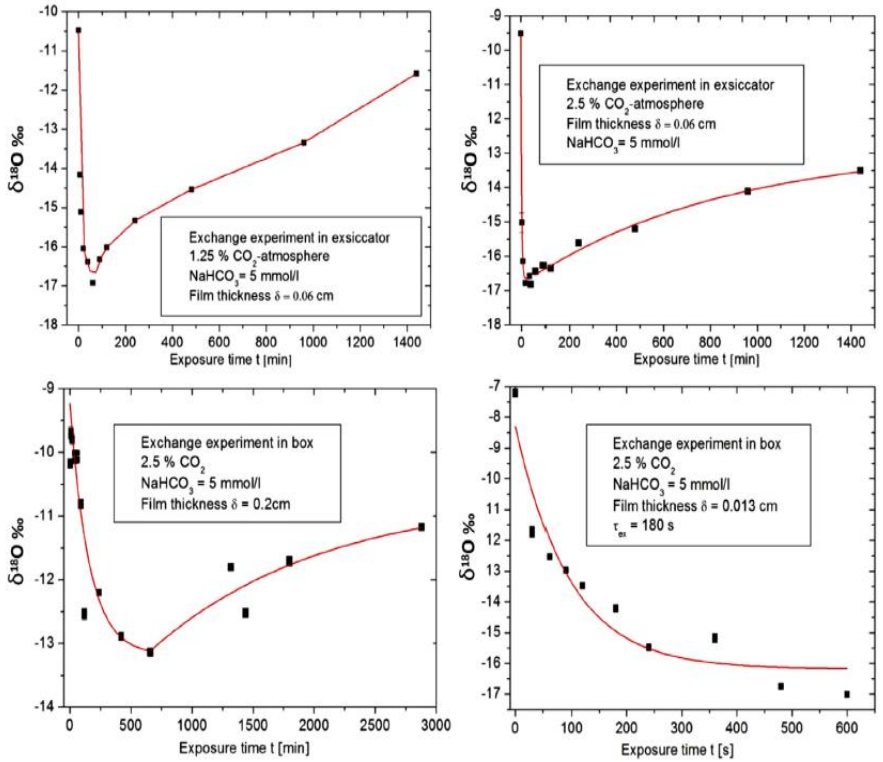

Fig. 3.4. Temporal evolution of the $\delta^{18}O$ (VPDB) values of the DIC after exposing the solution to a CO_2 atmosphere. Conditions are as in Fig. 3.3.

3.5.2 Oxygen isotope exchange

Oxygen isotope exchange between atmospheric CO_2 and the DIC in the water film is more complex due to exchange with a third large oxygen reservoir (i.e., H_2O). In this case, the temporal evolution of the concentration C of ^{18}O in the DIC in the film can be described by

$$\frac{dC}{dt} = -(C - C_{cave})/\tau_{cave} - (C - C_{eq})/\tau_{water}. \qquad (3.20)$$

The first term describes oxygen isotope exchange with the cave atmosphere (i.e., between CO_2 and DIC). Consequently, $\tau_{cave} = \tau_{ex}$. The second term describes oxygen isotope exchange with the water (i.e., between H_2O and DIC) with the exchange time $\tau_{water} = \tau_{eq}^{H2O}$. C_{cave} denotes the concentration of ^{18}O in DIC in equilibrium with the CO_2 of the atmosphere, and C_{eq} is the concentration of ^{18}O in isotope equilibrium with the water. In our experiments the CO_2 in the atmosphere is not in isotope equilibrium with the water. For an infinite reservoir of water and CO_2 inside the cave, C_{cave} and C_{eq} can be regarded as constant in time.

The solution of this differential equation is

$$C(t) = (C_0 - C_{eff})\exp(-t/\tau) + C_{eff};\ C_{eff} = \frac{C_{cave}\cdot\tau_{water} + C_{eq}\cdot\tau_{cave}}{\tau_{cave} + \tau_{water}};\quad \tau = \frac{\tau_{cave}\cdot\tau_{water}}{\tau_{cave} + \tau_{water}} \qquad (3.21)$$

This describes an exponential decay from initial concentration C_0 to a steady-state concentration, $C_\infty = C_{eff}$, which is established when the rate $(C - C_{cave})/\tau_{cave}$ of addition of ^{18}O to the DIC due to oxygen isotope exchange with the cave CO_2 is equal to the rate $(C - C_{eq})/\tau_{water}$ of withdrawal of ^{18}O from the DIC by oxygen isotope exchange with the water. In this case, $dC/dt = 0$, and a steady-state is established. Note that this relation is only valid if both reservoirs (i.e., CO_2 and H_2O) can be regarded as infinite in comparison to the DIC, which is a reasonable assumption for cave systems. In this process, isotopic equilibrium of DIC with respect to water and the CO_2 of the atmosphere is not attained. There is only a net flux of the heavy isotope from the CO_2 in the cave to the water in the film. Since these two reservoirs are regarded as infinitely large, the concentrations C_{cave} and C_{eq} remain constant. If, however, the reservoir of CO_2 in the air is finite, as in our experiments, this net flux of the heavy oxygen reduces its concentration in the surrounding atmosphere and oxygen isotope equilibrium between the DIC of the water film and CO_2 in the atmosphere is established. Since the water reservoir of oxygen is much larger isotope exchange continues until the final concentration of ^{18}O in the DIC is reached when isotopic equilibrium between all three reservoirs has been established.

Table 3.1: Experimental and theoretical exchange times for all experiments.

Experiment	film thickness a [cm]	[$NaHCO_3$] mmol/l	p_{CO2} [%]	τ^{ex} experimental [s]	τ^{ex} theoretical [s]	τ_{red}^{ex} experimental [s]	τ_{red}^{ex} theoretical [s]	$\delta^{13}C$ DIC t = 0 [‰]	$\delta^{13}C$ DIC final [‰]	Δ [‰]
1	0.06	5	2.5	570±60	582	97	99	-6.53	-30.7	24.2
2	0.06	10	2.5	1110±90	1164	94	99	-7.47	-31.9	24.4
3	0.06	5	1.25	900±90	1164	77	99	-7.69	-31.2	23.5
4	0.089	5	2.5	590±90	845	117	144	-7.53	-32.5	25
5	0.013	5	2.5	180±30	278	31	47	-7.1	-34.8	27.7
6	0.013	5	0.05	7000±1000	10200	40	47	-7.8	-38.3	30.5
7	0.06	5	2.5	636±60	582	108	99	-6.71	-37.3	29.7
8	0.2	5	2.5	2160±120	1893	367	322	-7.57	-37.7	32.5

Table 3.3: Luer-Lock®-Test.

Time t [min]	$\delta^{13}C$	±	$\delta^{18}O$	±
0	-33.00	0.0682	-8.60	0.0307
15	-31.76	0.0318	-8.74	0.0281
30	-33.01	0.0990	-8.60	0.0175
45	-32.01	0.2598	-8.82	0.0099
60	-32,64	0.1326	-8.82	0.0160
Average value	-32.48	0.5747	-8.72	0.1128

Table 3.2: Reproducibility of the precipitation method.

Sample	$\delta^{13}C$[‰]	±	$\delta^{18}O$[‰]	±
Filter 1 complete 1	-31.67	0.027	-8.68	0.052
Filter 1 complete 2	-31.95	0.020	-8.73	0.028
Filter 1 complete 3	-31.96	0.021	-8.75	0.048
Filter 1 complete 4	-31.89	0.032	-8.77	0.029
Filter 1 complete 5	-31.72	0.026	-8.67	0.042
Filter 1 complete 6	-31.86	0.020	-8.88	0.036
Filter 1 complete 7	-31.96	0.025	-8.70	0.034
Filter 1 complete 8	-31.70	0.021	-8.80	0.032
Filter 1 complete 9	-31.91	0.023	-8.86	0.035
Filter 1 complete 10	-31.83	0.019	-8,89	0.034
Filter 1 complete 11	-31.57	0.019	-8.76	0.029
Filter 1 complete 12	-31.57	0.011	-8.74	0.039
Filter 1 complete 13	-31.81	0.018	-8.72	0.059
Filter 1 complete 14	-31.78	0.018	-8.79	0.041
Filter 2-1	-31.70	0.022	-8.90	0.028
Filter 2-2	-31.57	0.017	-8.92	0.027
Filter 3-1	-32.02	0.022	-8.78	0.029
Filter 3-2	-31.82	0.022	-8.85	0.040
Filter 4-1	-31.47	0.014	-9.09	0.027
Filter 4-2	-31.54	0.031	-9.06	0.073
Filter 5-1	-31.99	0.018	-8.84	0.042
Filter 5-2	-32.12	0.028	-8.88	0.036

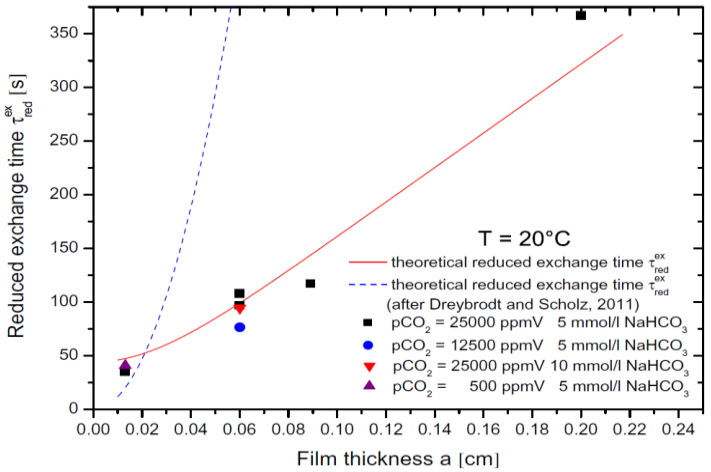

Fig. 3.5: Comparison of the theoretically derived reduced exchange times for ^{13}C, $\tau_{red}^{ex} = \tau_{ex} \cdot (K_H \cdot p_{CO_2}^{cave}) / [HCO_3^-]$, (full line) with the experimental results. Different plot symbols represent different experimental conditions. Black squares represent the experiments conducted with $[NaHCO_3] = 5$ mmol/l and $pCO_2 = 25{,}000$ ppmV. Circles depict $[NaHCO_3] = 5$ mmml/l and $pCO_2 = 12{,}500$ ppmV. The triangle at 0.06 cm shows the experiment with $[NaHCO_3] = 10$ mmml/l and $pCO_2 = 25{,}000$ ppmV. The upright triangle at $a = 0.013$ cm represents the experiment with the flowing water film with $[NaHCO_3] = 5$ mmol/l and $pCO_2 = 500$ ppmV. Also shown is the incorrect reduced exchange time (dotted line) derived by Dreybrodt and Scholz (2011), which deviates substantially for film depths $a > 0.03$ cm.

Fig. 3.4 depicts the temporal evolution of the $\delta^{18}O$ values of the DIC for the experiments shown in Fig. 3.3. Similar as for the evolution of the $\delta^{13}C$ values, the $\delta^{18}O$ values first decrease as $\delta^{13}C$. Then, however, after a minimum $\delta^{18}O$ value has been reached, the $\delta^{18}O$ values slowly increase. A constant $\delta^{18}O$ value, as observed for the $\delta^{13}C$ values, was not reached in our experiments suggesting that oxygen isotope equilibrium with the water had not been established yet. Considering the long isotope exchange times between HCO_3^- and water (Beck et al., 2005) as well as CO_2 and water of several ten hours (Affek, 2013; Hofmann et al., 2012), this is not surprising. This process, occurring on the time scale of hours to days, is not relevant for speleothem stable isotope signals in cave systems. However, the initial negative isotope shift occurring with the exchange time τ may imprint isotope signals in the DIC.

Calculating the expected equilibrium oxygen isotope values is more complex than for the carbon isotopes. Oxygen isotope exchange is based on three reservoirs: HCO_3^-, CO_2 and H_2O. As outlined in section 3.4.2, the distribution of the dissolved carbon species, calculated using PHREEQC, is 83.2 % HCO_3^- and 16.8 % aqueous CO_2. During precipitation as $SrCO_3$, the dissolved CO_2 is also precipitated. Due to mass balance, an additional oxygen atom is required, which comes from the OH^- of the solution (Beck et al., 2005; Usdowski et al., 1991) by the reaction $Sr^{2+} + OH^- + CO_2 \rightarrow SrCO_3 + H^+$.

For the experiments conducted in the box ($p_{CO2} = 25{,}000$ ppmV, [NaHCO3] = 5 mmol/l, and a = 0.06 cm), the largest oxygen reservoir is the CO_2 in the atmosphere. In this case, 93.64 % of the O-atoms are provided by the CO_2, and only 6.36 % come from the water. In the exsiccator, the largest reservoir for oxygen isotopes is the water with 72.8 %, whereas the CO_2 only provides 27.2 %. In both setups, the fraction of HCO_3^- provided by the $NaHCO_3$ is negligible. Note that we used the same water for the preparation of the solutions to establish a high relative humidity inside the box and the exsiccator, respectively. For the calculation of the $\delta^{18}O$ value of the DIC in equilibrium with water we neglect CO_3^{2-} at the pH of our experiments. The mass balance reads:

$$\delta^{18}O_{DIC,eq} = X_{CO2}\cdot(2/3\delta^{18}O_{CO2} + 1/3\delta^{18}O_{OH-}) + X_{HCO3-}\cdot\delta^{18}O_{HCO3-} \quad (3.22)$$

$$= X_{CO2}\cdot(2/3[\delta^{18}O_{H2O} + {}^{18}\varepsilon_{CO2/H2O}] + 1/3[\delta^{18}O_{H2O} + {}^{18}\varepsilon_{OH-/H2O}]) + x_{HCO3-}[\delta^{18}O_{H2O} + {}^{18}\varepsilon_{HCO3-/H2O}]$$

where X_{CO2} is the molar fraction of the dissolved CO_2 in the water film, X_{HCO3-} the molar fraction of the bicarbonate and the $\varepsilon_{HCO3-/H2O}$ are the corresponding fractionation factors between water and the different dissolved carbon species.

For the experiment with 5 mmol/l $NaHCO_3$, 20°C, and a pCO_2 of 25,000 ppmV in the climate box, with a $\delta^{18}O$ value of the water of -38.41 ± 0.1 ‰, ${}^{18}\varepsilon_{CO2g/H2O} = +42.31$ ‰, ${}^{18}\varepsilon_{HCO3-/H2O} = +32.55$ ‰ (Beck et al., 2005) and ${}^{18}\varepsilon_{OH-/H2O} = +34$ ‰ (Green and Taube, 1963;

Thornton, 1962), the expected equilibrium $\delta^{18}O$ value is -8.44 ‰. The experimental values range between -11.5 to -12.5 ‰ (Fig. 3.4). In both setups, we were not able to observe establishment of isotopic equilibrium. Thus, the equilibration process seems to be still in progress and obviously occurs on longer time scales as used for our experiments.

For natural caves, it is generally assumed that the CO_2 of the cave atmosphere is in oxygen isotope equilibrium with drip water. If this is true, oxygen isotope exchange does not affect the $\delta^{18}O$ values of speleothem calcite.

3.5.3 Exchange times for cave conditions

In our experiments, we have so far used CO_2 concentrations in the order of 10,000 ppmV, which are much higher than those in caves. The results motivated us to investigate the effects of stable isotope exchange for almost natural conditions. We used a thin film of a 5 mmol/L $NaHCO_3$ solution with a depth, a, of 0.013 cm flowing down a glass plate of 120 cm length, as described for the experiment above. To simulate real cave conditions, however, we exposed the solution to an atmosphere with a pCO_2 of 500 ppmV. For $T = 20°C$, this corresponds to a ratio of $\frac{[HCO_3^-]_{sol}}{[K_H \cdot p_{CO_{2\,cave}}]} = 256$.

Fig. 3.6 shows the temporal evolution of the $\delta^{13}C$ and $\delta^{18}O$ values as a function of flow or exposure time (i.e., the time the solution was exposed to the CO_2 atmosphere before it was collected). Since the exchange time, τ_{ex}, is much larger than the exposure time, the exponential Eq. (3.15) can be expanded to $\delta_{DIC}(t) = \delta_{DIC}(0) - (\delta_{DIC}(0) - \delta_{DIC}(eq))\frac{t}{\tau_{ex}}$ by using $\exp(-x) = 1 - x$.

τ_{ex} is then given by:

$$\tau_{ex} = \frac{\delta_{DIC}(eq) - \delta_{DIC}(0)}{\delta_{DIC}(t) - \delta_{DIC}(0)} t, \qquad (3.23)$$

where $\delta_{DIC}(eq) = \delta_{HCO_3}(eq) = \delta_{CO_2^{gas}} - \varepsilon_{CO_2^{gas}/HCO_3}$ is the $\delta^{13}C$ value in isotopic equilibrium and $\delta_{DIC}(0)$ is the initial $\delta^{13}C$ value. This equation is also valid for the oxygen isotope exchange because for such short exchange times, oxygen isotope exchange with the water can be neglected.

For $\delta^{13}C_{DIC}$ we find:

$$\delta^{13}C_{DIC}(t) = -7.83 - 0.0044 \cdot t, \qquad (3.24)$$

and for $\delta^{18}O_{DIC}$

$$\delta^{18}O_{DIC}(t) = -7.7 - 0.0018 \cdot t. \qquad (3.25)$$

The corresponding linear fits are shown as red lines in Fig. 3.6. The $\delta^{13}C$ value of the CO_2 used in this experiment was -46.8‰ and the $\delta^{18}O$ value was -30.21 ‰. For $t = 600$ s, $\delta^{13}C_{DIC}(600) - \delta^{13}C_{DIC}(0) = -2.7‰$, and $\delta^{18}O_{DIC}(600) - \delta^{18}O_{DIC}(0) = -1.1‰$, as derived from the corresponding fits. With $^{13}\varepsilon_{CO_2^{gas}/H^{13}CO_3} = -8.46‰$ (Mook et al., 1974), one gets $\delta^{13}C_{HCO_3}(\infty) = \delta^{13}C_{CO_2^{gas}} - \varepsilon_{^{13}CO_2^{gas}/H^{13}CO_3} = -38.34‰$. Using Eq. (3.22), one can obtain the corresponding exchange time, τ_{ex}, of 6780 s for carbon.

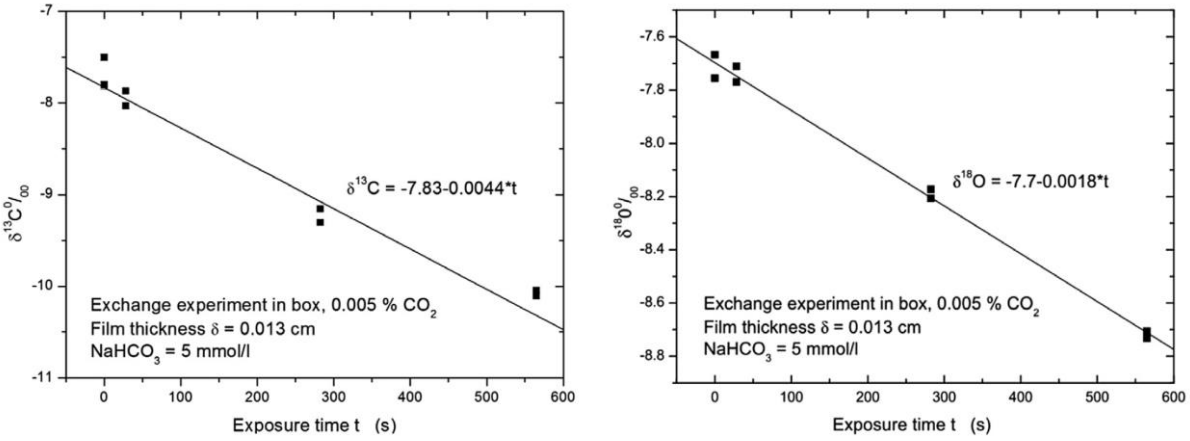

Fig. 3.6. Evolution of $\delta^{13}C$ (VPDB) and $\delta^{18}O$ (VPDB) after exposing the flowing water film with $[NaHCO_3] = 5$ mmol/l to a cave like CO_2 atmosphere with $pCO_2 = 500$ ppmV.

For the oxygen isotope exchange between CO_2 and DIC one has to consider also the exchange with the oxygen of water. From eqn. 3.21 we know, what is happening if the CO_2 and the water reservoir are infinitely large in contrast to our experimental conditions. Nevertheless we can assume that the initial evolutions of isotope composition for times $t << \tau_{ex}$ are very similar and therefore we estimate τ_{ex} from eqn. 3.21. From this one gets $\delta_{DIC}(\infty)$ to obtain.

$$\tau_{ex}^{18} = \frac{(\delta_{DIC}(\infty) - \delta_{DIC}(0))}{(\delta_{DIC}(t) - \delta_{DIC}(0))} \cdot t \qquad (3.26)$$

Since the δ-values are proportional to the concentrations of the rare isotope we get from eqn. 3.21

$$\delta_{DIC}(\infty) - \delta_{DIC}(0) = \frac{\delta_{cave} \cdot \tau_{water} + \delta_{eq} \cdot \tau_{cave}}{\tau_{cave} + \tau_{water}}, \qquad (3.27)$$

where δ_{cave} is the isotope composition of DIC in equilibrium with the CO_2 in the cave atmosphere and δ_{eq} is that of DIC in equilibrium with water. With ${}^{18}\varepsilon_{CO_2^{gas}/H^{18}CO_3} = +10.1‰$ one gets δ_{cave}= -40.31‰ and with ${}^{18}\varepsilon_{H_2O/H^{18}CO_3} = +32.5‰$ we have δ_{eq} = -5.91‰. Inserting into eqn. 3.27 and using $\tau_{water} = 10600$ s (Dreybrodt and Scholz, 2011) and τ_{cave}= 6780 s as derived for ^{13}C we find $\delta_{DIC}(\infty) - \delta_{DIC}(0)$ = -26.66‰. With this value we obtain $\tau^{18} = \tau^{18}_{ex} = 4110$ s from eqn. 3.26.

Note that τ^{18}_{ex} is the measured exchange time resulting from two mechanisms, exchange with the cave atmosphere and exchange with water in contrast to the measured exchange time of ^{13}C, which results from exchange with the cave atmosphere solely.

The time τ_{cave} in eqn. 3.21 is the exchange time which would result for oxygen, if τ_{water} were infinite or in other words exchange with water were absent. Therefore from eqn. 3.21:

$$\tau^{18}_{ex} = \frac{\tau_{cave} \cdot \tau_{water}}{\tau_{cave} + \tau_{water}} \qquad (3.21)$$

one calculates τ_{cave} = 6500 s for oxygen which compares well with the value for carbon exchange of 6780 s.

With the reduced exchange times, $\tau^{ex}_{red} = 40$ s, interpolated from the data shown in Fig. 3.1 and using K_H = 0.039 mol/atm, the theoretical prediction is $\tau^{theory}_{ex} = 10200$ s.

The experimental data are restricted by large errors in the value of $\delta DIC(t) - \delta DIC(0)$, which is a difference of large numbers. However, they are in the same range as the theoretically predicted values. Based on the reproducibility of our precipitation method (compare section 3.4.1), the error in the δ values is ±0.3‰. For $\delta DIC(t) - \delta DIC(0)$, this causes an error of ±0.4‰. τ^{13}_{ex} is then between 6000 and 8000 s and τ^{18}_{ex} is between 4000 s and 6000 s for 5 mmol/L $NaHCO_3$. For drip waters with typically 2.5 mmol/L of $CaCO_3$ τ^{13}_{ex} is 7000 s at a pCO_2 of 500 ppmV and 3500 s at a pCO_2 of 1000 ppmV.

3.5.4 Isotope exchange under cave analogue conditions of speleothem growth.

Speleothem growth is determined by the drip time T_{drip}, the cave temperature, the p_{CO2}^{cave} in the cave atmosphere, the DIC concentration $[HCO_3^-]_{sol}$ in the drip water, and the depth, a, of the water film. From these the exchange time can be calculated using eqn. 3.18.

Isotope exchange between the cave atmosphere and the DIC of the solution will only affect the isotopic composition of the calcite precipitated to the speleothem during its deposition.

Calcite deposition rates R are given by $R = \alpha(\tilde{C} - \tilde{C}_{eq})$,where $\tilde{C}$ is the actual calcium concentration, $\tilde{C}_{eq}$ the equilibrium concentration with respect to cave p_{CO2} , and α is a temperature dependent kinetic constant, $\alpha = (0.52 + 0.04 \cdot T + 0.004 \cdot T^2) \cdot 10^{-5}$. T is the temperature in °C , (Baker et al., 1998; Dreybrodt, 2012; Romanov et al., 2008a).

After the drop has impinged the surface of the stalagmite the deposition rates decrease exponentially by $R(t) = \alpha(\tilde{C}_i - \tilde{C}_{eq})\exp(-t/\tau_{pr})$ where $\tilde{C}_i$ is the initial concentration and the precipitation time is given by $\tau_{pr} = a/\alpha$. After the time $t = 3\tau_{pr}$ precipitation is practically completed. For, $a = 0.01$ cm, the corresponding values for τ_{pr} are $\tau_{pr}^{25} = 320\,s$, $\tau_{pr}^{15} = 500\,s$, and $\tau_{pr}^{5} = 1250\ s$ (Dreybrodt and Scholz, 2011). For, $a = 0.02$ cm, the values of τ_{pr} are higher by a factor of 2.

To estimate the impact of isotope exchange we assume a stagnant film model, (Romanov et al., 2008a), where the water film resides on the surface of the stalagmite until it is replaced by a new drop. When the new drop hits the water film some part of the water is lost from it by splashing (Curl, 1973; Mühlinghaus et al., 2007). If one assumes that after the splash the water of the new drop mixes with the solution of the water film one can introduce a mixing factor, Φ, such that the new mixed calcium excess concentration in the water film is given by

$(\tilde{C}_{new} - \tilde{C}_{eq}) = (\tilde{C}_{drop} - \tilde{C}_{eq}) \cdot \Phi + (\tilde{C}_{film} - \tilde{C}_{eq}) \cdot (1 - \Phi)$, equivalent to $\tilde{C}_{new} = \tilde{C}_{drop} \cdot \Phi + \tilde{C}_{film} \cdot (1 - \Phi)$.

If $\Phi = 1$, the drop replaces the water film completely. The calcium excess concentration of the existing solution layer decreases during the last drip interval to $(\tilde{C}_{film} - \tilde{C}_{eq})\exp(-T_{drip}/\tau_{pr})$. This solution mixes with the drip water. The result is

$(\tilde{C}^1_{new} - \tilde{C}_{eq}) = (\tilde{C}_{drop} - C_{eq}) \cdot \Phi + (\tilde{C}_{film} - \tilde{C}_{eq}) \cdot \exp(-T_{drip}/\tau_{pr}) \cdot (1 - \Phi)$. Repeating this mixing process (Mühlinghaus et al., 2007) after n drops the excess concentration immediately after each new drop is given by

$$\tilde{C}^{n}_{new} - \tilde{C}_{eq} = \lambda^{Ca}_{n} \cdot (\tilde{C}_{drop} - \tilde{C}_{eq}) \tag{3.28}$$

with

$$\lambda^{ca}_{n} = \left[(1-\Phi)\cdot \exp(-T_{drip}/\tau_{pr})\right]^{n} + \Phi \cdot \left[1 + \sum_{k=1}^{n-1}\left[(1-\Phi)\cdot \exp(-T_{drip}/\tau_{pr})\right]^{k}\right] \tag{3.29}$$

This geometric series converges rapidly (after n<100 iterations) to the impact factor

$$\lambda^{ca} = \frac{\Phi}{1-(1-\Phi)\exp(-T_{drip}/\tau_{pr})}. \tag{3.30}$$

The same arguments hold for isotope excess of ^{13}C, $\Delta = \delta^{13}HCO^{-}_{3\,i} - \delta^{13}HCO^{-}_{3\,f}$ = (δCO_2^{cave}-$\delta CO_2^{film} + \varepsilon_{CO2_{gas}/CO\,2_{liq}}$).

With

$(\delta^{1}_{new} - \delta_{eq}) = (\delta_{drop} - \delta_{eq})\cdot\Phi + (\delta_{film} - \delta_{eq})\cdot F_{ex}(t)\cdot(1-\Phi)$, where $F_{ex}(t)$ is the function describing the time dependence one finds by the same arguments $\Delta^{iso} = \lambda^{iso}\cdot\Delta$ with isotope impact factor

$$\lambda^{iso} = \frac{\Phi}{1-(1-\Phi)\cdot F_{ex}(t)} \tag{3.31}$$

Values of the isotope impact factor λ^{iso} are shown in Fig. 3.7 for various values of $F_{ex}(T_{drip})$.

From Δ^{iso} the isotope composition of the DIC in the water film immediately after a drop has fallen, is found by

$$\delta(T_{drip}) = \lambda^{iso}\cdot(\delta^{13}HCO^{-}_{3\,i} - \delta^{13}HCO^{-}_{3\,f}) + \delta^{13}HCO^{-}_{3\,f} \tag{3.32}$$

If $\Phi = 1, \lambda = 1$ and the water film is replaced completely by the drop. In this case isotope exchange has no effect on the δ-value of the DIC and consequently on the calcite precipitated. For $\Phi < 1, \lambda < 1$ and isotope exchange shifts the value of $\delta(T_{drip})$ closer to $\delta^{13}HCO^{-}_{3\,f}$. With decreasing Φ the impact of isotope exchange increases until at $\Phi = 0$, $\delta(T_{drip}) = \delta^{13}HCO^{-}_{3\,f}$.

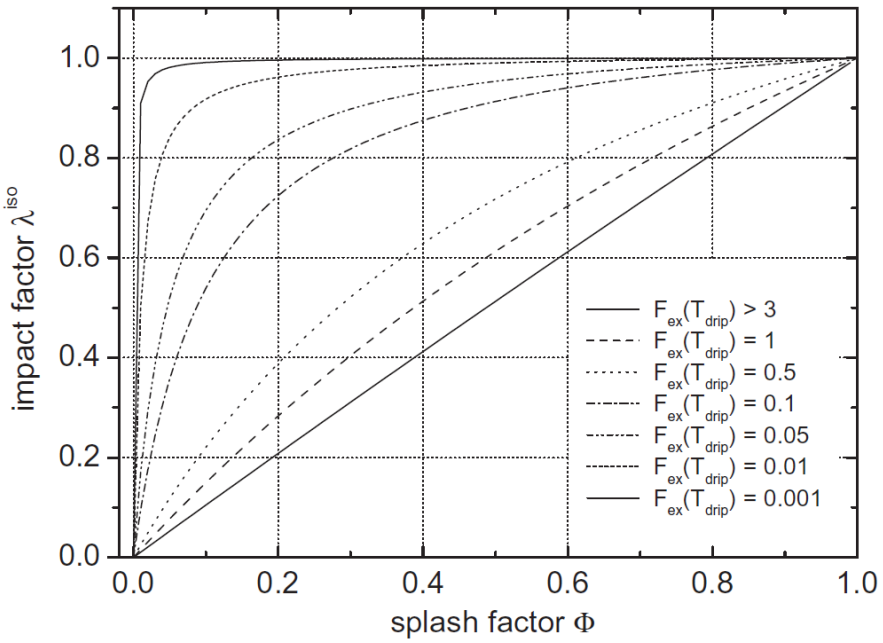

Fig. 3.7. Isotope impact factor λ_{iso} as function of splash factor ϕ for various values $F_{ex}(T_{drip})$.

With this information we can now estimate the impact of isotope exchange to the calcite deposited onto the speleothem.

The isotope shift in the calcite precipitated is found by

$$\Delta_{Ca}(T_{drip}) = \frac{\int_0^{T_{drip}} R(t)\cdot\Delta(t)\,dt}{\int_0^{T_{drip}} R(t)\cdot dt} = \frac{\int_0^{T_{drip}} \lambda^{pr}\alpha(\tilde{C}_i - \tilde{C}_{eq})\exp(-t/\tau_{pr})\cdot\lambda^{iso}\cdot(\delta^{13}HCO_{3i}^- - \delta^{13}HCO_{3f}^-)\cdot F_{ex}(t)dt}{\int_0^{T_{drip}} \lambda^{pr}\alpha(\tilde{C}_i - \tilde{C}_{eq})\exp(-t/\tau_{pr})\cdot dt} \quad (3.33)$$

For $F_{ex}(T_{drip}) < 0.99$ one gets $\Delta_{Ca}(T_{drip}) > 0.95\cdot\lambda^{iso}\cdot(\delta^{13}HCO_{3i}^- - \delta^{13}HCO_{3f}^-)$ for splash factors $\Phi>0.2$, as one can read from Fig.7. Consequently, under these conditions the impact of isotope exchange is negligible.

If $\tau_{pr} << \tau_{ex}$ one finds $\Delta_{Ca}(T_{drip}) = \lambda^{iso}\cdot(\delta^{13}HCO_{3i}^- - \delta^{13}HCO_{3f}^-)$. For $F(T_{drip}) = 0.37$ and $\Phi = 0.6$ from Fig. 3.7 one gets $\lambda^{iso} = 0.6$. Thus for splash factors less than 0.6 the impact of isotope exchange becomes significant.

In summary, eqn. 3.33 and eqn. 3.30 (Fig. 3.7) allow to obtain the impact of isotope exchange with the CO_2 of the cave atmosphere.

From these findings some rules for the selection of stalagmites in a cave can be suggested. To select samples, which do not carry imprints by isotope exchange with the cave atmosphere, drip times should be less than 100 s. Therefore stalagmites with a diameter of at least 11 cm are suitable (Dreybrodt, 2008). To avoid small splash factors, Φ, the fall height of the drops feeding the stalagmite should be less than one meter. Low splash factors reduce the growth rate of the stalagmite by a factor of λ^{ca} (Curl, 1973; Mühlinghaus et al., 2007). Growth rates become low as well, if T_{drip} becomes large compared to τ_{pr}. Therefore stalagmites with low growth rates of less than 0.01 cm/year are likely to carry imprints of exchange.

All arguments given above are also valid for ^{18}O provided the exchange time τ_{water} of oxygen isotopes with the water is large compared to T_{drip}.

3.6 Conclusions

We present a theoretical derivation of the exchange time, τ_{ex}, needed to establish isotopic equilibrium between atmospheric CO_2 and dissolved HCO_3^- using a diffusion- reaction equation. The result is $\tau_{ex} = \tau_{red}^{ex} \cdot [HCO_3^-] / (K_H \cdot p_{CO_2}^{cave})$. The reduced exchange time τ_{red}^{ex} is found to be a function of temperature and the depth, a, of the water film.

To test the theoretically predicted values, we prepared stagnant or flowing thin films of a $NaHCO_3$ solution and exposed them to a CO_2 atmosphere at 20°C. The $\delta^{13}C$ and $\delta^{18}O$ values of the DIC were measured as a function of the exposure time. The $\delta^{13}C$ values exhibit an exponential approach towards isotope equilibrium with the atmospheric CO_2 with the exchange time, τ_{ex}. The $\delta^{18}O$ values first evolve towards isotopic equilibrium with atmospheric CO_2, reach a minimum value and then drift away from the isotopic equilibrium with atmospheric CO_2. This behavior results from the fact that oxygen isotope equilibrium between the CO_2 contained in the experimental vessel and the water of the solution is established. The experimental values are in satisfactory agreement with the theoretical predictions.

Finally, a water film with a depth of 0.013 cm flowing down an inclined borosilicate glass plate was exposed to an atmosphere with $p_{CO2} = 500$ ppmV at 20°C. The $\delta^{13}C$ and $\delta^{18}O$ values were measured as a function of flow (exposure) time, t. From these data an exchange time τ_{ex} of 7000 s was determined.

From our experiments we are confident that the theoretical exchange times are sufficiently close to nature. This enables us to calculate them as function of the cave environment: temperature, p_{CO2} in the cave, DIC in the drip water, and the depth of the water layer on the

speleothem. Using this exchange time it is possible to obtain the isotope composition of the calcite precipitated in dependence on the drip time, exchange time, time of precipitation of calcite and the splash factor, which accounts for splashing and mixing when the drop hits the water layer covering the stalagmite. This can help to select stalagmites suitable for climate records.

Acknowledgements

M. Hansen, W. Dreybrodt and D. Scholz acknowledge funding by the Deutsche Forschungsgemeinschaft (DFG) through grants SCHO 1274/8-1 and DR 79/14-1. We are also thankful to C. Spötl for stable isotope analysis of the water samples and providing helpful comments to the manuscript. We thank Nicole Schindler and Madlaine Peine for assistance in the laboratory in the framework of their B.Sc-thesis. We thank B. R. Schöne for providing isotopic analysis from his lab. Furthermore we are thankful to the workshop of the Institutes for Geosciences and Physics of the Atmosphere, University of Mainz, and in particular S. Klumb for technical support and constructing the climate box for our experiments. We thank Chris Day and three anonymous reviewers for their suggestions, which helped to improve the manuscript. We highly appreciate the editorial work of AE Miryam Bar-Matthews.

3.7 References

Affek, H.P. (2013) Clumped isotopic equilibrium and the rate of isotope exchange between CO_2 and water. American Journal of Science **313**, 309-325.

Baker, A., Genty, D., Dreybrodt, W., Barnes, W.L., Mockler, N.J., Grapes, J. (1998) Testing Theoretically Predicted Stalagmite Growth Rate with Recent Annually Laminated Samples: Implications for Past Stalagmite Deposition. Geochimica et Cosmochimica Acta **62**, 393-404.

Baldini, J.U.L., McDermott, F., Hoffmann, D.L., Richards, D.A., Clipson, N. (2008) Very high-frequency and seasonal cave atmosphere P_{CO2} variability: Implications for stalagmite growth and oxygen isotope-based paleoclimate records. Earth and Planetary Science Letters **272**, 118-129.

Baskaran, M., Krishnamurthy, R.V. (1993) Speleothems as proxy for the carbon isotope composition of atmospheric CO_2. Geophysical Research Letters **20**, 2905-2908.

Beck, W.C., Grossman, E.L., Morse, J.W. (2005) Experimental studies of oxygen isotope fractionation in the carbonic acid system at 15°, 25°, and 40°C. Geochimica et Cosmochimica Acta **69**, 3493-3503.

Cowan, B.D., Osborne, M.C., Banner, J.L. (2013) Temporal variability of cave-air CO_2 in central Texas. Journal of Cave and Karst Studies **75**, 38-50.

Crank, J. (1979) The mathematics of diffusion. Oxford university press.

Curl, R.L. (1973) Minimum diameter stalagmites. Bulletin National Speleological Society of America (Nat. Speleol. Soc. Bull) **35**, 1-9.

Deininger, M., Fohlmeister, J., Scholz, D., Mangini, A. (2012) Isotope disequilibrium effects: The influence of evaporation and ventilation effects on the carbon and oxygen isotope composition of speleothems – A model approach. Geochimica et Cosmochimica Acta **96**, 57-79.

Dreybrodt, W. (2008) Evolution of the isotopic composition of carbon and oxygen in a calcite precipitating $H_2O–CO_2–CaCO_3$ solution and the related isotopic composition of calcite in stalagmites. Geochimica et Cosmochimica Acta **72**, 4712-4724.

Dreybrodt, W. (2011) Comments on processes contributing to the isotope composition of ^{13}C and 18O in calcite deposited to speleothems. Acta Carsologica 40, 233-238.

Dreybrodt, W. (2012) Comment on "Oxygen isotopes in calcite grown under cave-analogue conditions" by C.C. Day and G.M. Henderson. Geochimica et Cosmochimica Acta **85**, 383-387.

Dreybrodt, W., Deininger, M. (2014) The impact of evaporation to the isotope composition of DIC in calcite precipitating water films in equilibrium and kinetic fractionation models. Geochimica et Cosmochimica Acta **125**, 433-439.

Dreybrodt, W., Scholz, D. (2011) Climatic dependence of stable carbon and oxygen isotope signals recorded in speleothems: From soil water to speleothem calcite. Geochimica et Cosmochimica Acta **75**, 734-752.

Frisia, S., Fairchild, I.J., Fohlmeister, J., Miorandi, R., Spötl, C., Borsato, A. (2011) Carbon mass-balance modelling and carbon isotope exchange processes in dynamic caves. Geochimica et Cosmochimica Acta **75**, 380-400.

Green, M., Taube, H. (1963)Isotopic fractionation in the OH^--H_2O exchange reaction. The Journal of Physical Chemistry **67**, 1565-1566.

Hansen, M., Dreybrodt, W., Scholz, D. (2013) Chemical evolution of dissolved inorganic carbon species flowing in thin water films and its implications for (rapid) degassing of CO_2 during speleothem growth. Geochimica et Cosmochimica Acta **107**, 242-251.

Hofmann, M.E.G., Horváth, B., Pack, A. (2012) Triple oxygen isotope equilibrium fractionation between carbon dioxide and water. Earth and Planetary Science Letters **319–320**, 159-164.

Kim, S.-T., Coplen, T.B., Horita, J. (2015) Normalization of stable isotope data for carbonate minerals: Implementation of IUPAC guidelines. Geochimica et Cosmochimica Acta **158**, 276-289.

Kowalczk, A.J., Froelich, P.N. (2010) Cave air ventilation and CO_2 outgassing by radon-222 modeling: How fast do caves breathe? Earth and Planetary Science Letters 289, 209-219.

Mandić, M., Mihevc, A., Leis, A., Bronić, I.K. (2013) Concentration and stable carbon isotopic composition of CO_2 in cave air of Postojnska jama, Slovenia. International Journal of Speleology **42**, 279-287.

Mickler, P.J., Banner, J.L., Stern, L., Asmerom, Y., Edwards, R.L., Ito, E. (2004) Stable isotope variations in modern tropical speleothems: Evaluating equilibrium vs. kinetic isotope effects 1. Geochimica et Cosmochimica Acta **68**, 4381-4393.

Mook, W.G., Bommerson, J.C., Staverman, W.H. (1974) Carbon isotope fractionation between dissolved bicarbonate and gaseous carbon dioxide. Earth and Planetary Science Letters **22**, 169-176.

Mühlinghaus, C., Scholz, D., Mangini, A. (2007) Modelling stalagmite growth and $\delta^{13}C$ as a function of drip interval and temperature. Geochimica et Cosmochimica Acta **71**, 2780-2790.

Parkhurst, D., Apello, C. (1999) User's Guide to PHREEQC (V2). US Geol. Surv 312.

Richards, D.A., Dorale, J.A. (2003) Uranium-series chronology and environmental applications of speleothems. Reviews in Mineralogy and Geochemistry **52**, 407-460.

Riechelmann, D.F.C., Deininger, M., Scholz, D., Riechelmann, S., Schröder-Ritzrau, A., Spötl, C., Richter, D.K., Mangini, A., Immenhauser, A. (2013) Disequilibrium carbon and oxygen isotope fractionation in recent cave calcite: Comparison of cave precipitates and model data. Geochimica et Cosmochimica Acta **103**, 232-244.

Romanov, D., Kaufmann, G., Dreybrodt, W. (2008) Modeling stalagmite growth by first principles of chemistry and physics of calcite precipitation. Geochimica et Cosmochimica Acta **72**, 423-437.

Scholz, D., Mühlinghaus, C., Mangini, A. (2009) Modelling $\delta^{13}C$ and $\delta^{18}O$ in the solution layer on stalagmite surfaces. Geochimica et Cosmochimica Acta **73**, 2592-2602.

Scholz, D., Hoffmann, D. (2008) $^{230}Th/U$-dating of fossil corals and speleothems. Eiszeitalter und Gegenwart **57**, 52-76.

Spötl, C. (2005) A robust and fast method of sampling and analysis of $\delta^{13}C$ of dissolved inorganic carbon in ground waters. Isotopes in Environmental and Health Studies **41**, 217-221.

Thornton, E.R. (1962) Solvent Isotope Effects in H_2O^{16} and H_2O^{18}. Journal of the American Chemical Society **84**, 2474-2475.

Usdowski, E., Michaelis, J., Bottcher, M., Hoefs, J. (1991) Factors for the oxygen isotope equilibrium fractionation between aqueous and gaseous CO_2, carbonic-acid, bicarbonate, carbonate, and water (19-degrees-C). ZEITSCHRIFT FUR PHYSIKALISCHE CHEMIE-INTERNATIONAL JOURNAL OF RESEARCH IN PHYSICAL CHEMISTRY & CHEMICAL PHYSICS **170**, 237-249.

Vogel, J.C., Grootes, P.M., Mook, W.G. (1970) Isotopic fractionation between gaseous and dissolved carbon dioxide. Zeitschrift für Physik **230**, 225-238.

3.8 Supplementary information

Supplementary 3.1: Experimental set-up for the experiments in the exsiccator.

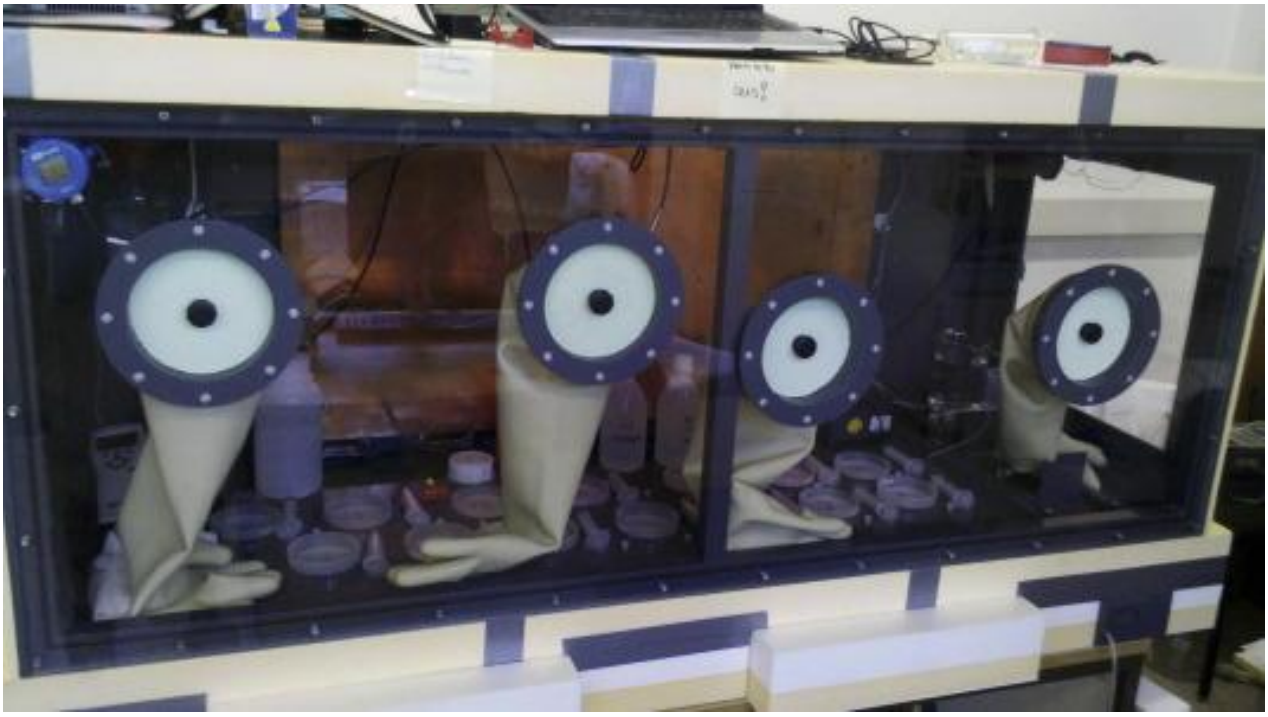

Supplementary 3.2: Experimental set-up for the experiments in the glove box.

Chapter 4: Manuscript II

Carbon isotope exchange between gaseous CO_2 and thin solution films:

Artificial cave experiments and a complete diffusion-reaction model

Maximilian Hansen[1*], Denis Scholz[1], Marie-Louise Froeschmann[1], Bernd R. Schöne[1], Christoph Spötl[2]

Manuscript in press in Geochimica et Cosmochimica Acta.

*corresponding author: m.hansen@uni-mainz.de

[1] Institute of Geosciences, University of Mainz, Germany

[2]Institute of Geology, University of Innsbruck, Austria

Hansen, M., Scholz, D., Froeschmann, M.-L., Schöne, B.R., Spötl, C. (in press) Carbon isotope exchange between gaseous CO_2 and thin solution films: Artificial cave experiments and a complete diffusion-reaction model. Geochimica et Cosmochimica Acta.

Abstract

Speleothem stable carbon isotope ($\delta^{13}C$) records provide important paleoclimate and paleo-environmental information. However, the interpretation of these records in terms of past climate or environmental change remains challenging because of various processes affecting the $\delta^{13}C$ signals. A process that has only been sparsely discussed so far is carbon isotope exchange between the gaseous CO_2 of the cave atmosphere and the dissolved inorganic carbon (DIC) contained in the thin solution film on the speleothem, which may be particularly important for strongly ventilated caves.

Here we present a novel, complete reaction diffusion model describing carbon isotope exchange between gaseous CO_2 and the DIC in thin solution films. The model considers all parameters affecting carbon isotope exchange, such as diffusion into, out of and within the film, the chemical reactions occurring within the film as well as the dependence of diffusion and the reaction rates on isotopic mass and temperature. To verify the model, we conducted laboratory experiments under completely controlled, cave-analogue conditions at three different temperatures (10, 20, 30 °C). We exposed thin (≈ 0.1 mm) films of a $NaHCO_3$ solution with four different concentrations (1, 2, 5 and 10 mmol/l, respectively) to a nitrogen atmosphere containing a specific amount of CO_2 (1000 and 3000 ppmV). The experimentally observed temporal evolution of the pH and $\delta^{13}C$ values of the DIC is in good agreement with the model predictions. The carbon isotope exchange times in our experiments range from ca. 200 to ca. 16,000 s and strongly depend on temperature, film thickness, atmospheric pCO_2 and the concentration of DIC. For low pCO_2 (between 500 and 1000 ppmV, as for strongly ventilated caves), our time constants are substantially lower than those derived in a previous study, suggesting a potentially stronger influence of carbon isotope exchange on speleothem $\delta^{13}C$ values. However, this process should only have an influence in case of very long drip intervals and slow precipitation rates.

4.1 Introduction

Speleothems have become well-established paleoclimate archives over the last decades, in particular because they can be dated very precisely with U-series disequilibrium methods (Richards and Dorale, 2003; Scholz and Hoffmann, 2008). The most frequently used paleoclimate proxies in speleothems are the stable oxygen and carbon isotope ratios ($\delta^{18}O$ and $\delta^{13}C$ values) of the speleothem calcite. These can be measured at high spatial resolution and provide long and often uninterrupted paleoclimate records. Most speleothem paleoclimate records are based on changes in speleothem $\delta^{18}O$ values (e.g., Cheng et al., 2016; Frisia et al., 2005; Wong et al., 2015), which are related to changes in the $\delta^{18}O$ value of precipitation and thus provide important information on past changes in temperature (Mangini et al., 2005), precipitation (Frisia et al., 2005), water vapor sources and atmospheric circulation (Wackerbarth et al., 2012).

Although all $\delta^{18}O$ records are accompanied by $\delta^{13}C$ records of the same resolution (due to analysis of CO2, carbon and oxygen isotopes of speleothem calcite are measured simultaneously, e.g., Spötl and Vennemann, 2003), speleothem $\delta^{13}C$ records have been less often utilized for paleoclimate reconstructions. The major reason for this is that speleothem $\delta^{13}C$ values are influenced by a variety of processes occurring in the soil and karst above the cave as well as inside the cave during precipitation of speleothem calcite (Dreybrodt and Scholz, 2011; McDermott, 2004) and are thus often assumed to reflect local environmental change rather than (supra)regional climate variability. Nevertheless, speleothem $\delta^{13}C$ records have provided important information on past climate change. For instance, Hellstrom et al. (1998) interpreted variations in the $\delta^{13}C$ values of stalagmites from New Zealand in terms of changes in vegetation productivity. A similar interpretation of a Holocene $\delta^{13}C$ record in terms of vegetation productivity and recharge has recently been provided by Mischel et al. (2016), who corroborated their interpretation by high-resolution trace element data. Genty et al. (2003) found rapid changes in the $\delta^{13}C$ values of a stalagmite from south-west France and interpreted them as reflecting dramatic vegetation changes in response to Dansgaard-Oeschger and Heinrich events. Scholz et al. (2012) observed a relationship between lamina thickness and lower $\delta^{13}C$ values on an annual timescale in a stalagmite from north-eastern Italy reflecting warmer winter temperatures. On the millennial time-scale, changes in $\delta^{13}C$ have been interpreted to reflect the progressive evolution of the soil. A monthly resolved $\delta^{13}C$ speleothem record has been shown to provide information on past changes in rainfall in Belize (Ridley et al., 2015), related to shifts of the position of the Intertropical Convergence Zone. Furthermore, Meyer et al. (2014) conducted a detailed cave monitoring study in central Texas and concluded that speleothem $\delta^{13}C$ values from temperate/subtropical regions may serve as a proxy for aridity. They also suggested that

speleothem $\delta^{13}C$ values potentially record seasonal changes in cave ventilation, which then could be used as a geochronological tool. These examples highlight the large potential of speleothem $\delta^{13}C$ data for various paleoclimatic and environmental applications. For some cave systems, speleothem $\delta^{13}C$ values may even be more sensitive to climate change than $\delta^{18}O$ values (Scholz et al., 2012).

Despite these successful studies, the interpretation of speleothem $\delta^{13}C$ signals in terms of past climate variability or environmental change is complex, because of the various processes occurring in the soil, the epikarst and inside the cave, where speleothem calcite is eventually precipitated (Cerling, 1984; Dorale et al., 1998; Dreybrodt and Scholz, 2011; McDermott, 2004; Rudzka et al., 2011). According to several studies, isotope fractionation effects occurring during the precipitation of calcite on the speleothem surface may obscure potential paleoclimate signals (e.g., Deininger et al., 2012; Dreybrodt and Scholz, 2011; Hendy, 1971; Mickler et al., 2006; Riechelmann et al., 2013). A process that has only been sparsely discussed in the speleothem community, so far, is carbon and oxygen isotope exchange between the gaseous CO_2 of the cave atmosphere and the dissolved inorganic carbon (DIC) contained in the solution film on the speleothem. The $\delta^{13}C$ value of the CO_2 of the cave atmosphere depends strongly on its origin. In general, it consists of a mixture between atmospheric CO_2 (currently ca. -8.5 ‰, Keeling, 2005) and CO_2 originating from the epikarst or the decomposition of organic matter in the soil (13C ≈ -22 ‰, Frisia et al., 2011; Gázquez et al., 2016; Kowalczk and Froelich, 2010). The $\delta^{13}C$ value of cave air CO_2 varies between these values, for instance, due to seasonal changes in cave ventilation (e.g., Baldini et al., 2008; Gázquez et al., 2016; Mandić et al., 2013; Mattey et al., 2008; Spötl et al., 2005). In a cave system, CO_2 either degasses from or diffuses into the solution after the water has entered the cave, depending on the difference between the pCO_2 of the solution and the cave atmosphere. If the $\delta^{13}C$ values of the DIC species contained in the film (aqueous CO_2, HCO_3^- and CO_3^{2-}) are not in isotopic equilibrium with the gaseous CO_2 of the cave atmosphere, carbon isotope exchange will occur and potentially affect the $\delta^{13}C$ values of the DIC.

Dreybrodt et al. (2016) were the first to systematically investigate isotope exchange between gaseous CO_2 and thin solution films in laboratory experiments and also derived an equation to calculate the time constant for isotope exchange depending on different parameters such as cave pCO_2, the HCO_3^- concentration of the solution, temperature and film thickness. For the laboratory experiments, they used very high pCO_2 values (up to 25,000 ppmV). This is not only much higher than in most cave systems, but also results in significant changes in pH and, consequently, substantial shifts in the distribution of the DIC species. For the theoretical

derivation of the time constants of isotope exchange, however, they considered the concentration of dissolved HCO_3^- to be constant in time.

Here we present new experiments aiming to simulate the conditions in a cave. We produced thin films (ca. 0.1 mm in thickness) of a $NaHCO_3$ solution which were exposed to an atmosphere with a pCO_2 of 1000 and 3000 ppmV at different temperatures. We also introduce a complete diffusion-reaction model to describe our experimental data as well as the previous data from Dreybrodt et al. (2016). Our data generally confirm the temporal evolution of the $\delta^{13}C$ values of the DIC derived by Dreybrodt et al. (2016). However, for low pCO_2 and relatively high concentrations of dissolved $NaHCO_3$, the time constants for carbon isotope exchange show large differences of up to 200,000 s.

4.2 Experimental methods

Different solutions were prepared by dissolving specific amounts of $NaHCO_3$ ($\delta^{13}C$ = -6.0 ‰) in pure MQ water (1, 2, 5 and 10 mmol/L, respectively). Prior to the addition of $NaHCO_3$, we sparged the MQ water with argon for several minutes. Thus, the water contained no dissolved CO_2. We prepared large amounts of solution (4 L), which were stored in narrow mouth bottles with a screw plug and additionally sealed with Parafilm® in order to minimize contamination. The bulk solutions were regularly sampled using a Luer-Lock® syringe, DIC was precipitated as $SrCO_3$, and the $\delta^{13}C$ values were measured in order to control the distribution of the dissolved carbon species and to detect contamination at an early stage of the experiments.

To closely simulate a cave system, the entire experimental setup was placed in a climate box, which allowed to control all parameters such as temperature, relative humidity and pCO_2. The total volume of the box was 500 L, and it was equipped with rubber gloves, which enabled to perform and adjust the experiments when the system was closed. The box is equipped with a small opening at the bottom (15 ×10 cm), which can be sealed by a sliding gate (the “sewer port”). This allows introducing and taking out items and solutions during the experiments without affecting the box atmosphere. The experiments were conducted at 10, 20 and 30 °C, respectively, and temperature was controlled via a LAUDA® TUK 30 thermostat pumping a tempered coolant through the box. Inside the box, temperature was monitored by five temperature probes (Tinytag® and Hobo®). To keep the temperature constant, the box was isolated with 60 mm thick Styrodur® plates. To maintain a high relative humidity, the atmosphere in the box was continuously pumped through a water column via glass frites using a membrane pump. Relative

humidity was logged during the experiments using a Tinytag® humidity probe. Two small ventilators were used to homogenize the atmosphere at very low ventilation rates.

Prior to each experiment, we established the experimental temperatures in the climate box, and stored the solutions for at least 3 days at this temperature to establish chemical and isotopic equilibrium between all dissolved species. Then, the box was flushed with N_2 until a minimum pCO_2 of ca. 40 - 50 ppmV was reached. Subsequently, the pCO_2 of the atmosphere was adjusted to 1000 or 3000 ppmV by adding a defined amount of CO_2 into the system which had a very different $\delta^{13}C$ value (ca. -37 ‰) than the $NaHCO_3$ solution (ca. -6 ‰). During the experiments, the pCO_2 was monitored using a Vaisala® MI 70 GMP222 probe. In order to control the $\delta^{13}C$ values of the atmospheric CO_2, we sampled the box atmosphere during every experiment by opening, slewing and closing off exetainers inside the box, which were pre-flushed with Ar.

We then pumped the $NaHCO_3$ solution onto an inclined, sandblasted borosilicate glass plate using a peristaltic pump. Drip interval (4.6 s, corresponding to a drip rate of 13 drips per min) and drip volume (0.05 ml) were identical for all experiments. In order to avoid splashing effects, a low drip height of ca. 1 cm was used. As a consequence, no splashing was visible during the experiments. This resulted in a film with a thickness between ca. 0.11 and 0.14 mm flowing down the plate (Dreybrodt et al., 2016; Hansen et al., 2013). After different distances of flow (5, 20, 50, 80 and 100 cm) and thus, residence times on the plate, the solution dripped via a small funnel through the sewer port into 5 ml test glasses. The maximum exposure time of the solution to the atmosphere ranged from 450 to 570 s. In addition, one sample was collected by pumping the solution on the very end of the plate (corresponding to a distance of flow of 0 cm). From there, the solution directly dripped into the sewer port via a small funnel. We note that splashing effects cannot be excluded for these samples.

Subsequently, the solution was immediately isolated from the box atmosphere by transferring the solution in an Ar-flushed Luer-Lock® syringe containing 1N NaOH and 1.5N $SrCl_2$. As a consequence, the DIC was immediately completely precipitated as solid $SrCO_3$, which was then rinsed with methanol to establish a neutral pH and dried in an exsiccator. The samples were stored under dry conditions in order to avoid isotope exchange with atmospheric CO_2. The precipitation method and its precision is described in detail in Dreybrodt et al. (2016). Figure 4.1 shows a schematic of the experimental setup. The parameters of all experiments (temperature, pCO_2, concentration of $NaHCO_3$ and $\delta^{13}C$ value of the atmosphere) are summarized in supplemental Table S4.1. The evolution of the $\delta^{13}C$ values as a function of residence time on the plate enabled us to monitor the $\delta^{13}C$ values of the DIC in response to carbon isotope exchange and to determine the exchange time, τ_{ex}, under cave analogue conditions. Note that we used a $NaHCO_3$

rather than a $CaCO_3$ solution in order to avoid precipitation of $CaCO_3$ along the plate. This would affect the $\delta^{13}C$ values of the DIC and thus superpose the effects of carbon isotope exchange (Dreybrodt, 2008; Dreybrodt et al., 2016; Hendy, 1971; Polag et al., 2010; Scholz et al., 2009; Wiedner et al., 2008). We also measured the evolution of the pH along the flow path using a Mettler-Toledo® InLab® Surface probe, which allowed in-situ measurements of the solution film. Measurements were conducted at the same distances (exposure times) as the DIC measurements. The relatively large diameter of the probe (12 mm) did not allow to directly determine the initial pH value of the film (i.e., when the drip impinges on the plate). Thus, ca. 3 ml of solution were collected in small test tubes prior to dripping onto the plate and the pH value was determined.

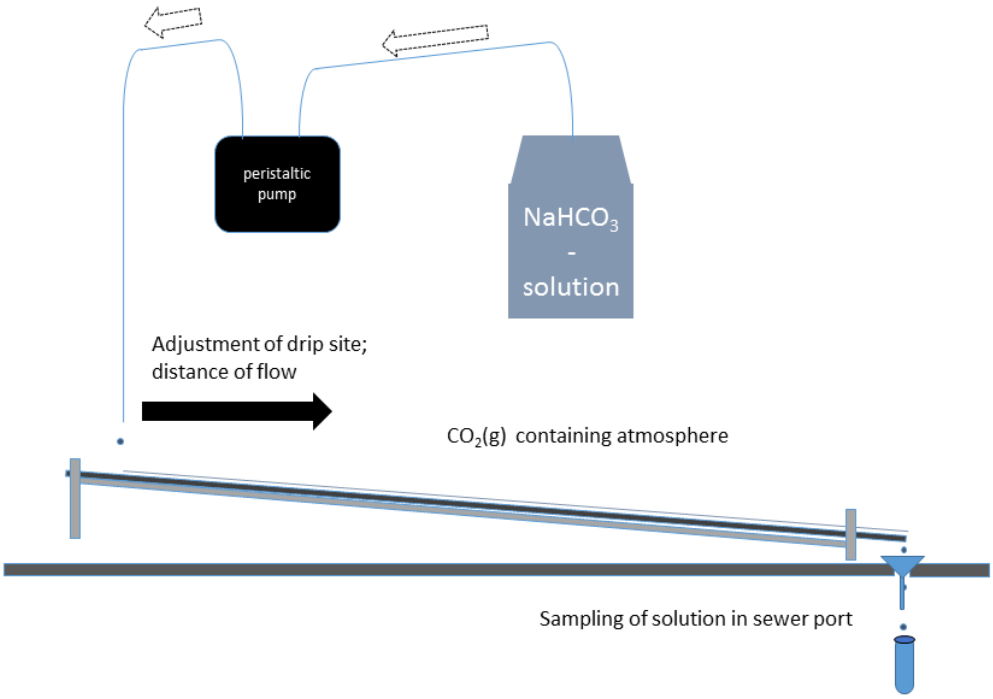

Fig. 4.1: Schematic drawing of the experimental setup inside the climate box. The drip site can be adjusted to different distances of flow and, thus, to different exposure times on the plate. Samples are collected in a sewer port and precipitated as $SrCO_3$.

Stable isotope analyses of the CO_2 of the box atmosphere were conducted at the University of Innsbruck. CO_2 was collected in glass vials, rushed into the laboratory and analyzed within less than three days to guarantee no significant leakage of the septa (see Spötl, 2004). $\delta^{13}C_{CO2}$ values were determined using a Delta^{plus}XL mass spectrometer calibrated against in-house calcite reference material, whose $\delta^{13}C$ value was previously calibrated against NBS-19. The 1σ-analytical uncertainty for $\delta^{13}C_{CO2}$ is 0.10 ‰.

Stable isotope analyses of the $SrCO_3$ samples were performed at the Institute of Geosciences, University of Mainz, using a Thermo Finnigan MAT 253 continuous flow-isotope ratio mass spectrometer coupled to a GasBench II. Samples were dissolved in concentrated phosphoric acid in helium-flushed borosilicate exetainers at 72 °C. Isotope data were calibrated against an NBS-19 calibrated Carrara marble standard distributed by IVA Analysentechnik e.K. (Düsseldorf, Germany) ($\delta^{18}O = -1.91$ ‰, $\delta^{13}C = +2.01$ ‰). On average, internal precision (1σ) and accuracy were better than 0.04 and 0.02 ‰, respectively. The isotope values are reported relative to the Vienna Pee Dee Belemnite scale (McKinney et al., 1950).

4.3 Theoretical background - quantitative modeling of carbon isotope exchange

4.3.1 General description of the model

When the $NaHCO_3$ solution is exposed to gaseous CO_2, CO_2 diffuses into the solution and is converted to aqueous CO_2. At the same time, aqueous CO_2 is lost from the solution by diffusive degassing. This triggers a variety of chemical reactions aiming to re-establish both chemical and isotopic equilibrium between the individual DIC species. The diffusion coefficients as well as the rate constants of the individual reactions are slightly different for the different isotopes. The chemical reactions occurring within the solution have been discussed in detail and quantitatively modeled (including carbon isotope fractionation) for the marine carbonate system (termed the complete chemical system, Schulz et al., 2006; Zeebe et al., 1999a; Zeebe and Wolf-Gladrow, 2001; Zeebe et al., 1999b). Here we extend this model to thin films on the surface of a speleothem, which requires including diffusion of gaseous CO_2 into and out of the film as well as diffusion of the dissolved species within the film.

The following reactions of the carbonate system are considered (Schulz et al., 2006):

$$CO_2 + H_2O \underset{k_{-1}}{\overset{k_{+1}}{\leftrightarrow}} HCO_3^- + H^+ \tag{4.1}$$

$$CO_2 + OH^- \underset{k_{-4}}{\overset{k_{+4}}{\leftrightarrow}} HCO_3^- \tag{4.2}$$

$$CO_3^{2-} + H^+ \underset{k_{-5}^{H^+}}{\overset{k_{+5}^{H^+}}{\leftrightarrow}} HCO_3^- \tag{4.3}$$

$$HCO_3^- + OH^- \underset{k_{-5}^{OH^-}}{\overset{k_{+5}^{OH^-}}{\leftrightarrow}} CO_3^{2-} + H_2O \quad (4.4)$$

$$H_2O \underset{k_{-6}}{\overset{k_{+6}}{\leftrightarrow}} H^+ + OH^- \quad (4.5)$$

Boron species, which are important in seawater (Zeebe and Wolf-Gladrow, 2001), can be neglected for cave water. The corresponding reaction constants, k, are compiled in supplemental Table S4.2. To include carbon isotope fractionation, the species containing the heavy and the light carbon isotopes can be divided into two compartments (Zeebe and Wolf-Gladrow, 2001; Zeebe et al., 1999b). These compartments can be considered as two independent systems that are, however, coupled via H^+ and OH^- (Eqs. 4.6-4.8). The corresponding chemical reactions for the heavy carbon isotope are:

$$^{13}CO_2 + H_2O \underset{k'_{-1}}{\overset{k'_{+1}}{\leftrightarrow}} H^{13}CO_3^- + H^+ \quad (4.6)$$

$$^{13}CO_2 + OH^- \underset{k'_{-4}}{\overset{k'_{+4}}{\leftrightarrow}} H^{13}CO_3^- \quad (4.7)$$

$$^{13}CO_3^{2-} + H^+ \underset{k'^{H^+}_{-5}}{\overset{k'^{H^+}_{+5}}{\leftrightarrow}} H^{13}CO_3^- \quad (4.8)$$

$$H^{13}CO_3^- + OH^- \underset{k'^{OH^-}_{-5}}{\overset{k'^{OH^-}_{+5}}{\leftrightarrow}} {}^{13}CO_3^{2-} + H_2O \quad (4.9)$$

As indicated by the prime, the reaction constants for the heavy isotopes are slightly different (Zeebe et al., 1999b). Here we used the values compiled by Zeebe et al. (1999b). For some reaction constants, however, no values for the heavy isotopes are available. In this case, we followed the approach of Zeebe et al. (1999b) and assumed the same value for the reaction constant of the heavy and the light isotope for the forward reaction and calculated the reaction constants for the backward reaction from equilibrium isotope fractionation. A compilation of the reaction constants for the heavy carbon isotope is provided in Table S4.2. The fractionation factors used in the model are compiled in Table S3. Based on the reactions described by Eqs. (4.1) – (4.9), a coupled system of differential equations describing the temporal evolution of both the chemical and the isotopic system can be set up (Schulz et al., 2006; Zeebe and Wolf-Gladrow, 2001; Zeebe et al., 1999b). The solution of this system has already been presented and discussed in detail for the marine carbonate system (Zeebe and Wolf-Gladrow, 2001; Zeebe et al., 1999b).

For the thin film on the surface of speleothems, diffusion of gaseous CO_2 into, out of and within the film needs to be taken into account. This can be done by including an additional term in the individual differential equations accounting for diffusion of the corresponding species:

$$\frac{d[^{12}CO_2]}{dt} = (k_{-1}[H^+] + k_{-4})\left[H^{12}CO_3^-\right] - (k_{+1} + k_{+4}[OH^-])\left[^{12}CO_2\right] + D_{^{12}CO_2}\frac{\partial^2[^{12}CO_2]}{\partial x^2} \quad (4.10)$$

$$\frac{d[^{13}CO_2]}{dt} = (k'_{-1}[H^+] + k'_{-4})\left[H^{13}CO_3^-\right] - (k'_{+1} + k'_{+4}[OH^-])\left[^{13}CO_2\right] + D_{^{13}CO_2}\frac{\partial^2[^{13}CO_2]}{\partial x^2} \quad (4.11)$$

$$\frac{d[H^{12}CO_3^-]}{dt} = (k_{+1} + k_{+4}[OH^-])\left[^{12}CO_2\right] - (k_{-1}[H^+] + k_{-4})\left[H^{12}CO_3^-\right] + \left(k_{+5}^{H^+}[H^+] + k_{-5}^{OH^-}\right)\left[^{12}CO_3^{2-}\right] - \left(k_{-5}^{H^+} + k_{+5}^{OH^-}[OH^-]\right)[H^{12}CO_3^-] + D_{H^{12}CO_3^-}\frac{\partial^2[H^{12}CO_3^-]}{\partial x^2} \quad (4.12)$$

$$\frac{d[H^{13}CO_3^-]}{dt} = (k'_{+1} + k'_{+4}[OH^-])\left[^{13}CO_2\right] - (k'_{-1}[H^+] + k'_{-4})\left[H^{13}CO_3^-\right] + \left(k'^{H^+}_{+5}[H^+] + k'^{OH^-}_{-5}\right)\left[^{13}CO_3^{2-}\right] - \left(k'^{H^+}_{-5} + k'^{OH^-}_{+5}[OH^-]\right)[H^{13}CO_3^-] + D_{H^{13}CO_3^-}\frac{\partial^2[H^{13}CO_3^-]}{\partial x^2} \quad (4.13)$$

$$\frac{d[^{12}CO_3^{2-}]}{dt} = \left(k_{-5}^{H^+} + k_{+5}^{OH^-}[OH^-]\right)\left[H^{12}CO_3^-\right] - \left(k_{+5}^{H^+}[H^+] + k_{-5}^{OH^-}\right)\left[^{12}CO_3^{2-}\right] + D_{^{12}CO_3^{2-}}\frac{\partial^2[^{12}CO_3^{2-}]}{\partial x^2} \quad (4.14)$$

$$\frac{d[^{13}CO_3^{2-}]}{dt} = \left(k'^{H^+}_{-5} + k'^{OH^-}_{+5}[OH^-]\right)\left[H^{13}CO_3^-\right] - \left(k'^{H^+}_{+5}[H^+] + k'^{OH^-}_{-5}\right)\left[^{13}CO_3^{2-}\right] + D_{^{13}CO_3^{2-}}\frac{\partial^2[^{13}CO_3^{2-}]}{\partial x^2} \quad (4.15)$$

$$\frac{d[H^+]}{dt} = \left(k_{+1}\left[^{12}CO_2\right] + k'_{+1}[^{13}CO_2]\right) - \left(k_{-1}[H^+]\left[H^{12}CO_3^-\right] + k'_{-1}[H^+]\left[H^{13}CO_3^-\right]\right) + \left(k_{-5}^{H^+}\left[H^{12}CO_3^-\right] + k'^{H^+}_{-5}\left[H^{13}CO_3^-\right]\right) - \left(k_{+5}^{H^+}[H^+]\left[^{12}CO_3^{2-}\right] + k'^{H^+}_{+5}[H^+]\left[^{13}CO_3^{2-}\right]\right) + k_{+6} - k_{-6}[H^+][OH^-] + D_{H^+}\frac{\partial^2[H^+]}{\partial x^2} \quad (4.16)$$

$$\frac{d[OH^-]}{dt} = \left(k_{-4}\left[H^{12}CO_3^-\right] + k'_{-4}\left[H^{13}CO_3^-\right]\right) - \left(k_{+4}[OH^-]\left[^{12}CO_2\right] + k'_{+4}[OH^-][^{13}CO_2]\right) - \left(k_{+5}^{OH^-}[OH^-]\left[H^{12}CO_3^-\right] + k'^{OH^-}_{+5}[OH^-]\left[H^{13}CO_3^-\right]\right) + \left(k_{-5}^{OH^-}\left[^{12}CO_3^{2-}\right] + k'^{OH^-}_{-5}\left[^{13}CO_3^{2-}\right]\right) + k_{+6} - k_{-6}[H^+][OH^-] + D_{OH^-}\frac{\partial^2[OH^-]}{\partial x^2}, \quad (4.17)$$

where the *k's* are the corresponding reaction constants (Table S4.2), the *D's* are the diffusion coefficients for the different species (Table S4.4), and *x* denotes the depth in the solution film. Note, that there is no significant isotope fractionation associated with the diffusion of HCO_3^- and CO_3^{2-} (Zeebe and Wolf-Gladrow, 2001). Thus, $D_{H^{13}CO_3^-} = D_{H^{12}CO_3^-}$ and $D_{^{13}CO_3^{2-}} = D_{^{12}CO_3^{2-}}$.

We solved this coupled stiff system of differential equations numerically using the statistical software `R` (R Core Team, 2016) and the methods described by Soetaert et al. (2012).

In particular, we use the `R` packages `deSolve` (Soetaert et al., 2010) and `ReacTran` (Soetaert and Meysman, 2012). The latter offers grid generation routines and the discretization of the diffusive and advective transport terms on these grids. A detailed description including several examples is given by Soetaert et al. (2012). We used a grid consisting of n = 10 boxes for all calculations. For the terms describing diffusion of dissolved CO_2 (Eqs. (4.10) and (4.11)), we used the following boundary conditions: (i) no flux at the bottom of the film and (ii) constant concentrations of $[^{12}CO_2]$ and $[^{13}CO_2]$ at the top of the film. The second assumption is reasonable considering the very large reservoir of gaseous CO_2 in both our experiments and in natural caves. For the other dissolved species, the boundary conditions of the diffusion terms (Eqs. (4.12)-(4.17)) are no flux at the top and the bottom of the film.

4.3.2 Initial conditions

The model is able to simulate two cases: (i) carbon isotope exchange between gaseous CO_2 and the DIC in a natural system (termed "cave") and (ii) carbon isotope exchange between gaseous CO_2 and the DIC in our experiments (termed "lab"). The difference between the two cases is the calculation of the initial concentrations and $\delta^{13}C$ values of the individual species. For the natural system, we assumed that the solution has equilibrated with a specific pCO_2 and $\delta^{13}C$ value. These values may be very different in natural systems and depend, amongst other parameters, on the type and density of the vegetation above the cave, soil pCO_2, the $\delta^{13}C$ value of the soil gas, the $\delta^{13}C$ value of the host rock, and whether dissolution of $CaCO_3$ occurs under conditions of an open or a closed system (Dreybrodt and Scholz, 2011; Fohlmeister et al., 2011; Hendy, 1971; McDermott, 2004; Salomons and Mook, 1986). The concentration of the other species was calculated using Henry's law and accounting for charge balance as well as chemical equilibrium and isotope fractionation between the different species. For the laboratory experiments, in contrast, the initial values were determined by the concentration and $\delta^{13}C$ value of the dissolved $NaHCO_3$, again taking into account charge balance as well as chemical equilibrium and isotope fractionation between the different species.

Note that the concentrations of the individual molecules containing the heavy and the light isotopes of a corresponding species depend on the total concentration of the species as well as its $\delta^{13}C$ value. For instance, for a solution equilibrated with a specific pCO_2 and $\delta^{13}C$ value:

$$[CO_2]_{tot} = \left[^{12}CO_2\right] + \left[^{13}CO_2\right] = K_H\, pCO_2, \tag{4.18}$$

where K_H is the Henry constant for CO_2. The concentrations of the rare and the abundant isotopes are given by the isotope ratio, ^{13}R:

$$\frac{[^{13}CO_2]}{[^{12}CO_2]} = {}^{13}R_{CO_2} = (\delta^{13}C_{CO_{2,aq}} + 1)\,{}^{13}R_{VPDB}, \tag{4.19}$$

where $^{13}R_{VPDB}$ is the Vienna Pee Dee Belemnite standard. Note that, using this notation, δ-values should not be specified in per mil, but rather in their real (small) value (i.e., -13 ‰ = -0.013). The $\delta^{13}C$ value of the dissolved CO_2 is related to the $\delta^{13}C$ value of the gaseous CO_2 by:

$$\frac{(\delta^{13}C_{CO_{2,aq}}+1)}{(\delta^{13}C_{CO_{2,g}}+1)} = \varepsilon_{CO_2,aq/CO_2,g} + 1, \tag{4.20}$$

where $\delta^{13}C_{CO2,\,aq}$ and $\delta^{13}C_{CO2,\,g}$ correspond to the $\delta^{13}C$ values of the dissolved and gaseous CO_2, respectively, and $\varepsilon_{CO2,aq/CO2,g}$ is the fractionation between dissolved and gaseous CO_2 (Table S4.3).

This results in the following concentrations for $[^{12}CO_2]$ and $[^{13}CO_2]$, respectively:

$$\left[^{12}CO_2\right] = \frac{K_H\, pCO_2}{1 + \left(\delta^{13}C_{CO_{2,g}} + 1\right)\left(\varepsilon_{CO_{2_{aq}}/CO_{2_g}} + 1\right)\,{}^{13}R_{VPDB}}\ , \tag{4.21}$$

where $\varepsilon_{CO_{2_{aq}}/CO_{2_g}}$ denotes the fractionation between dissolved and gaseous CO_2 (Table 4.5), and

$$\left[^{13}CO_2\right] = K_H\, pCO_2 - [^{12}CO_2]\,. \tag{4.22}$$

4.3.3 Modeling results

Here we show and briefly discuss the results of the model. As an example, we used similar values as in the experiments of Dreybrodt et al. (2016). The temperature was set to 20 °C, and the film thickness assumed to be 0.01 cm. The initial conditions were calculated for a solution containing 5 mmol/l of $NaHCO_3$ with a $\delta^{13}C$ value of -6 ‰. The pH of this solution is 8.37. Note that this solution contained ca. 1 % of both $[CO_2]$ and $[CO_3^{2-}]$ due to chemical equilibration between the dissolved species. This solution was then exposed to a nitrogen atmosphere with a pCO_2 of 25,000 ppmV and a $\delta^{13}C$ value of -45 ‰.

Fig. 4.2 shows the temporal evolution of the mean concentration of the different dissolved carbon species in the film (i.e., the sum of the molecules containing the rare and the abundant carbon isotopes) as well as the pH. It is obvious that chemical equilibrium between all species is established quickly (i.e., within 5 to 15 s). The effect of dissolution of gaseous CO_2 into the film is clearly visible by the large increase in $[CO_2]$ (from 0.05 to 0.95 mmol/l) and accompanied by a decrease in pH from 8.37 to 7.10 (Fig. 4.2e). The concentration of the total DIC increases from 5 to almost 6 mmol/l (Fig. 4.2d). As a consequence of the change in pH, the distribution of the carbon species within the film changes dramatically. Whereas the fraction of CO_2 increases from

1 to 16 %, the relative fraction of HCO_3^- decreases from 98 to 84 % (Fig. 4.2f). Due to the total increase in DIC, however, the absolute concentration of HCO_3^- increases (Fig. 4.2b). Figure 4.3 shows the evolution of the concentration of the different dissolved carbon species, DIC as well as pH and pOH *within* the film. Diffusion of CO_2 into the film and the resulting gradient are clearly visible. This gradient is also reflected in the concentration of the other species, DIC, pH and pOH as a result of the conversion of CO_2 according to Eqs. (4.1) – (4.5).

Figure 4.4 shows the temporal evolution of the mean $\delta^{13}C$ value of the different carbon species within the 10 boxes of the film, weighted according to their concentration. It is obvious that the evolution of the $\delta^{13}C$ values of the dissolved CO_2 is very different from that of the $\delta^{13}C$ values of HCO_3^- and CO_3^{2-}. The reservoirs of HCO_3^- and CO_3^{2-} progressively approach isotopic equilibrium, which is finally reached after ca. 1200 s (Fig. 4.4). We emphasize the 60 times longer duration to establish isotopic compared to chemical equilibrium (ca. 20 s, Fig. 4.2). In contrast, the $\delta^{13}C$ values of the dissolved CO_2 reservoir show a very rapid initial drop to negative values, followed by a slow convergence to the final value expected under conditions of isotopic equilibrium (Fig. 4.4a). This value is reached after ca. 800 s. The $\delta^{13}C$ values of the DIC (Fig. 4.4b) are similar as those of the HCO_3^-, which is reasonable considering that HCO_3^- represents between 84 and 98 % of the DIC throughout the experiment (Fig. 4.2f).

In order to better resolve the evolution during the early stages of the experiment, we also show the temporal evolution of the average $\delta^{13}C$ values of the film on a logarithmic scale (Fig. 4.5). This reveals that the CO_2 reservoir almost reaches isotopic equilibrium within a few seconds. This is due to the very fast diffusion of CO_2 into the thin film (Dreybrodt and Scholz, 2011; Hansen et al., 2013). However, subsequently, the $\delta^{13}C$ value of the dissolved CO_2 increases again before it finally reaches isotopic equilibrium (Fig. 4.5a). This results from the initiation of carbon isotope exchange between the CO_2 and the HCO_3^- reservoirs. In other words, the $\delta^{13}C$ value of the CO_2 is balanced by the competing influence of diffusion of gaseous CO_2 - with a very negative $\delta^{13}C$ value of -45 ‰ - into the film and the conversion of HCO_3^- - with a comparably high $\delta^{13}C$ value of -6 ‰ - to dissolved CO_2 according to Eqs. (4.1) and (4.2). With the progressive approach of the $\delta^{13}C$ value of the HCO_3^- reservoir towards isotopic equilibrium, this effect diminishes (Fig. 4.5b). Note that this behavior is also visible in the evolution of the $\delta^{13}C$ value of the DIC, which is different from that of the HCO_3^- in the corresponding time range (Fig. 4.5d). Figure 4.6 shows the evolution of the $\delta^{13}C$ values of the different dissolved carbon species and DIC *within* the film. Diffusion of CO_2 with a very negative $\delta^{13}C$ value of -45 ‰ into the film and the resulting gradient is visible within the first few seconds. In contrast to the evolution of the concentrations of the individual species, this gradient is not reflected in the $\delta^{13}C$ values of the other species and DIC.

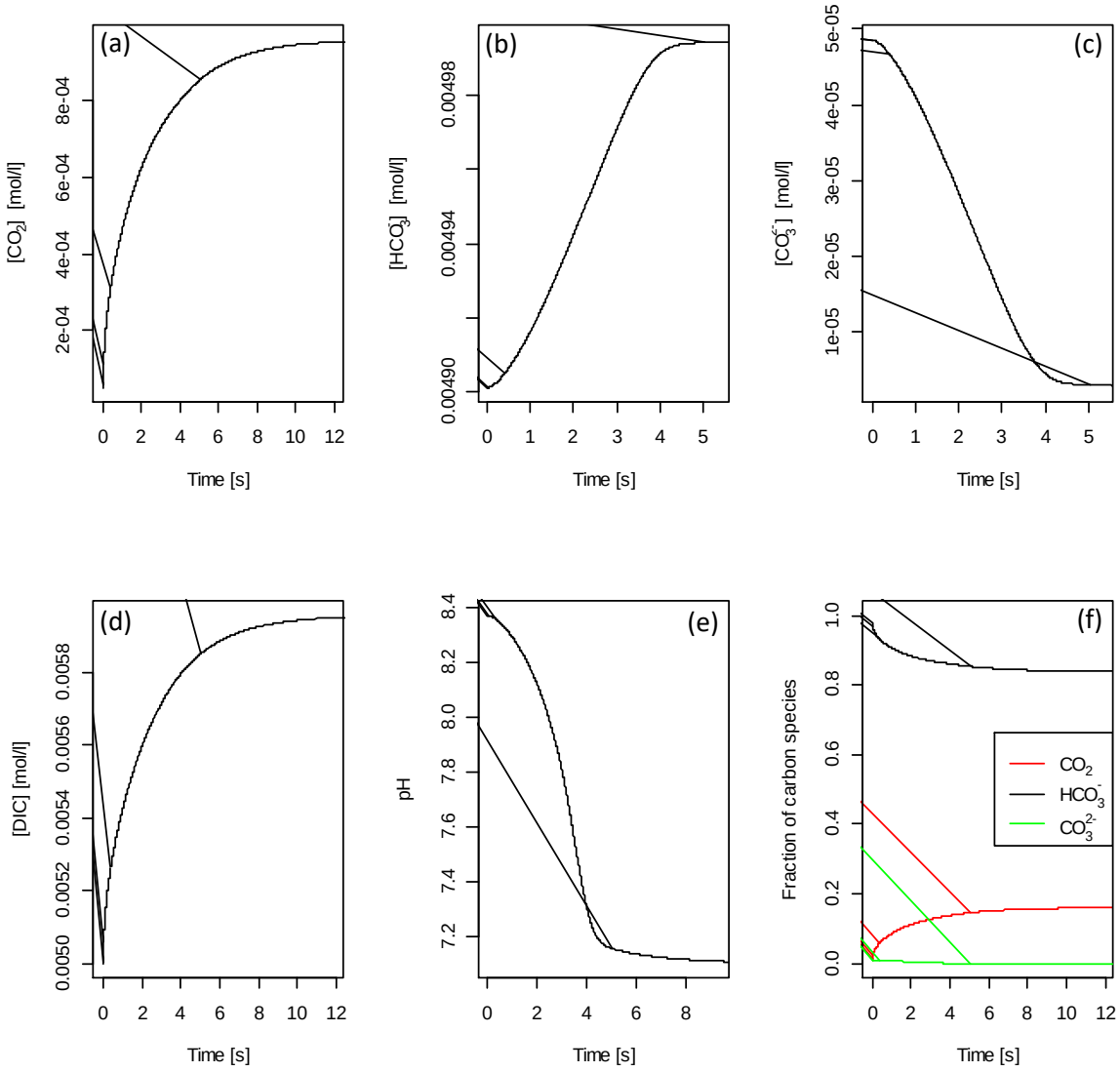

Fig. 4.2: Temporal evolution of the concentration of the different carbon species, DIC, pH as well as the distribution of species. The evolution is shown for an example initially containing 5 mmol/l of $NaHCO_3$ with a $\delta^{13}C$ value of -6 ‰, which is exposed to an atmosphere with a pCO_2 of 25,000 ppmV and a $\delta^{13}C$ value of -45 ‰. The time required to establish equilibrium is slightly different for the individual species, DIC and pH. This results in different scales on the x-axes.

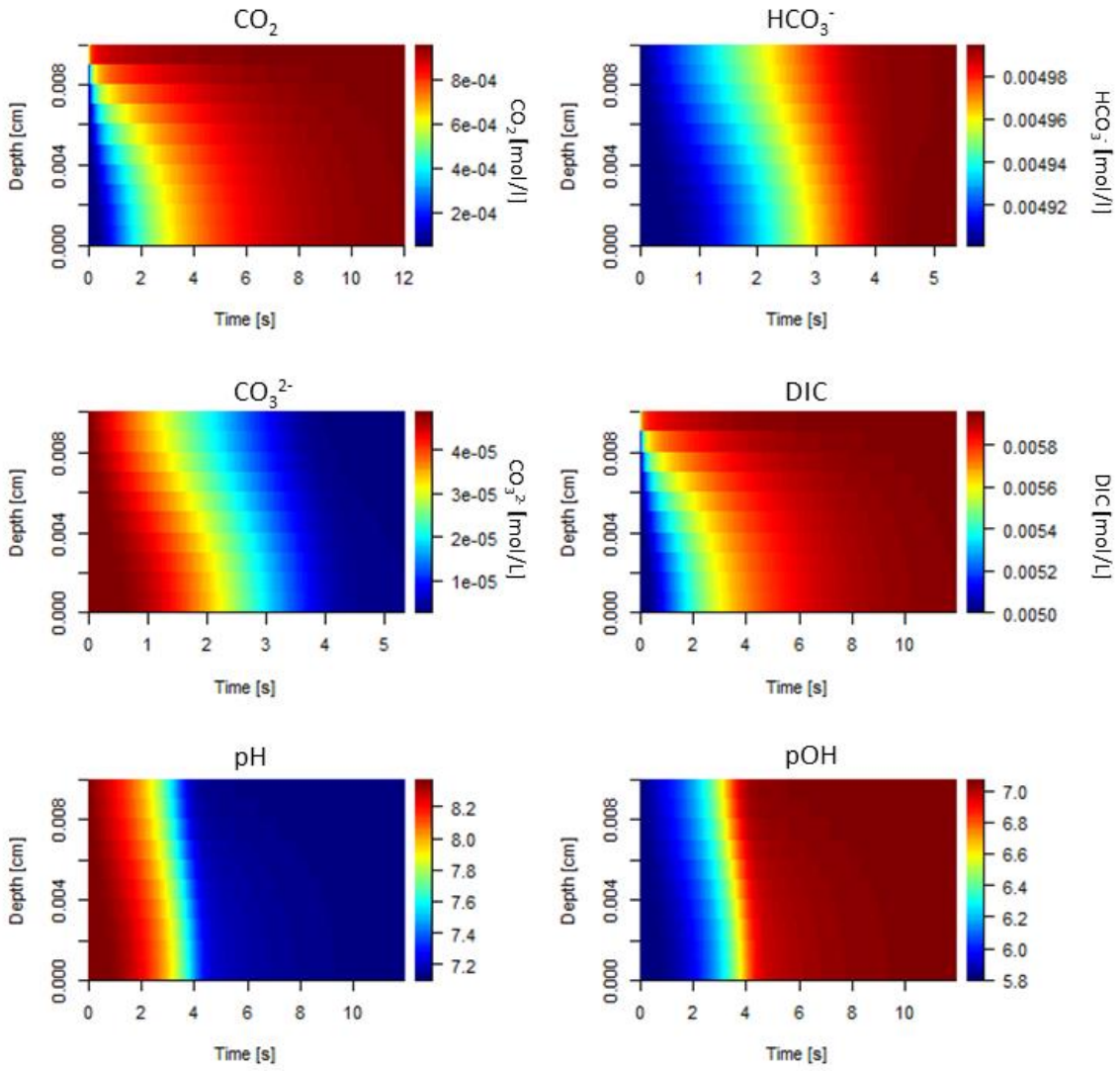

Fig. 4.3: Temporal evolution of the concentration of the different carbon species, DIC, pH as well as pOH within the thin film of solution. The evolution is shown for an example initially containing 5 mmol/l of $NaHCO_3$ with a $\delta^{13}C$ value of -6 ‰, which is exposed to an atmosphere with a pCO_2 of 25,000 ppmV and a $\delta^{13}C$ value of -45 ‰. The time required to establish equilibrium is slightly different for the individual species, DIC and pH. This results in different scales on the x-axes.

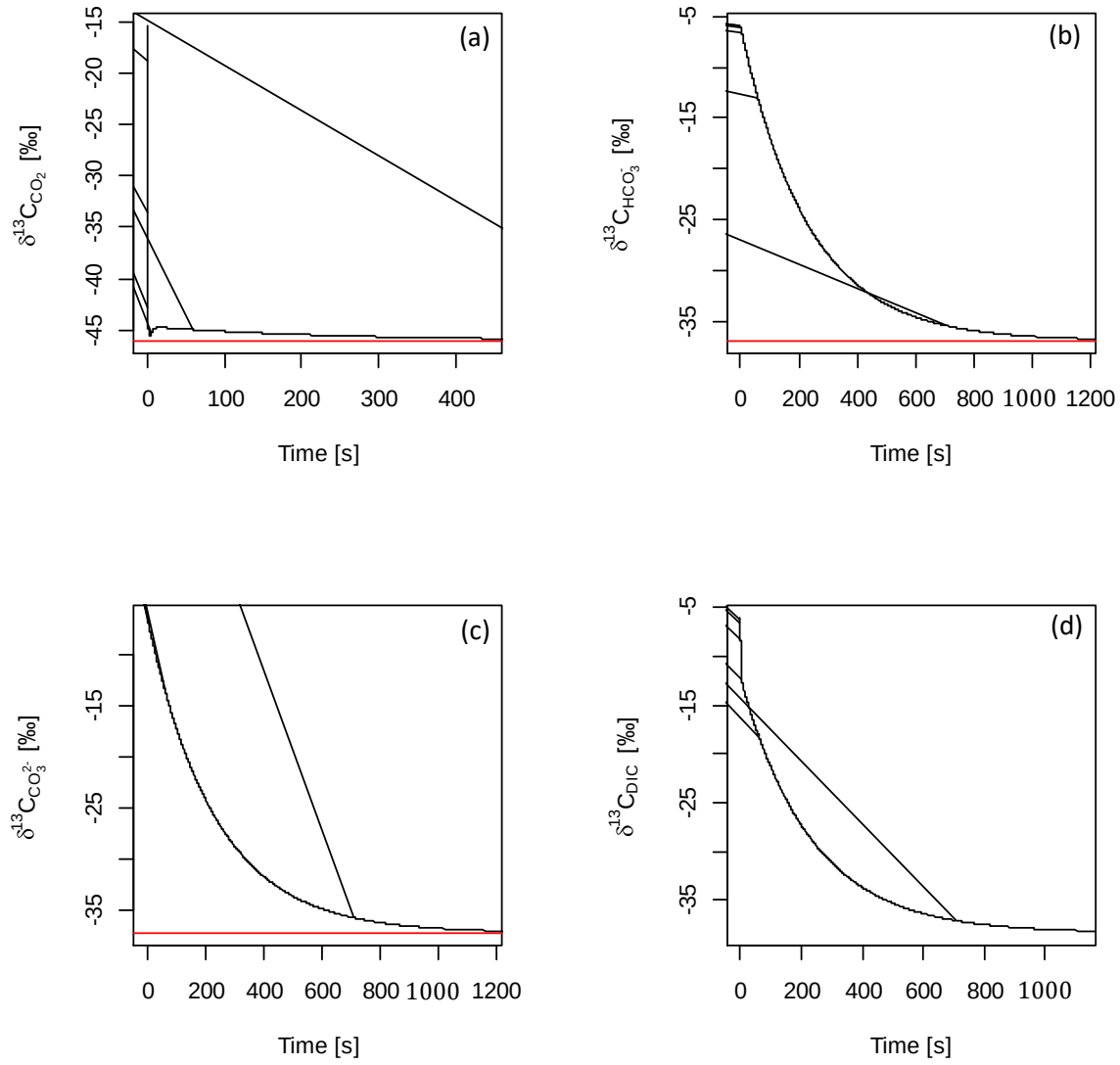

Fig. 4.4: Temporal evolution of the $\delta^{13}C$ values of the individual dissolved carbon species as well as the total DIC. The horizontal red lines denote the $\delta^{13}C$ values in equilibrium with the $\delta^{13}C$ value of gaseous CO_2 (-45 ‰ in this example). The evolution is shown for an example initially containing 5 mmol/l of $NaHCO_3$ with a $\delta^{13}C$ value of -6 ‰, which is exposed to an atmosphere with a pCO_2 of 25,000 ppmV and a $\delta^{13}C$ value of -45 ‰. The time required to establish isotopic equilibrium is different for the individual species and DIC. This results in different scales on the x-axes.

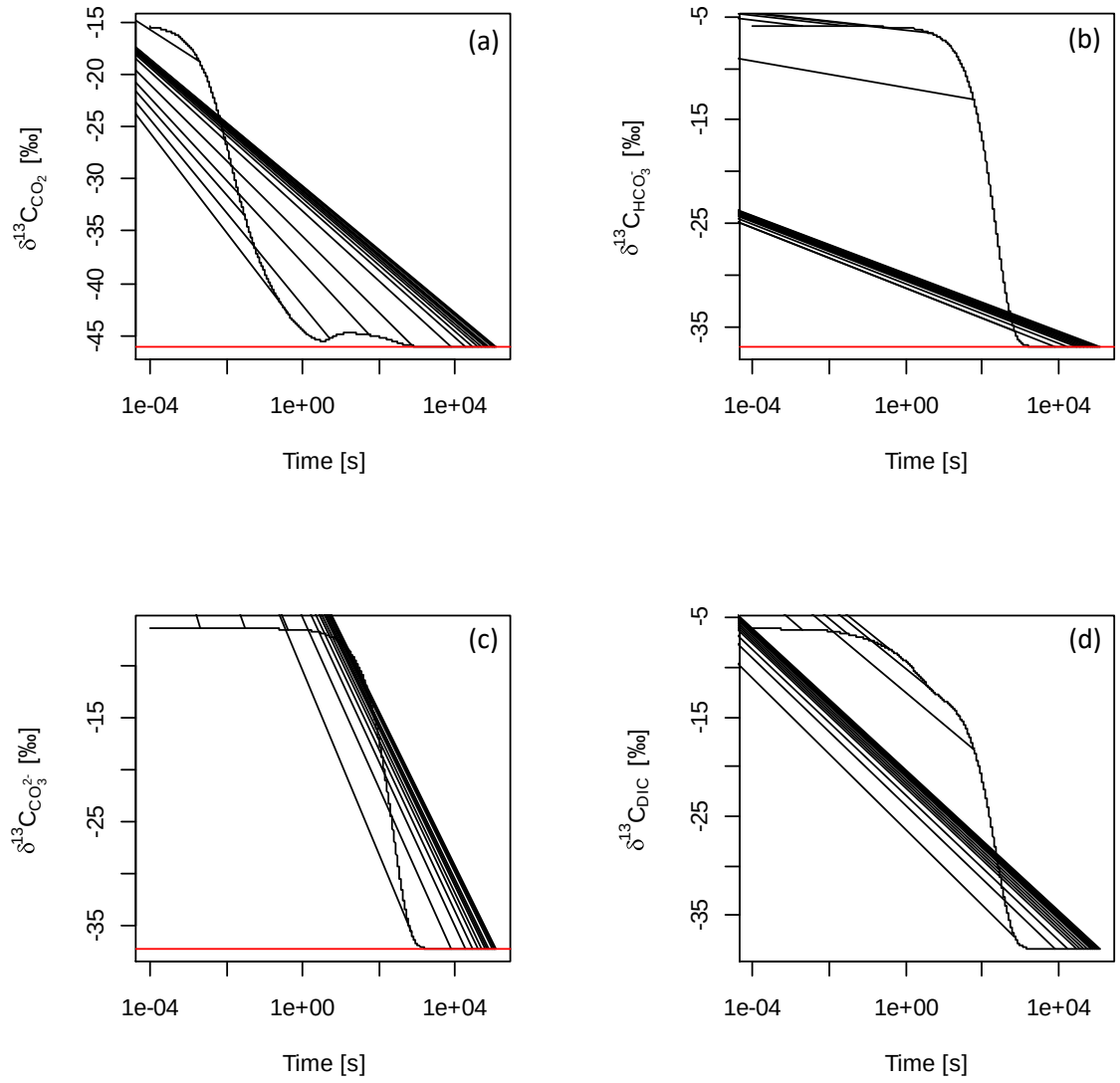

Fig. 4.5: Temporal evolution of the $\delta^{13}C$ values of the individual dissolved carbon species as well as the total DIC. The horizontal red lines denote the $\delta^{13}C$ values in equilibrium with the $\delta^{13}C$ value of gaseous CO_2 (-45 ‰ in this example). The x-axis is logarithmic. The evolution is shown for an example initially containing 5 mmol/l of $NaHCO_3$ with a $\delta^{13}C$ value of -6 ‰, which is exposed to an atmosphere with a pCO_2 of 25,000 ppmV and a $\delta^{13}C$ value of -45 ‰.

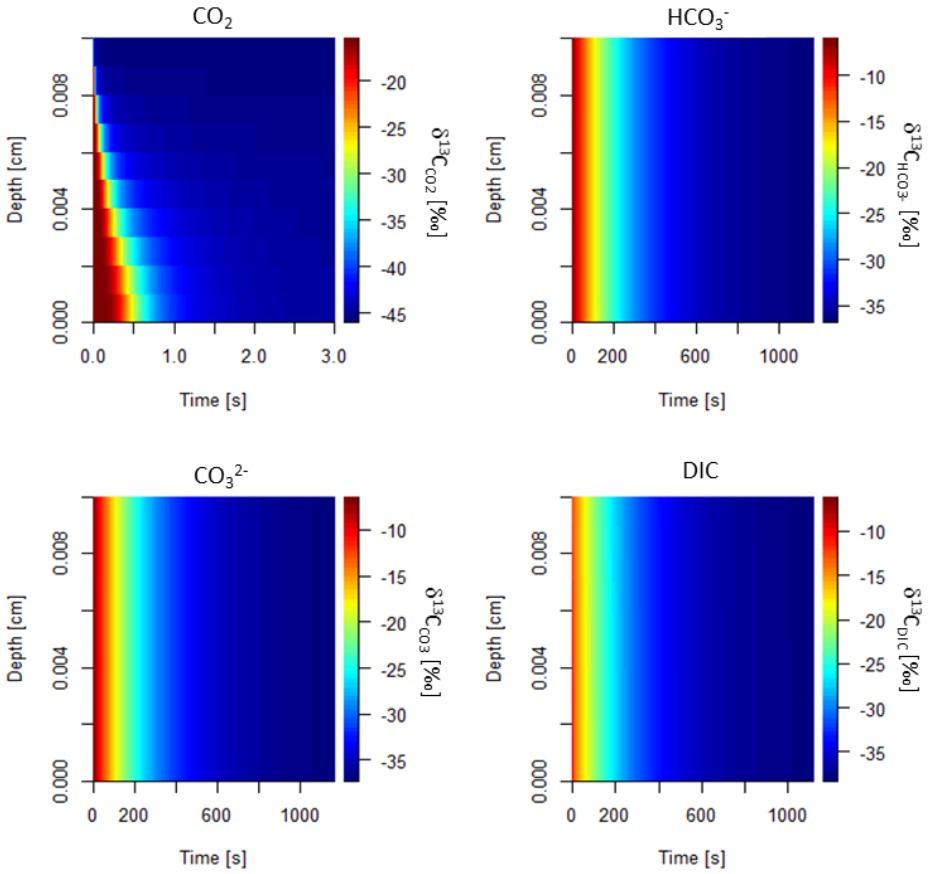

Fig. 4.6: Temporal evolution of the $\delta^{13}C$ values of the individual dissolved carbon species as well as the total DIC within the film. The evolution is shown for an example initially containing 5 mmol/l of $NaHCO_3$ with a $\delta^{13}C$ value of -6 ‰, which is exposed to an atmosphere with a pCO_2 of 25,000 ppmV and a $\delta^{13}C$ value of -45 ‰. The x-axes are scaled as in Fig. 4.4. The exception is the evolution of the $\delta^{13}C$ value of dissolved CO_2, which almost reaches isotopic equilibrium within a few seconds (compare Fig. 4.4a).

4.3.4 Determination of the time constants of the chemical and isotopic reactions

The temporal evolution of the concentrations and $\delta^{13}C$ values of the individual species of DIC as well as the total DIC reservoir are described by characteristic time constants. As is obvious from Figures 4.2 and 4.4, these may be very different for the different carbon species. Whereas all chemical reactions approach equilibrium within a maximum of 20 s (Fig. 4.2), isotopic equilibration of the reservoirs of HCO_3^-, CO_3^{2-} and DIC takes much longer (ca. 1500 s, Fig. 4.4). The adjustment of both chemical and isotopic equilibrium of the individual DIC species can be described by the following equation:

$$f(t) = \frac{\delta^{13}C(t) - \delta^{13}C_{eq}}{\delta^{13}C_0 - \delta^{13}C_{eq}}. \quad (4.23)$$

Eq. (4.23) describes the temporal evolution towards isotopic equilibrium. We note, however, that the same equation is valid for the temporal evolution of the concentrations of the individual species of DIC. The enumerator of Eq. (4.23) describes the current (i.e., at time, *t*) deviation from the equilibrium value, whereas the denominator is the initial deviation from the equilibrium value. For $t = 0$, f(t) is thus 1 (i.e., the maximum possible value of disequilibrium), whereas f(t) approaches zero for $t \rightarrow \infty$ (i.e., the initial disequilibrium has decayed away and equilibrium has been established). In other words, the temporal evolution of the $\delta^{13}C$ values is standardized to the initial deviation from isotopic equilibrium. If the evolution toward equilibrium is exponential, then

$$f(t) = e^{-\frac{t}{\tau_{ex}}}, \quad (4.24)$$

and the time constant for equilibration is given by τ_{ex}. Fig. 4.7 shows the equilibration of the $\delta^{13}C$ value of the HCO_3^- reservoir in our model. The logarithmic plot (Fig. 4.7b) confirms that the evolution towards isotopic equilibrium follows an exponential law. Fitting the data, thus, enables to determine the corresponding time constant τ_{ex} for isotopic equilibration, which is 232.1 s for this example. After a time of $5\tau_{ex}$, the value of Eq. (4.24) is exp(-5), which corresponds to -0.007. Thus, less than 1 % of the initial isotopic disequilibrium remains, and equilibrium can be considered to be established. In our example, this is the case after 1,161 s.

In contrast to the $\delta^{13}C$ values of the HCO_3^- reservoir, the equilibration of many other reservoirs in our model (e.g., the $\delta^{13}C$ values of CO_2 and DIC, Figs. 4.4 and 4.5, as well as the concentrations of HCO_3^- and CO_3^{2-}, Fig. 4.2) does not follow an exponential law, and an exponential fit of the data as well as the determination of a time constant, τ_{ex}, is not reasonable. In this case, the time when isotopic or chemical equilibrium is reached can be determined by the time corresponding to $f(t) = \exp(-5)$, which can be obtained from the numerical simulations. This enables us to derive equilibration times for the concentrations as well as the $\delta^{13}C$ values for all species of DIC. The deviation from the exponential law can be explained by the fact that observed shift in the $\delta^{13}C$ values is a combination of chemical equilibration with the new pCO_2 and carbon isotope exchange between the individual reservoirs of DIC. Strictly speaking, the term “isotope exchange” in isotope geochemistry describes an equilibrium isotope fractionation process without net mass transport (Mook and De Vries, 2000) and thus only occurs under conditions of chemical equilibrium. In this case, the evolution of the $\delta^{13}C$ values does follow an exponential law. Thus, the time constant, τ_{ex}, for carbon isotope exchange could be obtained from an exponential

fit of the $\delta^{13}C$ values when chemical equilibrium has been established. However, determination of the timing when chemical equilibrium has been established requires a complex geochemical model as developed in this study.

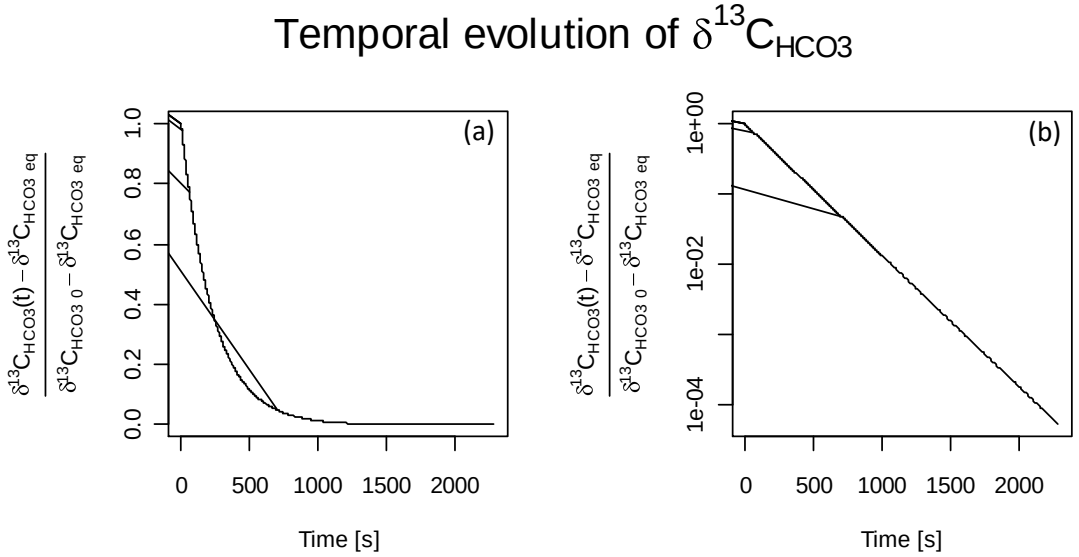

Fig. 4.7: Temporal evolution of the $\delta^{13}C$ values of the HCO_3^- reservoir standardized to the initial deviation from isotopic equilibrium. Black lines show the modeled $\delta^{13}C$ values on a linear (a) and a logarithmic (b) scale. The evolution is shown for an example initially containing 5 mmol/l of $NaHCO_3$ with a $\delta^{13}C$ value of -6 ‰, which is exposed to an atmosphere with a pCO_2 of 25,000 ppmV and a $\delta^{13}C$ value of -45 ‰.

4.4 Experimental results

4.4.1 Stability of the system during the experiments

The stability of the experimental system was systematically documented during the experiments. All parameters inside the climate box were logged. Temperature variability inside the box during the experiments was very low, the standard deviation (sd) ranged from $\pm$ 0.11 to $\pm$ 0.3° C. Relative humidity was also stable over the duration of an experiment and showed a maximum sd of $\pm$ 3 %. The sd of the pCO_2 of the atmosphere ranged from $\pm$ 15 to $\pm$ 45 ppmV for the individual experiments and was in the range of the precision of the probe. The $\delta^{13}C$ values of the atmospheric CO_2 ranged from -38.2 to –31.7 ‰ for the individual experiments and, thus, varied over the whole duration of the experiments (three weeks, Table S4.1). Within a single day and an individual

experiment, the variability was much smaller (2.5 ‰ at maximum). In general, the $\delta^{13}C$ values slightly increased during an experiment.

In order to control the stability of the distribution of the DIC species, the pH value of the bulk solution was monitored regularly and ranged from 7.8 to 8.8. The $\delta^{13}C$ values of the bulk solutions ranged from -7.5 to -12.5 ‰, with more negative $\delta^{13}C$ values for lower concentrations of $NaHCO_3$. These values are more negative than the $\delta^{13}C$ value of the $NaHCO_3$ that we used for the preparation of the solutions (-6 ‰).

4.4.2 Temporal evolution of pH

For experiments conducted at low concentrations of $NaHCO_3$, the pH decreased with increasing exposure time on the plates. In contrast, for high initial concentrations of $NaHCO_3$, the pH increased with time. The latter is the case for experiments 1, 9, 10, 17, 18, and 24 (Table S4.1). The two cases are shown for a low (2 mmol/L $NaHCO_3$, 20°C and pCO_2 = 1000 ppmV; Fig. 4.8a) and a high concentration (10 mmol/L $NaHCO_3$, 20°C and pCO_2 = 1000 ppmV; Fig 4.8b), respectively, and compared with the results of our model.

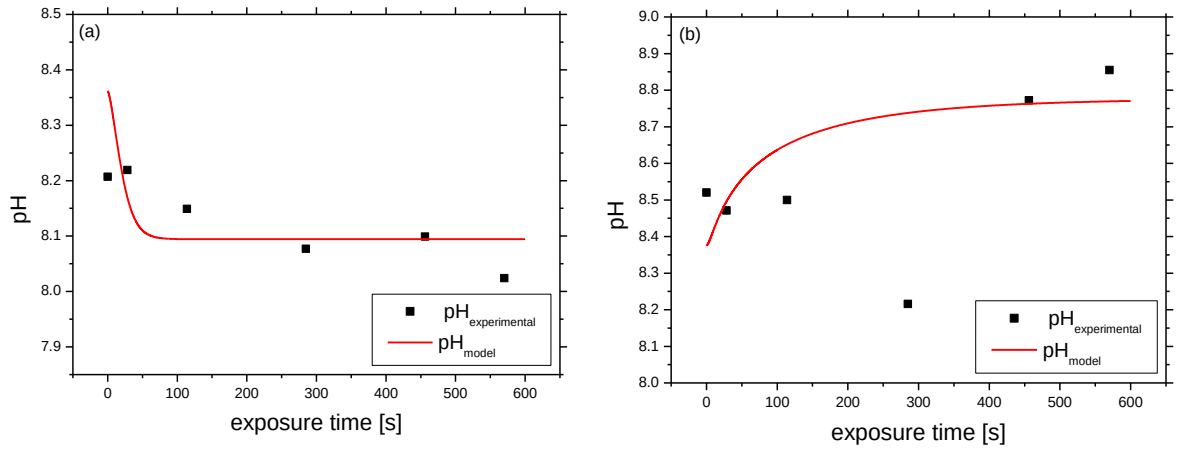

Fig. 4.8: Temporal evolution of the pH value of the solution with increasing residence time. (a) An example for decreasing pH during the experiment (2 mmol/l $NaHCO_3$, 20 °C and pCO_2 = 1000 ppmV). (b) Example for increasing pH during the experiment (10 mmol/l $NaHCO_3$, 20 °C and pCO_2 = 1000 ppmV).

4.4.3 Temporal evolution of the $\delta^{13}C$ values

In the experiments, we observed a significant decrease in the $\delta^{13}C$ values of the DIC with increasing residence time on the plate (Fig. 4.9). Depending on temperature and the concentration of $NaHCO_3$, this effect ranges from -0.04 to –10.6 ‰ and increases with decreasing $NaHCO_3$ concentrations. The data from all experiments are compiled in supplemental Table S4.5. Figures 4.9a and b show the temporal evolution of the $\delta^{13}C$ values for two experiments with different $NaHCO_3$ concentrations in comparison with our model. The effect for the 10 mmol/l solution (Fig. 4.9b) is -1.8 ‰, whereas it is -4.4 ‰ for the 2 mmol/l solution (Fig. 4.9a). Due to the relatively short exposure times on the plate (600 s at maximum), these experiments did not reach isotopic equilibrium. Most of the experimental data, thus, only show the initial part of the exponential evolution towards equilibrium (Fig. 4.7). The determination of a time constant for isotope exchange, τ_{ex}, according to Eq. (4.24) is, thus, not possible.

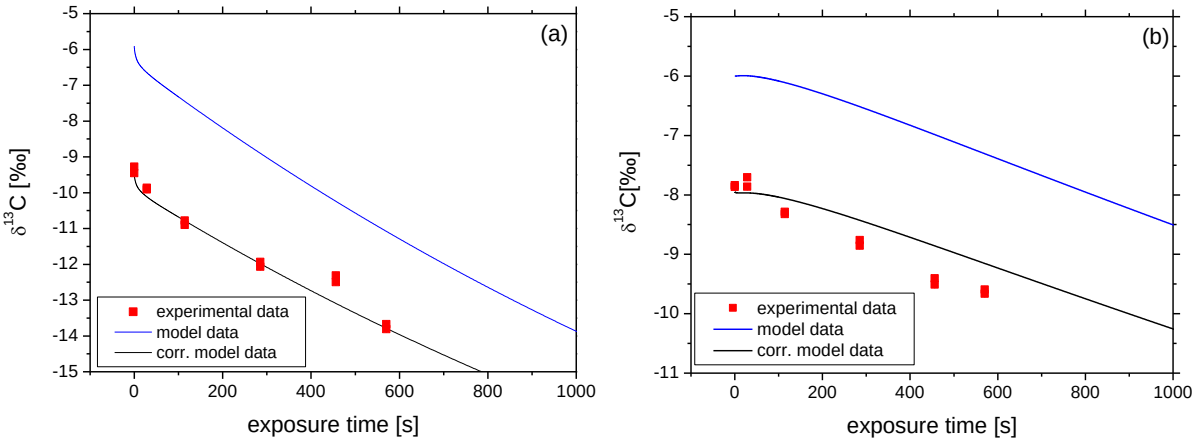

Fig. 4.9: Temporal evolution of the $\delta^{13}C$ values of the DIC compared with the results of our model (blue). (a) 2 mmol/l $NaHCO_3$, 20 °C, 1000 ppmV CO_2; (b) 10 mmol/l $NaHCO_3$, 20 °C, 1000 ppmV CO_2. The black line denotes the model prediction for the corrected initial $\delta^{13}C$ value of the DIC.

4.5 Discussion

4.5.1. Comparison of the experimental data with the model

To compare the model with the experimental data, we performed 400 model simulations using different initial and boundary conditions. We varied film thickness, temperature, pCO_2, concentration of $NaHCO_3$ and the $\delta^{13}C$ value of the CO_2 of the box atmosphere. These runs include all experiments from this study as well as the previous experiments performed by Dreybrodt et al. (2016).

4.5.1.1 pH values

Fig. 4.8 shows a comparison between the measured and the modeled evolution of pH along the plate for two examples (2 mmol/L $NaHCO_3$, 20°C and $pCO_2 = 1000$ ppmV, Fig. 4.8a; 10 mmol/L $NaHCO_3$, 20°C and $pCO_2 = 1000$ ppmV, Fig 4.8b). In general, the experimental data are in a good agreement with the predictions of the model (Fig. 4.8). Obvious outliers from the general trend (Fig. 4.8) may be due to problems during the pH measurements in the thin solution film. The adjustment of the pH probe in the center of the very thin film without disturbing the laminar flow of the solution is difficult. Thus, for some measurements, the membrane of the pH probe was probably not completely covered by the solution. Alternatively, the probe may have been dipped too deep into the film resulting in an influence from the surface of the glass plate. The initial pH value of the film (corresponding to a distance of flow of 0 cm, i.e., when the drip impinges on the plate) was not measured with the surface probe, but by collecting the solution in small test tubes. Diffusion of CO_2 out of or into the solution during collection is almost impossible to avoid. The initial offset from the model values (Fig. 4.8) may thus be due to uptake of gaseous CO_2 or degassing of dissolved CO_2 during collection inside the box. Thus, all pH measurements at the beginning of the plate must be considered to be affected by diffusion and degassing of CO_2.

For a better understanding of the experimental data, we show the temporal evolution of the concentrations of the different dissolved carbon species and pH for the two examples as predicted by the model (Figs. 4.10 and 4.11). For the relatively low concentration of 2 mmol/l $NaHCO_3$, the pH decreases with increasing residence time (Fig. 4.8a). This is caused by diffusion of CO_2 into the solution, which results in an increase of dissolved CO_2, HCO_3^- and total DIC (Figs. 4.10a, b and d). As a consequence, the pH value decreases, and the concentration of dissolved CO_3^{2-} is reduced (Fig. 4.10c). In total, the fraction of dissolved CO_2 slightly increases from ca. 1 to ca. 2 % (Fig. 4.10f). For the higher concentration of 10 mmol/l $NaHCO_3$, the pH increases

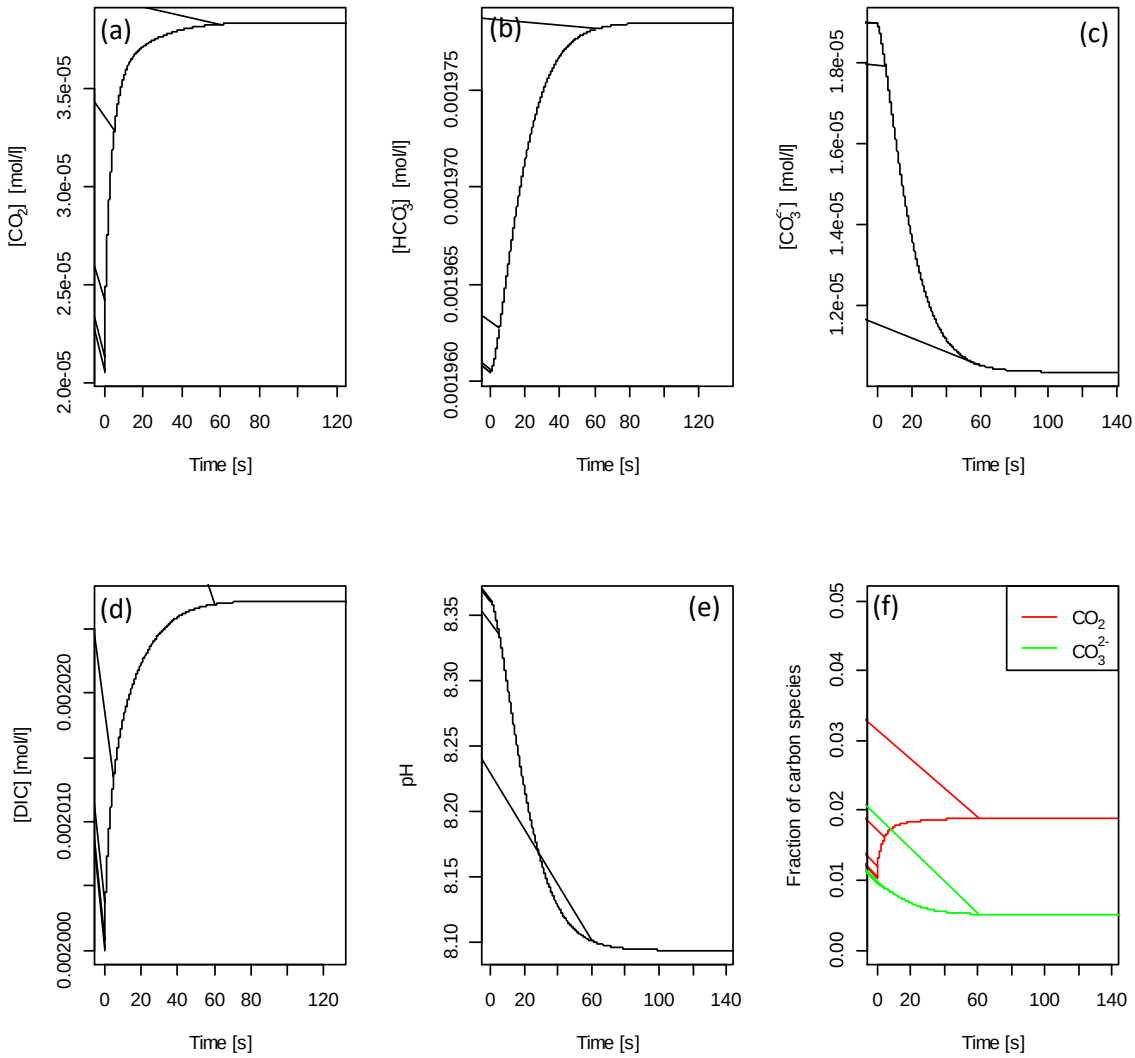

Fig. 4.10: Temporal evolution of the concentration of the different carbon species, DIC, pH as well as the distribution of species for a 2 mmol/l $NaHCO_3$ solution, which is exposed to an atmosphere with a pCO_2 of 1000 ppmV. The time required to establish equilibrium is slightly different for the individual species, DIC and pH. This results in different scales on the x-axes.

with increasing residence time (Fig. 4.8b). This results from diffusion of dissolved CO_2 out of the solution, which results in a decrease of dissolved CO_2, HCO_3^- and total DIC (Figs. 4.11a, b and d). As a consequence, both the pH value and the concentration of dissolved CO_3^{2-} increase (Fig. 4.11c). In total, the fraction of dissolved CO_2 slightly decreases from ca. 1 to ca. 0.5 %(Fig. 4.11f). It is important to note that the CO_2 initially contained in the solution (ca. 0.1 mmol/l, Fig. 4.11a, corresponding to ca. 1 % of total DIC, Fig. 4.11f) purely results from the dissolution of $NaHCO_3$ and equilibration of the chemical species. While the large volume of bulk solution is stored in narrow mouth bottles with a screw plug and additionally sealed with Parafilm®, degassing of CO_2 is

negligible. Once the solution is exposed as a thin film to the surrounding pCO_2 of 1000 ppmV, however, CO_2 degasses rapidly (Fig. 11a). As a consequence, further HCO_3^- is converted to CO_2, which then degasses until chemical equilibrium with the surrounding pCO_2 has been established (Fig. 4.11).

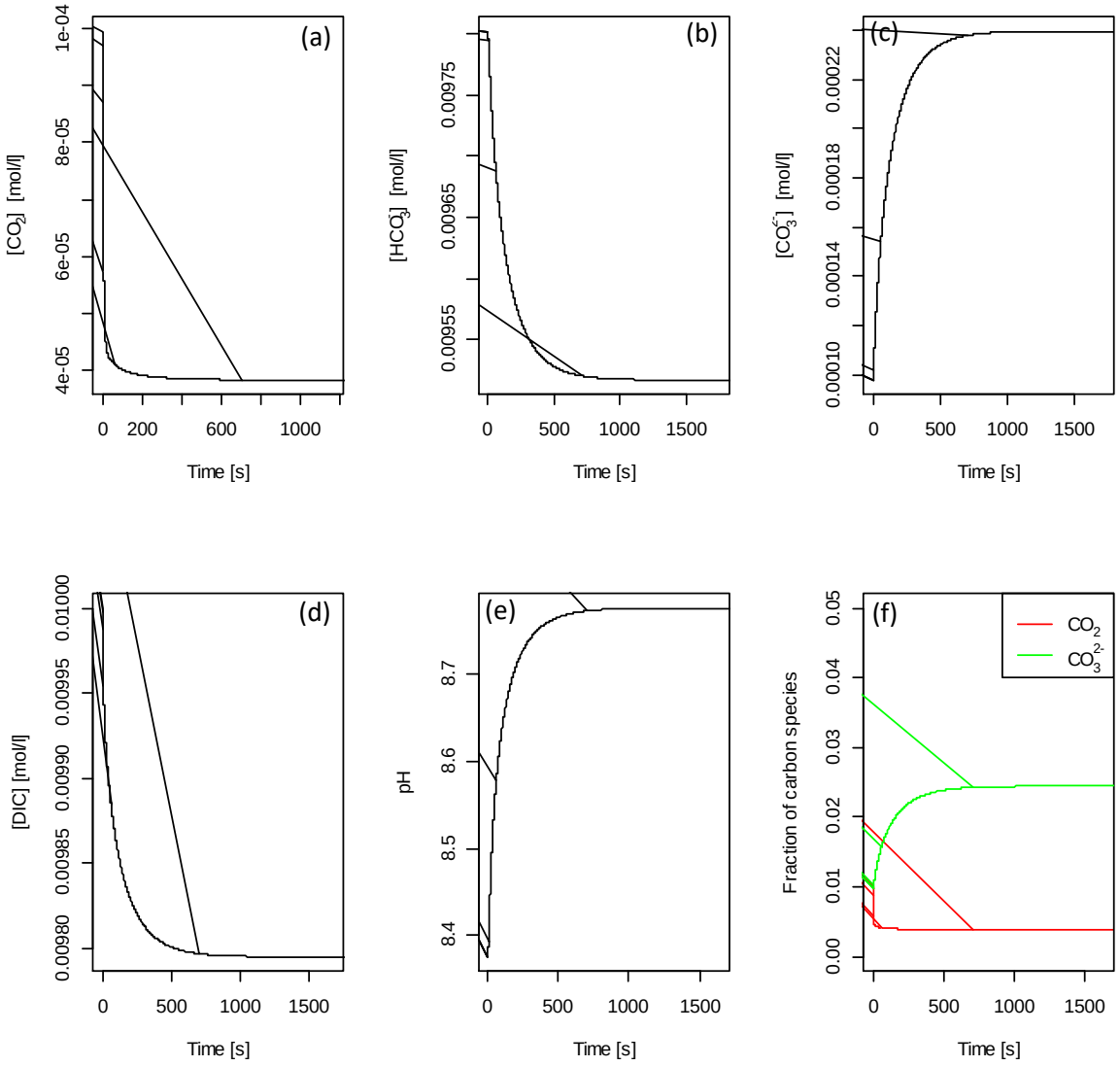

Fig. 4.11: Temporal evolution of the concentration of the different carbon species, DIC, pH as well as the distribution of species for a 10 mmol/l $NaHCO_3$ solution, which is exposed to an atmosphere with a pCO_2 of 1000 ppmV. The time required to establish equilibrium is slightly different for the individual species, DIC and pH. This results in different scales on the x-axes.

4.5.1.2 $\delta^{13}C$-values

Fig. 4.12 shows a compilation of the $\delta^{13}C$ values of the bulk solution and the initial $\delta^{13}C$ values on the plate (i.e., at 0 cm distance of flow). All values are more negative than expected from the $\delta^{13}C$ value of the $NaHCO_3$ (-6 ‰) used to prepare the solutions. The effect is more pronounced for lower concentrations of $NaHCO_3$ and higher pCO_2 (Fig. 4.12). In addition, the initial $\delta^{13}C$ values on the plate are generally lower than the corresponding $\delta^{13}C$ values of the bulk solution. For lower concentrations of $NaHCO_3$, the $\delta^{13}C$ values of the experiments conducted at different temperatures show a higher variability than at higher concentrations (Fig. 4.12). However, a systematic dependence on temperature is not visible, even if the lowest $\delta^{13}C$ values are observed for 30 °C and 1 mmol/l $NaHCO_3$. For the bulk solution samples, the effect is probably related to the sampling technique. The bulk solution was sampled using a Luer-Lock® syringe and then transferred via a small funnel into a 5 ml test glass in the sewer port. During injection of the solution into the test glass trough the funnel, the solution is unavoidably exposed to the box atmosphere for a short time (ca. 5 s). Since diffusion of CO_2 is fast (Hansen et al., 2013), carbon isotope exchange between the solution and the very negative box atmosphere ($\delta^{13}C$ = -37 ‰) during this short time span cannot be avoided. The effect of carbon isotope exchange is larger for lower concentrations of $NaHCO_3$ and higher pCO_2 and results in a negative shift of the $\delta^{13}C$ values of the DIC by up to -6.5 ‰ (Fig. 4.12).

The initial $\delta^{13}C$ values on the plate are consistently lower than the corresponding $\delta^{13}C$ values of the bulk solution (Fig. 4.12). In this case, the $NaHCO_3$ solution drips onto the very end of the glass plate and then into the funnel and the sewer port for sampling (Fig. 4.1). Even if the drip height was low (1 cm) in our experiments, splashing effects when the drip hits the plate cannot be excluded. During splashing, the drip breaks up into micro-droplets, which have a substantially larger ratio between surface and volume and thus a much higher potential for carbon isotope exchange driven by diffusion (Day and Henderson, 2011; Day and Henderson, 2013; Deininger et al., 2012; Mühlinghaus et al., 2007, 2009). For the higher concentrations of $NaHCO_3$ (> 5 mmol/l), the difference between the initial $\delta^{13}C$ values on the plate and the corresponding $\delta^{13}C$ values of the bulk solution is less than 1 ‰ (Fig. 4.12). For the lower concentrations, the effect may amount to 2-3 ‰ (Fig. 4.12), highlighting that splashing effects may, indeed, promote the effects of carbon isotope exchange driven by diffusion. However, in general, the effects of carbon isotope exchange due to splashing are lower than the general effects during the sampling procedure.

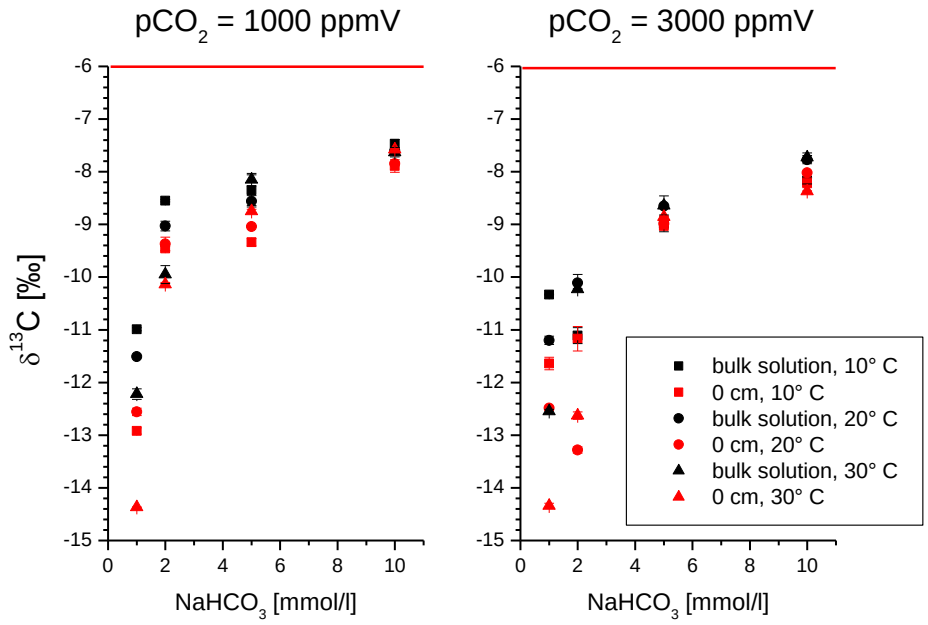

Fig. 4.12: Compilation of the $\delta^{13}C$ values of the bulk solution and the initial $\delta^{13}C$ values on the plate (i.e., at 0 cm distance of flow) against the concentration of $NaHCO_3$. The left panel shows the experiments conducted at a pCO_2 of 1000 ppmV, the right panel corresponds to 3000 ppmV. Different experimental temperatures are represented by different plot symbols.

We emphasize that this shift in the initial $\delta^{13}C$ values should not have an effect on the temporal evolution of isotope exchange, which is independent of the absolute $\delta^{13}C$ values. To account for this effect when comparing the experimental with model data, we used the experimentally observed initial $\delta^{13}C$ values as initial $\delta^{13}C$ values for the modeling. Figures 4.9a and b show the experimental data in comparison to the model predictions for two experiments conducted with a 2 mmol/L $NaHCO_3$ solution at 20°C and 1000 ppmV CO_2 (Fig. 4.9a, experiment #11, Table S4.1) as well as a 10 mmol/L $NaHCO_3$ solution at 20°C and 1000 ppmV CO_2 (Fig. 4.9b, experiment #9, Table S4.1). The black lines show the model data using the experimentally observed initial $\delta^{13}C$ values, the blue lines correspond to the model using the $\delta^{13}C$ value of the $NaHCO_3$, which was used for the preparation of the solutions (-6 ‰). It is clearly visible that the model and the experimental data show a similar evolution, independent of the initial $\delta^{13}C$ value of the solution. For experiment #11, the model agrees with the experimental data, except for the data points at a residence time of ca. 450 s, which plot slightly above the model curve (Fig. 4.9a). Even the fast decrease in the $\delta^{13}C$ values at the beginning of the plate, which is the result of the fast diffusion of CO_2 into the film, is reproduced by the data. For experiment #9, the experimental data plot ca. 0.5 ‰ below the model data, but show a similar trend (Fig. 4.9b). These two experiments

are representative of the whole data set. This confirms that our new exchange model adequately describes the temporal evolution of the $\delta^{13}C$ values and that the time constants for carbon isotope exchange between atmospheric CO_2 and the DIC in the thin solution film are reliable. It also confirms the applicability of the rate and diffusion constants used for the model (Tables S4.2 and S4.4).

We also applied our new model to the previous experiments by Dreybrodt et al. (2016). The main differences between their and the new experiments are that they used thicker, stagnant solution films in petri dishes and much longer residence times. The temporal evolution of the $\delta^{13}C$ values of their experiments is also well described by the new model (Fig. 4.13a). The experiments conducted in a desiccator show a similar temporal evolution as predicted by the model, but an offset of the equilibrium $\delta^{13}C$ value of up to +5 ‰ (Fig. 4.13b). This is caused by degassing of CO_2 during sampling and has been extensively discussed by Dreybrodt at al. (2016). For instance, at 25,000 ppmV CO_2 for a 5 mmol/l $NaHCO_3$ solution, about 16 % of the DIC are provided by aqueous CO_2, which degasses almost instantaneously when the solution is taken out of the desiccator.

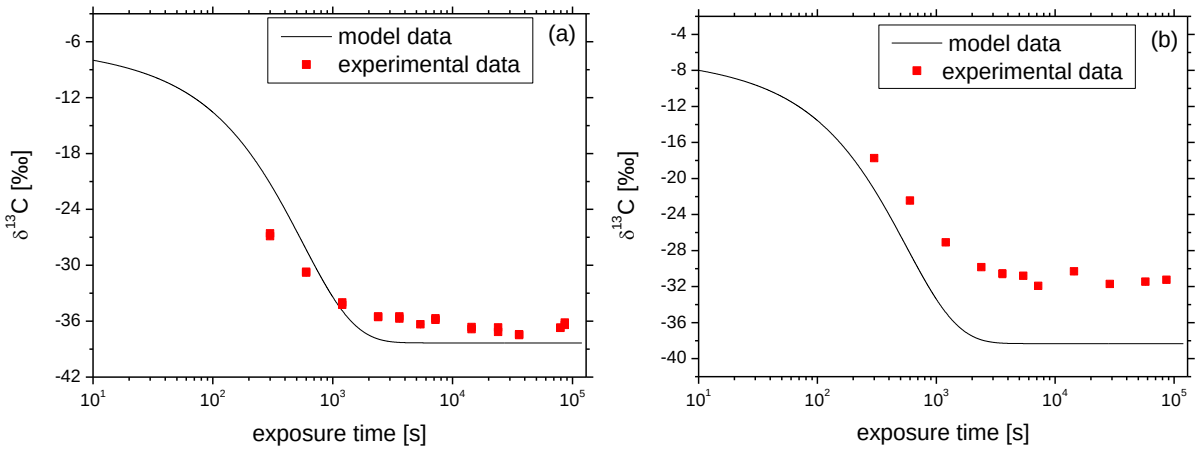

Fig. 4.13: (a) Comparison of experiments by Dreybrodt et al. (2016) with the new model, shown on a logarithmic x-axis. Temporal evolution of the $\delta^{13}C$ values for an experiment conducted in the climate box using a 5 mmol/l $NaHCO_3$ solution at 20°C, 25,000 ppmV CO_2 and a film thickness of 0.06 cm. (b) Corresponding experiment conducted in a desiccator.

In general, the good agreement of the model and the experimental data from this study and the previous experiments confirms that the new model adequately describes the temporal evolution of the $\delta^{13}C$ values of a thin film affected by isotope exchange.

4.5.2 Comparison with the approach of Dreybrodt et al. (2016)

The time constants calculated by our new model for all experiments of this study are given in Table 4.1. For comparison, the time constants calculated by the approach of Dreybrodt et al. (2016) are also shown. Figure 4.14 shows a comparison of the time constants for isotope exchange, τ_{ex}, calculated by the two models as a function of temperature, film thickness, concentration of HCO_3^- and pCO_2. In general, the magnitude of τ_{ex}, as calculated by both models, is similar. In addition, the dependence on film thickness and temperature is similar. In detail, however, the dependence on film thickness is slightly different for the two models. Whereas our new model calculates shorter exchange times for thin films, it calculates longer ones than the Dreybrodt et al. (2016) model for thicker films (Fig. 4.14c). More importantly, the two models show substantial deviations (up to 4000 s, i.e. more than 1 h) for the dependence of τ_{ex} on the concentration of dissolved HCO_3^- and pCO_2 (Figs. 4.14b and d). In particular, for low pCO_2 (Fig. 4.14b) and high concentrations of dissolved HCO_3^- (Fig. 4.14d), the time constants calculated by both models are substantially different. This suggests that isotope exchange may be much faster than suggested by the model of Dreybrodt et al. (2016). This is particularly important since most cave systems are characterized by seasonally low pCO_2 values (e.g., Breitenbach et al., 2015; Riechelmann et al., 2011; Spötl et al., 2005; Verheyden et al., 2008).

The approach of Dreybrodt et al. (2016) considers two processes: (i) diffusion of gaseous CO_2 into and out of the thin film of solution, and (ii) conversion of dissolved CO_2 to HCO_3^- according to Eq. (4.1). The time constant for carbon isotope exchange, τ_{ex}, is given by:

$$\tau_{ex} = \frac{\frac{d^2}{D_{CO_2}}}{\sqrt{\frac{k_{+1}d^2}{D_{CO_2}}}\tanh\left(\sqrt{\frac{k_{+1}d^2}{D_{CO_2}}}\right)} * \frac{[HCO_3^-]}{\left[K_H * p_{CO_2}\right]}, \tag{4.25}$$

where d is the film thickness, k_{+1} the corresponding rate constant for the conversion of CO_2 into HCO_3^-, D_{CO_2} the diffusion coefficient of CO_2, $[HCO_3^-]$ the concentration of dissolved bicarbonate, K_H Henry's constant and p_{CO_2} the partial pressure of the atmospheric CO_2.

For derivation of Eq. (4.25), Dreybrodt et al. (2016) assumed that the concentration of dissolved HCO_3^- remains constant during carbon isotope exchange. Thus, they assumed a classical "isotope exchange" scenario, which requires conditions of chemical equilibrium (compare section 4.3.4). However, as shown by our model, substantial shifts in pH, the concentrations of the individual species of DIC and their $\delta^{13}C$ values are possible. In addition, Dreybrodt et al. (2016) have not considered the second reaction converting dissolved CO_2 into HCO_3^-, which becomes relevant for high concentrations of OH^- and, thus, high pH values (Eq. (4.2)). This is the case for

low pCO_2 and/or high concentrations of HCO_3^-, the conditions showing the largest difference between the new model and their approach (Table 4.1). We discuss the effect of these two limitations using three extreme examples.

Table 4.1: Comparison of the time constants for the exchange, τ_{ex}, calculated by our model and the approach by Dreybrodt et al. (2016). Values are given for all experiments of this study and the experiments presented by Dreybrodt et al. (2016), which are marked by an asterisk.

[$NaHCO_3$] [mmol/l]	pCO_2 [ppmV]	T [°C]	Film thickness [mm]	τ_{new} [s]	$\tau_{Dreybrodt}$ [s]
1	1000	10	0.12	2465	2557
2	1000	10	0.12	4725	5115
5	1000	10	0.12	10333	12787
10	1000	10	0.12	15769	25573
1	1000	20	0,14	1154	1197
2	1000	20	0,14	2189	2394
5	1000	20	0,14	4752	5968
10	1000	20	0,14	7876	11972
1	1000	30	0.13	670	714
2	1000	30	0.13	1252	1429
5	1000	30	0.13	2613	5918
10	1000	30	0.13	4180	7146
1	3000	10	0.12	839	852
2	3000	10	0.12	1669	1705
5	3000	10	0.12	3999	4262
10	3000	10	0.12	7426	8524
1	3000	20	0.14	392	399
2	3000	20	0.14	778	798
5	3000	20	0.14	1853	1995
10	3000	20	0.14	3414	3991
1	3000	30	0.13	233	238
2	3000	30	0.13	458	476
5	3000	30	0.13	1067	1191
10	3000	30	0.13	1914	2382
5*	25,000	room temp	0.6	556	507
10*	25,000	room temp	0.6	1063	1013
5*	12,500	room temp	0.6	1064	1013
5*	25,000	room temp	0.89	882	723
5*	25,000	20	0.13	232	237
5*	500	20	0.13	7739	11837
5*	25,000	20	0.6	556	507
5*	25,000	20	2	2753	1653

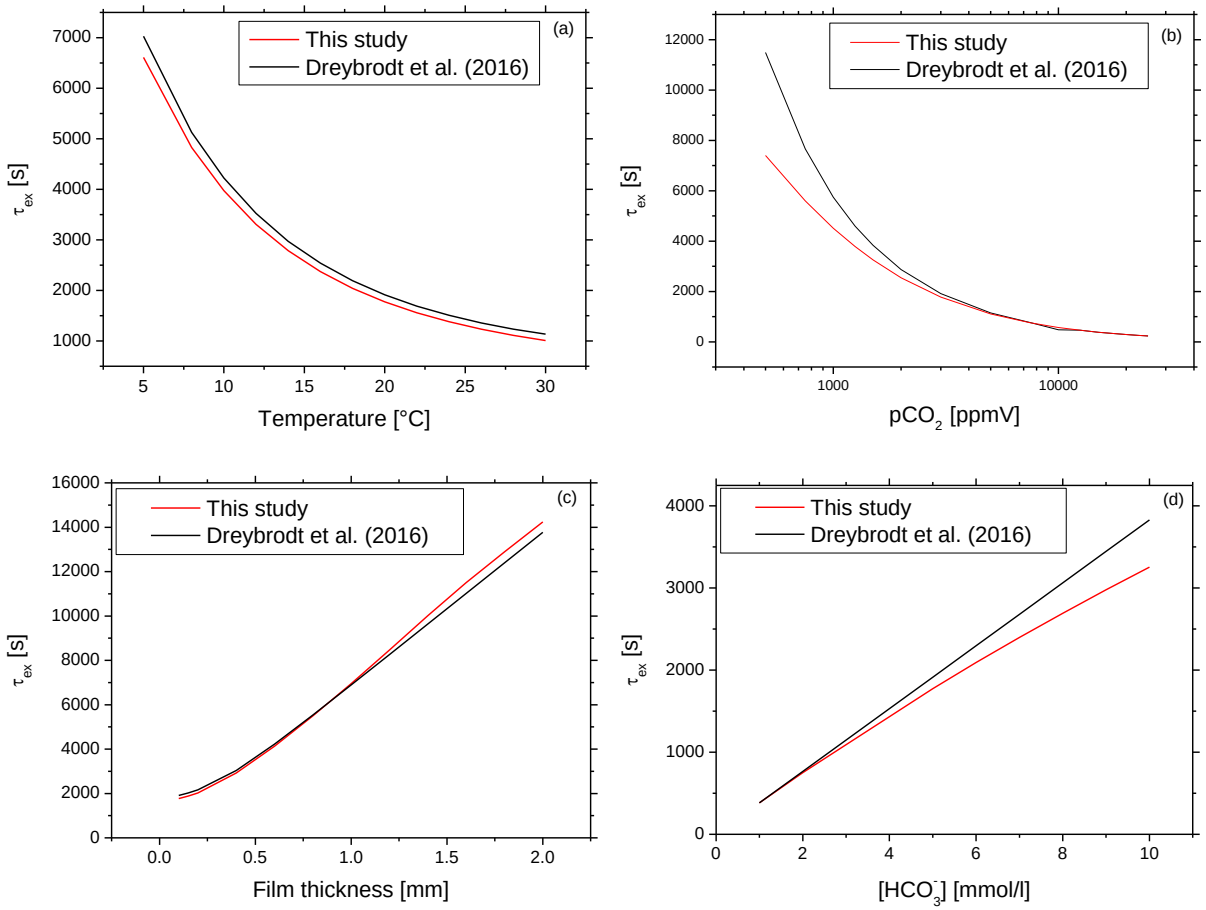

Fig. 4.14: Comparison of the time constant for carbon isotope exchange between gaseous CO_2 and the DIC in the thin solution film, τ_{ex}, calculated by our new model and the approach used by Dreybrodt et al. (2016). As an example, we show the evolution for a temperature of 20 °C, a HCO_3^- concentration of 5 mmol/l, 3000 ppmV CO_2 and a film thickness of 0.01 cm. (a) dependence on temperature; (b) dependence on pCO_2 on a logarithmic scale; (c) dependence on film thickness; (d) dependence on [HCO_3^-].

As a first example, we use a thin film containing 5 mmol/l $NaHCO_3$ and equilibrate it with a pCO_2 of 3000 ppmV. The $\delta^{13}C$ value of the gaseous CO_2 is -14.5 ‰. Subsequent to chemical equilibration, this solution contains 4.96 mmol/l of dissolved HCO_3^-, which is 1 % less than the initial concentration of $NaHCO_3$. This solution is then exposed to an atmosphere with the same pCO_2 (3000 ppmV), but with a lower $\delta^{13}C$ value of -45 ‰. Thus, this is an example for pure isotope exchange. Our model calculates a carbon isotope exchange time of 1773 s, whereas the approach of Dreybrodt et al. (2016) predicts an exchange time of 1915 s, which is higher by 8 %. This relatively large discrepancy between the two models cannot be explained by the small difference between the $NaHCO_3$ and the HCO_3^- concentration of ca. 1 %.

In a second example, we use a thin film of a pure 5 mmol/l $NaHCO_3$ solution with a $\delta^{13}C$ value of -6 ‰. After chemical equilibration, the concentration of dissolved HCO_3^- is 4.9 mmol/l. This solution is then exposed to an atmosphere with a high pCO_2 of 25,000 ppmV with a low $\delta^{13}C$ value of -45 ‰. For this scenario, the approach of Dreybrodt et al. (2016) yields almost the same carbon isotope exchange time ($\tau_{ex} = 230$ s) as our model (225 s). Due to the high pCO_2, the pH is relatively low for this example (7.1). Thus, the second reaction converting dissolved CO_2 into HCO_3^- (Eq. (4.2)) is of minor importance.

Finally, in a third example, we use a thin film of a pure 10 mmol/l $NaHCO_3$ solution with a $\delta^{13}C$ value of -6 ‰. After chemical equilibration, the concentration of dissolved HCO_3^- is 9.8 mmol/l. This solution is then exposed to an atmosphere with a pCO_2 of 1,000 ppmV with a low $\delta^{13}C$ value of -45 ‰. The carbon isotope exchange time calculated by our model is 7,399 s, whereas the approach of Dreybrodt et al. (2016) calculates a substantially longer exchange time of 11,488 s. Due to the low pCO_2, pH increases to 8.8 during the experiment. In this case (high concentration of OH^-), conversion of dissolved CO_2 into HCO_3^- is dominated by Eq. (4.2). Thus, this is obviously the major reason for the observed differences between the two models (Fig. 4.14).

4.5.3 Implications for the interpretation of speleothem $\delta^{13}C$ data

Carbon isotope exchange between the thin solution film on the speleothem surface and the CO_2 of the cave atmosphere may be recorded in the $\delta^{13}C$ values of the precipitated calcite. However, the effect is only relevant if the rate of isotope exchange is in the range of or faster than the precipitation rate of calcite. If precipitation occurs at a much faster rate than isotope exchange, the $\delta^{13}C$ values of the precipitated calcite will reflect the $\delta^{13}C$ values of the dissolved HCO_3^- prior to isotope exchange. Since we calculated significantly lower time constants for carbon isotope exchange than Dreybrodt et al. (2016), in particular for conditions closer to cave systems, isotope exchange might have an influence at an earlier stage. If a solution containing 5 mmol/l of HCO_3^- (corresponding to 2.5 mmol/l $[Ca^{2+}]$, i.e. the equilibrium value established for a soil pCO_2 of 25,000 ppmV) equilibrated with a soil $\delta^{13}C$ value of -20 ‰ is exposed to an atmosphere with a pCO_2 of 500 ppmV and a cave CO_2 $\delta^{13}C$ value of -8.5 ‰, the time constant for carbon isotope exchange between the atmosphere and the solution film, τ_{ex}, is 7,362 s. This is still very large (ca. 2 h) and would only have an effect for very slowly dripping sites. In addition, such a solution is strongly supersaturated with respect to calcite (the saturation index with respect to calcite would be 1.6) and immediately starts precipitating $CaCO_3$. The time constant for the precipitation of calcite, which is given by $\tau_{pr} = d/\alpha$, where d is the film thickness and α a kinetic constant (Baker

et al., 1998; Dreybrodt and Scholz, 2011), is 343 s for our example. Thus, >99 % of the calcite would have been precipitated after 5 τ_{pr} (i.e. 1,700 s). During this time interval, only 21 % of the total carbon isotope exchange has occurred (Eq. 4.23). For this example, carbon isotope exchange would, thus, only be relevant if large amounts of the new drops impinging on the surface of the stalagmite would be lost by splashing, which results in (i) very slow replacement/refreshment of the existing film, (ii) low supersaturation and (iii) slow precipitation rates. A speleothem growing under such conditions would show a very slow growth rate and a small diameter. Such a sample could be of interest for the reconstruction of past changes in the $\delta^{13}C$ value of cave air CO_2 and thus cave ventilation, which in turn may have an effect on .speleothem $\delta^{13}C$, $\delta^{18}O$ and trace element signals (Johnson et al., 2006; Mattey et al., 2010; Spötl et al., 2005; Wong et al., 2011).

4.6 Conclusions

We present results of new experiments examining carbon isotope exchange between gaseous CO_2 and the DIC in thin solution films on speleothem surfaces. In addition, we introduce a new complete diffusion reaction model, which considers all parameters affecting carbon isotope exchange, i.e. diffusion into, out of and within the film, chemical reactions occurring within the film, as described by the corresponding rate constants, as well as the dependence of diffusion and reaction rates on isotopic mass. The model and the experimental data are in good agreement. For low pCO_2 (i.e., between 500 and 1000 ppmV), as observed in many cave systems, the time constants calculated by our model are shorter than estimated by an alternative approach. (Dreybrodt et al., 2016).

For the interpretation of speleothem paleoclimate records, carbon isotope exchange may have an influence on the $\delta^{13}C$ values in case of very long drip intervals and slow precipitation rates. In addition, isotope exchange could be relevant if large amounts of drip water impinging on the speleothem surface are lost by splashing. Thus, cave monitoring programs studying present-day cave conditions (e.g., drip rate, drip water chemistry and cave pCO_2) are of great importance to assess the potential influence of carbon isotope exchange processes.

Acknowledgements

M. Hansen and D. Scholz acknowledge funding by the Deutsche Forschungsgemeinschaft (DFG) through grants SCHO 1274/8-1 and SCHO 1274/9-1. We thank Wolfgang Dreybrodt for discussion and comments on a previous version of the manuscript. Furthermore we are thankful to the workshop of the Institutes for Geosciences and Physics of the Atmosphere, University of Mainz, especially S. Klumb, for technical support during the experiments and to keep the climate box running reliably. Constructive and thorough comments by three anonymous reviewers were extremely helpful to improve the manuscript.

4.7 References

Baker, A., Genty, D., Dreybrodt, W., Barnes, W.L., Mockler, N.J., Grapes, J. (1998) Testing Theoretically Predicted Stalagmite Growth Rate with Recent Annually Laminated Samples: Implications for Past Stalagmite Deposition. Geochimica et Cosmochimica Acta **62**, 393-404.

Baldini, J.U.L., McDermott, F., Hoffmann, D.L., Richards, D.A., Clipson, N. (2008) Very high-frequency and seasonal cave atmosphere P_{CO2} variability: Implications for stalagmite growth and oxygen isotope-based paleoclimate records. Earth and Planetary Science Letters **272**, 118-129.

Breitenbach, S.F.M., Lechleitner, F.A., Meyer, H., Diengdoh, G., Mattey, D., Marwan, N. (2015) Cave ventilation and rainfall signals in dripwater in a monsoonal setting – a monitoring study from NE India. Chemical Geology **402**, 111-124.

Cerling, T.E. (1984) The stable isotopic composition of modern soil carbonate and its relationship to climate. Earth and Planetary Science Letters **71**, 229-240.

Cheng, H., Edwards, R.L., Sinha, A., Spötl, C., Yi, L., Chen, S., Kelly, M., Kathayat, G., Wang, X., Li, X., Kong, X., Wang, Y., Ning, Y., Zhang, H. (2016) The Asian monsoon over the past 640,000 years and ice age terminations. Nature **534**, 640-646.

Day, C.C., Henderson, G.M. (2011) Oxygen isotopes in calcite grown under cave-analogue conditions. Geochimica et Cosmochimica Acta **75**, 3956-3972.

Day, C.C., Henderson, G.M. (2013) Controls on trace-element partitioning in cave-analogue calcite. Geochimica et Cosmochimica Acta **120**, 612-627.

Deininger, M., Fohlmeister, J., Scholz, D., Mangini, A. (2012) Isotope disequilibrium effects: The influence of evaporation and ventilation effects on the carbon and oxygen isotope composition of speleothems – A model approach. Geochimica et Cosmochimica Acta **96**, 57-79.

Dorale, J.A., Edwards, R.L., Ito, E., González, L.A. (1998) Climate and Vegetation History of the Midcontinent from 75 to 25 ka: A Speleothem Record from Crevice Cave, Missouri, USA. Science **282**, 1871-1874.

Dreybrodt, W. (2008) Evolution of the isotopic composition of carbon and oxygen in a calcite precipitating $H_2O–CO_2–CaCO_3$ solution and the related isotopic composition of calcite in stalagmites. Geochimica et Cosmochimica Acta **72**, 4712-4724.

Dreybrodt, W., Hansen, M., Scholz, D. (2016) Processes affecting the stable isotope composition of calcite during precipitation on the surface of stalagmites: Laboratory experiments investigating the isotope exchange between DIC in the solution layer on top of a speleothem and the CO_2 of the cave atmosphere. Geochimica et Cosmochimica Acta **174**, 247-262.

Dreybrodt, W., Scholz, D. (2011) Climatic dependence of stable carbon and oxygen isotope signals recorded in speleothems: From soil water to speleothem calcite. Geochimica et Cosmochimica Acta **75**, 734-752.

Eigen, M. (1964) Proton Transfer, Acid-Base Catalysis, and Enzymatic Hydrolysis. Part I: ELEMENTARY PROCESSES. Angewandte Chemie International Edition in English **3**, 1-19.

Fohlmeister, J., Scholz, D., Kromer, B., Mangini, A. (2011) Modelling carbon isotopes of carbonates in cave drip water. Geochimica et Cosmochimica Acta **75**, 5219-5228.

Frisia, S., Borsato, A., Spötl, C., Villa, I.M., Cucchi, F. (2005) Climate variability in the SE Alps of Italy over the past 17 000 years reconstructed from a stalagmite record. Boreas **34**, 445-455.

Frisia, S., Fairchild, I.J., Fohlmeister, J., Miorandi, R., Spötl, C., Borsato, A. (2011) Carbon mass-balance modelling and carbon isotope exchange processes in dynamic caves. Geochimica et Cosmochimica Acta **75**, 380-400.

Gázquez, F., Quindós-Poncela, L., Sainz-Fernández, C., Fernández-Villar, A., Fuente-Merino, I., Celaya-Gonzalez, S. (2016) Spatiotemporal distribution of $\delta^{13}C_{CO2}$ in a shallow cave and its potential use as indicator of anthropic pressure. Journal of Environmental Management **180**, 421-432.

Genty, D., Blamart, D., Ouahdi, R., Gilmour, M., Baker, A., Jouzel, J., Van-Exter, S. (2003) Precise dating of Dansgaard-Oeschger climate oscillations in western Europe from stalagmite data. Nature **421**, 833-837.

Hansen, M., Dreybrodt, W., Scholz, D. (2013) Chemical evolution of dissolved inorganic carbon species flowing in thin water films and its implications for (rapid) degassing of CO_2 during speleothem growth. Geochimica et Cosmochimica Acta **107**, 242-251.

Hellstrom, J., McCulloch, M., Stone, J. (1998) A Detailed 31,000-Year Record of Climate and Vegetation Change, from the Isotope Geochemistry of Two New Zealand Speleothems. Quaternary Research **50**, 167-178.

Hendy, C.H. (1971) The isotopic geochemistry of speleothems—I. The calculation of the effects of different modes of formation on the isotopic composition of speleothems and their applicability as palaeoclimatic indicators. Geochimica et Cosmochimica Acta **35**, 801-824.

Jähne, B., Heinz, G., Dietrich, W. (1987) Measurement of the diffusion coefficients of sparingly soluble gases in water. Journal of Geophysical Research: Oceans **92**, 10767-10776.

Johnson, K.R., Lynn Ingram, B., Sharp, W.D., Zhang, P. (2006) East Asian summer monsoon variability during Marine Isotope Stage 5 based on speleothem $\delta^{18}O$ records from Wanxiang Cave, central China. Palaeogeography, Palaeoclimatology, Palaeoecology **236**, 5-19.

Johnson, K.S. (1982) Carbon dioxide hydration and dehydration kinetics in seawater. Limnol. Oceanogr **27**, 849-855.

Keeling, C.D.P., S. C.; Bacastow, R. B.; Wahlen, M.; Whorf, T. P.; Heimann, M.; Meijer, H. A., 2005. Atmospheric CO_2 and $^{13}CO_2$ exchange with the terrestrial biosphere and oceans from 1978 to 2000: observations and carbon cycle implications A history of Atmospheric CO_2 and its effects on Plants Animals and Ecosystems. Springer Verlag, New York, pp. 83 - 113.

Kowalczk, A.J., Froelich, P.N. (2010) Cave air ventilation and CO_2 outgassing by radon-222 modeling: How fast do caves breathe? Earth and Planetary Science Letters **289**, 209-219.

Li, Y.-H., Gregory, S. (1974) Diffusion of ions in sea water and in deep-sea sediments. Geochimica et Cosmochimica Acta **38**, 703-714.

Mandić, M., Mihevc, A., Leis, A., Bronić, I.K. (2013) Concentration and stable carbon isotopic composition of CO_2 in cave air of Postojnska jama, Slovenia. International Journal of Speleology **42**, 279-287.

Mangini, A., Spötl, C., Verdes, P. (2005) Reconstruction of temperature in the Central Alps during the past 2000 yr from a $\delta^{18}O$ stalagmite record. Earth and Planetary Science Letters **235**, 741-751.

Mattey, D., Lowry, D., Duffet, J., Fisher, R., Hodge, E., Frisia, S. (2008) A 53 year seasonally resolved oxygen and carbon isotope record from a modern Gibraltar speleothem: Reconstructed drip water and relationship to local precipitation. Earth and Planetary Science Letters **269**, 80-95.

Mattey, D.P., Fairchild, I.J., Atkinson, T.C., Latin, J.-P., Ainsworth, M., Durell, R. (2010) Seasonal microclimate control of calcite fabrics, stable isotopes and trace elements in modern speleothem from St Michaels Cave, Gibraltar. Geological Society, London, Special Publications **336**, 323-344.

McDermott, F. (2004) Palaeo-climate reconstruction from stable isotope variations in speleothems: a review. Quaternary Science Reviews **23**, 901-918.

McKinney, C.R., McCrea, J.M., Epstein, S., Allen, H.A., Urey, H.C. (1950) Improvements in Mass Spectrometers for the Measurement of Small Differences in Isotope Abundance Ratios. Review of Scientific Instruments **21**, 724-730.

Meyer, K.W., Feng, W., Breecker, D.O., Banner, J.L., Guilfoyle, A. (2014) Interpretation of speleothem calcite $\delta^{13}C$ variations: Evidence from monitoring soil CO_2, drip water, and modern speleothem calcite in central Texas. Geochimica et Cosmochimica Acta **142**, 281-298.

Mickler, P.J., Stern, L.A., Banner, J.L. (2006) Large kinetic isotope effects in modern speleothems. GSA Bulletin **118**, 65-81.

Mischel, S.A., Scholz, D., Spötl, C., Jochum, K.P., Schröder-Ritzrau, A., Fiedler, S. (2016) Holocene climate variability in Central Germany and a potential link to the polar North Atlantic: A replicated record from three coeval speleothems. The Holocene.

Mook, W.G., Bommerson, J.C., Staverman, W.H. (1974) Carbon isotope fractionation between dissolved bicarbonate and gaseous carbon dioxide. Earth and Planetary Science Letters 22, 169-176.

Mook, W.G., De Vries, J. (2000) Volume I: Introduction: Theory, Methods, Review. Environmental Isotopes in the Hydrological Cycle—Principles and Applications, International Hydrological Programme (IHP-V), Technical Documents in Hydrology (IAEA/UNESCO) No **39**, 75-76.

Mühlinghaus, C., Scholz, D., Mangini, A. (2007) Modelling stalagmite growth and $\delta^{13}C$ as a function of drip interval and temperature. Geochimica et Cosmochimica Acta **71**, 2780-2790.

Mühlinghaus, C., Scholz, D., Mangini, A. (2009) Modelling fractionation of stable isotopes in stalagmites. Geochimica et Cosmochimica Acta **73**, 7275-7289.

Nordstrom, D.K., Plummer, L.N., Langmuir, D., Busenberg, E., May, H.M., Jones, B.F., Parkhurst, D.L., 1990. Revised chemical equilibrium data for major water-mineral reactions and their limitations, ACS symposium series. Oxford University Press, pp. 398-413.

O'Leary, M.H., Madhavan, S., Paneth, P. (1992) Physical and chemical basis of carbon isotope fractionation in plants. Plant, Cell & Environment 15, 1099-1104.

Polag, D., Scholz, D., Mühlinghaus, C., Spötl, C., Schröder-Ritzrau, A., Segl, M., Mangini, A. (2010) Stable isotope fractionation in speleothems: Laboratory experiments. Chemical Geology 279, 31-39.

R Core Team, 2016. R: A Language and Environment for Statistical Computing. R Foundation for Statistical Computing, Vienna, Austria.

Richards, D.A., Dorale, J.A. (2003) Uranium-series chronology and environmental applications of speleothems. Reviews in Mineralogy and Geochemistry **52**, 407-460.

Ridley, H.E., Asmerom, Y., Baldini, J.U.L., Breitenbach, S.F.M., Aquino, V.V., Prufer, K.M., Culleton, B.J., Polyak, V., Lechleitner, F.A., Kennett, D.J., Zhang, M., Marwan, N., Macpherson, C.G., Baldini, L.M., Xiao, T., Peterkin, J.L., Awe, J., Haug, G.H. (2015) Aerosol forcing of the position of the intertropical convergence zone since ad 1550. Nature Geosci **8**, 195-200.

Riechelmann, D.F.C., Deininger, M., Scholz, D., Riechelmann, S., Schröder-Ritzrau, A., Spötl, C., Richter, D.K., Mangini, A., Immenhauser, A. (2013) Disequilibrium carbon and oxygen isotope fractionation in recent cave calcite: Comparison of cave precipitates and model data. Geochimica et Cosmochimica Acta **103**, 232-244.

Riechelmann, D.F.C., Schröder-Ritzrau, A., Scholz, D., Fohlmeister, J., Spötl, C., Richter, D.K., Mangini, A. (2011) Monitoring Bunker Cave (NW Germany): A prerequisite to interpret geochemical proxy data of speleothems from this site. Journal of Hydrology **409**, 682-695.

Rudzka, D., McDermott, F., Baldini, L.M., Fleitmann, D., Moreno, A., Stoll, H. (2011) The coupled $\delta^{13}C$-radiocarbon systematics of three Late Glacial/early Holocene speleothems; insights into soil and cave processes at climatic transitions. Geochimica et Cosmochimica Acta **75**, 4321-4339.

Salomons, W., Mook, W. (1986) Isotope geochemistry of carbonates in the weathering zone. Handbook of environmental isotope geochemistry **2**, 239-269.

Scholz, D., Frisia, S., Borsato, A., Spötl, C., Fohlmeister, J., Mudelsee, M., Miorandi, R., Mangini, A. (2012) Holocene climate variability in north-eastern Italy: potential influence of the NAO and solar activity recorded by speleothem data. Clim. Past **8**, 1367-1383.

Scholz, D., Hoffmann, D.L. (2008) ^{230}Th/U-dating of fossil reef corals and speleothems. E&G Quaternary Science Journal **57**, 52-77.

Scholz, D., Mühlinghaus, C., Mangini, A. (2009) Modelling $\delta^{13}C$ and $\delta^{18}O$ in the solution layer on stalagmite surfaces. Geochimica et Cosmochimica Acta **73**, 2592-2602.

Schulz, K.G., Riebesell, U., Rost, B., Thoms, S., Zeebe, R.E. (2006) Determination of the rate constants for the carbon dioxide to bicarbonate inter-conversion in pH-buffered seawater systems. Marine Chemistry **100**, 53-65.

Soetaert, K., Cash, J., Mazzia, F. (2012) Solving differential equations in R. Springer Science & Business Media.

Soetaert, K., Meysman, F. (2012) Reactive transport in aquatic ecosystems: Rapid model prototyping in the open source software R. Environmental Modelling & Software **32**, 49-60.

Soetaert, K.E.R., Petzoldt, T., Setzer, R.W. (2010) Solving differential equations in R: package deSolve. Journal of Statistical Software 33.

Spötl, C. (2004) A simple method of soil gas stable carbon isotope analysis. Rapid Communications in Mass Spectrometry **18**, 1239-1242.

Spötl, C., Fairchild, I.J., Tooth, A.F. (2005) Cave air control on dripwater geochemistry, Obir Caves (Austria): Implications for speleothem deposition in dynamically ventilated caves. Geochimica et Cosmochimica Acta **69**, 2451-2468.

Spötl, C., Vennemann, T.W. (2003) Continuous-flow isotope ratio mass spectrometric analysis of carbonate minerals. Rapid Communications in Mass Spectrometry **17**, 1004-1006.

Thode, H.G., Shima, M., Rees, C.E., Krishnamurty, K.V. (1965) CARBON-13 ISOTOPE EFFECTS IN SYSTEMS CONTAINING CARBON DIOXIDE, BICARBONATE, CARBONATE, AND METAL IONS. Canadian Journal of Chemistry **43**, 582-595.

Verheyden, S., Genty, D., Deflandre, G., Quinif, Y., Keppens, E. (2008) Monitoring climatological, hydrological and geochemical parameters in the Père Noël cave (Belgium): implication for the interpretation of speleothem isotopic and geochemical time-series. International Journal of Speleology **37**: p. 221-234.

Vogel, J.C., Grootes, P.M., Mook, W.G. (1970) Isotopic fractionation between gaseous and dissolved carbon dioxide. Zeitschrift für Physik **230**, 225-238.

Wackerbarth, A., Langebroek, P.M., Werner, M., Lohmann, G., Riechelmann, S., Borsato, A., Mangini, A. (2012) Simulated oxygen isotopes in cave drip water and speleothem calcite in European caves. Clim. Past **8**, 1781-1799.

Wiedner, E., Scholz, D., Mangini, A., Polag, D., Mühlinghaus, C., Segl, M. (2008) Investigation of the stable isotope fractionation in speleothems with laboratory experiments. Quaternary International **187**, 15-24.

Wong, C.I., Banner, J.L., Musgrove, M. (2011) Seasonal dripwater Mg/Ca and Sr/Ca variations driven by cave ventilation: Implications for and modeling of speleothem paleoclimate records. Geochimica et Cosmochimica Acta **75**, 3514-3529.

Wong, C.I., Banner, J.L., Musgrove, M. (2015) Holocene climate variability in Texas, USA: An integration of existing paleoclimate data and modeling with a new, high-resolution speleothem record. Quaternary Science Reviews **127**, 155-173.

Zeebe, R.E. (2011) On the molecular diffusion coefficients of dissolved CO_2, HCO_3^-, and CO_3^{2-} and and their dependence on isotopic mass. Geochimica et Cosmochimica Acta **75**, 2483-2498.

Zeebe, R.E., Bijma, J., Wolf-Gladrow, D.A. (1999a) A diffusion-reaction model of carbon isotope fractionation in foraminifera. Marine Chemistry **64**, 199-227.

Zeebe, R.E., Wolf-Gladrow, D. (2001) *CO_2 in Seawater: Equilibrium, Kinetics, Isotopes*. Amsterdam: Elsevier Science, B.V. 346 pp.

Zeebe, R.E., Wolf-Gladrow, D.A., Jansen, H. (1999b) On the time required to establish chemical and isotopical equilibrium in the carbon dioxide system in seawater. Marine Chemistry **65**, 135-153.

4.8 Supplementary information to "Carbon isotope exchange between gaseous CO_2 and thin solution films: Artificial cave experiments and a complete diffusion-reaction model".

Table S4.1: Overview of the experimental parameters of all experiments conducted within this study. $\delta^{13}C_{CO2}$ is the $\delta^{13}C$ value of the CO_2 of the box atmosphere during the experiment. Also shown are the experimentally observed $\delta^{13}C$ values for the DIC measurements at the beginning, $\delta^{13}C_{initial}$, and the end, $\delta^{13}C_{end}$, of the plate.

Experiment	[$NaHCO_3$] [mmol/l]	Temp [°C]	pCO_2 [ppmV]	$\delta^{13}C_{CO2}$ [‰]	$\delta^{13}C_{initial}$ [‰]	$\delta^{13}C_{end}$ [‰]
1	10	10	1000	-37.4	-12.9	-12.9
2	5	10	1000	-35.6	-9.5	-11.0
3	2	10	1000	-34.0	-9.3	-9.5
4	1	10	1000	-31.7	-7.9	-8.3
5	1	10	3000	-37.1	-11.6	-18.4
6	2	10	3000	-37.1	-11.2	-14.9
7	5	10	3000	-36.6	-9.0	-11.6
8	10	10	3000	-36.6	-8.2	-10.4
9	10	20	1000	-38.2	-12.6	-15.5
10	5	20	1000	-36.3	-9.4	-13.7
11	2	20	1000	-34.8	-8.6	-11.5
12	1	20 °	1000	-33.4	-7.9	-9.6
13	1	20	3000	-37.9	-12.5	-22.0
14	2	20	3000	-37.6	-13.3	-18.0
15	5	20	3000	-36.9	-9.0	-13.4
16	10	20	3000	-36.6	-8.0	-11.3
17	10	30	1000	-37.7	-14.4	-18.4
18	5	30	1000	-35.5	-10.1	-15.5
19	2	30	1000	-33.9	-8.8	-12.5
20	1	30	1000	-32.6	-7.5	-11.3
21	1	30	3000	-37.5	-14.3	-24.9
22	2	30	3000	-37.1	-12.6	-21.0
23	5	30	3000	-36.4	-8.9	-16.6
24	10	30	3000	-35.9	-8.4	-14.6

Table S4.2: Rate constants for the chemical reactions used in the model as well as their dependence on temperature.

Rate constant	Check value T = 293.15 K	Dependence on T	Reference
k_{+1}	0.02375 s^{-1}	exp(1246.98 - 6.19 * 10^4/T - 183 * ln(T))	Johnson (1982)
k'_{+1}	0.02345 s^{-1}	k_{+1}* 0.987	O'Leary et al.(1992)
k_{-1}	57231.08 kg mol^{-1} s^{-1}	k_{+1} / K_1	calculated
k'_{-1}	55948.46 kg mol^{-1} s^{-1}	k_{-1} * 0.987 * ($\varepsilon_{(CO2/HCO3)}$ / 1000 + 1)	calculated
k_{+4}	3454.087 kg mol^{-1} s^{-1}	A_4 * exp(-23.2 * 10^3/ R / T)	Johnson (1982)
k'_{+4}	3416.092 kg mol^{-1} s^{-}	k_{+4} * 0.989	Zeebe and Wolf-Gladrow (2001)
k_{-4}	5.649647 * 10^{-5} s^{-1}	k_{+4}* K_W / K_1	calculated
k'_{-4}	5.534223 * 10^{-5} s^{-1}	k_{-4} * 0.989 * ($\varepsilon_{(CO2/HCO3)}$ / 1000 + 1)	calculated
$k_{+5}^{H^+}$	5 * 10^{10} kg $mol^{-1}s^{-1}$	None	Eigen(1964)
$k'^{H^+}_{+5}$	5 * 10^{10} kg $mol^{-1}s^{-1}$	None	-
$k_{-5}^{H^+}$	2.105729 s^{-1}	$k_{+5}^{H^+}$ * K_5	calculated
$k'^{H^+}_{-5}$	2.104808 s^{-1}	$k_{-5}^{H^+}$ * ($\varepsilon_{(CO3/HCO3)}$ / 1000 + 1)	calculated
$k_{+5}^{OH^-}$	6 * 10^9 kg $mol^{-1}s^{-1}$	None	Eigen(1964)
$k'^{OH^-}_{+5}$	6 * 10^9 kg $mol^{-1}s^{-1}$	None	-
$k_{-5}^{OH^-}$	967243.6 s^{-1}	$k_{+5}^{OH^-}$ * K_w * K_2	calculated
$k'^{OH^-}_{-5}$	967666.9 s^{-1}	$k_{-5}^{OH^-}$ / ($\varepsilon_{(CO3/HCO3)}$ / 1000 + 1)	calculated
k_{+6}	1.4 * 10^{-3} mol kg^{-1} s^{-1}	None	Eigen (1964)
k_{-6}	2.0621 * 10^{11}	k_{+6}/ K_w	calculated
R	8.31451 J / mol	None	-
K_H	0.03835812 mol kg^{-1} atm^{-1}	3.3 * 10^{-4} * exp(2400 * (1 / T – 1 / 298.15)) * 101.325	Sander (2011)
A_4	4.7 * 10^7	None	Johnson (1982)
K_W	6.789177 * 10^{-15}	10^(-283,971 + 13323 / T - 0.05069842 * T + 102.24447 * $\log_{10}$(T) - 1119669 / T^2)	Nordstrom et al.(1990)
K_1	4.150774 * 10^{-7}	10^(-356.3094 - 0.06091964 * T + 21834.37 / T +126.8339 * $\log_{10}$(T) - 1684915 / T^2)	Nordstrom et al.(1990)
K_2	4.211458 * 10^{-11}	10^(-107.8871 - 0.03252849 * T + 5151.79 / T + 38.92561 * $\log_{10}$(T) - 563713.9 / T^2)	Nordstrom et al.(1990)

Table 4.3: Isotope fractionation factors used in the model and their dependence on temperature.

Fractionation	Check value T = 293.15 K [‰]	Dependence on T	Reference
$\varepsilon_{(CO2,aq/\ CO2,g)}$	-1.082386	-373 / T + 0.19	Vogel et al.(1970)
$\varepsilon_{(Diffusion,\ CO2)}$	-0.87	None	Jähne et al.(1987)
$\varepsilon_{(CO2/\ HCO3)}$	-9.535125	-9866 / T + 24.12	calculated
$\varepsilon_{(HCO3/CO2)}$	9.626919	(1 / ($\varepsilon_{(CO2/\ HCO3)}$ / 1000 + 1) - 1) * 1000	calculated
$\varepsilon_{(CO3/\ HCO3)}$	-0.4375303	-867 / T + 2.52	Thode et al.(1965)
$\varepsilon_{(CO2,g/\ HCO3)}$	-8.458627	-9483 / T + 23.89	Mook et al.(1974)
$\varepsilon_{(HCO3/CO2,g)}$	8.530786	(1 / ($\varepsilon_{(CO2,g/\ HCO3)}$ / 1000 + 1) - 1) * 1000	calculated
$\varepsilon_{(CO3/\ CO2,g)}$	8.089523	(((($\varepsilon_{(CO3/\ HCO3)}$ / 1000 + 1) * ($\varepsilon_{(HCO3/CO2,g)}$ / 1000 + 1)) – 1) * 1000	calculated

Table S4.4: Diffusion constants and their dependence on temperature.

Diffusion constant	Check value T = 293.15 K [cm²/s]	Dependence on T	Reference
D_{CO_2}	1.676235 * 10^{-5}	5019 * 10^{-5} * exp(-19.51 * 10^3 / R / T)	Jähne et al.(1987)
$D_{^{13}CO_2}$	1.674777 * 10^{-5}	($\varepsilon_{(Diffusion,\ CO2)}$ / 1000 + 1) * D_{CO_2}	calculated
$D_{HCO_3^-}$	9.657584 * 10^{-6}	7.0158 * 10^{-5} * ((T / 204.0282) - 1)$^{2.3942}$	Zeebe(2011)
$D_{CO_3^{2-}}$	7.072582 * 10^{-6}	- 5.4468 * 10^{-5} * ((T / 210.2646) - 1)$^{2.1929}$	Zeebe(2011)
D_{H^+}	8.528832 * 10^{-5}	-3.452133 * 10^{-4} + 1.468537 * 10^{-6} * T	Fitted based on the data of Li and Gregory(1974)
D_{OH^-}	4.719601 * 10^{-5}	-2.698935 * 10^{-4} + 1.081663 * 10^{-6} * T	Fitted based on the data of Li and Gregory(1974)

Table S4.5a: Results of the experiments conducted at 10 °C

Experiments 1000 ppmV																
10 mmol/l	Experiment No 1			5 mmol/l	Experiment No 2			2 mmol/l	Experiment No 3			1 mmol/l	Experiment No 4		
exposure time [s]	$pH_{experimental}$	$\delta^{13}C$ [‰]	± 1σ sd	exposure time [s]	$pH_{experimental}$	$\delta^{13}C$ [‰]	± 1σ sd	exposure time [s]	$pH_{experimental}$	$\delta^{13}C$ [‰]	± 1σ sd	exposure time [s]	$pH_{experimental}$	$\delta^{13}C$ [‰]	± 1σ sd
452	8.7	-8.32	0.15	452	8.5	-9.47	0.01	452	8.7	-10.97	0.11	452	8.0	-12.91	0.14
361	8.6	-8.31	0.16	361	8.4	-9.89	0.12	361	8.6	-10.86	0.05	361	7.4	-13.93	0.06
226	8.6	-8.11	0.21	226	8.4	-9.64	0.12	226	8.6	-10.40	0.07	226	8.1	-13.65	0.15
90	8.6	-8.01	0.02	90	8.4	-9.67	0.02	90	8.6	-10.28	0.06	90	7.8	-13.24	0.17
23	8.6	-8.22	0.00	23	8.4	-9.27	0.10	23	8.6	-10.06	0.04	23	8.0	-12.65	0.11
0	9.0	-7.89	0.12	0	8.6	-9.34	0.07	0	9.0	-9.46	0.04	0	8.2	-12.92	0.06
Reservoir		-7.47	0.08	Reservoir		-8.35	0.29	Reservoir		-8.55	0.02	Reservoir		-10.99	0.03
Experiments 3000 ppmV															
10 mmol/l	Experiment No 8			5 mmol/l	Experiment No 7			2 mmol/l	Experiment No 6			1 mmol/l	Experiment No 5		
exposure time [s]	$pH_{experimental}$	$\delta^{13}C$ [‰]	± 1σ sd	exposure time [s]	$pH_{experimental}$	$\delta^{13}C$ [‰]	± 1σ sd	exposure time [s]	$pH_{experimental}$	$\delta^{13}C$ [‰]	± 1σ sd	exposure time [s]	$pH_{experimental}$	$\delta^{13}C$ [‰]	± 1σ sd
452	8.3	-10.35	0.30	452	8.1	-11.59	0.23	452	7.9	-14.92	0.27	452	8.6	-18.37	0.17
361	8.3	-9.84	0.05	361	8.0	-11.82	0.03	361	7.7	-14.40	0.07	361	7.2	-17.50	0.07
226	8.3	-9.41	0.21	226	7.9	-10.58	0.02	226	7.7	-13.43	0.05	226	7.6	-16.74	0.01
90	8.4	-9.00	0.11	90	7.8	-9.91	0.01	90	7.9	-12.14	0.00	90	7.8	-14.32	0.14
23	8.4	-8.24	0.03	23	8.4	-9.72	0.21	23	7.7	-11.51	0.03	23	7.6	-12.98	0.12
0	8.5	-8.21	0.09	0	8.4	-9.03	0.04	0	8.3	-11.17	0.23	0	8.0	-11.64	0.12
Reservoir		-8.17	0.06	Reservoir		-8.99	0.15	Reservoir		-11.11	0.15	Reservoir		-10.33	0.01

Table S4.5b: Results of the experiments conducted at 20 °C

Experiments 1000 ppmV															
10 mmol/l	Experiment No 9			5 mmol/l	Experiment No 10			2 mmol/l	Experiment No 11			1 mmol/l	Experiment No 12		
exposure time [s]	$pH_{experimental}$	$\delta^{13}C$ [‰]	± 1σ sd	exposure time [s]	$pH_{experimental}$	$\delta^{13}C$ [‰]	± 1σ sd	exposure time [s]	$pH_{experimental}$	$\delta^{13}C$ [‰]	± 1σ sd	exposure time [s]	$pH_{experimental}$	$\delta^{13}C$ [‰]	± 1σ sd
570	8.9	-9.63	0.05	570	8.5	-11.54	0.26	570	8.0	-13.74	0.10	570	8.3	-15.48	0.01
456	8.8	-9.46	0.08	456	8.4	-10.62	0.12	456	8.1	-12.41	0.13	456	7.8	-15.47	0.02
285	8.2	-8.81	0.07	285	8.3	-9.92	0.01	285	8.1	-12.00	0.10	285	7.8	-14.77	0.01
114	8.5	-8.30	0.03	114	8.5	-9.39	0.10	114	8.1	-10.84	0.09	114	7.8	-13.60	0.04
29	8.5	-7.78	0.11	29	8.3	-9.12	0.19	29	8.2	-9.89	0.03	29	7.8	-12.71	0.11
0	8.5	-7.85	0.02	0	8.4	-9.04	0.00	0	8.2	-9.37	0.13	0	7.8	-12.56	0.07
Reservoir		-7.60	0.02	Reservoir		-8.56	0.11	Reservoir		-9.03	0.09	Reservoir		-11.51	0.02
Experiments 3000 ppmV															
10 mmol/l	Experiment No 16			5 mmol/l	Experiment No 15			2 mmol/l	Experiment No 14			1 mmol/l	Experiment No 13		
exposure time [s]	$pH_{experimental}$	$\delta^{13}C$ [‰]	± 1σ sd	exposure time [s]	$pH_{experimental}$	$\delta^{13}C$ [‰]	± 1σ sd	exposure time [s]	$pH_{experimental}$	$\delta^{13}C$ [‰]	± 1σ sd	exposure time [s]	$pH_{experimental}$	$\delta^{13}C$ [‰]	± 1σ sd
570	8.2	-11.33	0.23	570	8.0	-13.37	0.15	570	7.8	-18.03	0.04	570	7.4	-22.02	0.13
456	8.2	-11.01	0.16	456	8.0	-12.63	0.03	456	7.6	-17.08	0.03	456	7.0	-21.02	0.01
285	8.2	-9.96	0.03	285	7.9	-11.63	0.14	285	7.5	-15.72	0.01	285	7.2	-19.10	0.02
114	8.6	-8.87	0.02	114	8.4	-10.38	0.18	114	7.6	-13.85	0.17	114	7.5	-16.14	0.05
29	8.3	-8.56	0.15	29	8.0	-9.68	0.05	29	7.5	-13.37	0.05	29	7.3	-15.21	0.24
0	8.3	-8.02	0.02	0	8.2	-8.99	0.03	0	7.8	-13.28	0.06	0	7.6	-12.49	0.03
Reservoir		-7.77	0.08	Reservoir		-8.65	0.00	Reservoir		-10.11	0.16	Reservoir		-11.20	0.08

Table S4.5c: Results of the experiments conducted at 30 °C

Experiments 1000 ppmV																
10 mmol/l	**Experiment No 17**			**5 mmol/l**	**Experiment No 18**			**2 mmol/l**	**Experiment No 19**			**1 mmol/l**	**Experiment No 20**		
exposure time [s]	**$pH_{experimental}$**	**$\delta^{13}C$ [‰]**	**± 1σ sd**	**exposure time [s]**	**$pH_{experimental}$**	**$\delta^{13}C$ [‰]**	**± 1σ sd**	**exposure time [s]**	**$pH_{experimental}$**	**$\delta^{13}C$ [‰]**	**± 1σ sd**	**exposure time [s]**	**$pH_{experimental}$**	**$\delta^{13}C$ [‰]**	**± 1σ sd**
500	8.7	-11.29	0.02	500	8.5	-12.49	0.02	500	8.1	-15.53	0.08	500	7.7	-18.44	0.05
400	8.4	-10.50	0.18	400	8.1	-12.35	0.24	400	7.7	-15.36	0.00	400	7.6	-17.75	0.10
250	8.6	-9.45	0.10	250	8.4	-10.43	0.04	250	7.3	-13.55	0.10	250	7.2	-16.84	0.07
100	8.7	-8.16	0.01	100	8.4	-9.37	0.08	100	7.6	-11.66	0.04	100	7.8	-13.76	0.25
25	8.5	-7.85	0.05	25	8.3	-8.59	0.11	25	7.7	-11.18	0.12	25	7.7	-13.77	0.09
0	8.4	-7.58	0.02	0	8.3	-8.75	0.04	0	8.0	-10.14	0.04	0	7.8	-14.37	0.01
Reservoir		-7.63	0.09	Reservoir		-8.15	0.12	Reservoir		-9.95	0.17	Reservoir		-12.22	0.10
Experiments 3000 ppmV																
10 mmol/l	**Experiment No 24**			**5 mmol/l**	**Experiment No 23**			**2 mmol/l**	**Experiment No 22**			**1 mmol/l**	**Experiment No 21**		
exposure time [s]	**$pH_{experimental}$**	**$\delta^{13}C$ [‰]**	**± 1σ sd**	**exposure time [s]**	**$pH_{experimental}$**	**$\delta^{13}C$ [‰]**	**± 1σ sd**	**exposure time [s]**	**$pH_{experimental}$**	**$\delta^{13}C$ [‰]**	**± 1σ sd**	**exposure time [s]**	**$pH_{experimental}$**	**$\delta^{13}C$ [‰]**	**± 1σ sd**
500	8.3	-14.61	0.28	500	8.0	-16.63	0.01	500	7.6	-21.01	0.07	500	7.3	-24.95	0.03
400	7.8	-13.49	0.03	400	7.6	-15.69	0.03	400	7.4	-20.49	0.12	400	7.0	-24.19	0.05
250	8.1	-12.18	0.27	250	7.7	-13.39	0.06	250	7.5	-18.36	0.23	250	6.9	-21.80	0.18
100	8.2	-9.74	0.03	100	7.6	-10.77	0.16	100	7.5	-15.26	0.18	100	7.5	-17.28	0.12
25	8.4	-8.65	0.05	25	7.7	-9.71	0.05	25	7.7	-13.78	0.05	25	7.4	-15.52	0.03
0	8.3	-8.37	0.01	0	8.1	-8.86	0.02	0	7.7	-12.63	0.07	0	7.4	-14.34	0.05
Reservoir		-7.73	0.09	Reservoir		-8.64	0.18	Reservoir		-10.23	0.01	Reservoir		-12.55	0.04

4.7.1 Supplemental References

Eigen, M. (1964) Proton Transfer, Acid-Base Catalysis, and Enzymatic Hydrolysis. Part I: ELEMENTARY PROCESSES. *Angewandte Chemie International Edition in English* **3**, 1-19.

Jähne, B., Heinz, G., Dietrich, W. (1987) Measurement of the diffusion coefficients of sparingly soluble gases in water. *Journal of Geophysical Research: Oceans* **92**, 10767-10776.

Johnson, K.S. (1982) Carbon dioxide hydration and dehydration kinetics in seawater. *Limnol. Oceanogr* **27**, 849-855.

Li, Y.-H., Gregory, S. (1974) Diffusion of ions in sea water and in deep-sea sediments. *Geochimica et Cosmochimica Acta* **38**, 703-714.

Mook, W.G., Bommerson, J.C., Staverman, W.H. (1974) Carbon isotope fractionation between dissolved bicarbonate and gaseous carbon dioxide. *Earth and Planetary Science Letters* **22**, 169-176.

Nordstrom, D.K., Plummer, L.N., Langmuir, D., Busenberg, E., May, H.M., Jones, B.F., Parkhurst, D.L., 1990. Revised chemical equilibrium data for major water-mineral reactions and their limitations, ACS symposium series. Oxford University Press, pp. 398-413.

O'Leary, M.H., Madhavan, S., Paneth, P. (1992) Physical and chemical basis of carbon isotope fractionation in plants. *Plant, Cell & Environment* **15**, 1099-1104.

Sander, S. P., Abbatt, J., Barker, J. R., Burkholder, J. B., Friedl, R. R., Golden, D. M., Huie, R. E., Kolb, C. E., Kurylo, M. J., Moortgat, G. K., Orkin, V. L., Wine, P. H. (2011) Chemical Kinetics and Photochemical Data for Use in Atmospheric Studies. Evaluation No. **17**, JPL Publication 10-6, Jet Propulsion Laboratory, Pasadena, available at: http://jpldataeval.jpl.nasa.gov (last access: 10 April 2015)

Thode, H.G., Shima, M., Rees, C.E., Krishnamurty, K.V. (1965) CARBON-13 ISOTOPE EFFECTS IN SYSTEMS CONTAINING CARBON DIOXIDE, BICARBONATE, CARBONATE, AND METAL IONS. *Canadian Journal of Chemistry* **43**, 582-595.

Vogel, J.C., Grootes, P.M., Mook, W.G. (1970) Isotopic fractionation between gaseous and dissolved carbon dioxide. *Zeitschrift für Physik* **230**, 225-238.

Zeebe, R.E. (2011) On the molecular diffusion coefficients of dissolved CO_2, HCO_3^-, and CO_3^{2-} and and their dependence on isotopic mass. *Geochimica et Cosmochimica Acta* **75**, 2483-2498.

Zeebe, R.E., Wolf-Gladrow, D. (2001) *CO_2 in Seawater: Equilibrium, Kinetics, Isotopes*. Amsterdam: Elsevier Science, B.V. 346 pp.

Chapter 5: Manuscript III

Simulating speleothem growth in the laboratory. Part I: Stable carbon isotope fractionation during precipitation of speleothem calcite

Maximilian Hansen[1*], Denis Scholz[1], Bernd R. Schöne[1], Christoph Spötl[2]

Manuscript in preparation for submission to Chemical Geology

*corresponding author: m.hansen@uni-mainz.de
[1]Institute for Geosciences, University of Mainz, Germany
[2]Institute of Geology, University of Innsbruck, Austria

Abstract

Stable carbon isotopes in speleothem $CaCO_3$ are of great importance for reconstruction of past climate and environmental changes. The interpretation of these paleoclimate records, however, is challenging because various processes may bias the climate signal until speleothem calcite is deposited. The basic mechanisms of stable isotope fractionation are still a matter of a lively debate, especially whether kinetic, equilibrium or disequilibrium fractionation are the dominant processes. Here we present novel laboratory experiments, performed under controlled, cave analogues conditions, ,which allow for the first time to directly investigate the stable carbon isotope fractionation between $CaCO_3$ and all other involved dissolved carbon species (HCO_3^-, CO_2) in a thin film of solution as they occur on the surface of speleothems at the same time. All chemical parameters, such as pH, electrical conductivity, and, thus, precipitation rate as well as time constant for precipitation of $CaCO_3$ are in agreement with previous theoretical studies (e.g., Baker et al., 1998; Buhmann and Dreybrodt, 1985a; Dreybrodt et al., 1997).

For both, the dissolved inorganic carbon (DIC) and $CaCO_3$, a strong enrichment of $\delta^{13}C$ values is observed. The temporal evolution of $\delta^{13}C_{DIC}$ can be well explained using a Rayleigh distillation model, as proposed by Scholz et al. (2009). The total fractionation $^{13}\varepsilon_{tot}$, is much larger than expected from isotope equilibrium with values up to + 13.7 ‰. The fractionation between $CaCO_3$ and DIC, $^{13}\varepsilon_{CaCO3/HCO3-}$, is negative for all experiments. With increasing residence time, and thus decreasing supersaturation with respect to calcite, the fractionation becomes smaller, approaching isotope equilibrium values. Hence, stable carbon isotope fractionation seems to be coupled to reaction kinetics, especially if precipitation rates are high at the beginning of the experiments (corresponding e.g. to the growth axis of a stalagmite). Consequently, the assumption of previous modelling studies (e.g., Dreybrodt, 2008; Scholz et al., 2009) of a static fractionation factor might not be entirely correct, as the results of this study suggest that the fractionation factors for speleothem calcite additionally seems to be coupled to reaction kinetics. These are important information for paleoclimate reconstruction from speleothems. Rate dependent (negative) fractionation processes might lead to an overestimation of $\delta^{13}C$ values in terms of cave ventilation or (paleo-)vegetation changes. Thus the interpretation of $\delta^{13}C$ speleothem records should always be handled with care,

5.1. Introduction

In the last decades, speleothems have been established as an important palaeoclimate archive (Fairchild and Baker, 2012). The most commonly used paleoclimate proxies in speleothems are the stable isotopes of carbon and oxygen ($\delta^{13}C$ and $\delta^{18}O$), which can be measured at high temporal resolution. In combination with precise U-series dating (e.g., Scholz, 2008), this allows to generate long and often continuous records of continental climate (e.g., Asmerom et al., 2010; Bar-Matthews et al., 2003; Boch et al., 2011; Cheng et al., 2016; Cruz et al., 2005; Fleitmann et al., 2004). However, the interpretation of speleothem stable isotope data in terms of past climate variability (i.e., amount of meteoric precipitation and temperature) is complex, particularly because the $\delta^{18}O$ and $\delta^{13}C$ values depend on various processes occurring in the atmosphere, the soil and the karst above the cave as well as inside the cave, which may all have an influence on the signals finally recorded in the cave carbonates. Most speleothem paleoclimate studies are based on $\delta^{18}O$ data (e.g., Cheng et al., 2016; Fleitmann et al., 2004; Spötl et al., 2008), which are in most cases interpreted as reflecting changes in the $\delta^{18}O$ values of precipitation above the cave. This has provided important information on past precipitation (e.g., Bar-Matthews et al., 2003; Cheng et al., 2016), temperature (e.g., Mangini et al., 2005), water vapor source and atmospheric circulation (e.g., Cruz et al., 2005; Wassenburg et al., 2016).

Even though mass spectrometric analyses of carbonate samples typically yield both $\delta^{13}C$ and $\delta^{18}O$ values, $\delta^{13}C$ data of speleothem have been utilized to a lesser extent than $\delta^{18}O$ data. The major reason for this is that $\delta^{13}C$ values are influenced by complex processes in the soil, the epikarst, and inside the cave during precipitation of speleothem calcite (Dreybrodt and Scholz, 2011; McDermott, 2004). However, various studies have documented the large potential of paleoclimate information preserved in speleothem $\delta^{13}C$ records. For example, Genty et al. (2003) interpreted rapid changes in the $\delta^{13}C$ values of a stalagmite from southwest France as reflecting dramatic changes in vegetation above the cave related to Dansgaard-Oeschger events. Similarly, Mischel et al. (2016) and Hellstrom and McCulloch (2000) interpreted speleothem $\delta^{13}C$ records in terms of changes in vegetation and recharge and supported their interpretation by trace elements. Scholz et al. (2012) showed a relationship between thicker annual laminae and lower $\delta^{13}C$ values in a speleothem from northeastern Italy reflecting warmer winter temperatures on annual timescales. On the millennial timescale, they interpreted changes in $\delta^{13}C$ values as reflecting the progressive evolution of the soil profile in the catchment of the cave´s drip water. In a recent study, Ridley et al. (2015) generated monthly resolved $\delta^{13}C$ data from a speleothem from Belize providing information on past changes in rainfall, which in turn are related to changes in the Intertropical Convergence Zone. Additionally, Breecker (2017) showed, that globally

averaged speleothem $\delta^{13}C$ records potentially record changes in atmospheric pCO_2 for the Pleistocene and could thus be used as a radiometric chronometer for ice cores via correlation with speleothem records. All these examples emphasize the large potential of speleothem $\delta^{13}C$ records for a number of paleoclimate and environmental applications.

Since the early attempts to utilize speleothems for palaeoclimate reconstruction (e.g., Fornaca-Rinaldi et al., 1968; Hendy and Wilson, 1968), there is an ongoing discussion about stable isotope fractionation during precipitation of speleothem calcite. In particular it is a matter of debate whether precipitation occurs under conditions close to isotopic equilibrium or involves kinetic isotope fractionation (e.g., Mickler et al., 2006). A pioneering theoretical work about stable isotope fractionation in speleothems was presented by Hendy (1971). He suggested that a progressive increase of $\delta^{13}C$ and $\delta^{18}O$ values as well as a positive correlation between $\delta^{13}C$ and $\delta^{18}O$ values along individual growth layers is an indication for disequilibrium isotope fractionation. This was subsequently established as the "Hendy test" and has been widely applied to test the suitability of speleothems for paleoclimate reconstruction (e.g., Dorale and Liu, 2009). In the last decade, a number of theoretical studies have been published aiming to quantitatively describe the isotope fractionation processes during precipitation of speleothem calcite. In particular, two models have been proposed: a so-called 'kinetic' fractionation model (Dreybrodt, 2008; Dreybrodt and Scholz, 2011) and a Rayleigh distillation model (Scholz et al., 2009). The model of Scholz et al. (2009) provides the basis for a more sophisticated model also accounting for changes in cave temperature, cave and soil pCO_2, drip rate and splashing effects (Mühlinghaus et al., 2007, 2009). In addition, models describing the effects of evaporation (Deininger et al., 2012; Dreybrodt and Deininger, 2014) as well as isotope exchange between gaseous cave CO_2 and the dissolved inorganic carbon (DIC) in the thin film of solution on the surface of a speleothem (Dreybrodt et al., 2016; Dreybrodt and Romanov, 2016; Hansen et al., accepted) have been developed. A detailed discussion of these models and their applicability for the description of stable isotope fractionation in speleothems can be found elsewhere (Dreybrodt, 2008; Dreybrodt and Romanov, 2016; Dreybrodt and Scholz, 2011; Scholz et al., 2009). Irrespective of the current debate which model is better suited to describe the temporal evolution of the $\delta^{13}C$ and $\delta^{18}O$ values of the DIC during precipitation of speleothem calcite (Dreybrodt, 2016), all models rely on equilibrium isotope fractionation factors. This is simply due to the lack of suitable kinetic or disequilibrium isotope fractionation factors, which have not yet been determined for speleothems.

Isotope fractionation processes during precipitation of speleothem calcite have also been investigated in several laboratory experiments using synthetic carbonates. Early experiments were conducted by Emrich et al. (1970), who performed bulk experiments investigating carbon

isotope fractionation during precipitation of $CaCO_3$ at different temperatures. Subsequently, Fantidis and Ehhalt (1970) observed increasing stable isotope values along an individual growth layer of a stalagmite and conducted calcite precipitation experiments under laboratory atmosphere in glass tubes, which confirmed the isotopic enrichment observed in the stalagmite. In recent years, several studies aiming to simulate isotope fractionation during precipitation of speleothem calcite were performed under better controlled conditions. Wiedner et al. (2008) and Polag et al. (2010) carried out experiments in a refrigerator and precipitated calcite in a pure N_2 atmosphere by mixing a $NaHCO_3$ and a $CaCl_2$ solution in a glass tube and using a glass fiber stripe as a crystallization substrate. Both studies observed increasing $\delta^{13}C$ and $\delta^{18}O$ values with increasing distance of flow of the solution and thus confirmed the theoretical predictions of Hendy (1971). Using a different setup, Day and Henderson (2011) observed a similar result for $\delta^{18}O$ values using a $CaCO_3$-CO_2-H_2O solution dripping onto seeded glass plates under an atmosphere containing CO_2. All these setups have specific advantages and disadvantages. However, they all have in common that they only investigated the spatial and temporal evolution of the isotope composition of the precipitated calcite. They did not directly investigate the temporal evolution of the $\delta^{13}C$ and $\delta^{18}O$ values of the DIC, pH and the Ca^{2+} concentration of the solution during the course of the experiments. Thus, determination of the fractionation factors between DIC and $CaCO_3$ as a function of the experimental conditions, as would be required for the models described above, has not achieved so far.

Here we present results of novel laboratory experiments simulating all potential processes affecting the $\delta^{13}C$ value during precipitation of $CaCO_3$ from a flowing thin layer of solution as on the surface of a speleothem. We quantify the temporal evolution of the $\delta^{13}C$ values of both DIC and the precipitated $CaCO_3$ as well as pH and the precipitation rate of calcite. This enables us to study isotope fractionation between different species in the carbonate system (i.e., HCO_3^-, CO_2, $CaCO_3$). In this publication we focus on carbon isotopes; oxygen isotopes will be discussed in a forthcoming paper (Part II).

5.2 Theoretical background

5.2.1 Chemical evolution of a calcite precipitating solution

Meteoric precipitation above the cave seeps through the soil, where pCO_2 may reach values of up to a few percent (Fairchild and Baker, 2012). This leads to formation of carbonic acid, resulting in relatively low pH values of the solution (5.1):

$$CO_2(g) + H_2O \Leftrightarrow H_2O + CO_2(aq) \Leftrightarrow H_2CO_3. \quad (5.1)$$

Note that the total DIC at low pH values is mainly represented by $CO_{2(aq)}$, whereas the proportion of carbonic acid is about 600 times smaller (e.g., Appelo and Postma, 2004).

When the solution comes into contact with the carbonate host rock $CaCO_3$ is being dissolved. The overall reaction is:

$$CO_2 + H_2O + CaCO_3 \Leftrightarrow Ca^{2+} + 2\ HCO_3^-. \quad (5.2)$$

Thus, dissolution of each molecule of $CaCO_3$ consumes one molecule of CO_2. This reaction is reversible, depending on the availability of CO_2 and, thus, on the pH of the solution. The distribution of the different species of DIC is also controlled by the pCO_2 and thus the pH of the solution. In detail, these reactions are considerably more complex because they involve a series of slow and fast reactions, controlled by diffusion and/or different reaction constants (e.g., Dreybrodt, 1988; Dreybrodt et al., 1997; Zeebe and Wolf-Gladrow, 2001).

Subsequently, the solution enters the cave system, where the pCO_2 is generally several orders of magnitude lower than in the soil and epikarst zone. The drip water dripping onto the top of a stalagmite forms a thin layer of solution, usually about 0.1 mm in thickness, from which the dissolved CO_2 degasses in the range of a few seconds (Hansen et al., 2013); Hansen et al., under review). This is followed by an increase in pH to ca. 8. As a consequence, HCO_3^- becomes the dominant species of DIC (about 95 %), the solution reaches supersaturation with respect to calcite and eventually calcite is precipitated (e.g., Dreybrodt et al., 1997). When the solution flows down the stalagmite, $CaCO_3$ progressively precipitates resulting in incremental growth of the stalagmite (e.g., Mühlinghaus et al., 2007; Romanov et al., 2008a). The precipitation rate, F [mmol/cm²s], for calcite has been described by Plummer et al. (1978):

$$F = k_1 * [H^+]_s + k_2 * [H_2CO_3]_s + k_3 - k_4 * [Ca^{2+}]_s * [HCO_3^-], \quad (5.3)$$

where the brackets denote the concentration of the individual molecules at the calcite surface, k_1, k_2, k_3 are temperature-dependent rate constants for dissolution, and k_4 is the rate constant for precipitation of $CaCO_3$, which also depends on the pCO_2 of the solution. If the system is

supersaturated with respect to calcite, the precipitation term is dominant. If F approaches 0, the system is in chemical equilibrium. The CO_2 molecules produced according to Eq. (5.2) are almost instantaneously released to the atmosphere by molecular diffusion. This step also involves the relatively slow conversion of H_2CO_3 into H_2O and CO_2. The precipitation rate is, thus, also limited by the conversion of HCO_3^- into CO_2. By combining all three processes the precipitation rate of $CaCO_3$ from a thin film as on the surface of a speleothem was derived (Buhmann and Dreybrodt, 1985a; Dreybrodt et al., 1997):

$$F = \kappa * ([Ca^{2+}] - [Ca^{2+}]_{eq}) \text{ [mol*cm}^{-2}\text{*s}^{-1}\text{]} \quad (5.4)$$

$$\kappa = (0.52 + 0.04*T + 0.004*T^2) * 10^{-5} \text{ cm/s}, \quad (5.5)$$

where κ is a rate constant, T the temperature in °C, $[Ca^{2+}]$ is the Ca^{2+} concentration at time t and $[Ca^{2+}]_{eq}$ is the equilibrium concentration which depends on the cave pCO_2. For the film thicknesses observed in caves, κ is independent of the film thickness and only depends on temperature (Baker et al., 1998; Romanov et al., 2008a). Consequently, supersaturation with respect to calcite decreases exponentially during precipitation of calcite with a characteristic decay time, τ_{pr} (Dreybrodt, 1988), and the temporal evolution of the concentration of $[Ca^{2+}]$ and $[HCO_3^-]$ is given by (Buhmann and Dreybrodt, 1985a):

$$[Ca^{2+}](t) = \left([Ca^{2+}]_0 - [Ca^{2+}]_{eq}\right)\left(exp^{\left(-t/\tau_{pr}\right)}\right) + [Ca^{2+}]_{eq} \quad (5.6)$$

$$\tau_{pr} = d/\kappa \ , \quad (5.7)$$

where $[Ca^{2+}]_0$ is the initial concentration and d is the film thickness of the solution.

5.2.2 The essential stable isotope geochemistry for understanding speleothem $\delta^{13}C$ data

The chemical and physical behavior of the heavy and the light isotope of a specific element are slightly different. These differences are caused by the mass differences of the atomic nuclei of the different isotopes. The heavier isotopes are characterized by larger binding energies and a generally lower mobility. As a consequence, the light isotopes of an element react faster than the heavier ones in a chemical reaction. The resulting isotope effect, referred to as isotope fractionation, is expressed by a fractionation factor, α. Isotope effects are generally small. Thus, isotope effects are commonly expressed by the fractionation, ε, defined as the deviation of α from 1 in permil (see e.g., Mook and De Vries, 2000, for details):

$$\varepsilon_{B/A} = \alpha_{B/A} - 1 = \frac{R_B}{R_A} - 1 \ (* 10^3‰), \quad (5.8)$$

In general, there are three kinds of isotope fractionation: equilibrium, disequilibrium and kinetic fractionation. Equilibrium fractionation is characterized by a processes in which an (isotope) flux between two different reservoirs are equal in both directions with a corresponding equilibrium fractionation factor. Kinetic fractionation, in constrast, describes an irreversible, one-way process. Most natural fractionation processes are neither completely kinetic nor completely in equilibrium. Such processes are often referred to as disequilibrium fractionation. The term kinetic isotope fractionation has, in particular in the speleothem literature, frequently been used to describe a deviation of the $\delta^{13}C$ value of the precipitated calcite from the value expected under conditions of isotope equilibrium and been associated with rapid degassing of CO_2 (e.g., Hendy, 1971; Mickler et al., 2006). However, strictly speaking, this is misleading, because the term kinetic isotope fractionation is used to describe one-dimensional, rate-dependent, irreversible processes resulting in strong, negative isotope fractionation (e.g., Mook and De Vries, 2000; Sharp, 2007). Thus, we use the classical definition of kinetic isotope fractionation here and refer to disequilibrium isotope fractionation to describe a deviation from the values expected under conditions of equilibrium.

The most commonly used fractionation factors for $^{13}\varepsilon_{CaCO3/HCO3-}$ and $^{13}\varepsilon_{CO2(aq)/HCO3-}$ were determined in laboratory experiments by precipitating synthetic $CaCO_3$ from a bulk solution and measuring all species in the system (DIC, $CaCO_3$ and CO_2(g)) as a function of temperature and/or precipitation rate (e.g., Emrich et al., 1970; McCrea, 1950; Mook et al., 1974; Romanek et al., 1992; Vogel et al., 1970). However, for the interpretation of speleothem stable isotope data, these values may not be suitable, because the physical and chemical processes in these very thin films of solution are considerably different than in a large bulk solution. For larger volumes of solution, diffusion is the rate-limiting step for the chemical reactions. In contrast, for thin solution films, diffusion is very fast (e.g., Hansen et al., 2013) and thus not rate-limiting.

5.2.3 Modeling stable isotope fractionation in speleothems

The temporal evolution of the $\delta^{13}C$ values of the dissolved HCO_3^- as well as the precipitated $CaCO_3$ have been described by two different approaches, which have been controversially discussed. They are briefly described in the following.

5.2.3.1 Rayleigh distillation model

Precipitation of $CaCO_3$ from a solution and the corresponding temporal evolution of the $\delta^{13}C$ values has often been described by a Rayleigh distillation model (e.g., Bar-Matthews et al., 1996; Mickler et al., 2004; Mook and De Vries, 2000; Romanov et al., 2008b; Salomons and Mook, 1986; Scholz et al., 2009). During precipitation, carbon isotopes are incorporated into the $CaCO_3$ on the speleothem surface as well as released to the atmosphere via conversion to CO_2 (Eq. (5.2)). Thus, the DIC reservoir progressively loses C atoms. This process is accompanied by a carbon isotope fractionation, which is the classical case of a Rayleigh fractionation process (removal of a substance from a reservoir accompanied by isotope fraction), which is widely applied in isotope geochemistry (e.g., Mook and De Vries, 2000). Thus, when calcite precipitates from a DIC reservoir containing N_0 carbon atoms with an isotope ratio R_0 at time $t = 0$ with a characteristic time constant τ_{pr} (Eq. (5.6)), this results in a progressive change in the isotope ratio, R(t), of the DIC. Note, that isotope fractionation may be different for the different sinks, which is described by the corresponding fractionation factors, ε. For precipitation of $CaCO_3$, the total fractionation, ε_{tot}, is a combination of $½\ \varepsilon_{CaCO3/HCO3^-} + ½\ \varepsilon_{CO2(g)/HCO3^-}$ (Mickler et al., 2004; Scholz et al., 2009).

Scholz et al. (2009) derived the temporal evolution of the $\delta^{13}C$ value of the DIC in the thin film on the surface of a speleothem using a Rayleigh distillation approach:

$$\frac{\delta^{13}C(t)+1000}{\delta^{13}C_0+1000} = \frac{[Ca^{2+}](t)^{\varepsilon_{tot}}}{[Ca^{2+}]_0} = \left(exp^{\frac{-t}{\tau_{pr}}} + \left(\frac{[Ca^{2+}]_{eq}}{[Ca^{2+}]_0}\right) * \left(1 - exp^{\frac{-t}{\tau_{pr}}}\right)\right)^{\varepsilon_{tot}} \quad (5.9)$$

where δ denotes the corresponding $\delta^{13}C$ values at time t and the initial isotope ratio, $[Ca^{2+}]$, is the concentration of Ca^{2+} in solution at time t and the initial $[Ca^{2+}]$ concentration at $t = 0$. The corresponding evolution is shown by the black curve in Fig. 5.1.

5.2.3.2 'Kinetic' fractionation model by Dreybrodt (2008)

Using an alternative approach, Dreybrodt (2008) derived a 'kinetic fractionation model', which is based on the assumption that the light and heavy isotopes are precipitated independently from

each other. Due to isotope effects, two slightly different time constants for the precipitation of the heavy and the light isotope as well as a 'kinetic' constant, γ, were introduced. γ determines the $\delta^{13}C$ value of the DIC in equilibrium and depends on processes occurring at the calcite surface (Dreybrodt, 2008). Note, that γ is currently only of theoretical nature and has not yet been determined experimentally. The corresponding temporal evolution of the $\delta^{13}C$ values according to the 'kinetic' model is shown by the red curve in Fig. 5.1. Since kinetic isotope fractionation factors for precipitation of speleothem calcite are not available, the ratio between the two different time constants, which determines the degree of isotope fractionation in the model, has been described using equilibrium isotope fractionation factors (Dreybrodt, 2008; Dreybrodt and Scholz, 2011). Thus, the term 'kinetic' fractionation model is, strictly speaking, misleading. Recently, Dreybrodt and Romanov (2016) extended this model by introducing isotope exchange between the DIC and the gaseous CO_2 of the cave atmosphere as well as evaporation. For further details the reader is referred to Dreybrodt (2008), Dreybrodt and Scholz (2011), Dreybrodt and Romanov (2016) and Dreybrodt (2016).

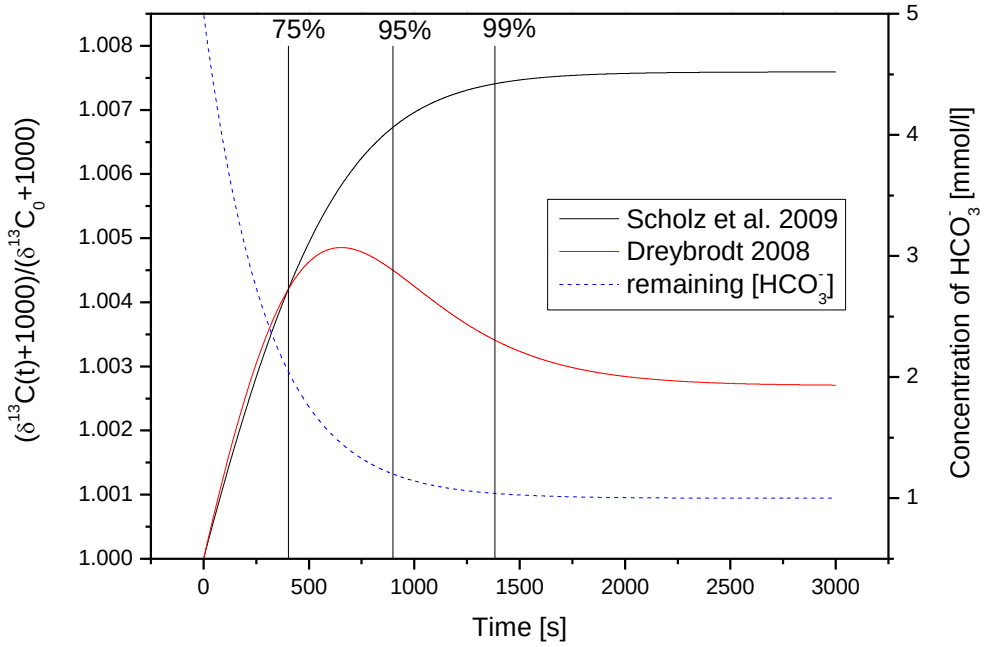

Fig. 5.1: Comparison of the two available models describing the temporal evolution of the $\delta^{13}C$ value of DIC in a thin film on the surface of a speleothem during calcite precipitation (Dreybrodt, 2008; Scholz et al., 2009). Also shown is the corresponding exponential decrease of $[HCO_3^-]$ in the solution with increasing precipitation. Initial $[HCO_3^-]$ was 5 mmol/l and τ_{pr} was set to 300 s (modified from Scholz et al., 2009).

5.2.3.3 Comparison of the two models

Dreybrodt and Scholz (2011) state that the "Rayleigh distillation concept is basically an equilibrium model" suggesting that the Rayleigh approach can – in contrast to the 'kinetic' model – only be used to describe equilibrium isotope fractionation processes. However, in principle, kinetic fractionation can also be described by a Rayleigh process if kinetic isotope fractionation factors are used in Eq. (5.9). Furthermore, if the same fractionation factors are used, the 'kinetic' and the Rayleigh model are identical until ca. 75 % of the excess Ca^{2+} has precipitated (Fig. 5.1, also see Scholz et al., 2009). Subsequently, the two models show a considerably different evolution (Fig. 1). Whereas Scholz et al. (2009) predict a progressive exponential growth until an equilibrium state has been reached (Fig. 5.1, black line), the Dreybrodt (2008) model suggests a maximum value of isotopic enrichment, followed by a decrease to the equilibrium value defined by the value of γ (Fig. 5.1, red line). For a more detailed discussion, the reader is referred to Dreybrodt (2016).

5.3 Experimental methods

5.3.1 Basic concept of the experiments

The basic idea of our experiments is to simulate all natural processes, which potentially influence the $\delta^{13}C$ values of speleothems in the laboratory as close to a natural cave system as possible. For this purpose, we developed a "climate box", in which our experiments are conducted and which allows to control all experimental parameters, such as relative humidity, temperature, pCO_2 and the $\delta^{13}C$ value of gaseous CO_2. Rubber gloves allow to perform the experiments without opening the box and contaminating the atmosphere (Dreybrodt et al., 2016). Prior to each experiment, the box was equipped with the experimental material and then sealed for at least three days to establish the experimental temperature and a high relative humidity by bubbling the box atmosphere through two water columns. Note that we used the same water for preparation of all solutions and for establishment of the humidity in the system. To control the pCO_2 inside the box, the air of the box was flushed with nitrogen for about 15 h using a gas washer. After a minimum pCO_2 value of ca. 40 ppmV had been reached, a defined amount of CO_2, preliminarily equilibrated with the water used for the experiments, was injected into the system.

In the experiments, $CaCO_3$-CO_2-H_2O solutions of different initial concentrations flew down on an inclined marble or borosilicate glass plate. We used thin solution films of about 0.1 mm in thickness (Hansen et al., 2013). The Ca^{2+} concentrations of the solutions were 2, 3 and 5 mmol/L.

5 L of solution were prepared for each experiment. The experiments were conducted at three temperatures (10, 20 and 30 °C) and two different pCO_2 values (1000 and 3000 ppmV). During the experiments, we measured the temporal evolution of the $\delta^{13}C$ values of DIC, the precipitated $CaCO_3$ as well as of the CO_2 of the atmosphere. In addition, the temporal evolution of the pH and the conductivity of the solution was measured. This enables the determination of isotope fractionation between the precipitated calcite and the DIC as well as of the precipitation rate at any time during the experiment.

The ambient conditions inside the box were logged using instruments also commonly used in cave monitoring. Five Hobo® and Tinytag® temperature probes were used to measure the temperature on the surface of the plates and of the atmosphere in the box. The average precision was $\pm$ 0.15 °C and relative humidity was measured using a Tinytag® humidity probe. Another important experimental parameter is the stability of the pCO_2 of the box atmosphere during the experiments, which was logged using a Vaisala® MI70 instrument with a GMP 222 probe (average experimental precision $\pm$ 27 ppmV). During the experiments, gaseous CO_2 was released into the box due to degassing of dissolved CO_2 during chemical equilibration and precipitation of $CaCO_3$. In a natural cave, this effect is negligible, because the pCO_2 of the cave atmosphere can be regarded as constant between two subsequent drops. Since the volume of the climate box is finite, we continuously monitored the pCO_2. When the pCO_2 value increased significantly (up to + 100 ppmV), the system was shortly flushed with N_2.

The experiments are divided into two parts, one to study the dissolved inorganic carbon (DIC) and another one for the $CaCO_3$.

5.3.2 Preparation of solutions

For each experiment, we prepared a $CaCO_3$-CO_2-H_2O solution by dissolving Merck® high grade pure $CaCO_3$ powder ($\delta^{13}C \approx$ - 6 ‰) in 5 L of pure MQ water by bubbling CO_2 ($\delta^{13}C \approx$ - 45 ‰) through the water column. When the solution was clear without any visible particles of $CaCO_3$ the pH was ca. 5. Considering the distribution of the different species of DIC, which depends on temperature and the concentration of Ca^{2+}, about 80 % of the DIC is represented by dissolved CO_2. This solution is undersaturated with respect to calcite. For a typical cave drip water, which remained sufficiently long in the aquifer above the cave to establish chemical equilibrium with the carbonate host rock, the saturation index (SI) is expected to be close to 0 (e.g., Dreybrodt and Scholz, 2011). Hence, we subsequently adjusted the solutions to a saturation index of ca. 0 by sparging the solution off CO_2 with argon and measuring pH and electrical conductivity. The

corresponding pH value and the mass balance were calculated for each experiment using PhreeqC (Parkhurst and Apello, 1999). For example, for a 5 mmol/L $CaCO_3$ solution at 20 °C, SI ≈ 0 is reached at a pH value of 6.5, with 40 % of the DIC constituted by dissolved CO_2. After the saturation index for the corresponding experimental temperature had been adjusted, the solutions were stored inside the box for 4 days at the experimental temperature in order to establish isotope equilibrium between all dissolved carbon species.

5.3.3 Experimental setup for the DIC experiments

In the first part of the experiments, the temporal evolution of the DIC was investigated. The previously equilibrated $CaCO_3$-CO_2-H_2O solution was pumped via a peristaltic pump from the reservoir onto a small upper marble plate (the "equilibration plate", Fig. 5.2), where the solution then flew down as a thin (ca. 0.1 mm) film. On this plate, the dissolved CO_2 degasses in the range of a few seconds, the pH rises to values of about 8 and the solution reaches supersaturation with respect to calcite (Hansen et al., 2013). The distance of flow required for chemical equilibration of the solution with the pCO_2 of the box atmosphere was individually evaluated for each experimental run by measuring the pH and electrical conductivity at the end of the equilibration plate. The corresponding equilibration distance was then determined by comparing the values with those expected for chemical equilibrium with the box atmosphere as calculated using PhreeqC.

The solution then dripped onto a lower, larger marble plate, where a thin, laminar solution film was established and calcite progressively precipitated onto the plate (Fig. 5.2). In order to mimic the carbonate surface of a stalagmite, a Carrara marble plate was used. Prior to all experiments, the film thickness and flow velocity were determined by measuring the maximum flow speed and the supply rate at the end of the plate as described by Hansen et al. (2013). With this information, the residence time of the film on the plate can be calculated. A sketch of the experimental setup inside the climate box is shown in Fig. 5.2.

During the experiments, the distance of flow on the lower plate was adjusted by shifting the equilibration plate relative to the lower plate (Fig. 5.2). At the end of the lower plate, the solution dripped into a sewer port, where it was collected. This allowed to study the solution after different distances of flow and, thus, residence times on the plate. For every distance of flow, two samples were taken. The first sample was used to determine pH and electrical conductivity [µS/cm], which enabled us to monitor the temporal evolution of carbonate chemistry of the film and to determine the time constants and precipitation rate of $CaCO_3$. The second sample was taken

out of the sewer port after collection and then immediately precipitated as $SrCO_3$ for stable isotope analyses by adding the sample to a specific amount of a $CaCl_2$ and NaOH solution under an argon atmosphere in a Luer-Lock® syringe. Thereby, the pH of the sample was instantaneously shifted to high values (pH ≈ 12), and as a consequence, DIC is completely precipitated as $SrCO_3$. Subsequently, the sample was rinsed in methanol in order to neutralize the pH of the precipitate and dried in an evacuated desiccator to avoid contamination (Beck et al., 2005). This allowed to "freeze" the $\delta^{13}C$ value of the DIC for the corresponding distance of flow and to determine its temporal evolution. The precipitation method and its precision is described in detail in Dreybrodt et al. (2016). Note, that especially for the short distances of flow the solution may still contain very small amounts of dissolved CO_2 which then is also precipitated with all other carbonate species as $SrCO_3$.

In addition, the box atmosphere was sampled at regular intervals in order to monitor the stability of the $\delta^{13}C$ value of the atmosphere. This was done by opening, slewing and closing exetainers, which were previously flushed by Ar.

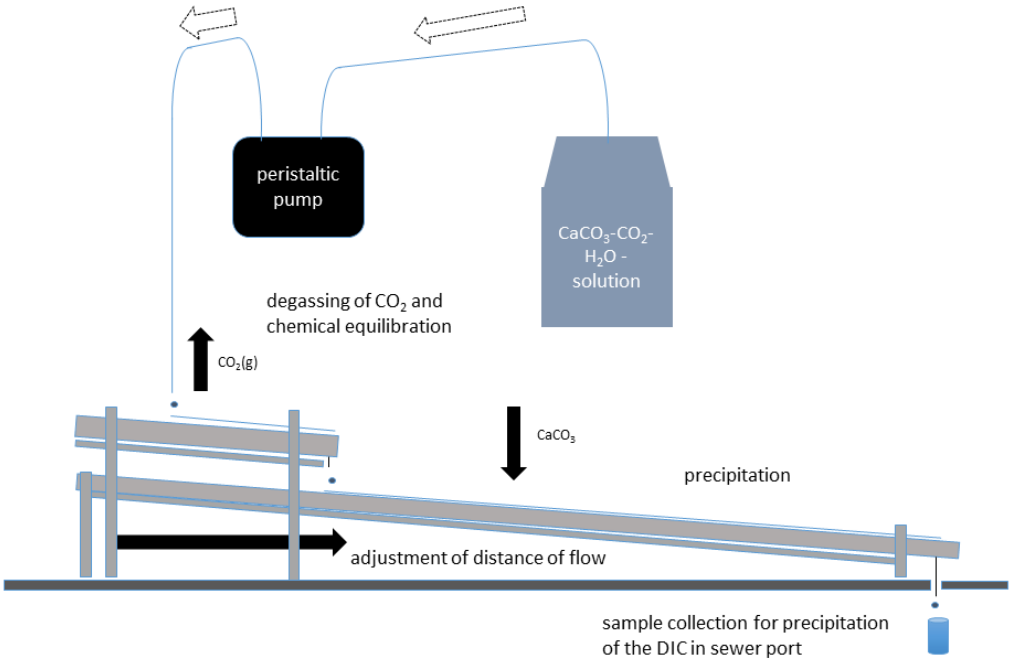

Fig. 5.2: Sketch of the experimental setup of the DIC experiment. Degassing of dissolved CO_2 and adjustment to the new pH take place on the upper equilibration plate. Precipitation of $CaCO_3$ occurs on the lower plate.

5.3.4 Experimental setup for the $CaCO_3$ experiments

In the second part of the experiments, the temporal evolution of the $\delta^{13}C$ values of the precipitated $CaCO_3$ was investigated. The previously described setup was slightly modified by replacing the two marble plates by a single sand-blasted borosilicate glass plate. Afterwards, the box was sealed again, and the system was flushed with N_2 with subsequent adjustment of the pCO_2 as described above. Then the remaining solution ($\approx$ 4 L) was pumped onto the glass plate. The distance of flow was increased by the equilibration distance, as previously determined on the equilibration plate for the corresponding DIC experiment. The same film thickness was established as in the DIC experiments ($\approx$ 0.1 mm). During the experiments, $CaCO_3$ was progressively precipitated onto the glass plate along the flow path. The duration of one such experiment was about four days. As described for the DIC experiment, the box atmosphere was regularly sampled in order to control the stability of the $\delta^{13}C$ value of the CO_2 in the box.

Electrical conductivity was measured at the end of the glass plate at regular intervals in order to ensure that the precipitation rate was in the same range for both experiments (i.e., the DIC and the $CaCO_3$ experiment). Subsequent to the $CaCO_3$ experiment, the distance of flow on the glass plate was adjusted according to the DIC experiments, and, as in the latter, samples of solution were collected and electrical conductivity measured. This allowed to test whether the time constant for precipitation of DIC and $CaCO_3$ was on the same order of magnitude. Finally, the experiment was stopped, and the precipitate was left to dry inside the box. Subsequently, the plate was removed from the system, and $CaCO_3$ samples were scratched off using a spatula at the same distances of flow as for the DIC experiments for stable isotope analysis.

5.3.4 Stable isotope analysis

Stable isotope analyses of the sampled CO_2 of the box atmosphere were conducted at the University of Innsbruck. 10 ml Labco glass vials containing CO_2 from the experiments were rushed to the laboratory within a few days immediately after completion of an experiment to ensure no leakage of the septa (see Spötl, 2004). $\delta^{13}C_{CO2}$ values were measured using a Delta^{plus}XL mass spectrometer and calibrated against calcite standards. Long-term precision was $\pm$0.15 ‰.

Stable isotope analysis of the $SrCO_3$ and $CaCO_3$ samples were performed at the Institute of Geosciences, University of Mainz using a Thermo Finnigan MAT 253 continuous flow-isotope ratio mass spectrometer coupled to a GasBench II. Samples were dissolved in concentrated phosphoric

acid in helium-flushed borosilicate exetainers at 72 °C. Isotope data were calibrated against an NBS-19 calibrated Carrara marble standard distributed by IVA Analysentechnik e.K. (Düsseldorf, Germany) ($\delta^{13}C = +2.01$ ‰). On average, internal precision (1σ) and accuracy were better than 0.04 and 0.02 ‰, respectively. The isotope values are reported relative to the Vienna Pee Dee Belemnite scale.

5.4 Results

5.4.1 DIC experiments

5.4.1.1 Degassing of CO_2, chemical equilibration and establishment of supersaturation

The chemical processes occurring during degassing of CO_2 from a thin film of water – comparable to those occurring in cave environments – were experimentally studied and discussed by Hansen et al. (2013). Here, we briefly show the results of our measurements on the small equilibration plate. In addition to measurements of pH and electrical conductivity, we sampled the reservoir as well as the solution film at the start and the end of the equilibration plate and precipitated DIC as $SrCO_3$ for isotope analysis. The equilibration distance for an experiment with a 5 mmol/L $CaCO_3$ solution at 20 °C and 1000 ppmV CO_2 is 8 cm, which corresponds to a residence time of 34 s. The pH is 6.6 for the reservoir and 6.7 at the start of the film on the equilibration plate. During the 34 s on the equilibration plate, the pH rose to 8.0 and the conductivity decreased from 883 to 790 µS/cm (Fig. 5.3). Degassing of CO_2 and chemical equilibration is also apparent from the $\delta^{13}C$ values of DIC. The DIC of the reservoir had a $\delta^{13}C$ value of -37.6 ‰ and the $\delta^{13}C$ value at the beginning of the equilibration plate was -37.1 ‰. At the end of the equilibration plate, the $\delta^{13}C$ value of the DIC was -33.7 ‰ (Fig. 5.3). This clearly demonstrates (fast) degassing of CO_2. At pH 6.6, about 40 % of the DIC is provided by dissolved CO_2, resulting in more negative $\delta^{13}C$ values of DIC. After degassing, at a pH of 8.0, about > 98 % of DIC are provided by HCO_3^-, and the $\delta^{13}C$ value increased by about 3.4 ‰.

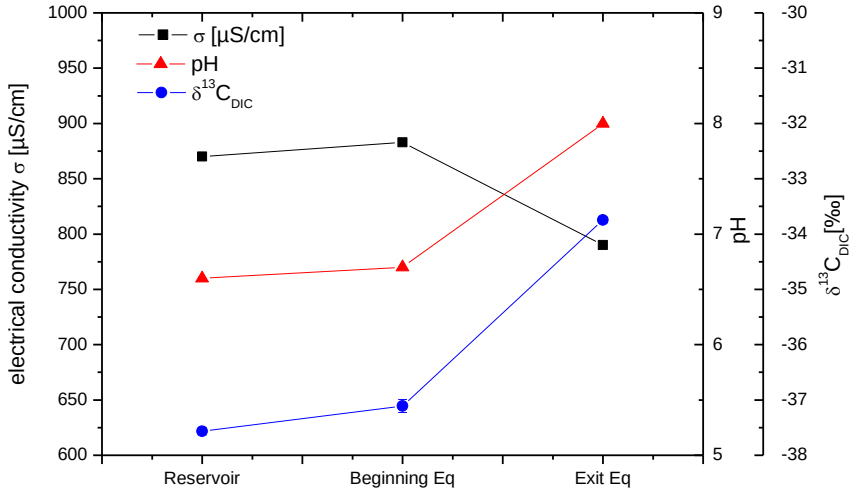

Fig. 5.3: Chemical and isotopic evolution on the upper equilibration marble plate.

5.4.1.2 Temporal evolution of the Ca^{2+} concentration and precipitation rate

The electrical conductivity of the solution is proportional to the Ca^{2+} concentration, and the corresponding Ca^{2+} concentration can be calculated using PhreeqC (for details, see Hansen et al., 2013). Thus, the temporal evolution of electrical conductivity reflects the evolution of the Ca^{2+} concentration in solution. Fig. 5.4 for example shows the temporal evolution of electrical conductivity against residence time on the lower marble plate for three experiments conducted using a 5 mmol/L $CaCO_3$ solution at 10, 20 and 30°C and a pCO_2 of 1000 and 3000 ppmV, respectively. All experiments show decreasing conductivity with increasing residence time on the plates, documenting progressive precipitation of $CaCO_3$. As expected by theoretical predictions (Baker et al., 1998), the highest precipitation rate was observed at the highest temperature.

Since electrical conductivity is representative of the concentration of Ca^{2+}, the time constant for precipitation of calcite, τ_{pr}, can be obtained by fitting the conductivity data according to Eq. (5.6). The time constants for all experiments are compiled in Table 5.1. Also shown in Table 5.1 are the theoretical time constants calculated according to Eq. 5.7. Within uncertainty, all experimentally determined time constants are in good agreement with the values predicted by the theory. Due to the lower precipitation rates at low temperatures, chemical equilibrium was not established for the 10 °C experiments. Thus, the data only show the linear part of the exponential function, which results in larger errors of the fit. For the experiments conducted using a 2 mmol/L $CaCO_3$ solution at 10 and 20 °C, the amount of calcite precipitated on the plates was not large enough to determine the $\delta^{13}C$ values.

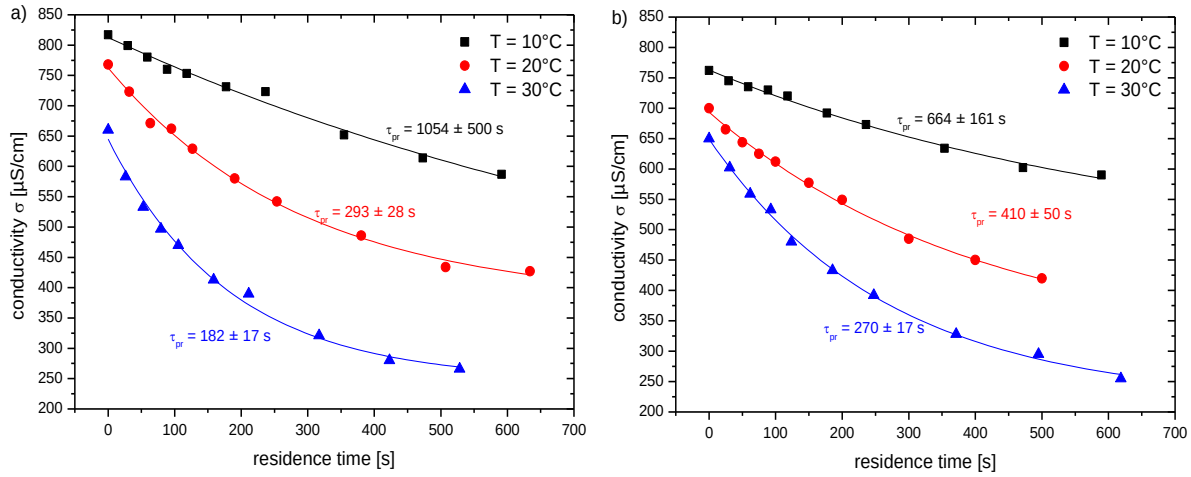

Fig. 5.4: Temporal evolution of electrical conductivity in dependence of the residence time on the marble plates for experiments conducted using a $CaCO_3$ concentration of 5 mmol/L and an ambient pCO_2 of 1000 (a) and 3000 ppmV (b). The solid lines are exponential fits of the experimental data according to Eq. (5.6).

The change in $[Ca^{2+}]$ concentration can be calculated by differentiating Eq. (5.6):

$$\frac{d[Ca^{2+}](t)}{dt} = \frac{1}{\tau_{pr}} * \left([Ca^{2+}]_0 - [Ca^{2+}]_{eq}\right) * exp^{\frac{-t}{\tau pr}}, \tag{5.10}$$

where t is the residence time on the plate, $[Ca^{2+}]_0$ and $[Ca^{2+}]_{eq}$ are the initial and equilibrium concentrations of $[Ca^{2+}]$ in solution, and τ_{pr} is the time constant for precipitation. During the experiments electrical conductivity is measured, which was converted into $[Ca^{2+}]$ concentrations using PhreeqC (Parkhurst and Apello, 1999). By combination with the corresponding film thickness, d, the precipitation rate, F (moles of $CaCO_3$ precipitated per time and area), was determined. All experimentally observed values are in good agreement with the theoretically expected values calculated using the approach of Buhmann et al. (1985a) and Dreybrodt et al. (1997).

5.4.1.3 Temporal $\delta^{13}C$ evolution of DIC

The $\delta^{13}C$ values of DIC show a progressive increase with increasing residence time along the marble plate. Fig. 5.5 exemplarily shows the evolution of the $\delta^{13}C$ values for experiments conducted using a 5 mmol/L $CaCO_3$ solution at 1000 (Fig. 5.5a) and 3000 ppmV CO_2 (Fig. 5.5b). The enrichment of the experiments conducted at a pCO_2 of 1000 ppmV ranges from + 3.6 at 10 °C to + 8.7 ‰ at 30 °C (Fig. 5.5a). Experiments conducted at a higher pCO_2 of 3000 ppmV show a lower enrichment ranging from + 2.4 at 10 °C to + 5.9 ‰ at 20 °C. In general, the enrichment

increases with increasing temperature. The $\delta^{13}C$ values of the experiment conducted at 30 °C and a pCO_2 of 3000 ppmV (blue symbols in Fig. 5.5b) also show a progressive increase until a residence time of approximately 400 s. Subsequently, the $\delta^{13}C$ values reach a plateau and then decrease again.

The results of the experiments conducted using solutions of 2 and 3 mmol/L $CaCO_3$ show a similar evolution. As stated above, from the experiments conducted using a 2 mmol/L $CaCO_3$ solution, only the 30 °C experiment yielded enough $CaCO_3$ to determine the $\delta^{13}C$ values.. The corresponding enrichment is + 2.1 ‰. The experiment conducted using a 3 mmol/L $CaCO_3$-solution at 20 °C shows an enrichment of + 5.4 ‰. The $\delta^{13}C_{DIC}$ values of all experiments are compiled in supplemental Table S 5.1.

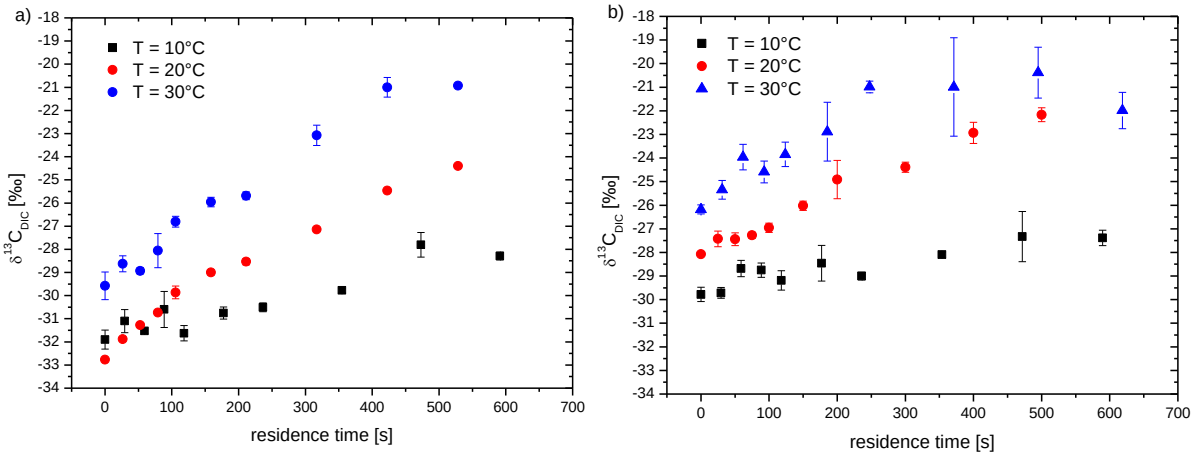

Fig. 5.5: Temporal evolution of the $\delta^{13}C$ values of the DIC for experiments conducted using a 5 mmol/L $CaCO_3$ solution and an ambient pCO_2 of 1000 (a) and 3000 ppmV (b).

5.4.2 $CaCO_3$ experiments

5.4.2.1 Mineralogy of the precipitated $CaCO_3$

We studied $CaCO_3$ from all experiments using Raman spectroscopy. The samples were taken at the same distances as the samples for stable isotope analysis. Almost all precipitates consist of calcite. Only for the experiments conducted at high supersaturation (5 mmol/L $CaCO_3$ at 30°C), a few aragonite crystals were observed. The corresponding sections were avoided for stable isotope analysis. Thus, we consider our results as representative of speleothem calcite.

Furthermore, optical microscopy was performed. Fig. 5.6 exemplarily shows pictures from four different experiments. The $CaCO_3$ from all experiments shows the typical rhombohedral

habitus of calcite crystals, which confirms that the main fraction of the precipitated $CaCO_3$ consists of calcite. Apparently, the size of the crystals is inversely related to the precipitation rate. The smallest crystals are observed for the experiment with the highest precipitation rate (30 °C, 5 mmol/l, Fig. 5.6a), and the crystal size increases at lower temperatures and lower concentrations.

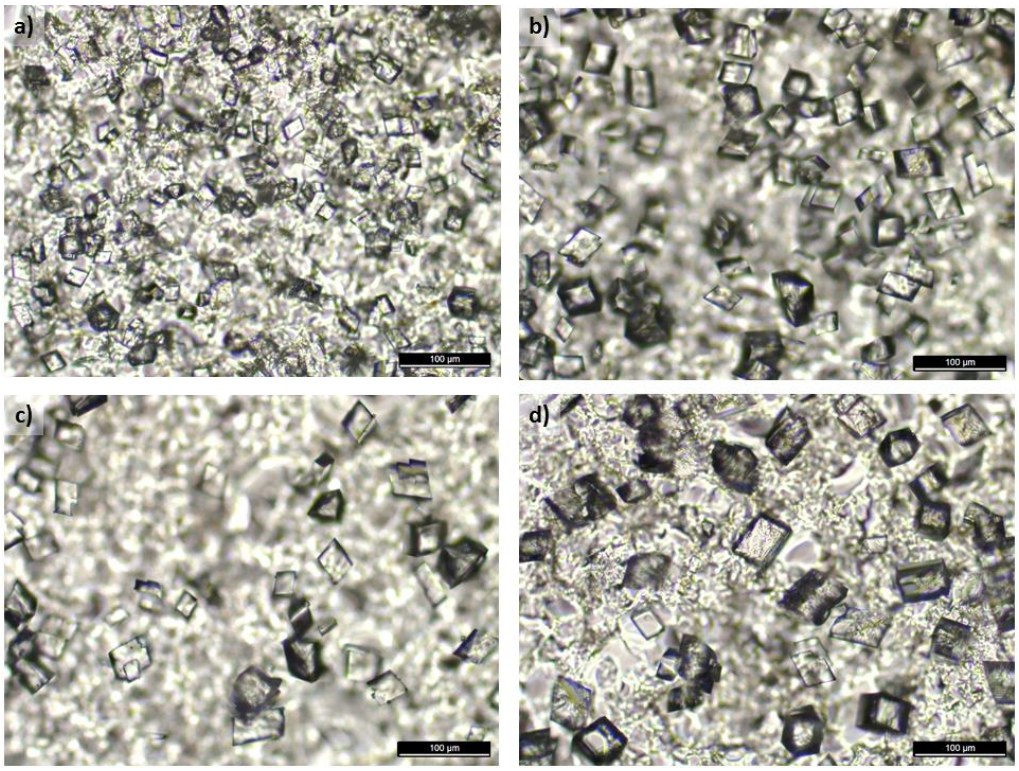

Fig. 5.6: Transmitted-light photomicrographs of the $CaCO_3$ precipitates on glass plates in four different experiments: (a) 5 mmol/L $CaCO_3$ solution at 30 °C and an ambient pCO_2 of 3000 ppmV; (b) 5 mmol/L $CaCO_3$ solution at 20 °C and an ambient pCO_2 of 1000 ppmV; (c) 5 mmol/L $CaCO_3$ solution at 10 °C and an ambient pCO_2 of 3000 ppmV; (d) 3 mmol/L $CaCO_3$ solution at 20 °C and an ambient pCO_2 of 1000 ppmV.

5.4.2.2 Temporal $\delta^{13}C$ evolution of $CaCO_3$

The $\delta^{13}C$ values of $CaCO_3$ precipitated on the glass plates show a similar trend as the $\delta^{13}C$ values of DIC. All experiments show a progressive increase in $\delta^{13}C$ values with increasing residence time due to progressive precipitation of $CaCO_3$. Fig. 5.7 exemplarily shows the corresponding data for experiments conducted using a 5 mmol/L $CaCO_3$ solution at 10, 20 and 30 °C with a pCO_2 of 1000 and 3000 ppmV, respectively. The enrichment for the 1000 ppmV experiments ranges from

+5.8 ‰ at 10 °C to +9.7 ‰ at 30 °C (Fig. 5.7 a). As observed in the DIC experiments, the enrichment is lower for the higher pCO_2 of 3000 ppmV. The corresponding values range from +4.0 ‰ at 10 °C to +7.1 ‰ at 20 °C (Fig. 5.7 b). As for the DIC experiments, the overall enrichment increases with increasing temperature (Fig. 5.7). In general, the enrichment observed in the $CaCO_3$ experiments is up to +2.2 ‰ larger than in the DIC experiments. The experiments performed at a pCO_2 of 3000 ppmV and 30 °C show a progressive increase in the $\delta^{13}C$ values until a residence time of ca. 300 s. Subsequently, the $\delta^{13}C$ values reach a plateau followed by a decreasing trend (Fig. 5.7 b). A similar evolution was observed for the corresponding DIC experiment (Fig. 5.5b).

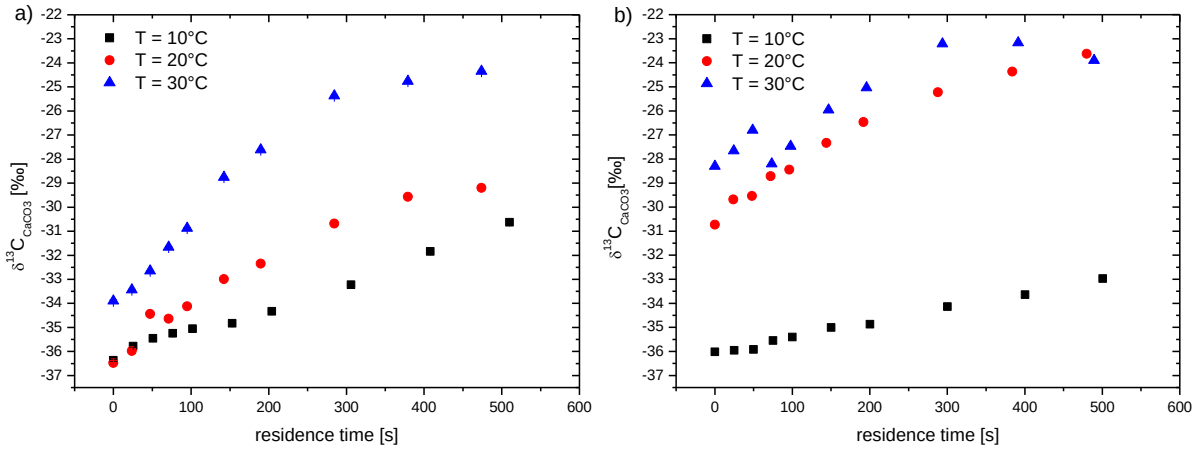

Fig. 5.7: Temporal evolution of the $\delta^{13}C$ values of the precipitated $CaCO_3$ on the glass plates for experiments conducted using a 5 mmol/L $CaCO_3$ solution and an ambient pCO_2 of 1000 (a) and 3000 ppmV (b).

The initial $\delta^{13}C$ values (i.e., at the beginning of the glass plate) shown an increasing trend with temperature (Fig. 5.7). This is particularly pronounced for the experiment conducted at 10 °C and a pCO_2 of 3000 ppmV, which are substantially lower than those of the 20 and 30°C experiments (Fig. 5.7 b).

The experiments performed using 2 and 3 mmol/L $CaCO_3$ concentration show a similar evolution, and the enrichment ranges from +3.9 to +8 ‰. As stated above, the amount of $CaCO_3$ precipitated during the experiments conducted using a 2 mmol/L $CaCO_3$ solution at 10 and 20 °C was too low to determine the stable isotope values. The enrichment in the $\delta^{13}C$ values of the $CaCO_3$ experiments is again slightly larger than for the corresponding DIC experiments. All $\delta^{13}C_{CaCO3}$ values are compiled in supplemental Table S 5.1

5.5 Discussion

5.5.1 Physical and chemical consistency of the DIC and the $CaCO_3$ experiments

There are two major differences between the DIC and the $CaCO_3$ experiments: (i) the material of the plate (marble vs. glass) and (ii) the absence of the equilibration plate in the $CaCO_3$ experiments. The comparability of the DIC and $CaCO_3$ experiments was determined by measuring electrical conductivity at the end of the glass plate inside the box. During the first hours of the $CaCO_3$ experiment (24 h at maximum), the conductivity values at the end of the glass plate continuously decreased indicating increasing precipitation rates. This probably documents the progressive seeding of the glass plate. Subsequently, the plate was seeded with $CaCO_3$ crystals, and the electrical conductivity at the end of the glass plates reached the same value as at the end of the marble plates. This is in agreement with the observations of Stockmann et al. (2014), who performed $CaCO_3$ precipitation experiments using different substrates and found that precipitation rates are independent from the substrate once nucleation has occurred. The conductivity values still slightly decreased after 24 h, but this effect is very small. In addition, the flow velocity on the glass plates was slightly faster than on the marble plates. Flow velocity is related to film thickness, which, in turn, is related to the time constants for precipitation of $CaCO_3$ (Eq. (5.6)). After about 100 h, the precipitation times for the $CaCO_3$ experiment were determined by adjusting the distances of flow according to the distances of the corresponding DIC experiment and measuring electrical conductivity. The time constants are in good agreement within the corresponding errors. For instance, for the experiment performed using a 3 mmol/L $CaCO_3$ solution, at 20 °C and 1000 ppmV CO_2, the time constants for the DIC and the $CaCO_3$ experiment are 436 $\pm$51 and 539 $\pm$45 s, respectively.

As described in section 5.3.1 the pCO_2 of the box atmosphere was kept constant during and logged during the experiments. For example, for the 3 mmol/L $CaCO_3$ solution, the average pCO_2 value was 1065 ppmV with a 1σ-standard deviation of $\pm$ 20 ppmV. Thus, the stability of the box atmosphere was within the range of the precision of the CO_2 probe. In addition, the $\delta^{13}C$ value of the box atmosphere was measured regularly. The $\delta^{13}C$ values only showed a small drift towards positive values from – 40.5 to – 38.5 ‰ and were thus almost constant over the duration of an experiment. The pCO_2 and $\delta^{13}C$ values of the box atmosphere are compiled in Table 5.1.

5.5.2 Modeling $\delta^{13}C$ of the DIC experiments

Scholz et al. (2009) described the temporal evolution of the $\delta^{13}C$ values of the DIC during precipitation of speleothem calcite with a Rayleigh approach. In the following, we apply their model to our experimental data. As discussed in section 5.2.3.1, a calcite-precipitating solution fractionates carbon isotopes into two different sinks: $CaCO_3$ and CO_2 (Eq. (5.2)). Isotope fractionation is described by the corresponding fractionation factors. The combination of these fractionation factors results in a total fractionation factor for the precipitation of speleothem $CaCO_3$. According to the classical Rayleigh distillation model (Eq. (5.9)), the increase in $\delta^{13}C$ depends on the Ca^{2+} fraction remaining in solution. Thus, the temporal evolution of the $\delta^{13}C$ (t) values can be written as:

$$\delta(t) = \left(\frac{\sigma(t)}{\sigma_0}\right)^{\varepsilon_{tot}} * (\delta_0 + 1000) - 1000 \qquad (5.11)$$

Fig. 5.8 shows the $\delta^{13}C$ values in dependence of the Ca^{2+} fraction remaining in solution (σ/σ_0) for the experiments conducted using a 5 mmol/L $CaCO_3$ solution and an ambient atmosphere of 1000 (a) and 3000 ppmV (b) CO_2. The total isotope fractionation, ε_{tot}, can be obtained by fitting the experimental data according to Eq. (5.11). For the data shown in Fig. 5.8, ε_{tot} ranges from -7.4 ± 0.8 to -13.7 ± 0.7 ‰. ε_{tot} is compiled for all experiments in Table 5.1.

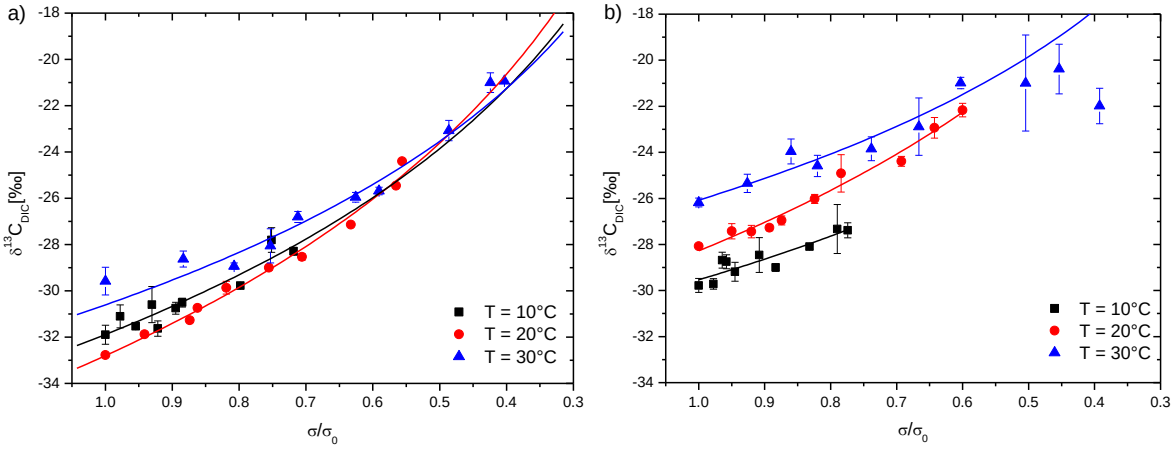

Fig. 5.8: Evolution of $\delta^{13}C_{DIC}$ in dependence of the Ca^{2+} fraction remaining in solution for the experiments conducted using a 5 mmol/L $CaCO_3$ solution at 10, 20 and 30 °C and an ambient pCO_2 of 1000 (a) and 3000 ppmV (b). The solid lines are the corresponding fits according to Eq. (5.11).

Table 5.1: Experimental values of the experiments of this study.

Experiment No.		[$CaCO_3$] [mmol/L]	Temp[°C]	pCO_2 [ppmV]	rH [%]	Film thickness [mm]	$\delta^{13}C_{CO2}$ [‰]	τ_{pr} [s]	$^{13}\varepsilon_{tot}$ [‰]
1	DIC	5	10 ± 0.5	1038 ± 21	80.5 ± 2	0.11	- 45.8 - - 44.4	1054 ± 543	- 11.92 ±0.15
	$CaCO_3$		10.1 ± 0.02	1029 ± 48	89.2 ± 1	0.11	- 46.1 - - 48.5		
2	DIC	5	19.9 ± 0.3	1030 ± 18	91.1 ± 1.5	0.16	- 44.8 - - 42.9	244 ± 24	- 13.67 ± 0.67
	$CaCO_3$		19.7 ± 0.1	1053 ± 42	98.7 ± 1.2	0.1	- 46.5 - - 45.5		
3	DIC	5	30.6 ± 0.2	1033 ± 38	96.5 ± 1.6	0.1	- 46.0 - - 43.9	182 ± 17	- 10.48 ± 0.65
	$CaCO_3$		30.7 ± 0.3	1007 ± 42	97.5 ± 1.2	0.1	- 45.4 - - 43.2		
4	DIC	5	9.9 ± 0.1	2980 ± 28	82.1 ± 1.2	0.11	- 47.6 - - 44.8	644 ± 161	- 7.38 ± 0.83
	$CaCO_3$		9.7 ± 0.1	3020 ± 28	89.8 ± 1.2	0.12	- 46.0 - - 45.5		
5	DIC	5	20.3 ± 0.2	3046 ± 27	88.0 ± 1.3	0.12	- 39.2 - - 39.7	410 ± 50	- 12.08 ± 0.61
	$CaCO_3$		20.0 ± 0.1	3060 ± 35	95.6 ± 0.7	0.11	- 40.3 - - 40.0		
6	DIC	5	31.0 ± 0.2	3069 ± 29	98.4 ± 2.7	0.1	- 38.1 - - 38.9	270 ± 17	- -9.2 ± 1.24
	$CaCO_3$		30.7 ± 0.1	3076 ± 56	99.9 ± 0.6	0.11	- 39.9 - - 39.3		
7*	DIC	2	10.0 ± 0.1	1042 ± 13	77.7 ± 1.7	0.12	- 38.1 - - 38.9	----	---
	$CaCO_3$		9.9 ± 0.2	1030 ± 18	86.4 ± 1.6	0.14	- 39.9 - - 39.3		
8*	DIC	2	20.3 ± 0.1	1099 ± 16	99.7 ± 0.3	0.13	- 40.3 - - 39.3	----	---
	$CaCO_3$		20 ± 0.1	1062 ± 14	100 ± 0.0	0.11	- 40.6 - - 36.7		
9	DIC	2	30.8 ± 0.1	1075 ± 13	95.2 ± 2.2	0.11	- 35.4 - - 34.8	270 ± 33	- 4.73 ± 0.44
	$CaCO_3$		30.6 ± 0.1	1066 ± 17	99.0 ± 0.6	0.11	- 35.2 - - 31.4		
10	DIC	3	20.3 ± 0.1	1071 ± 10	100 ± 0	0.14	- 39.7 - - 37.6	436 ± 51	- 9.8 ± 3.18
	$CaCO_3$		20.2 ± 0.1	1065 ± 20	100 ± 0	0.12	- 40.5 - - 38.5		

* The experiments conducted using 2 mmol/L $CaCO_3$ at 10 and 20 °C did not yielded enough calcite to determine $\delta^{13}C$ and therefore no τ_{pr} and $^{13}\varepsilon_{tot}$ values are given.

By inserting Eq. (5.6) into Eq. (5.11) the temporal evolution along the plate can be derived (Eq. (5.9)). This equation combines the total isotope fractionation in a Rayleigh model with the precipitation rate of calcite and is identical with Eq. (5.7) from Scholz et al. (2009) in the delta notation. All parameters (τ_{pr}, δ_0, σ_{eq}, σ_0, ε_{tot}) can be obtained from our experimental data. Inserting the previously determined parameters into Eq. (5.9) enables to test whether the model adequately describes the temporal evolution of the $\delta^{13}C$ values. Fig. 5.9 exemplarily shows a comparison between model and data for a 5 mmol/L $CaCO_3$ solution at 1000 (Fig. 5.9 a) and 3000 ppmV pCO_2 (Fig. 5.9 b). The straight lines show the modeled $\delta^{13}C_{DIC}$ values, the dashed lines show the corresponding uncertainties, which were calculated by error propagation of the uncertainties obtained from the fits of the experimental data (Figs. 5.4 and 5.8). The experimental data are in very good agreement with the model demonstrating the general applicability of the Rayleigh distillation model to our data.

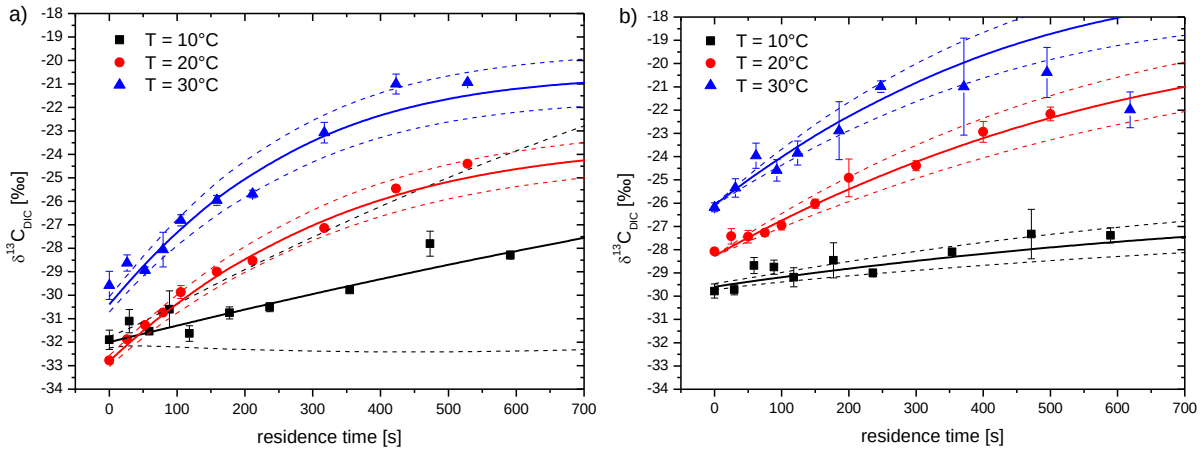

Fig. 5.9: Temporal evolution of $\delta^{13}C_{DIC}$ as a function of the residence time for experiments conducted using a 5 mmol/L $CaCO_3$ solution at 10, 20 and 30 °C and a pCO_2 of 1000 (a) and 3000 ppmV (b). The solid lines show the modeled evolution according to Eq. (5.9). The dashed lines are the corresponding uncertainties.

For the experiment conducted at 30 °C and 3000 ppmV CO_2 the $\delta^{13}C$ values reach a plateau and then decrease again to lower values (Figs. 5.8 b and 5.9 b). This is not in agreement with the Rayleigh model, which predicts an increase followed by the establishment of an equilibrium $\delta^{13}C$ value in chemical equilibrium. Thus, we excluded the last three data points from the fit. The shift towards more negative $\delta^{13}C$ values subsequent to the plateau could be explained by fractionation processes occurring at the calcite surface, as proposed by Dreybrodt (2008) and Dreybrodt and Romanov (2016). In this case, they would be related to the constant γ, which describes the equilibrium $\delta^{13}C$ value, but is so far an unknown quantity (section 5.2.3.2). However, since we

observed this phenomenon only in one of our experiments, our experimental data do neither allow to validate nor reject their model.

Another explanation for the decreasing isotope values at the end of the plate in this experiment is carbon isotope exchange with the (isotopically very negative) CO_2 of the box atmosphere. With increasing residence time the amount of DIC (and the $[Ca^{2+}]$ concentration) in the solution progressively decreases due to precipitation of $CaCO_3$. Simultaneously, the precipitation rate decreases and the solution finally approaches chemical equilibrium (Fig. 5.4). The higher the experimental temperature the higher the precipitation rates (cf. experiments conducted at 30 °C in Fig. 5.4). Thus, the $[Ca^{2+}]$ concentration, and thereby the concentration of DIC, at the end of the plate are much lower for these experiments than for the experiments conducted at lower temperatures (Fig. 5.4). In this case, carbon isotope exchange with the CO_2 atmosphere, which pulls back the $\delta^{13}C$ values of the DIC towards more negative values, may become significant. This is reasonable because the effect is only visible for the experiment conducted at higher pCO_2.

To further evaluate this assumption, we calculated the time constants for carbon isotope exchange for the corresponding experiment using a diffusion-reaction model (Hansen et al., under review). This model calculates the temporal evolution of pH, the concentration of all DIC species and the corresponding $\delta^{13}C$ values if a thin film of solution is exposed to gaseous CO_2. For the initial conditions of the experiment (5 mmol/l $[Ca^{2+}]$, corresponding to 10 mmol/l of $[HCO_3^-]$), the carbon isotope exchange time, τ_{ex}, is 1800 s. Compared to the corresponding time constants for the precipitation of $CaCO_3$ for this experiment ($\tau_{pr} = 270$ s) the exchange times are about 6 times larger and isotope exchange should be negligible. However, at the end of the plate, 61 % of the initial $[HCO_3^-]$ has been lost to the carbonate surface due to precipitation of calcite, which corresponds to a $[HCO_3^-]$ of 3.9 mmol/L (after a residence time of about 600 s). As a consequence the corresponding carbon isotope exchange time also decreases during the experiment, for the final experimental concentration τ_{ex} is 800 s. This is close to the maximum residence time on the plate (600 s). Thus, carbon isotope exchange is very likely to have an influence on the $\delta^{13}C$ values of this experiment, at least for longer residence times. The effect is also visible in the data of the corresponding $CaCO_3$ experiment (Figs. 5.7, 5.8 and 5.9). Note, that the time constant for the precipitation, τ_{pr}, is substantially shorter than the exchange time, τ_{ex}, and is actually not resolved in our experiments. Only the experiment conducted at 30 °C and 3000 ppmV shows a small effect of about – 1.5 ‰.

5.5.3 Comparison of the DIC and the $CaCO_3$ experiments – determination of fractionation factors

5.5.3.1 Fractionation between DIC and $CaCO_3$ – determination of $^{13}\varepsilon_{CaCO3/HCO3-}$

In order to determine the carbon isotope fractionation between DIC and the precipitated calcite, we compare the $\delta^{13}C$ values from the DIC experiment with the corresponding $\delta^{13}C$ values from the $CaCO_3$ experiment. The carbon isotope fractionation between $CaCO_3$ and DIC, $^{13}\varepsilon_{CaCO3/HCO3-}$, is then simply given by the difference between the corresponding $\delta^{13}C$ values (Eq. 5.12):

$$^{13}\varepsilon_{CaCO_3/HCO_3^-}(t) = \delta^{13}C_{CaCO_3}(t) - \delta^{13}C_{HCO_3^-}(t), \quad (5.12)$$

It is essential, however, that the residence times and, thus, the fraction of $[Ca^{2+}]$ remaining in solution is identical for both $\delta^{13}C$ values. Due to the slightly different setup of the DIC and the $CaCO_3$ experiment, the residence times are not identical in both experiments (compare Figs. 5.5 and 5.7). Thus, the values cannot be compared directly. However, as described in section 5.4.2.1, the flow velocity and the precipitation rates on the marble and glass plates are very similar. The temporal evolution of the $\delta^{13}C$ values of the DIC are described by Eq. (5.9). This allows to calculate the $\delta^{13}C$ values of the DIC experiments for the residence time of the corresponding $CaCO_3$ experiments.

Fig. 5.10 exemplarily shows the $\delta^{13}C$ values of the DIC and $CaCO_3$ for selected experiments. In addition, the $\delta^{13}C$ values expected for the $CaCO_3$ for equilibrium carbon isotope fractionation between HCO_3^- and $CaCO_3$ are shown. These were calculated using the fractionation factor of Emrich et al. (1970). All experiments show a large negative carbon isotope fractionation between $CaCO_3$ and DIC (Fig. 5.10). However, with increasing residence time on the plate the difference becomes smaller. The fractionation expected for carbon isotope equilibrium, in contrast, is small and positive. The decreasing isotope fractionation between $CaCO_3$ and DIC with increasing residence time is most obvious for the experiment using a 2 mmol/L $CaCO_3$ solution at 30 °C and 1000 ppmV (Fig. 5.10 d). After about 540 s, the fractionation even becomes positive, but is still 1 ‰ more negative than expected under conditions of isotope equilibrium. For some experiments, the error bars are relatively large (e.g., Fig 5.10 a). However, even considering these large errors, we observe a strong negative carbon isotope fractionation between $CaCO_3$ and DIC for all experiments, which decreases with increasing residence time and, thus, precipitation rate,

Strong, negative and rate-dependent isotope fractionation effects are usually associated with kinetic isotope fractionation processes (Mook and De Vries, 2000; Sharp, 2007). For precipitation of $CaCO_3$, a strong negative fractionation has also been interpreted as 'kinetic' isotope fractionation (Dandurand et al., 1982; Millo et al., 2012; Usdowski et al., 1979). We

emphasize that our approach avoids the effect of isotope fractionation between DIC and CO_2, because we directly compare the $\delta^{13}C$ values of the DIC and the precipitated calcite. The effect of rapid degassing of CO_2, which has often been used to explain speleothem calcite $\delta^{13}C$ values not in equilibrium with the DIC (Hendy, 1971; Mickler et al., 2006), can thus be neglected.

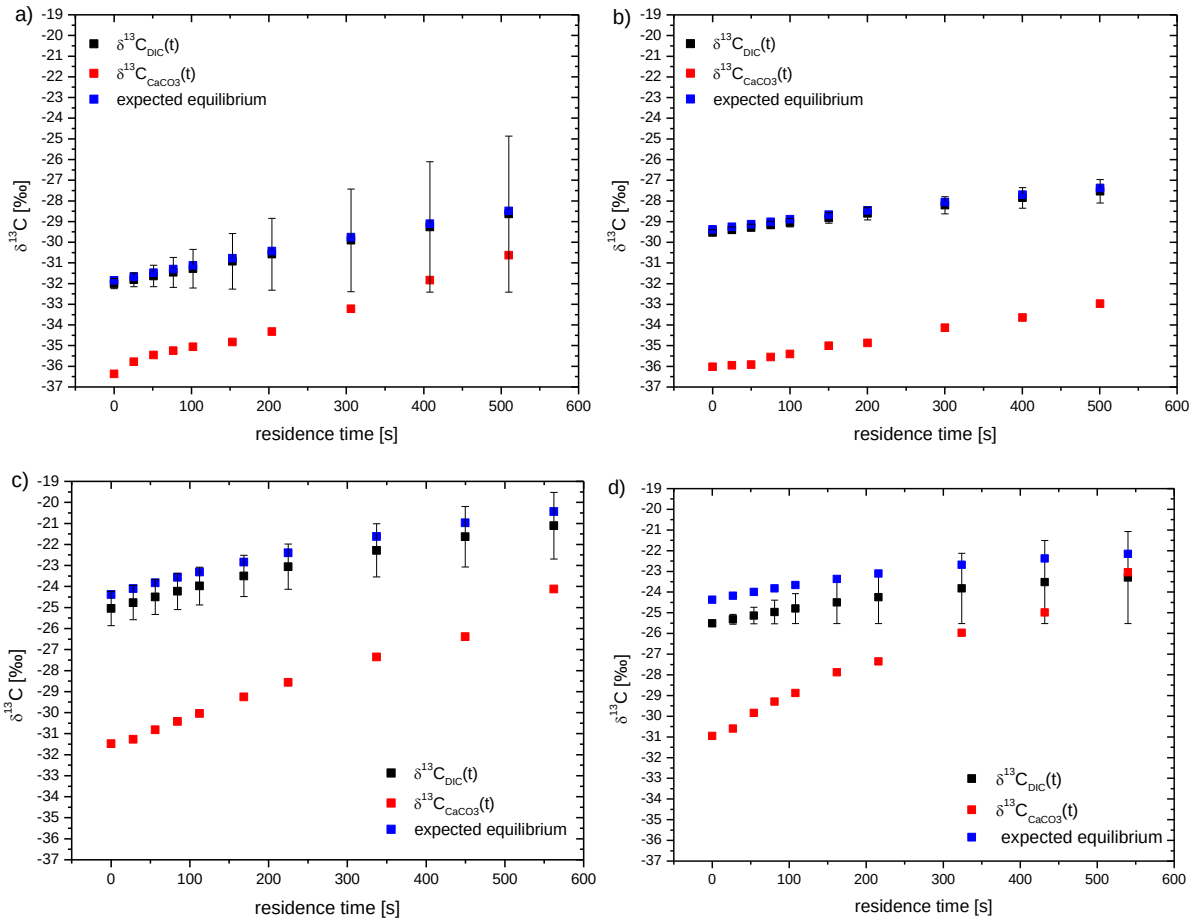

Fig. 5.10: Comparison of the $\delta^{13}C$ values of DIC (black) and the precipitated $CaCO_3$ (red). Also shown are the $\delta^{13}C$ values expected for $CaCO_3$ precipitated under conditions of isotope equilibrium (blue). Exemplarily shown are the results for experiments conducted using (a) 5 mmol/L $CaCO_3$ solution at 10 °C and 1000 ppmVCO_2; (b) 5 mmol/L $CaCO_3$ solution at 10 °C and 3000 ppmV CO_2; (c) 3 mmol/L at 20 °C and 1000 ppmV CO_2; and (d) 2 mmol/L $CaCO_3$ solution at 30 °C and 1000 ppmV. Error bars for the $\delta^{13}C$ values of the DIC were calculated by error propagation using Eq. (9) and the errors from the fits of the experimental data.

Fig. 5.11 shows the relationship between carbon isotope fractionation between $CaCO_3$ and DIC, $^{13}\varepsilon_{CaCO3/HCO3}$, and precipitation rate. The uncertainty of the $\delta^{13}C$ values of the DIC (Fig. 5.10) was propagated to the calculated fractionation factors. For some experiments, the uncertainties are relatively large (e.g. Fig. 5.11 a). All experiments clearly show decreasing isotope fractionation

with decreasing precipitation rate demonstrating a strong influence of precipitation rate on (kinetic) isotope fractionation. Thus, carbon isotope fractionation seems to directly depend on the reaction kinetics during $CaCO_3$ precipitation. However, the absolute values of $^{13}\varepsilon_{CaCO3/HCO3-}$ of the individual experiments show a strong variability ranging from -6.5 to +0.3 ‰. This variability does not show a clear relationship with temperature, pCO_2 or concentration of $[Ca^{2+}]$. For example for the experiment conducted at 10 °C, 5 mmol/l and 1000 ppmV CO_2 (Fig. 5.11a) $^{13}\varepsilon_{CaCO3/HCO3-}$ ranges from -1.9 to -4.4 ‰. The experiment conducted at 10 °C and 5 mmol/l but at 3000 ppmV CO_2 (Fig 5.11b) shows much lower values, ranging from -5.1 to -6.4 ‰.

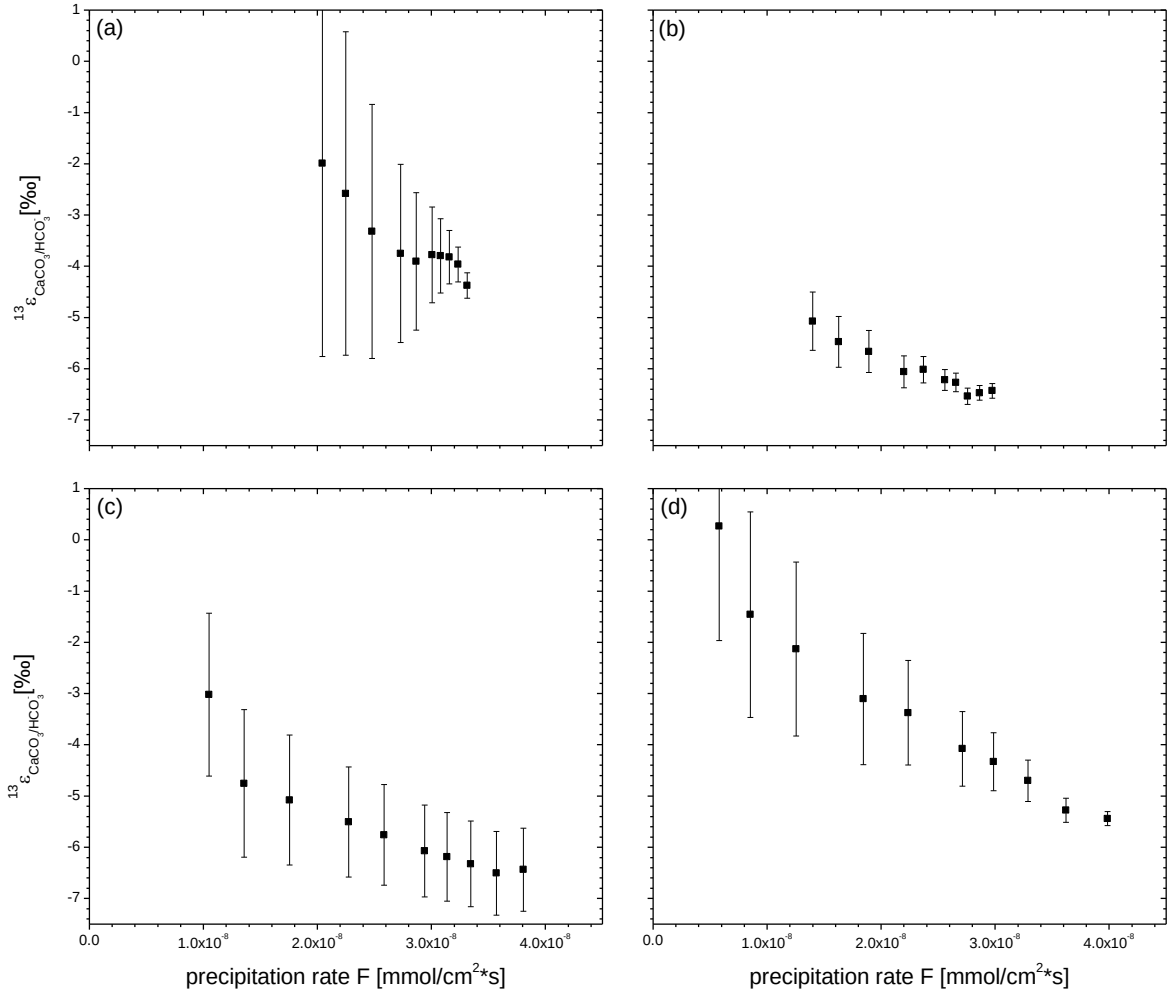

Fig. 5.11: Carbon isotope fractionation between $CaCO_3$ and HCO_3^-, $^{13}\varepsilon_{CaCO3/HCO3-}$, as a function of precipitation rate. Exemplarily shown are the results of the experiments conducted using (a) 5 mmol/L $CaCO_3$ solution at 10 °C and 1000 ppmV CO_2; (b) 5 mmol/L $CaCO_3$ solution at 10 °C and 3000 ppmV CO_2; (c) 3 mmol/L at 20 °C and 1000 ppmV CO_2; and (d) 2 mmol/L $CaCO_3$ solution at 30 °C and 1000 ppmV.

This suggests that the different experiments are not directly comparable and it is therefore not possible to estimate, for instance, the dependence of $^{13}\varepsilon$ on temperature. The relatively large degree of scatter is caused by several minor uncertainties associated with the different experimental setups: (i) the DIC and $CaCO_3$ experiments were conducted using slightly different setups (one glass plate vs. two marble plates); (ii) the flow velocities and the corresponding film thicknesses were slightly different for the DIC and the $CaCO_3$ experiments; (iii) the distances required for chemical equilibration was different for different experiments. Thus, in particular for the DIC experiments, even co-precipitation of small amounts of dissolved CO_2 and, thus, slightly biased $\delta^{13}C$ values for small distances of flow cannot be completely excluded. Most importantly, however, the large degree of scatter between the different experiments is related to initial (isotopic) conditions. As described in the methods (section 5.3) the SI of the solution was adjusted to values of about 0, by sparging the excess CO_2 with argon and carefully measuring the pH values. This is, however, very difficult and deviations from $SI = 0$ cannot be excluded. This is, for example, visible in the initial $\delta^{13}C$ values, which show an increasing trend with temperature (Fig. 5.7). In particular for the experiment conducted at 10 °C and a pCO_2 of 3000 ppmV, which shows substantially lower initial $\delta^{13}C$ values than those of the 20 and 30°C experiments (Fig. 5.7 b). This may be related to the chemical equilibration of the reservoir. At lower temperatures, the solubility of CO_2 in water increases (e.g., Murray and Riley, 1971). Thus, at lower temperatures, the fraction of dissolved CO_2 (with a more negative $\delta^{13}C$ value) of the total DIC is higher than at higher temperatures. However, for the 10 °C experiment, we cannot exclude that the saturation index of the solution was still slightly lower than 0 prior to equilibration of the reservoir. Thus, for this experiment, the fraction of dissolved CO_2 may have been larger than for the other experiments leading to more negative initial $\delta^{13}C$ values of the $CaCO_3$. This effect is also visible in the DIC experiments (compare Fig. 5.5 b), but more obvious in the $CaCO_3$ experiments.

In summary, our experiments clearly show a rate dependence of $^{13}\varepsilon_{CaCO3/HCO3-}$. However, absolute values and their dependence on temperature and precipitation rate cannot be determined.

5.5.3.2 Fractionation between HCO_3^- and CO_2 – determination of $^{13}\varepsilon_{CO2/HCO3-}$

Based on the total isotope fractionation, ε_{tot}, calculated in section 5.1 and the isotope fractionation between $CaCO_3$ and HCO_3, the isotope fractionation- between HCO_3^- and CO_2 can be calculated by subtracting $^{13}\varepsilon_{CaCO3/HCO3-}$ from the total isotope fractionation (see section 5.2.2.2 and 5.5.1):

$$^{13}\varepsilon_{CO_2\ /HCO_3^-} = \left(^{13}\varepsilon_{tot} - 0.5 * {}^{13}\varepsilon_{CaCO_3/HCO_3^-}\right) * 2. \quad (5.13)$$

At isotopic equilibrium, values between -7.29 and -9.47 ‰ are expected for $\varepsilon_{CO2/HCO3-}$ at the temperatures of our experiments (Emrich et al., 1970). The average values in our experiments range from -11.3 ‰ to -24 ‰ and are, thus much more negative than expected under conditions of isotope equilibrium. This indicates kinetic isotope fractionation between CO_2 and HCO_3^- during precipitation of speleothem calcite, as observed for $\varepsilon_{CaCO3/HCO3-}$. In the previous section, we have shown a strong dependence of $^{13}\varepsilon_{CaCO3/HCO3-}$ on precipitation rate. Thus, $^{13}\varepsilon_{CaCO3/HCO3-}$ is not constant along the plates, but becomes more positive with increasing residence time. However, using a Rayleigh approach, ε_{tot}, in contrast, is constant by definition (Eq. (5.11)). As a result, the values for $^{13}\varepsilon_{CO2/HCO3-}$ calculated with Eq. (5.13) are not constant, but become more negative with increasing residence time. However, it is likely that $^{13}\varepsilon_{CO2/HCO3-}$ also depends on precipitation rate. Thus, the values calculated for $^{13}\varepsilon_{CO2/HCO3-}$ should be considered as an estimate rather than a precise determination.

5.5.3.3 Limitations of the experiments

All our experimental results can be described using the Rayleigh model proposed by Scholz et al. (2009) by inserting the experimentally determined fractionation factors. The 'kinetic' model proposed by Dreybrodt (2008) is considerably more complex. The differences between both models only become relevant after about 75 % of the Ca^{2+} has precipitated to the carbonate surface. Prior to this, the temporal evolution of both models are very similar (Dreybrodt and Scholz, 2011; Scholz et al., 2009). During our experiments, at maximum ca. 60 % of the $[Ca^{2+}]$ in solution precipitated, which is still far from chemical equilibrium of the precipitating solution. Thus, the 'kinetic' model proposed by Dreybrodt (2008) can neither be validated nor rejected with these experimental data.

Both models have in common that they use a constant fractionation factor to describe isotope fractionation, which only depends on temperature, independently on whether a 'kinetic' or an 'equilibrium' fractionation factor is used. Our experimental data, however, show a very different "behavior" of carbon isotope fractionation. All experiments show a strong dependence

of the fractionation factor on precipitation rate, which, in turn, is related to temperature. Further experimental work is required to determine whether the 'kinetic' or the Rayleigh approach is more suitable, or a new model is required in which the fractionation factors are related to the precipitation kinetics. Essential in this context are longer residence times on the plates as well as lower concentrations/supersaturation of the solution, which would allow getting closer to the chemical equilibrium.

5.6. Conclusions

The cave analogue experiments presented in this study allow, for the first time, to directly determine the isotope fractionation between $CaCO_3$ and all other involved dissolved carbon species (HCO_3^-, CO_2) in a thin water film, comparable to the surface of speleothems. All chemical parameters, including precipitation rate, time constants of precipitation and pH are in agreement with previously published theoretical studies (e.g., Baker et al., 1998; Buhmann and Dreybrodt, 1985a; Dreybrodt et al., 1997) and show the expected temperature dependence.

We observe a strong enrichment of the $\delta^{13}C$ values of up to + 8.7 ‰ in both the DIC and the $CaCO_3$ experiments. The temporal evolution of the $\delta^{13}C_{DIC}$ values can be explained by a Rayleigh distillation model, as suggested by Scholz et al. (2009). The total carbon isotope fractionation, $^{13}\varepsilon_{tot}$, in dependence of the solution chemistry, seems to be much larger than expected from isotope equilibrium, with values up to + 13.7 ‰. All experiments show a large negative fractionation between DIC and $CaCO_3$, $^{13}\varepsilon_{CaCO3/HCO3-}$, which decreases with increasing residence time on the plates and are, thus, strongly dependent on precipitation rate. However, with increasing residence time and, thus, decreasing supersaturation and precipitation rate the fractionation becomes smaller and even positive approaching equilibrium. This suggests, that the assumption of previous studies (e.g., Dreybrodt, 2008; Dreybrodt and Scholz, 2011; Scholz et al., 2009) of a static fractionation factor may not entirely correct, as this study shows that the fractionation factors also seem to be coupled to chemical kinetics, especially if the precipitation rate is high at the beginning of an experiment (equivalent to calcite precipitating at the top of a stalagmite as opposed to the flanks). A final validation which model (i.e., Dreybrodt, 2008; vs Scholz et al., 2009) is more suitable for the interpretation of speleothem isotope records is not possible within the resolution of this study. In order to investigate these mechanisms in more detail it is necessary to perform experiments with a longer duration and solutions closer to chemical equilibrium.

The rate-dependent (negative) fractionation processes may lead to an overestimation of isotope values in terms of cave ventilation or (paleo-)vegetation changes. Thus, for paleoclimate purpose, stable carbon isotope records should be interpreted with care. Thoroughly conducted

monitoring studies, testing the present-day in-situ conditions of fractionation processes inside a cave, may provide important constraints on the most suitable fractionation factors for interpretation of the corresponding speleothem record for this particular site.

Acknowledgements

M. Hansen and D. Scholz acknowledge funding by the Deutsche Forschungsgemeinschaft (DFG) through grants SCHO 1274/8-1 and SCHO 1274/9-1. We thank Wolfgang Dreybrodt for discussion and comments on the manuscript. Furthermore we are thankful to the workshop of the Institutes for Geosciences and Physics of the Atmosphere, University of Mainz, especially S. Klumb, for technical support during the experiments and to keep the climate box running reliably.

5.7. References

Appelo, C.A.J., Postma, D. (2004) *Geochemistry, groundwater and pollution*. CRC press.

Asmerom, Y., Polyak, V.J., Burns, S.J. (2010) Variable winter moisture in the southwestern United States linked to rapid glacial climate shifts. *Nature Geosci* **3**, 114-117.

Baker, A., Genty, D., Dreybrodt, W., Barnes, W.L., Mockler, N.J., Grapes, J. (1998) Testing Theoretically Predicted Stalagmite Growth Rate with Recent Annually Laminated Samples: Implications for Past Stalagmite Deposition. *Geochimica et Cosmochimica Acta* **62**, 393-404.

Bar-Matthews, M., Ayalon, A., Gilmour, M., Matthews, A., Hawkesworth, C.J. (2003) Sea–land oxygen isotopic relationships from planktonic foraminifera and speleothems in the Eastern Mediterranean region and their implication for paleorainfall during interglacial intervals. *Geochimica et Cosmochimica Acta* **67**, 3181-3199.

Bar-Matthews, M., Ayalon, A., Matthews, A., Sass, E., Halicz, L. (1996) Carbon and oxygen isotope study of the active water-carbonate system in a karstic Mediterranean cave: Implications for paleoclimate research in semiarid regions. *Geochimica et Cosmochimica Acta* **60**, 337-347.

Beck, W.C., Grossman, E.L., Morse, J.W. (2005) Experimental studies of oxygen isotope fractionation in the carbonic acid system at 15°, 25°, and 40°C. *Geochimica et Cosmochimica Acta* **69**, 3493-3503.

Boch, R., Cheng, H., Spötl, C., Edwards, R., Wang, X., Häuselmann, P., 2011. NALPS: a precisely dated European climate record 120–60 ka, Clim. Past, 7, 1247–1259.

Breecker, D.O. (2017) Atmospheric pCO_2 control on speleothem stable carbon isotope compositions. *Earth and Planetary Science Letters* **458**, 58-68.

Buhmann, D., Dreybrodt, W. (1985) The kinetics of calcite dissolution and precipitation in geologically relevant situations of karst areas: 1. Open system. *Chemical Geology* **48**, 189-211.

Cheng, H., Edwards, R.L., Sinha, A., Spötl, C., Yi, L., Chen, S., Kelly, M., Kathayat, G., Wang, X., Li, X., Kong, X., Wang, Y., Ning, Y., Zhang, H. (2016) The Asian monsoon over the past 640,000 years and ice age terminations. *Nature* **534**, 640-646.

Cruz, F.W., Burns, S.J., Karmann, I., Sharp, W.D., Vuille, M., Cardoso, A.O., Ferrari, J.A., Silva Dias, P.L., Viana, O. (2005) Insolation-driven changes in atmospheric circulation over the past 116,000 years in subtropical Brazil. *Nature* **434**, 63-66.

Dandurand, J.L., Gout, R., Hoefs, J., Menschel, G., Schott, J., Usdowski, E. (1982) Kinetically controlled variations of major components and carbon and oxygen isotopes in a calcite-precipitating spring. *Chemical Geology* **36**, 299-315.

Day, C.C., Henderson, G.M. (2011) Oxygen isotopes in calcite grown under cave-analogue conditions. *Geochimica et Cosmochimica Acta* **75**, 3956-3972.

Deininger, M., Fohlmeister, J., Scholz, D., Mangini, A. (2012) Isotope disequilibrium effects: The influence of evaporation and ventilation effects on the carbon and oxygen isotope composition of speleothems – A model approach. *Geochimica et Cosmochimica Acta* **96**, 57-79.

Dorale, J.A., Liu, Z. (2009) Limitations of Hendy test criteria in judging the paleoclimatic suitability of speleothems and the need for replication. *Journal of Cave and Karst Studies* **71**, 73-80.

Dreybrodt, W. (1988) *Processes in Karst Systems*. Series in Physical Environment, Vol. **4**, Springer, Heidelberg.

Dreybrodt, W. (2008) Evolution of the isotopic composition of carbon and oxygen in a calcite precipitating H_2O–CO_2–$CaCO_3$ solution and the related isotopic composition of calcite in stalagmites. *Geochimica et Cosmochimica Acta* **72**, 4712-4724.

Dreybrodt, W. (2016) Problems in using the approach of Rayleigh distillation to interpret the ^{13}C and ^{18}O isotope compositions in stalagmite calcite. *Acta Carsologica* **45**.

Dreybrodt, W., Deininger, M. (2014) The impact of evaporation to the isotope composition of DIC in calcite precipitating water films in equilibrium and kinetic fractionation models. *Geochimica et Cosmochimica Acta* **125**, 433-439.

Dreybrodt, W., Eisenlohr, L., Madry, B., Ringer, S. (1997) Precipitation kinetics of calcite in the system $CaCO_3$-H_2O-$C0_2$: The conversion to CO_2 by the slow process $H^+ + HCO_3^- \rightarrow CO_2 + H_2O$ as a rate limiting step. *Geochimica et Cosmochimica Acta* **61**, 3897-3904.

Dreybrodt, W., Hansen, M., Scholz, D. (2016) Processes affecting the stable isotope composition of calcite during precipitation on the surface of stalagmites: Laboratory experiments investigating the isotope exchange between DIC in the solution layer on top of a speleothem and the CO_2 of the cave atmosphere. *Geochimica et Cosmochimica Acta* **174**, 247-262.

Dreybrodt, W., Romanov, D. (2016) The evolution of ^{13}C and ^{18}O isotope composition of DIC in a calcite depositing film of water with isotope exchange between the DIC and a CO_2 containing

atmosphere, and simultaneous evaporation of the water. Implication to climate proxies from stalagmites: A theoretical model. *Geochimica et Cosmochimica Acta* **195**, 323-338.

Dreybrodt, W., Scholz, D. (2011) Climatic dependence of stable carbon and oxygen isotope signals recorded in speleothems: From soil water to speleothem calcite. *Geochimica et Cosmochimica Acta* **75**, 734-752.

Emrich, K., Ehhalt, D.H., Vogel, J.C. (1970) Carbon isotope fractionation during the precipitation of calcium carbonate. *Earth and Planetary Science Letters* **8**, 363-371.

Fairchild, I.J., Baker, A. (2012) *Speleothem science: from process to past environments*. John Wiley & Sons.

Fantidis, J., Ehhalt, D.H. (1970) Variations of the carbon and oxygen isotopic composition in stalagmites and stalactites: Evidence of non-equilibrium isotopic fractionation. *Earth and Planetary Science Letters* **10**, 136-144.

Fleitmann, D., Burns, S.J., Neff, U., Mudelsee, M., Mangini, A., Matter, A. (2004) Palaeoclimatic interpretation of high-resolution oxygen isotope profiles derived from annually laminated speleothems from Southern Oman. *Quaternary Science Reviews* **23**, 935-945.

Fornaca-Rinaldi, G., Panichi, C., Tongiorgi, E. (1968) Some causes of the variation of the isotopic composition of carbon and oxygen in cave concretions. *Earth and Planetary Science Letters* **4**, 321-324.

Genty, D., Blamart, D., Ouahdi, R., Gilmour, M., Baker, A., Jouzel, J., Van-Exter, S. (2003) Precise dating of Dansgaard-Oeschger climate oscillations in western Europe from stalagmite data. *Nature* **421**, 833-837.

Hansen, M., Dreybrodt, W., Scholz, D. (2013) Chemical evolution of dissolved inorganic carbon species flowing in thin water films and its implications for (rapid) degassing of CO_2 during speleothem growth. *Geochimica et Cosmochimica Acta* **107**, 242-251.

Hellstrom, J.C., McCulloch, M.T. (2000) Multi-proxy constraints on the climatic significance of trace element records from a New Zealand speleothem. *Earth and Planetary Science Letters* **179**, 287-297.

Hendy, C.H. (1971) The isotopic geochemistry of speleothems—I. The calculation of the effects of different modes of formation on the isotopic composition of speleothems and their applicability as palaeoclimatic indicators. *Geochimica et Cosmochimica Acta* **35**, 801-824.

Hendy, C.H., Wilson, A.T. (1968) Palaeoclimatic Data from Speleothems. *Nature* **219**, 48-51.

Mangini, A., Spötl, C., Verdes, P. (2005) Reconstruction of temperature in the Central Alps during the past 2000 yr from a $\delta^{18}O$ stalagmite record. *Earth and Planetary Science Letters* **235**, 741-751.

McCrea, J.M. (1950) On the isotopic chemistry of carbonates and a paleotemperature scale. *The Journal of Chemical Physics* **18**, 849-857.

McDermott, F. (2004) Palaeo-climate reconstruction from stable isotope variations in speleothems: a review. *Quaternary Science Reviews* **23**, 901-918.

Mickler, P.J., Banner, J.L., Stern, L., Asmerom, Y., Edwards, R.L., Ito, E. (2004) Stable isotope variations in modern tropical speleothems: Evaluating equilibrium vs. kinetic isotope effects 1. *Geochimica et Cosmochimica Acta* **68**, 4381-4393.

Mickler, P.J., Stern, L.A., Banner, J.L. (2006) Large kinetic isotope effects in modern speleothems. *Geological Society of America Bulletin* **118**, 65-81.

Millo, C., Dupraz, S., Ader, M., Guyot, F., Thaler, C., Foy, E., Ménez, B. (2012) Carbon isotope fractionation during calcium carbonate precipitation induced by ureolytic bacteria. *Geochimica et Cosmochimica Acta* **98**, 107-124.

Mischel, S.A., Scholz, D., Spötl, C., Jochum, K.P., Schröder-Ritzrau, A., Fiedler, S. (2016) Holocene climate variability in Central Germany and a potential link to the polar North Atlantic: A replicated record from three coeval speleothems. *The Holocene*.

Mook, W.G., Bommerson, J.C., Staverman, W.H. (1974) Carbon isotope fractionation between dissolved bicarbonate and gaseous carbon dioxide. *Earth and Planetary Science Letters* **22**, 169-176.

Mook, W.G., De Vries, J. (2000) Volume I: Introduction: Theory, Methods, Review. *Environmental Isotopes in the Hydrological Cycle—Principles and Applications, International Hydrological Programme (IHP-V), Technical Documents in Hydrology (IAEA/UNESCO) No* **39**, 75-76.

Mühlinghaus, C., Scholz, D., Mangini, A. (2007) Modelling stalagmite growth and $\delta^{13}C$ as a function of drip interval and temperature. *Geochimica et Cosmochimica Acta* **71**, 2780-2790.

Mühlinghaus, C., Scholz, D., Mangini, A. (2009) Modelling fractionation of stable isotopes in stalagmites. *Geochimica et Cosmochimica Acta* **73**, 7275-7289.

Murray, C.N., Riley, J.P. (1971) The solubility of gases in distilled water and sea water—IV. Carbon dioxide. *Deep Sea Research and Oceanographic Abstracts* **18**, 533-541.

Parkhurst, D., Apello, C. (1999) User's Guide to PHREEQC (V2). *US Geol. Surv* **312**.

Plummer, L., Wigley, T., Parkhurst, D. (1978) The kinetics of calcite dissolution in CO_2-water systems at 5 degrees to 60 degrees C and 0.0 to 1.0 atm CO_2. *American Journal of Science* **278**, 179-216.

Polag, D., Scholz, D., Mühlinghaus, C., Spötl, C., Schröder-Ritzrau, A., Segl, M., Mangini, A. (2010) Stable isotope fractionation in speleothems: Laboratory experiments. *Chemical Geology* **279**, 31-39.

Ridley, H.E., Asmerom, Y., Baldini, J.U.L., Breitenbach, S.F.M., Aquino, V.V., Prufer, K.M., Culleton, B.J., Polyak, V., Lechleitner, F.A., Kennett, D.J., Zhang, M., Marwan, N., Macpherson, C.G., Baldini, L.M., Xiao, T., Peterkin, J.L., Awe, J., Haug, G.H. (2015) Aerosol forcing of the position of the intertropical convergence zone since ad 1550. *Nature Geosci* **8**, 195-200.

Romanek, C.S., Grossman, E.L., Morse, J.W. (1992) Carbon isotopic fractionation in synthetic aragonite and calcite: Effects of temperature and precipitation rate. *Geochimica et Cosmochimica Acta* **56**, 419-430.

Romanov, D., Kaufmann, G., Dreybrodt, W. (2008a) Modeling stalagmite growth by first principles of chemistry and physics of calcite precipitation. *Geochimica et Cosmochimica Acta* **72**, 423-437.

Romanov, D., Kaufmann, G., Dreybrodt, W. (2008b) $\delta^{13}C$ profiles along growth layers of stalagmites: Comparing theoretical and experimental results. *Geochimica et Cosmochimica Acta* **72**, 438-448.

Salomons, W., Mook, W. (1986) Isotope geochemistry of carbonates in the weathering zone. *Handbook of environmental isotope geochemistry* **2**, 239-269.

Scholz, D., Frisia, S., Borsato, A., Spötl, C., Fohlmeister, J., Mudelsee, M., Miorandi, R., Mangini, A. (2012) Holocene climate variability in north-eastern Italy: potential influence of the NAO and solar activity recorded by speleothem data. *Clim. Past* **8**, 1367-1383.

Scholz, D., Mühlinghaus, C., Mangini, A. (2009) Modelling $\delta^{13}C$ and $\delta^{18}O$ in the solution layer on stalagmite surfaces. *Geochimica et Cosmochimica Acta* **73**, 2592-2602.

Scholz, D., Hoffmann, D. (2008) $^{230}Th/U$-dating of fossil corals and speleothems. *Eiszeitalter und Gegenwart* **57**, 52-76.

Sharp, Z. (2007) *Principles of stable isotope geochemistry*. Pearson Education Upper Saddle River, NJ.

Spötl, C. (2004) A simple method of soil gas stable carbon isotope analysis. *Rapid Communications in Mass Spectrometry* **18**, 1239-1242.

Spötl, C., Scholz, D., Mangini, A. (2008) A terrestrial U/Th-dated stable isotope record of the Penultimate Interglacial. *Earth and Planetary Science Letters* **276**, 283-292.

Stockmann, G.J., Wolff-Boenisch, D., Bovet, N., Gislason, S.R., Oelkers, E.H. (2014) The role of silicate surfaces on calcite precipitation kinetics. *Geochimica et Cosmochimica Acta* **135**, 231-250.

Usdowski, E., Hoefs, J., Menschel, G. (1979) Relationship between13C and18O fractionation and changes in major element composition in a recent calcite-depositing spring — A model of chemical variations with inorganic CaCO3 precipitation. *Earth and Planetary Science Letters* **42**, 267-276.

Vogel, J.C., Grootes, P.M., Mook, W.G. (1970) Isotopic fractionation between gaseous and dissolved carbon dioxide. *Zeitschrift für Physik* **230**, 225-238.

Wassenburg, J.A., Dietrich, S., Fietzke, J., Fohlmeister, J., Jochum, K.P., Scholz, D., Richter, D.K., Sabaoui, A., Spotl, C., Lohmann, G., Andreae, M.O., Immenhauser, A. (2016) Reorganization of the North Atlantic Oscillation during early Holocene deglaciation. *Nature Geosci* **advance online publication**.

Wiedner, E., Scholz, D., Mangini, A., Polag, D., Mühlinghaus, C., Segl, M. (2008) Investigation of the stable isotope fractionation in speleothems with laboratory experiments. *Quaternary International* **187**, 15-24.

Zeebe, R.E., Wolf-Gladrow, D. (2001) *CO_2 in Seawater: Equilibrium, Kinetics, Isotopes*. Elsevier Science.

5.8 Supplementary Information

Table S5.1 a: Experimental results for experiment #1, conducted using a 5 mmol/l $CaCO_3$ solution at 10° C and a pCO_2 of 1000 ppmV.

distance of flow [cm]	residence time DIC [s]	electrical conductivity σ [µS/cm]	pH	$\delta^{13}C_{DIC}$ [‰]	±	residence time $CaCO_3$ [s]	$\delta^{13}C_{CaCO3}$ [‰]	±
100	591	587	8.20	-28.29	0.17	510	-30.63	0.06
80	473	614	8.21	-27.80	0.53	408	-31.84	0.04
60	355	652	8.10	-29.77	0.10	306	-33.23	0.03
40	236	723	8.19	-30.51	0.19	204	-34.33	0.04
30	177	731	8.04	-30.75	0.26	153	-34.83	0.04
20	118	753	8.14	-31.63	0.33	102	-35.05	0.04
15	89	760	8.12	-30.60	0.78	76.5	-35.25	0.03
10	59	780	7.89	-31.53	0.10	51	-35.46	0.03
5	30	799	7.87	-31.10	0.50	25.5	-35.78	0.05
0	0	817	7.79	-31.90	0.41	0	-36.37	0.05

Table S5.1 b: Experimental results for experiment #2, conducted using a 5 mmol/l $CaCO_3$ solution at 20° C and a pCO_2 of 1000 ppmV.

distance of flow [cm]	residence time DIC [s]	electrical conductivity σ [µS/cm]	pH	$\delta^{13}C_{DIC}$ [‰]	±	residence time $CaCO_3$ [s]	$\delta^{13}C_{CaCO3}$ [‰]	±
100	634	427	8.10	-24.40	0.08	474	-29.20	0.02
80	507	434	8.10	-25.46	0.07	379	-29.57	0.02
60	380	486	8.10	-27.14	0.05	284	-30.68	0.02
40	254	542	8.10	-28.54	0.13	190	-32.35	0.02
30	190	580	8.03	-29.00	0.11	142	-33.00	0.02
20	127	629	8.05	-29.86	0.28	95	-34.12	0.02
15	95	662	7.99	-30.74	0.01	71	-34.64	0.01
10	63	671	8.02	-31.27	0.10	47	-34.44	0.02
5	32	723	7.98	-31.88	0.07	24	-35.98	0.01
0	0	768	7.81	-32.77	0.04	0	-36.48	0.03

Table S5.1 c: Experimental results for experiment #3, conducted using a 5 mmol/l $CaCO_3$ solution at 30° C and a pCO_2 of 1000 ppmV.

distance of flow [cm]	residence time DIC [s]	electrical conductivity σ [µS/cm]	pH	$\delta^{13}C_{DIC}$ [‰]	±	residence time $CaCO_3$ [s]	$\delta^{13}C_{CaCO3}$ [‰]	±
100	528	266	7.999	-20.93	0.01	474	-24.34	0.01
80	423	280	8.164	-21.00	0.43	379	-24.76	0.01
60	317	321	8.159	-23.07	0.44	284	-25.37	0.03
40	211	390	8.199	-25.69	0.17	190	-27.61	0.02
30	159	413	8.058	-25.96	0.21	142	-28.75	0.01
20	106	470	8.055	-26.81	0.24	95	-30.87	0.02
15	79	497	8	-28.06	0.74	71	-31.66	0.02
10	53	533	8.016	-28.93	0.13	47	-32.65	0.02
5	26	583	7.9	-28.63	0.35	24	-33.44	0.02
0	0	660	8.086	-29.58	0.60	0	-33.90	0.04

Table S5.1 d: Experimental results for experiment #4, conducted using a 5 mmol/l $CaCO_3$ solution at 10° C and a pCO_2 of 3000 ppmV.

distance of flow [cm]	residence time DIC [s]	electrical conductivity σ [µS/cm]	pH	$\delta^{13}C_{DIC}$ [‰]	±	residence time $CaCO_3$ [s]	$\delta^{13}C_{CaCO3}$ [‰]	±
100	589.69	590	7.94	-27.39	0.33	501	-32.97	0.04
80	471.75	602	7.98	-27.33	1.06	400	-33.64	0.02
60	353.82	634	7.93	-28.10	0.11	300	-34.14	0.01
40	235.88	673	7.87	-29.00	0.16	200	-34.87	0.03
30	176.91	692	7.87	-28.46	0.75	150	-35.01	0.02
20	117.94	720	7.91	-29.18	0.41	100	-35.40	0.01
15	88.45	730	7.88	-28.75	0.31	75	-35.55	0.02
10	58.97	735	7.86	-28.97	0.02	50	-35.92	0.02
5	29.48	745	7.86	-29.72	0.03	25	-35.96	0.02
0	0.00	762	7.82	-29.74	0.03	0	-36.02	0.04

Table S5.1 e: Experimental results for experiment #5, conducted using a 5 mmol/l $CaCO_3$ solution at 20° C and a pCO_2 of 3000 ppmV.

distance of flow [cm]	residence time DIC [s]	electrical conductivity σ [µS/cm]	pH	$\delta^{13}C_{DIC}$ [‰]	±	residence time $CaCO_3$ [s]	$\delta^{13}C_{CaCO3}$ [‰]	±
100	500	420	8.05	-22.17	0.29	480	-23.63	0.02
80	400	450	8.08	-22.93	0.45	384	-24.37	0.02
60	300	485	8.03	-24.39	0.21	288	-25.22	0.03
40	200	549	8.02	-24.91	0.81	192	-26.47	0.02
30	150	577	8.01	-26.03	0.20	144	-27.34	0.03
20	100	612	7.98	-26.96	0.20	96	-28.45	0.03
15	75	625	7.97	-27.28	0.13	72	-28.72	0.02
10	50	644	7.94	-27.44	0.27	48	-29.54	0.03
5	25	665	7.93	-27.43	0.34	24	-29.68	0.02
0	0	700	7.95	-28.07	0.06	0	-30.73	0.02

Table S5.1 f: Experimental results for experiment #6, conducted using a 5 mmol/l $CaCO_3$ solution at 30° C and a pCO_2 of 3000 ppmV.

distance of flow [cm]	residence time DIC [s]	electrical conductivity σ [µS/cm]	pH	$\delta^{13}C_{DIC}$ [‰]	±	residence time $CaCO_3$ [s]	$\delta^{13}C_{CaCO3}$ [‰]	±
100	591	255	7.88	-21.98	0.77	489	-23.90	0.03
80	473	295	7.89	-20.38	1.08	392	-23.16	0.03
60	355	328	7.93	-20.99	2.08	294	-23.21	0.04
40	236	392	7.98	-20.99	0.25	196	-25.04	0.03
30	177	433	7.87	-22.89	1.25	147	-25.96	0.03
20	118	480	7.88	-23.85	0.52	98	-27.47	0.03
15	89	533	7.81	-24.59	0.46	73	-28.20	0.02
10	59	559	7.81	-23.96	0.54	49	-26.80	0.02
5	30	602	7.80	-25.35	0.40	24	-27.65	0.02
0	0	650	7.79	-26.18	0.19	0	-28.30	0.04

Table S5.1 h: Experimental results for experiment #9, conducted using a 2 mmol/l $CaCO_3$ solution at 30° C and a pCO_2 of 1000 ppmV.

distance of flow [cm]	residence time DIC [s]	electrical conductivity σ [µS/cm]	pH	$\delta^{13}C_{DIC}$ [‰]	±	residence time $CaCO_3$ [s]	$\delta^{13}C_{CaCO3}$ [‰]	±
100	655	202	8.21	-22.91	0.20	540	-23.04	0.11
80	524	216	8.20	-23.51	0.04	432	-24.98	0.08
60	393	238	8.15	-23.67	0.03	324	-25.96	0.03
40	262	252	8.18	-23.87	0.05	216	-27.36	0.05
30	197	267	8.17	-24.22	0.05	162	-27.88	0.02
20	131	282	8.18	-24.47	0.08	108	-28.88	0.03
15	98	299	8.15	-25.12	0.06	81	-29.30	0.02
10	66	316	8.15	-25.11	0.36	54	-29.84	0.03
5	33	327	8.15	-25.54	0.12	27	-30.60	0.01
0	0	348	8.04	-25.13	0.03	0	-30.95	0.03

Table S5.1 i: Experimental results for experiment #10, conducted using a 3 mmol/l $CaCO_3$ solution at 20° C and a pCO_2 of 1000 ppmV.

distance of flow [cm]	residence time DIC [s]	electrical conductivity σ [µS/cm]	pH	$\delta^{13}C_{DIC}$ [‰]	±	residence time $CaCO_3$ [s]	$\delta^{13}C_{CaCO3}$ [‰]	±
100	693	308	8.18	-20.66	0.04	562	-24.13	0.03
80	555	327	8.18	-21.75	0.25	450	-26.39	0.01
60	416	356	8.17	-21.28	0.14	337	-27.36	0.02
40	277	382	8.17	-21.73	0.07	225	-28.56	0.02
30	208	404	8.16	-23.75	0.20	169	-29.26	0.02
20	139	433	8.14	-25.03	0.01	112	-30.05	0.01
15	104	444	8.23	-20.41	0.49	84	-30.41	0.02
10	69	454	8.20	-24.33	0.31	56	-30.81	0.01
5	35	469	8.20	-25.11	0.28	28	-31.27	0.01
0	0	498	7.96	-26.14	0.17	0	-31.48	0.02

Chapter 6: Manuscript IV

Simulating speleothem growth in the laboratory Part II: Determination of stable oxygen isotope fractionation between DIC, $CaCO_3$ and water

Maximilian Hansen[1*], Denis Scholz[1], Bernd R. Schöne[1], Christoph Spötl[2]

Manuscript in preparation for submission to Chemical Geology

*corresponding author: m.hansen@uni-mainz.de

[1] Institute for Geosciences, University of Mainz, Germany

[2]Institue of Geology, University of Innsbruck, Austria

Abstract

Here we present cave analogue experiments, enabling for the first time to directly investigate stable oxygen isotope fractionation between all involved species in the carbonate system (HCO_3^-, CO_2, $CaCO_3$ and H_2O) at the same time. During the experiments thin films of different concentrated $CaCO_3$ solutions are caused to flow down an inclined marble of glass plate. After different distances of flow and, thus, residence times on the plates all chemical parameters (pH, electrical conductivity, supersaturation with respect to calcite, precipitation rate) as well as the $\delta^{18}O$ values of the DIC and the directly precipitated $CaCO_3$ are investigated.

The precipitation of $CaCO_3$ is accompanied by isotope fractionation, the corresponding temporal evolution $\delta^{18}O$ values for both the dissolved inorganic carbon (DIC) and the $CaCO_3$ can be well explained by applying a Rayleigh fractionation model as predicted by Scholz et al. (2009). The overall enrichment, the total fractionation, $^{18}\varepsilon_{tot}$, ranges between – 0.38 and – 3.3 ‰. The initial fractionation between $CaCO_3$ and DIC, $^{18}\varepsilon_{CaCO3/HCO3-}$, for all experiments is in good agreement with combined fractionation factors observed in natural cave systems (e.g., Johnston et al., 2013; Tremaine et al., 2011). With decreasing supersaturation and, thus, decreasing precipitation rates the fractionation between DIC and $CaCO_3$ become smaller approaching values as proposed by Coplen (2007)and Watkins et al.(2014; 2013). The initial fractionation between DIC and water can be well explained using "equilibrium" fractionation factors, $^{18}\varepsilon_{HCO3-/H2O}$, by Beck et al. (2005). With progressive precipitation of $CaCO_3$ the system is forced out of equilibrium because the time required to re-equilibrate the DIC with the water is substantially longer than the residence time on the plates. The initial $\delta^{18}O$ fractionation between $CaCO_3$ and water is in good agreement to values observed in natural cave systems (e.g., Johnston et al., 2013; Tremaine et al., 2011) and provide a very similar temperature dependence. However, with progressive precipitation of $CaCO_3$, the fractionation $1000\ln^{18}\alpha$ increases and approaches different values as proposed by Coplen (2007) and Watkins et al.(2014; 2013). These findings suggest (i) that our system closely resembles a natural system because our observed values corresponds best to those observed in natural cave systems; (ii) reaction kinetics have to be taken into account for interpretation of speleothem $\delta^{18}O$ records.

6.1. Introduction

Speleothems are unique paleoclimate archives providing important information on past climate variability in a wide range of climatic zones (Fairchild and Baker, 2012). They can be dated very precisely using U-series disequilibrium methods (Richards and Dorale, 2003; Scholz, 2008). In combination with the most abundantly used paleoclimate proxies for speleothems, the stable carbon and oxygen isotopes ($\delta^{13}C$ and $\delta^{18}O$) may provide continuous long term paleoclimate records (e.g., Asmerom et al., 2010; Bar-Matthews et al., 2003; Boch et al., 2011; Cheng et al., 2016; Cruz et al., 2005; Fleitmann et al., 2004). However, the stable isotope signals in a speleothem depend on various processes occurring in the atmosphere, the soil and inside the cave and might be obscured until speleothem calcite is deposited. Thus, the interpretation of $\delta^{13}C$ and $\delta^{18}O$ records in terms of past climate and /or precipitation variability remains challenging. Many speleothem paleoclimate studies are based on interpreting the changes in $\delta^{18}O$ signals of speleothem calcite (e.g., Cheng et al., 2016; Fleitmann et al., 2004; Spötl et al., 2008). The $\delta^{18}O$ record of a speleothem might provide important information about changes in past precipitation patterns above the cave (e.g., Bar-Matthews et al., 2003; Cheng et al., 2016), the source of the corresponding water vapor and atmospheric circulation (e.g., Cruz et al., 2005; Wassenburg et al., 2016), as well as the temperature (Mangini et al., 2005).

In an ideal setting the $\delta^{18}O$ signal of meteoric precipitation above a cave would be directly incorporated into speleothem calcite. In a natural environment, however, the mechanisms behind the incorporation of the $\delta^{18}O$ signal into speleothem calcite depend on various parameters. These could be saturation state (i.e. degree of supersaturation) of the solution entering the cave, evaporation (controlled by relative humidity inside the cave), temperature and whether chemical equilibrium is established during precipitation of (speleothem) $CaCO_3$. Since the early studies trying to exploit speleothem isotope records as paleoclimate proxies (e.g., Fornaca-Rinaldi et al., 1968; Hendy and Wilson, 1968) stable isotope fractionation has been discussed controversially, especially whether “kinetic” or equilibrium fractionation processes are more suitable to describe stable isotope fractionation in speleothems (e.g., Mickler et al., 2006). One of the first theoretical approaches for evaluating the suitability of speleothems for paleoclimate purposes was postulated by Hendy (1971). He divided the stable isotope fractionation during precipitation of calcite into equilibrium and kinetic processes, controlled by slow and fast loss of CO_2 from the precipitating solution and the presence or absence of evaporation. Based on this study the “Hendy test” was established, using a positive correlation between $\delta^{13}C$ and $\delta^{18}O$ values along one growth layer as an indicator for a disequilibrium fractionation process, rendering the usability of the corresponding sample, thus, less suitable for paleoclimate reconstruction. This has, however, been

questioned since the "Hendy test" does not account for initial disequilibrium (e.g., when the solution reaches the tip of a stalagmite) (e.g., Day and Henderson, 2011; Dorale and Liu, 2009).

In more recent years a number of theoretical studies were published, aiming to more quantitatively describe the fractionation processes during precipitation of speleothem calcite. Dreybrodt (2008) and Dreybrodt and Scholz (2011) described stable isotope fractionation in a 'kinetic' fractionation model, whereas Scholz et al. (2009) used a Rayleigh distillation model. In addition, modelling studies showed, that the degree of enrichment of the stable isotope signal could be linked to mixing effects on top of a speleothem, as well as changes in drip rates (Deininger et al., 2012; Mühlinghaus et al., 2009). These models use equilibrium fractionation factors to describe the temporal evolution of the stable isotope signal, mainly due to the lack of suitable "kinetic" or disequilibrium fractionation factors, since they have not been quantified yet.

Additionally, a few studies have attempted to test these theoretical models for a cave setting in the laboratory, by precipitation experiments in the laboratory with synthetic carbonates. Fantidis and Ehhalt (1970) performed experiments by precipitating calcite in a glass tube under laboratory atmosphere, showing increasing isotope values with increasing distance of flow. Their findings were confirmed by similar observations within one growth layer of a stalagmite. Later on Polag et al. (2010) and Wiedner et al. (2008) conducted experiments under controlled conditions in a refrigerator by mixing a $NaHCO_3$ and a $CaCl_2$ solution in a glass tube containing a glass fiber mat as crystallization substrate under a pure N_2 atmosphere. They both observed increasing $\delta^{18}O$ and $\delta^{13}C$ values with increasing distance of flow, as well as fractionation factors which differed from the commonly used equilibrium values. In a different approach Day and Henderson (2011) more closely simulated a natural system by dripping a $CaCO_3$-CO_2-H_2O solution onto seeded inclined glass plates in a CO_2 containing atmosphere. They also observed a temperature dependent fractionation for $\alpha_{calcite\text{-}water}$ and increasing $\delta^{18}O$ values with increasing distance from the impinging point of their drips. These laboratory experiments provided very important information and improved the understanding of the controls on stable isotope values in a speleothem record. However, some problems still remain unsolved. All these studies were only able to provide information about the temporal evolution of the stable isotopes of precipitated calcite as a function of temperature and / or drip rate. They had no control on the experiment once it was started and, direct investigations of the temporal evolution of the solution, such as pH values, Ca^{2+} concentration and the isotope composition of the dissolved inorganic carbon (DIC) were not possible. Thus, direct determinations of oxygen fractionations factors between all participating species, DIC, $CaCO_3$ and H_2O were not feasible.

Here we present novel laboratory experiments aiming to closely resemble a natural cave system and providing the possibility to simulate all processes affecting the $\delta^{18}O$ values during precipitation of $CaCO_3$ from a thin flowing solution layer, like they occur on the surface of speleothems. During the experiments all surrounding conditions are carefully controlled and adjusted to cave analogues conditions, which enables us to quantify the stable oxygen isotope fractionation ($\delta^{18}O$) between the DIC, the directly precipitated $CaCO_3$ and the water and to determine the precipitation rates as a function of the experimental parameters, such as temperature, super saturation with respect to calcite and (cave) air pCO_2. Along with Part I, this is the first study which enables the determination of stable isotope fractionation between *all* different species in the system (here HCO_3^-, CO_2, $CaCO_3$, H_2O) *at the same time*.

6.2. Theoretical background

6.2.1 Chemical background for oxygen isotope during precipitation of $CaCO_3$

The main source of oxygen isotopes in a natural cave environment is provided by meteoric precipitation. Rainfall above a cave seeps through the soil, where the pCO_2 is much higher than in the atmosphere, these values may reach to about a few percent (Fairchild and Baker, 2012). This causes relatively low pH values of the percolating water, due to the formation of carbonic acid (6.1):

$$CO_2(g) + H_2O \Leftrightarrow H_2O + CO_2(aq) \Leftrightarrow H_2CO_3. \quad (6.1)$$

If this solution seeps further down and enters the carbonate host rock through joints and fissures $CaCO_3$ is dissolved. The overall reaction then is:

$$CO_2 + H_2O + CaCO_3 \Leftrightarrow Ca^{2+} + 2\,HCO_3^- \quad . \quad (6.2)$$

Thus, each Ca^{2+} consumes one molecule CO_2 and one H_2O. Depending on the availability of CO_2 and, thus, on the prevailing pH value this reaction is reversible. The distribution of the individual carbon species is controlled by the pH (and, thus, pCO_2) of the solution. In detail these reactions consist of a complex interplay between different fast and slow reactions, induced by diffusion and/or different rate constants (see e.g., Dreybrodt, 1988; Dreybrodt et al., 1997; Zeebe and Wolf-Gladrow, 2001). For a natural environment the residence time of the solution in the karst aquifer is sufficient long to establish isotope equilibrium between the water and the dissolved carbon species (e.g., CO_2 and HCO_3^-).

After the water enters a cavity or a cave system, the pCO_2 is usually several orders of magnitude lower than in the overlying epikarst. This results in a gradient of pCO_2 between the solution and the (cave) atmosphere. Drip water, dripping to the apex of a stalagmite forms a thin layer of solution, about 0.1 mm in thickness, from which the excess dissolved CO_2 degasses in the range of a few seconds (Hansen et al., 2013). As a result the pH value of the solution increases to values of about 8, the solution becomes supersaturated with respect to calcite and consequently calcite is precipitated to the speleothem surface (e.g., Dreybrodt et al., 1997). Subsequently to the formation of the thin film, the solution flows down the flanks of the stalagmite in a laminar flow, progressively precipitating $CaCO_3$ in thin layers, resulting in the growth of a stalagmite (e.g., Mühlinghaus et al., 2007; Romanov et al., 2008a). Plummer et al. (1978) quantified the rate of calcite precipitation, which has later on been transferred to the applicability for calcite precipitation during formation of speleothems by including diffusion in thin solution films (see also e.g., Buhmann and Dreybrodt, 1985a; Dreybrodt et al., 1997).

According to Dreybrodt and Scholz (2011) the change in $[Ca^{2+}]$, accompanied by change in $[HCO_3^-]$, during precipitation of $CaCO_3$ can be described as:

$$[Ca^{2+}](t) = \left([Ca^{2+}]_0 - [Ca^{2+}]_{eq}\right)\left(exp^{\left(-t/\tau_{pr}\right)}\right) + [Ca^{2+}]_{eq} \tag{6.3}$$

$$\tau_{pr} = {}^{d}/_{\kappa} \ , \tag{6.4}$$

with τ_{pr} as time constant for the exponential decrease in $[Ca^{2+}]$, d is the thickness of the solution film, $[Ca^{2+}]$ (t) is the concentration at time t, $[Ca^{2+}]_0$ the initial and $[Ca^{2+}]_{eq}$ the equilibrium value of $[Ca^{2+}]$, k is a rate constant (for details see e.g., Buhmann and Dreybrodt, 1985a; Dreybrodt et al., 1997). The processes of precipitation and dissolution has already been described in detail in Part I of this study.

2.2 The basic stable isotope geochemistry for understanding $\delta^{18}O$ speleothem records

The chemical and physical behavior of the heavy and the light isotope of a specific element are slightly different. This is caused by small differences in the mass of the atomic nuclei of the different isotopes of an element. In general the heavier isotopes of an element show a lower mobility and are characterized by higher binding energies, consequently the corresponding light isotopes exhibit a higher responsiveness in chemical reactions. This results in an isotope effect, which is commonly expressed as isotope fractionation α. Since the isotope effects are small, the fractionation, ε, is defined as the deviation of α from 1:

$$\varepsilon_{B/A} = \alpha_{B/A} - 1 = \frac{R_B}{R_A} - 1 \ (* 10^3‰), \quad (6.5),$$

where, R_A is the isotope ratio of the abundant isotope and R_B the ratio of the rare isotope, ε, denotes the enrichment (or depletion) of the rare isotope (for details see e.g., Mook and De Vries, 2000). The fractionation processes can be divided into three basic types of fractionation: equilibrium, non-equilibrium and kinetic fractionation. Kinetic isotope fractionation has often been used in the speleothem literature for isotope values which cannot be explained by equilibrium fractionation factors. In a natural environment, however, most processes underlie neither a complete equilibrium nor a strict one dimensional kinetic fractionation process, but rather a non-equilibrium fractionation. Here we use the term kinetic fractionation and refer to a disequilibrium isotope fractionation to describe a deviation from the values which would be expected under conditions of equilibrium.

In general there are a number of stable isotope fractionation factors for $^{18}\alpha_{calcite\text{-}water}$ available, which have been mostly evaluated in laboratory experiments by precipitating calcite from a bulk solution under accurate and controlled conditions and simultaneously measuring the $\delta^{18}O$ values of the precipitated calcite and the water. Performing these kind of experiments at a range of temperatures enables to estimate the temperature dependence of the equilibrium fractionation (e.g., Friedman and O'Neil, 1977; Kim and O'Neil, 1997; McCrea, 1950; O'Neil et al., 1969). The most widely applied fractionation factors, also in the speleothem community, are those by Kim and O'Neil (1997). Fractionation factors between water and HCO_3^-, $^{18}\alpha_{HCO3\text{-}H2O}$, and for $^{18}\alpha_{CO2\text{-}H2O}$ have been provided by Beck et al. (2005) who performed equilibration experiments for the carbonate system with a $NaHCO_3$ solutions at different pH values and temperatures. However, other studies recently showed that the previously postulated equilibrium fractionation factors might not be valid for all natural settings and depend on additional controls such as precipitation rate (Dietzel et al., 2009; Watkins et al., 2014), the reaction kinetics (Watkins et al., 2013) or pH (Watkins et al., 2014; Zeebe et al., 1999b). This might have important implications for the interpretation of speleothem $\delta^{18}O$ records and corresponds to fractionation factors which were determined by measurements of calcite and water in a natural cave environments. Tremaine et al. (2011) investigated a higher $\alpha_{calcite\text{-}water}$ than Kim and O'Neil (1997) from comparing in situ framed calcite compared to drip water $\delta^{18}O$. Even larger values for $\alpha_{calcite\text{-}water}$ were previously reported by Coplen (2007) from Devils Hole who performed measurements of slowly precipitating calcite from a water filled calcite vein. These findings are important in the view of paleoclimate reconstruction from speleothem isotope records and urge to carefully reassess the mechanisms behind isotope fractionation for speleothem calcite.

6.2.3. Modeling stable isotope oxygen fractionation $\delta^{18}O$ in speleothems

For the stable oxygen isotope fractionation in the carbonate system CO_2, HCO_3^-, and H_2O are involved in the carbonate reactions, depending on the pH of the solution. Each participating species has an own fractionation factor. The temporal evolution of $\delta^{18}O$ of a calcite precipitating solution for the DIC as well as the precipitated $CaCO_3$ have been controversially discussed in two different approaches.

6.2.3.1 Rayleigh distillation model

The change of isotope composition of a $CaCO_3$ precipitating solution have often been described using a Rayleigh distillation model (e.g., Bar-Matthews et al., 1996; Mickler et al., 2004; Mook and De Vries, 2000; Mühlinghaus et al., 2009; Romanov et al., 2008b). Regarding the overall reaction for precipitation of $CaCO_3$, Eqn. (6.2) from right to left for each Ca^{2+} precipitated to the speleothem surface there is a "flux" of isotopes into different sinks with different corresponding fractionation factors. Thus, the DIC and the $CaCO_3$ reservoirs change progressively with increasing (precipitation) time. This reaction involves isotope fractionation, which can be described by a classical Rayleigh fractionation model. At the beginning of the reaction a DIC reservoir contais $[Ca^{2+}]$ molecules with a isotope ratio $\delta^{18}O_{DIC}$ at time $t = 0$. During progressive precipitation of $CaCO_3$ the amount of DIC ($[Ca^{2+}](t)$) in the solution decreases with a characteristic time constant τ_{pr}. Simultaneously, there is a flux of oxygen isotopes into the three different sinks ($CaCO_3$, CO_2 and H_2O) with the corresponding fractionation factors. Mass balance defines that 1/6 of the oxygen atoms portion is incorporated into H_2O, 2/6 into CO_2 and 3/6 into $CaCO_3$, the total fractionation, ε_{tot}, then is a combination of the fractionation $1/3\ \varepsilon_{CaCO3/H2O-} + 1/2\ \varepsilon_{CaCO3/CO2} + 3/6\varepsilon_{CaCO3\ /\ HCO3-}$ (e.g., Mickler et al., 2006) (Scholz et al., 2009).

The temporal evolution of the $\delta^{18}O$ values of a calcite precipitating from a thin layer of solution has been derived by Scholz et al. (2009) using a classical Rayleigh distillation approach:

$$\frac{\delta^{18}O(t)+1000}{\delta^{18}O_0+1000} = \frac{[Ca^{2+}](t)}{[Ca^{2+}]_0}^{\varepsilon_{tot}} = \left(exp^{\frac{-t}{\tau_{pr}}} + \left(\frac{[Ca^{2+}]_{eq}}{[Ca^{2+}]_0} \right) * \left(1 - exp^{\frac{-t}{\tau_{pr}}} \right) \right)^{\varepsilon_{tot}}. \quad (6.6)$$

For a more detailed deviation we refer the readers to the studies of Dreybrodt and Scholz (2011) and Scholz et al. (2009).

6.2.3.2. 'Kinetic fractionation model' by Dreybrodt (2008) and differences of both approaches

In a previous study Dreybrodt (2008) proposed an alternative, 'kinetic fractionation' model. This approach is based on the assumption, that the heavy and the light isotopes are precipitated independently from each other. This results in slightly different time constants and rate constants for the precipitation of the heavy and light isotopes respectively. Additionally, a 'kinetic' constant is introduced, which determines the isotope composition of the DIC in equilibrium and is dependent on processes at the calcite surface. Kinetic isotope fractionation factors have not been determined so far, thus, the degree of isotope fractionation has been described using equilibrium fractionation factors (Dreybrodt, 2008; Dreybrodt and Scholz, 2011). Strictly speaking, the term 'kinetic' model in the context of distinguishing between kinetic isotope fractionation and other fractionation processes may be misleading.

However, when kinetic fractionation factors are available a Rayleigh distillation model can in principle be used to describe the temporal evolution of the isotope composition of a calcite precipitating solution. Figure 6.1 shows a comparison of the two models for a calcite precipitating solution plotted against residence time on the stalagmite surface. The black line denotes the model as postulated by Scholz et al. (2009), the red line shows the 'kinetic' model by Dreybrodt (2008) and the blue graph depicts the evolution of the [HCO_3^-] concentration in solution. The Rayleigh model by Scholz et al. (2009) expects an exponential increase in isotope values until a maximum is reached. With increasing residence time on the stalagmite surface and decreasing HCO_3^- concentration, due to precipitation of $CaCO_3$, isotope exchange with the CO_2 of the cave atmosphere, as well as with the water isotopes of the solution might become significant, thus the Rayleigh model predicts a trend to more negative values until an equilibrium values close to the initial isotope composition of the solution is reached. This is reasonable, since water is by far the biggest reservoir for oxygen isotopes. The approach by Dreybrodt (2008) also estimates a strong initial increase in $\delta^{18}O$ values until a maximum is reached. Afterwards, the model predicts a decrease with an over swing below the initial isotope ratio followed by an increase to a final, 'steady state' value. The reason for this is the kinetic constant (in the model, Dreybrodt, 2008), which the Rayleigh approach does not account for. In practice, this is unlikely since this effect could only be related to another source of oxygen isotopes than the solution, which again is unlikely because water is the biggest reservoir for $\delta^{18}O$. Interestingly both approaches show an almost identical behavior until approx. 75 % (vertical straight lines, Fig. 6.1) of the precipitation reaction is completed, if the same fractionation factors are used. For a detailed discussion on these differences the reader is referred to Dreybrodt (2016). However, neither the Rayleigh model nor the 'kinetic' model with the different time constants and the kinetic constants have been confirmed by experiments so far.

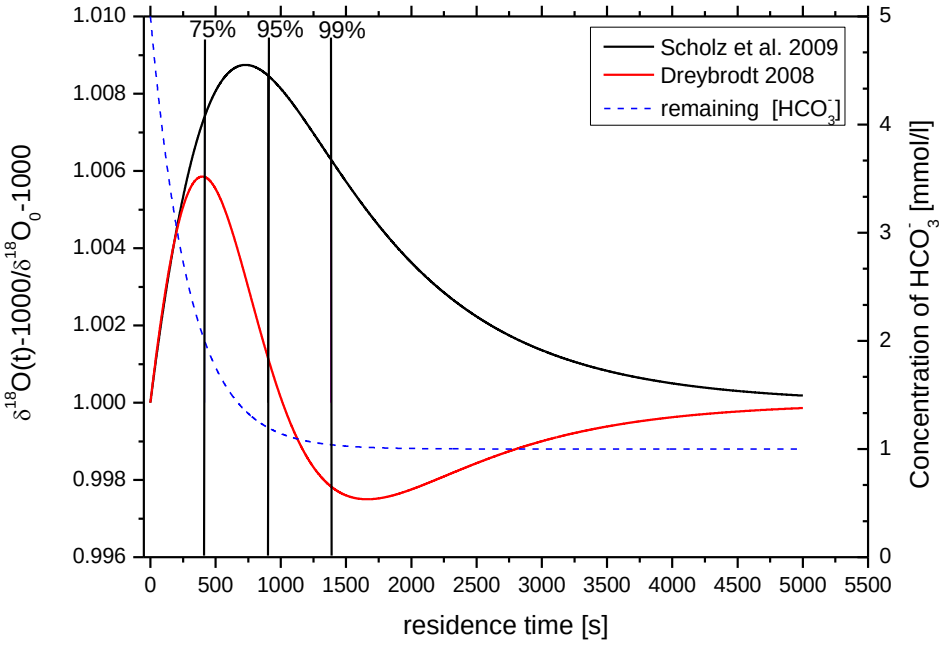

Fig. 6.1: Comparison of the fractionation models for $\delta^{18}O$ from Dreybrodt (2008) and Scholz et al. (2009) during precipitation of speleothem calcite. Also shown is the corresponding exponential decrease of $[HCO_3^-]$ in solution with increasing (precipitation) time (after Scholz et al., 2009). The shown example is for a solution of initial 5 mmol/l $[HCO_3^-]$, the equilibrium concentration is 1 mmol/l, τ_{pr} is 300 s and the exchange time with water is set to 1000 s.

6.3. Experimental methods

Here we present experiments performed under completely controlled, cave analogues conditions aiming to improve the understanding of the basic processes affecting the fractionation of $\delta^{18}O$ during precipitation of speleothem calcite. This enables us, for the *first* time, to determine the fractionation factors between all participating carbon species in the system in dependence of the temperature and chemical properties of the solution. The experimental procedure and setup has been described in detail in Part I ($\delta^{13}C$) of this study, thus, we focus on the essential experimental steps and the additional sampling methods for understanding the stable isotope signals here.

The solutions for the experiments were prepared by dissolving Merck® high grade pure $CaCO_3$ powder ($\delta^{18}O \approx -18$ ‰) in 5 L of pure MQ water by bubbling CO_2 ($\delta^{18}O \approx -44$ ‰) through

the water column. After the $CaCO_3$ powder was dissolved, the solution was clear without any visible particles of $CaCO_3$ powder and the pH was ca. 5. In a natural cave environment the solution in the epikarst is commonly expected to stay sufficient long in the aquifer above the cave to establish chemical equilibrium with the carbonate host rock (e.g., Dreybrodt and Scholz, 2011). Thus, the bulk solution for the experiments was adjusted to a saturation index (SI) of about 0 by cautiously sparging the solution off the excess CO_2 and measuring the pH and electrical conductivity. For each experiment the SI and the corresponding pH value and its mass balance were calculated using PhreeqC (Parkhurst and Apello, 1999). Subsequent to the adjustment of SI, pH and corresponding experimental temperature, the solutions were stored for at least four days at the experimental temperature in order to establish oxygen isotope equilibrium between all dissolved carbon species and the water.

The experimental setup is placed inside a climate box, in which all surrounding parameters such as pCO_2, the $\delta^{18}O$ value of the CO_2, temperature and relative humidity can be adjusted closely to a natural cave environment. This allows to simulate all natural processes, which could influence the stable isotope signal in speleothem calcite. The experiments can be adjusted with rubber gloves inside the sealed box without opening the system and to avoid contamination of the box atmosphere (Dreybrodt et al., 2016; Hansen et al.). Prior to each experiment, the box was equipped with all experimental material and was then sealed to establish the experimental temperature and relative humidity by bubbling the box atmosphere through two water columns. Note, that the same water for establishment of the humidity as well as for the preparation of all solutions was used. In order to control the isotope composition and the pCO_2, the climate box was flushed with pure nitrogen for about 15 h through a gas washer to maintain a high relative humidity prior to the experiments (Hansen et al., accepted). Subsequently, after a minimum pCO_2 of about 20 – 40 ppmV was reached, a defined amount of CO_2 which was previously equilibrated with the same water used in the experiments was injected into the system.

The experiments are divided into two parts, one for the analysis of DIC and one for the $CaCO_3$. During the experiments, thin films of $CaCO_3$-CO_2-H_2O solutions (ca. 0.1 mm in thickness) with different initial concentrations are caused to flow down an inclined marble (part one) or borosilicate glass plate (part two). A detailed sketch of the $CaCO_3$ setup inside the box is given in Figure 6.2. The initial $[Ca^{2+}]$ were 5, 3 and 2 mmol/l, for each experiment 5 l of solution were prepared. The surrounding conditions for the experiments were adjusted to temperatures of 10, 20 and 30 °C and two different pCO_2 of the atmosphere of 1000 and 3000 ppmV. During the experiments the temporal evolution of the solution chemistry was monitored by measuring pH and electrical conductivity. Additionally the temporal evolution of the $\delta^{18}O$ values for both the dissolved inorganic carbon (DIC, precipitated as $SrCO_3$), the directly precipitated $CaCO_3$, as well

as of the atmospheric CO_2 and the $\delta^{18}O$ of the water were investigated. This allows the determination of stable isotope fractionation between all involved species (DIC, directly precipitated $CaCO_3$ and the water), as well as the precipitation rates as a function of the experimental conditions.

All physical parameters inside the box were logged by instruments that are also commonly used in cave monitoring programs. The pCO_2 was measured using a Vaisala® MI70 instrument with a GMP 222 probe, relative humidity was logged using a Tinytag® humidity probe. Five temperature probes by Hobo® and Tinytag® were used to measure the temperatures inside the artificial cave on the surface of the plates on the atmosphere.

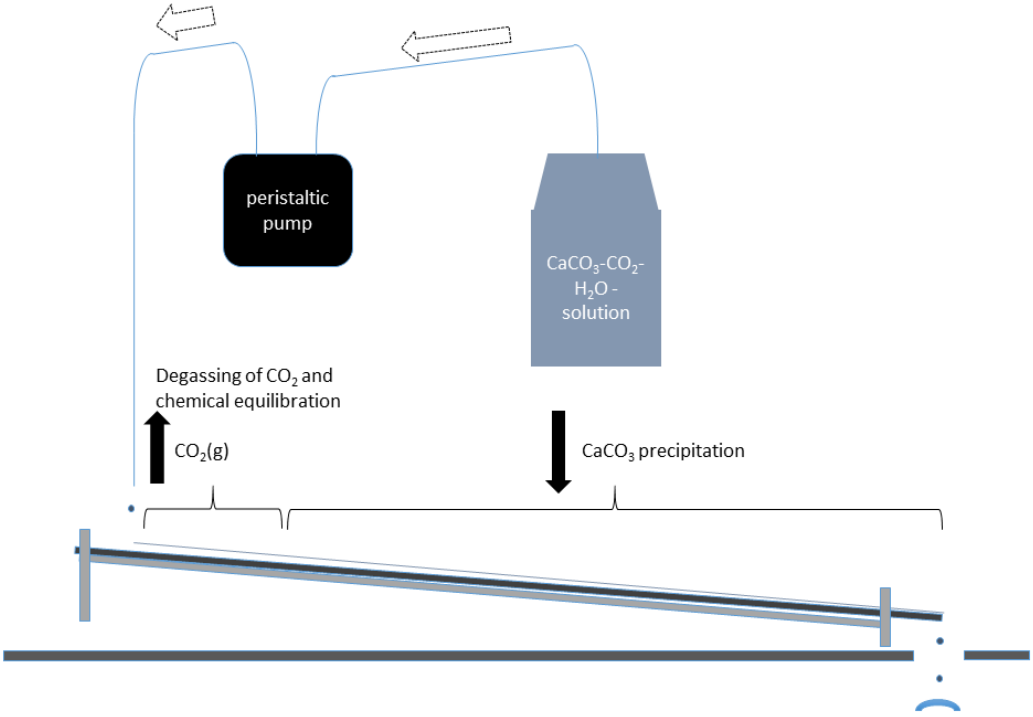

Fig. 6.2: Schematic sketch of the experimental setup for the $CaCO_3$ experiment. Note, that the distance of flow on the glass plate is increased by the equilibration distance on the upper marble plate from the DIC experiment (described in detail in Part I of this study).

6.3.4 Stable isotope analyses

Stable isotope analyses of the sampled CO_2 of the box atmosphere and the measurements of the water samples were conducted at the University of Innsbruck. The exetainers containing CO_2 from the experiments were rushed into the laboratory within a few days, subsequently to an experiment to ensure no leakage from the septa (see Spötl, 2004). $\delta^{18}O_{CO2}$ values were measured using a Delta^{plus}XL mass spectrometer and calibrated against calcite standards.

Stable isotope analyses of the $SrCO_3$ samples were performed at the Institute of Geosciences, University of Mainz, using a Thermo Finnigan MAT 253 continuous flow-isotope ratio mass spectrometer coupled to a GasBench II. Samples were dissolved in concentrated phosphoric acid in helium-flushed borosilicate exetainers at 72 °C. Isotope data were calibrated against an NBS-19 calibrated Carrara marble standard distributed by IVA Analysentechnik e.K. (Düsseldorf, Germany) ($\delta^{18}O = -1.91$ ‰). On average, internal precision (1σ) and accuracy were better than 0.04 ‰, respectively. The isotope values are reported relative to the Vienna Pee Dee Belemnite scale (McKinney et al., 1950).

6.4 Results

6.4.1 DIC experiments

6.4.1.1 Degassing of CO_2, chemical equilibration and establishment of supersaturation

The samples from which the data for this study are generated are the same as for Part I from this study. Therefore all the physical data like pH and electrical conductivity, as well as the surrounding conditions are the same as in the preceding study. However, in Part I the results showed rising pH as indication for fast degassing of dissolved CO_2 and the corresponding establishment of supersaturation with respect to calcite. Figure 6.3 shows, representative for the whole data set, the evolution of pH, electrical conductivity and $\delta^{18}O$ from the reservoir to the exit of the equilibration plate for an experiment with a 5 mmol/l $CaCO_3$ solution, 20 °C and 1000 ppmV CO_2. The equilibration distance is 8 cm which corresponds to 34 s residence time. The enrichment of $\delta^{18}O$ on the equilibration plate is + 4.8 ‰, which documents the degassing of excess CO_2.

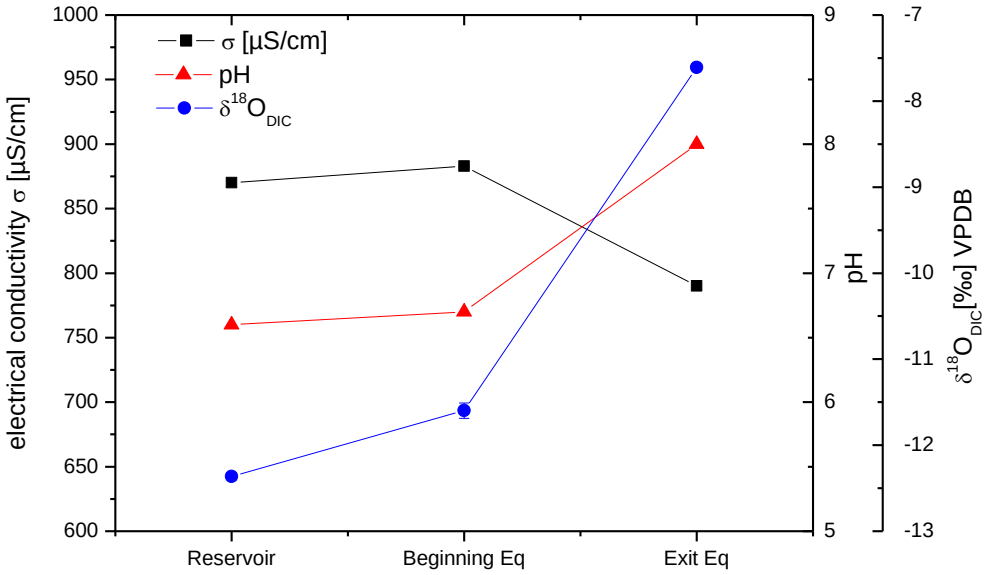

Fig. 6.3: Chemical and isotopic evolution on the upper equilibration marble plate.

6.4.1.2 Temporal evolution of the Ca^{2+} concentration of the solution

The temporal evolution of the [Ca^{2+}] has also been described in detail in Part I of this study. As mentioned above all samples have been already used in Part I, we here present the results for the stable oxygen isotopes. All measured physical and chemical parameters are the same as presented in Part I, thus we refer the reader to the preceding manuscript for more details. Basically the electrical conductivity reflect the decreasing [Ca^{2+}] of the solution due to progressive precipitation of $CaCO_3$ along the flow path. The experimentally observed values can be fitted by an exponential decay function (Eq. 6.3), which then provides the time constant, τ_{pr}, for the precipitation of $CaCO_3$. The lowest temperature corresponds to the longest time constant. All time constants are provided in Table 6.1. The electrical conductivity and pH values of the experiments are provided in supplemental Table S 6.1.

6.4.1.3 Temporal evolution of the $\delta^{18}O_{DIC}$ values

During the DIC experiments the $\delta^{18}O_{DIC}$ values get enriched with increasing residence time on the marble plate. This clearly documents isotope fractionation due to degassing of CO_2 and progressive precipitation of $CaCO_3$. However, the observed enrichments for the stable oxygen isotopes are much lower than for the $\delta^{13}C$ values (Part I of this study).

Figure 6.4 shows the temporal evolution of $\delta^{18}O$ values for the DIC of a calcite precipitating solution for experiments conducted with a 5 mmol/l $CaCO_3$-solution at 10, 20 and 30 °C in a 1000 (Fig, 6.4a) and a 3000 ppmV CO_2 (Fig. 6.4b) atmosphere. The enrichments, $\Delta^{18}O$, for the experiments conducted at a pCO_2 of 1000 ppmV range from + 0.4 ‰ at 10 °C to + 2 ‰ at 20 °C (Fig. 6.4a). For the experiments conducted at higher pCO_2 of 3000 ppmV the total enrichment is lower and ranges around 1 ‰ (Fig 6.4b). A clear, temperature dependent fractionation effect is visible in all data, the higher the temperature, the lower the initial $\delta^{18}O_{DIC}$ value due to isotope fractionation between the water and the HCO_3^- of the solution. The experiments conducted at 30 °C for both pCO_2 show a progressive increase in $\delta^{18}O_{DIC}$ values until a maximum is reached and then the values, however, tend to decrease again, after ca. 400 s at 1000 ppmV and after ca. 350 s at 3000 ppmV CO_2 (blue symbols in Fig. 6.4). This phenomenon is more pronounced for the higher pCO_2 atmosphere.

Table 6.1: Compilation of experimentally observed values of the experiments of this study.

Experiment No.		[$CaCO_3$] [mmol/l]	Temp[°C]	pCO_2 [ppmV]	rH [%]	Film thickness [mm]	$\delta^{18}O_{CO2}$ [‰]	τ_{pr}, [s]	$^{18}\varepsilon_{tot}$ [‰]	$1000\ln^{18}\alpha$
1	DIC	5	10 ± 0.5	1038 ± 21	80.5 ± 2	0.11	- -8.2 - - 7.2	1054 ± 543	- 1.81 ±0.5	32.34
	$CaCO_3$		10.1 ± 0.02	1029 ± 48	89.2 ± 1	0.11	- 6.4 - - 5.5			
2	DIC	5	19.9 ± 0.3	1030 ± 18	91.1 ± 1.5	0.16	- 7.4 - - 6.9	244 ± 24	- 3.3 ± 0.19	29.87
	$CaCO_3$		19.7 ± 0.1	1053 ± 42	98.7 ± 1.2	0.1	-27.3 - - 9.4***			
3	DIC	5	30.6 ± 0.2	1033 ± 38	96.5 ± 1.6	0.1	- 10.22 - - 9.89	182 ± 17	- 1.78 ± 0.3	**
	$CaCO_3$		30.7 ± 0.3	1007 ± 42	97.5 ± 1.2	0.1	-11.5 - - 9.4			
4	DIC	5	9.9 ± 0.1	2980 ± 28	82.1 ± 1.2	0.11	- -7 - - 5.7	644 ± 161	- 2.5 ± 0.34	32.24
	$CaCO_3$		9.7 ± 0.1	3020 ± 28	89.8 ± 1.2	0.12	- 14.9 - - 6***			
5	DIC	5	20.3 ± 0.2	3046 ± 27	88.0 ± 1.3	0.12	- 8 - - 7.8	410 ± 50	- 2.61 ± 0.22	30.12
	$CaCO_3$		20.0 ± 0.1	3060 ± 35	95.6 ± 0.7	0.11	- 9.5 - - 6.4			
6	DIC	5	31.0 ± 0.2	3069 ± 29	98.4 ± 2.7	0.1	- 8.4 - - 8.1	270 ± 17	-1.44 ± 0.22	28.55
	$CaCO_3$		30.7 ± 0.1	3076 ± 56	99.9 ± 0.6	0.11	- 8.5 - - 8.2			
7*	DIC	2	10.0 ± 0.1	1042 ± 13	77.7 ± 1.7	0.12	- 7 - - 6.3	----	---	---
	$CaCO_3$		9.9 ± 0.2	1030 ± 18	86.4 ± 1.6	0.14	- 7.4 - -4.7			
8*	DIC	2	20.3 ± 0.1	1099 ± 16	99.7 ± 0.3	0.13	- 10.3 - - 9.4	----	---	---
	$CaCO_3$		20 ± 0.1	1062 ± 14	100 ± 0.0	0.11	- 11.4 - -9.3			
9	DIC	2	30.8 ± 0.1	1075 ± 13	95.2 ± 2.2	0.11	**	270 ± 33	- 3.26 ± 0.3	H_2O value not measured so far
	$CaCO_3$		30.6 ± 0.1	1066 ± 17	99.0 ± 0.6	0.11				
10	DIC	3	20.3 ± 0.1	1071 ± 10	100 ± 0	0.14	- 7.7 - - 7.4	436 ± 51	- 0.38 ± 1.48	H_2O value not measured so far
	$CaCO_3$		20.2 ± 0.1	1065 ± 20	100 ± 0	0.12	- 8.7 - - 7.5			

*The experiments conducted with 2 mmol/L $CaCO_3$ at 10 and 20 °C yielded not enough calcite to determine $\delta^{13}C$ values and therefore also τ_{pr}, $^{18}\varepsilon_{tot}$ and $1000\ln^{18}\alpha$.

**$\delta^{18}O_{CO2}$ values were not provided during measurement of isotope composition of the CO_2

***The amount of pre-equilibrated CO_2 was too low to establish the required pCO_2 in the climate box, therefore small amounts of non-equilibrated CO_2 were added. Note that within a few hours of the experimental run the isotope composition of the CO_2 approached an equilibrium value.

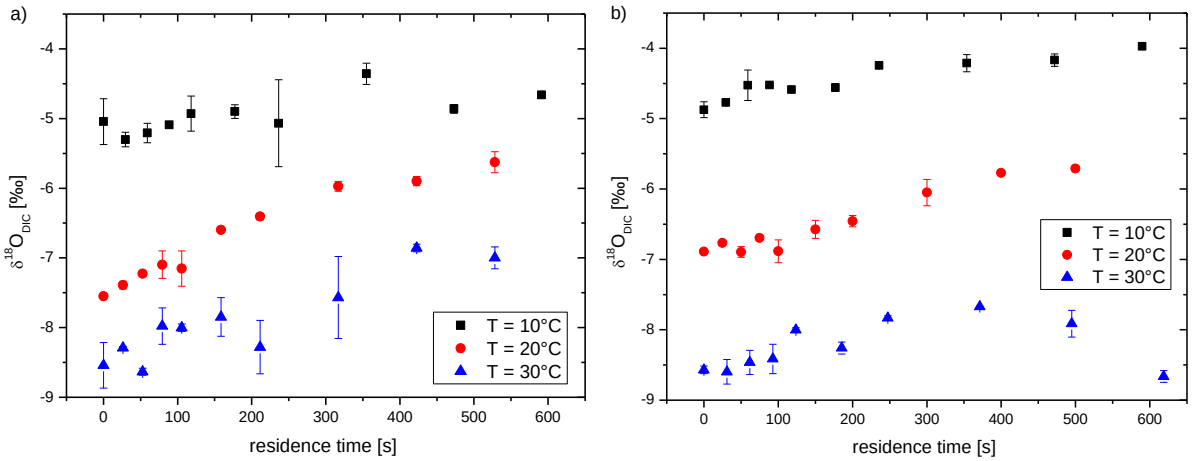

Fig. 6.4: Temporal evolution of the $\delta^{18}O_{DIC}$ values on the marble plate for the experiments conducted with a 5 mmol/L $CaCO_3$-solution and a pCO_2 of 1000 (a) and 3000 ppmV CO_2 (b). $\delta^{18}O_{DIC}$ values are calibrated vs. VPDB.

The results of the experiments conducted with 2 and 3 mmol/L show a similar temporal evolution. However, for the experiments conducted with a 2 mmol/L $CaCO_3$-solution only the experiment conducted at 30 °C provided reliable data, because the amount of precipitated $CaCO_3$ along the flow path was too low to provide reliable data for both electrical conductivity and stable isotopes. For the experiment conducted with a 3 mmol/L $CaCO_3$-solution at 20 °C and 1000 ppmV CO_2 the observed enrichment is $\Delta^{18}O = +0.9$ ‰. All isotope values for $\delta^{18}O_{DIC}$ and the corresponding residence times are provided in supplemental Table S 6.1.

6.4.1.4 Temporal evolution of the $\delta^{18}O_{water}$ values during the DIC experiments

The water isotopes of the solution were measured regularly during the experiments for the reservoir, the entry and exit of the equilibration plate, as well as after longer and shorter residence times on the lower marble plate. The enrichment in water values is generally low with a maximum value of + 0.9 ‰. Thus, evaporation cannot be completely excluded, however, the observed isotope effect in $\delta^{18}O_{DIC}$ shows a clear trend which corresponds well to the observed behavior for the $\delta^{13}C$ values of Part I of this study. All measured water values for the DIC experiments are compiled in supplemental Table S 6.1.

6.4.2 $CaCO_3$-experiments

The second part of the experiments investigated the temporal evolution of the directly precipitated $CaCO_3$. To ensure, that the main fraction of the precipitated material is calcite, Raman spectroscopy was performed on crystals of all experiments. This has already been described in detail in Part I of this study, but briefly almost all investigated sections consist of about 100 % calcite, only a very few aragonite and vaterite crystals were found for high temperatures and very high precipitation rates. Sections which did not consist of pure calcite were avoid to sample for isotope analyses. For pictures and a detailed discussion the reader is referred to Part I of this study.

6.4.2.1 Temporal evolution of $\delta^{18}O_{CaCO3}$ values

The temporal evolution of $\delta^{18}O$ values of the directly precipitated $CaCO_3$ on the glass plates shows a similar trend as the $\delta^{18}O$ values of the DIC. They get enriched towards more positive values with increasing residence time on the plates. Figure 6.5 shows the results for experiments conducted with 5 mmol/l $CaCO_3$-solutions at 10, 20 and 30 °C with an ambient pCO_2 of 1000 (Fig. 6.5a) and 3000 ppmV (Fig. 6.5b). For 1000 ppmV the total enrichments range from $\Delta^{18}O = +1.4$ ‰ at 10 °C up to $\Delta^{18}O = +2.8$ ‰ at 30 °C (Fig. 6.5a). Similar to the observations for the DIC experiments the overall enrichment at a pCO_2 of 3000 ppmV is lower and ranges from $\Delta^{18}O = +0.6$ ‰ at 10 °C to $\Delta^{18}O = +2.1$ ‰ at 30 °C (Fig. 6.5 b). For both pCO_2 the highest temperature exhibits the highest enrichment. In general, the observed enrichment is larger as for the DIC part, a similar observation has already been made for $\delta^{13}C$ in Part I of this study. The experiments conducted at 30 °C, and especially the experiment conducted at 30 °C and 3000 ppmV CO_2 (blue symbols, Fig. 6.5b) show an initial increase in $\delta^{18}O$ values, which then reach a plateau and afterwards decrease back to more negative values for the high pCO_2 experiment.

Another characteristic is the clearly visible temperature dependence of the initial values. These are directly linked to isotope fractionation with the $\delta^{18}O$ of the water and the precipitated $CaCO_3$. At lower temperatures the fractionation between calcite and water is larger than for higher temperatures. However, for the experiments conducted at 1000 ppmV and 20 and 30 °C (red and blue symbols in Fig. 6.5a) seems to have similar initial values. This is linked to the corresponding $\delta^{18}O$ value of the water. For the experiment conducted at 20 °C the values were more negative than for 10 and 20 °C (- 10 ‰ compared to – 9.3 . and – 9.6 ‰ calibrated vs. VSMOW).

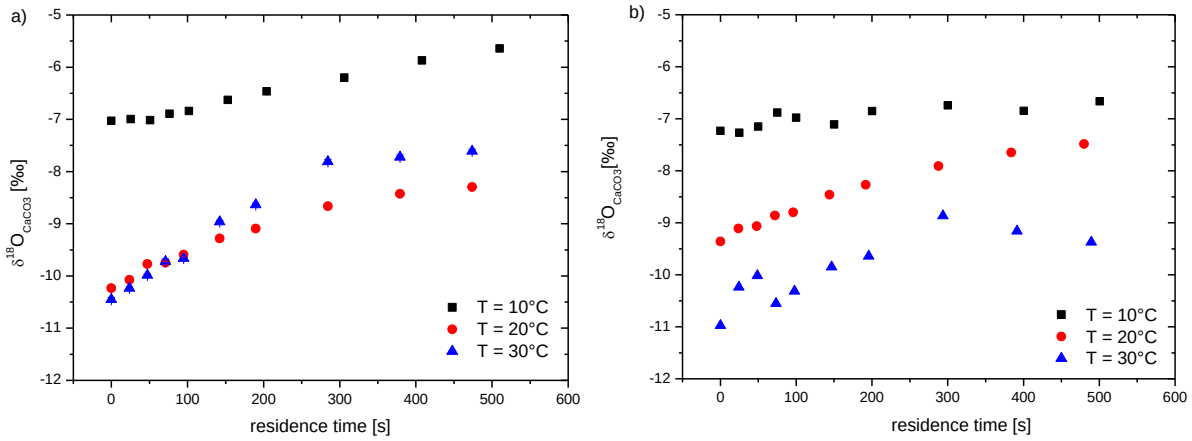

Fig. 6.5: Temporal evolution of the $\delta^{18}O_{CaCO3}$ values of the directly precipitated $CaCO_3$ on the glass plate, exemplarily shown for experiments conducted with a 5 mmol/L $CaCO_3$-solution and an ambient pCO_2 of 1000 (a) and 3000 ppmV (b).

The temporal evolution of the $\delta^{18}O_{CaCO3}$ values of the experiments conducted with 2 and 3 mmol/L show similar developments, analogous to the results of the DIC experiments. The enrichments of these experiments are $\Delta^{18}O = +2.6$ ‰ (2 mmol/L and 30 °C) and $\Delta^{18}O = +1.5$ ‰ (3 mmol/L and 20 °C). The observed enrichment is again slightly larger than for the corresponding DIC experiments. As already mentioned above the amount of precipitated $CaCO_3$ of the experiments performed at 10 and 20 °C with a 2 mmol/L $CaCO_3$ solution was unfortunately too low to generate reliable data. All $\delta^{18}O_{CaCO3}$ values and the corresponding residence time on the glass plates are provided in supplemental Table S 6.1.

6.4.2.2 Temporal evolution of the $\delta^{18}O_{water}$ values during the $CaCO_3$ experiments

As for the DIC experiments, the water of the solution was sampled regularly at the end of the glass plate, as well as prior to the experiment of the reservoir and at the entry of the glass plate. The difference in $\delta^{18}O_{H2O}$ values between the entries of the glass plate vs. exit (i.e. 100 cm distance of flow) is generally low. However, at the beginning of the experiments the enrichment in $\delta^{18}O_{H2O}$ ranges from + 0.4 ‰ up to + 1 ‰. With increasing duration of the experiment, especially within the first ~ 24 h, this isotope effect decreases significantly until values from + 0.4 ‰ to + 0.01 ‰. The enrichment of $\delta^{18}O_{CaCO3}$ values observed during precipitation of $CaCO_3$ is much larger than the isotope effect observed in $\delta^{18}O_{H2O}$ of the water samples. Nevertheless small effects of evaporation cannot be completely excluded, although this should not have an influence on the DIC or $CaCO_3$ isotope values, since isotope exchange between water and the carbonate species happens on much

larger time scales than our maximum temporal resolution of the experiments. The Water values measured during the experiments are compiled in supplemental Table S 6.1.

6.5 Discussion

6.5.1 Physical and chemical consistency during the experiments

The main difference between the DIC and $CaCO_3$ setup is that (i) the DIC experiments are conducted on a Carrara marble surface, whereas the $CaCO_3$ experiments are performed on a sand blasted borosilicate glass plate and (ii) the $CaCO_3$ experiments had no equilibration plate. To ensure the comparability between the both setups, the electrical conductivity, and thus the precipitation rates were compared. In the first 24 h of the $CaCO_3$ experiments, the conductivity values at the end of the glass plate progressively decrease and finally approach the same values as in the corresponding DIC experiments. The same is valid for the time constants for the precipitation of $CaCO_3$, τ_{pr}, which are equal in the range of the experimental errors. This has already discussed in more detail in Part I of this study. Note, that the residence times on the marble plate and the glass plates are also slightly different (see also supplemental Table S 1).

In order to keep the pCO_2 stable during the experiments, these values were monitored continuously. During precipitation of $CaCO_3$ gaseous CO_2 is released into the box atmosphere due to degassing, while the solution equilibrates with the pCO_2 of the climate box and due to precipitation of $CaCO_3$ (Eq. 6.2). In a natural setting the volume of the (cave) atmosphere is large and the pCO_2 can be regarded as infinite and stable for the time interval between two drips. In our laboratory setup, however, the box volume is finite, thus, we shortly flushed the system with N_2 whenever the pCO_2 value raised significantly (up to + 100 ppmV). The average (1σ) precision of pCO_2 for all experiments was $\pm$ 30 ppmV, which is in the range of the precision of the CO_2 probe. Additionally the stability of $\delta^{18}O$ of the artificial cave atmosphere was investigated regularly during the experiments. The average (1σ) stability of the $\delta^{18}O_{CO2}$ was $\pm$ 2.2 ‰, but are in general much lower (see Table 6.1). All experiments slightly tend to more positive values with increasing duration, this might be due to continuous dilution of the atmosphere during flushing with N_2 and corresponding isotope fractionation. However, this effect is very small and should have no or only very, limited effect on the isotope results of the experiments since most experiments should not be influenced by isotope exchange with the box atmosphere. All pCO_2 and corresponding $\delta^{18}O$ values of the CO_2 are compiled in Table 6.1.

6.5.2 Modeling the $\delta^{18}O$ values of the DIC experiments using a Rayleigh approach

In the following the experimentally observed data are applied to a classical Rayleigh distillation approach, which has been used in a theoretical study modelling isotope fractionation during calcite precipitation by Scholz et al. (2009). According to section 6.2.3.1 a calcite precipitating solution fractionates oxygen isotopes into three different sinks (Eq. (6.2)): $CaCO_3$, CO_2, and H_2O with the corresponding fractionation factors. The combination of all three factors then provides the total fractionation for the complete reaction. The (total) enrichment in $\delta^{18}O$ depends on the remaining $[Ca^{2+}]$ fraction and the temporal evolution of $\delta^{18}O(t)$ is then in accordance to a classical Rayleigh distillation model (Eq. (6.6)) and can be written as:

$$\delta(t) = \left(\frac{\sigma(t)}{\sigma_0}\right)^{\varepsilon_{tot}} * (\delta_0 + 1000) - 1000 \qquad (6.7)$$

In Figure 6.6 the $\delta^{18}O$ values of the DIC are plotted against the remaining fraction of $[Ca^{2+}]$ in solution (σ_t/σ_0), as an example shown for the experiments performed with a 5 mmol/l $CaCO_3$ at 10, 20 and 30 °C and a pCO_2 of 1000 (Fig. 6.6a) and 3000 ppmV (Fig. 6.6b). By fitting the experimentally observed data according to Eq. 6.7, the total fractionation $^{18}\varepsilon_{tot}$ can be determined. For the examples shown in Fig. 6.6, $^{18}\varepsilon_{tot}$ ranges from -1.8 ± 0.3 to -3.3 ± 0.2 ‰. The total fractionation for all experiments are summarized in Table 6.1.

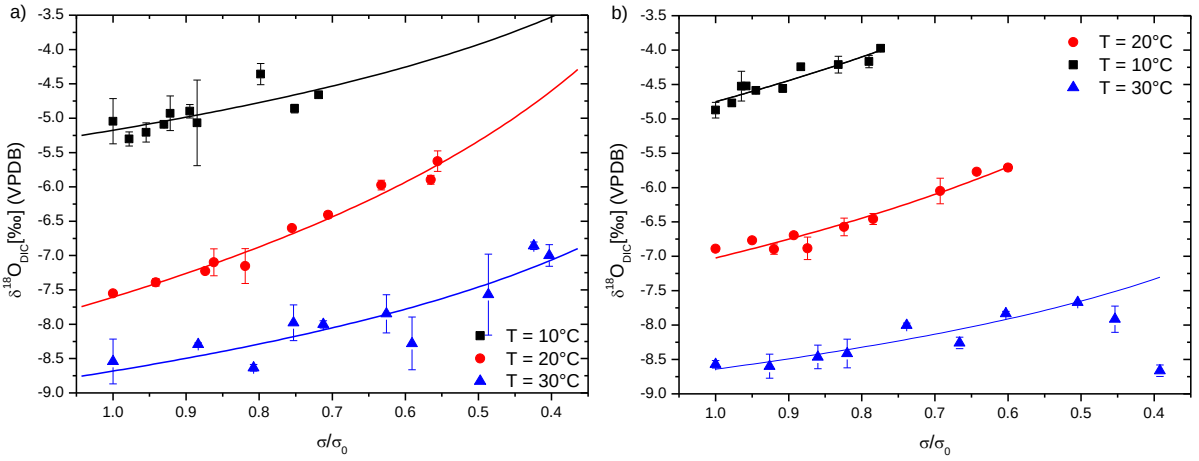

Fig. 6.6: $\delta^{18}O_{DIC}$ plotted versus the remaining fraction of $[Ca^{2+}]$ for experiments performed with a 5 mmol/L at 10, 20, 30 °C and a pCO_2 of 1000 (a) and 3000 ppmV (b). The solid lines are the corresponding fits according to Eq. (6.10).

The combination of Eq. (6.5) and Eq. (6.7) provides the temporal evolution of $\delta^{18}O$ values along the plates during precipitation of $CaCO_3$. Eq. (6.8) combines the precipitation process of calcite with the total fractionation in a Rayleigh model, equivalent to Eq. (6.7) from Scholz et al. (2009):

$$\delta(t) = (\delta_0 + 1000) * \left(exp^{\frac{-t}{\tau pr}} + \left(\frac{\sigma_{eq}}{\sigma_0}\right) * \left(1 - exp^{\frac{-t}{\tau pr}}\right)\right)^{\varepsilon_{tot}} - 1000. \quad (6.8)$$

Note that all constants (ε_{tot}, σ_{eq}, σ_0, δ_0, τ_{pr}) are obtained from the experimental data. Using these data, Eq. (6.8) can be applied to the experimental data in order to test the accuracy of the model predictions compared to the experimentally observed temporal evolution of $\delta^{18}O$ values. Figure 6.7 shows the corresponding example to Figure 6.6, the temporal evolution of $\delta^{18}O$ values for a 5mmol/l $CaCO_3$-solution for the 1000 (Fig. 6.7a) and 3000 ppmV (Fig. 6.7b) experiments with the corresponding model fed with the experimentally determined parameters (Eq. (6.8)). The solid lines denote the modeled $\delta^{18}O_{DIC}$ values, whereas the dashed lines show the corresponding uncertainties calculated applying a Gaussian error propagation by using the respective error from the fits of the experimental data. The experimentally observed temporal evolution of $\delta^{18}O_{DIC}$ values are in very good agreement with the model. This clearly shows a general applicability of a classical Rayleigh distillation model to describe the temporal evolution of DIC isotope values of a (speleothem) calcite precipitating solution.

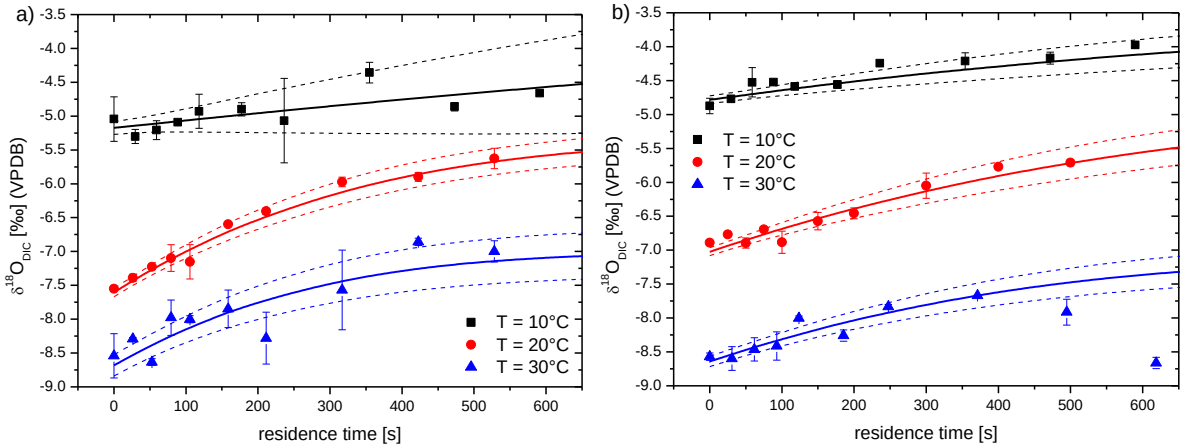

Fig. 6.7: Temporal evolution of the $\delta^{18}O_{DIC}$ values plotted against the residence time on the marble plate exemplarily shown for experiments performed at 10, 20 and 30 °C with a 5 mmol/L $CaCO_3$-solution and a pCO_2 of 1000 (a) and 3000 ppmV (b). The black, red and blue solid lines show the Rayleigh model data according to Eq. (6.8). The dashed lines are the corresponding uncertainties of the model.

However, for the interpretation of the experiments conducted at 30 °C and 3000 ppmV CO_2 (Fig. 6.6b and 6.7b) the last two data points were excluded from the fit based on a Rayleigh distillation, because the data gets enriched until about 350 s and then decreases to lower values again. This is cannot be explained with a classical Rayleigh approach, which predicts an initial increase followed by the establishment of some kind of equilibrium state when approaching

chemical equilibrium. Including these data points into the fit would lead to a flatter slope, approaching biased, more negative values than the initial increase would suggest.

This trend to more negative values for longer residence times could be caused by different processes. On the one hand this could be related to fractionation processes as proposed by Dreybrodt (2008) and Dreybrodt and Romanov (2016). After reaching the maximum the tendency to more negative values would then be related to their kinetic constant, γ, which has not been validated experimentally yet. However, the temporal resolution of our experiments is not high enough to confirm or quantify this model, as we observe this phenomenon only in one of the experiments (5 mmol/l, 30 °C, 3000 ppmV CO_2).

On the other hand, the decreasing isotope values could also very likely be related to beginning isotope exchange processes with the gaseous CO_2 of the box atmosphere or with the water reservoir (also often referred to "buffering") affecting both the DIC and the precipitated $CaCO_3$. The precipitation rate of the solution decreases with increasing residence times on the plate, due to progressive loss of Ca^{2+} to the carbonate surface and, thus, progressive decrease in supersaturation, approaching chemical equilibrium. When the rates become slower, isotope exchange between H_2O, HCO_3^- and CO_2 might get significant and is also imprinted into the isotope signature of the DIC and $CaCO_3$, respectively. Since the CO_2 used in the experiments was previously equilibrated with the water used for all solutions in the experiments, it is very likely that, if isotope exchange becomes significant, the $\delta^{18}O$ values tend to establish isotope equilibrium with the (initial) water values. The assumption of isotope exchange is reasonable, as this phenomenon is more pronounced for the experiment performed at higher pCO_2 (compare Fig. 6.7a and 6.7b). This observation is not only visible in the $\delta^{18}O$ values of the DIC, but also in the temporal isotope evolution of the corresponding $CaCO_3$ experiment (blue symbols in Fig. 6.5b).

The possible isotope exchange between the solution and the box atmosphere is also obvious in the $\delta^{13}C$ values of the corresponding experiment. This has been discussed in detail in Part I of this study.

6.5.3 Comparison of the DIC and the $CaCO_3$ experiments – determination of fractionation factors

6.5.3.1 Fractionation between DIC and $CaCO_3$ – determination of $^{18}\varepsilon_{CaCO3/HCO3-}$

The investigation of the temporal evolution of stable isotopes for both, the DIC and the $CaCO_3$ enables to directly determine the fractionation between the respective carbonate species. Therefore, the $\delta^{18}O$ values of the $CaCO_3$ experiment need to be compared with those of the DIC.

The fractionation is then simply given by the differences between the corresponding isotope values. Since the two experiments are conducted on two different plates the residence times on the plates (glass vs. marble) are slightly different (compare Fig. 6.4 and Fig. 6.5). Thus, it is essential to synchronize the residence times and to ensure that the precipitation rates are of the same magnitude. However, although the residence times are not exactly identical they are very similar on the glass and the marble plates. The temporal evolution of the $\delta^{18}O_{DIC}$ values can be described by Eqn. (6.8) (Section 6.5.1), this enables to calculate the isotope composition of the DIC for the residence times of the corresponding $CaCO_3$ experiment and to calculate the fractionation. The isotope fractionation, $^{18}\varepsilon_{CaCO3/HCO3-}$, can then be calculated for all experimental times by subtracting the $\delta^{18}O$ value of the HCO_3^- from the corresponding $\delta^{18}O$ value of the $CaCO_3$:

$$^{18}\varepsilon_{CaCO_3/HCO_3^-}(t) = \delta^{18}O_{CaCO_3}(t) - \delta^{18}O_{HCO_3^-}(t), \quad (6.9)$$

Figure 6.8 shows the $\delta^{18}O$ values of the DIC and the $CaCO_3$ for selected experiments, as well as a comparison to $\delta^{18}O_{CaCO3}$ values as they would be expected from isotope equilibrium obtained from the experimentally observed $\delta^{18}O_{DIC}$ values. The uncertainty of the $\delta^{18}O$ values of the DIC (Fig. 6.8) were calculated by a Gaussian error propagation. Since there are no direct fractionation factors for the fractionation between HCO_3^- and $CaCO_3$ available it is necessary to combine the available fractionation factors for the interfaces $CaCO_3/H_20$ and HCO_3^-/H_2O. The fractionation is then given by (e.g., Mühlinghaus et al., 2009):

$$^{18}\varepsilon_{CaCO_3/HCO_3^-} = {}^{18}\varepsilon_{HCO_3^-/H_2O} + {}^{18}\varepsilon_{CaCO_3/H_2O}, \quad (6.10)$$

We here use the combination of the fractionation for $^{18}\varepsilon_{HCO_3^-/H_2O}$ by Beck et al. (2005) and four different fractionation factors for $^{18}\varepsilon_{CaCO_3/H_2O}$ by Coplen (2007) (green solid line in Fig 6.8), Tremaine et al. (2011) (blue solid line in Fig 6.8), Johnston et al. (2013) (orange solid line in Fig 6.8) and Kim and O'Neil (1997) (purple solid line in Fig 6.8) which has often been used in speleothem literature.

The fractionation, $^{18}\varepsilon_{CaCO3/HCO3-}$, observed in our experiments ranges from – 0.34 to – 2.55 ‰ (Fig. 6.8). The initial values are in good agreement to the theoretical predictions using the fractionation factor calculated using Tremaine et al. (2011) (blue solid lines Fig. 6.8) and Johnston et al. (2013) (orange lines in Fig 6.8). With increasing residence time on the plates the fractionation between $\delta^{18}O_{HCO3-}$ and $\delta^{18}O_{CaCO3}$ of our experimental values becomes smaller, mostly approaching the theoretical predictions by Coplen (2007) (green solid line, Fig. 6.8 a, b, d). Both, $\delta^{18}O_{HCO3-}$ and $\delta^{18}O_{CaCO3}$ become enriched due to progressive precipitation of $CaCO_3$. With increasing residence time, however, we observe a progressively decreasing fractionation in most of our experiments (Fig. 6.8a, c, e, f, g, h). This is a hint for a disequilibrium process most probably

coupled to the precipitation kinetics of $CaCO_3$. In other words: the system has an initial equilibrium state, which is then forced out of equilibrium during precipitation of calcite.

This is also visible in Figure 6.9, where the relation between the oxygen isotope fractionation, $^{18}\varepsilon_{CaCO3/HCO3-}$, and the precipitation rate is shown. The fractionation is not constant along our plates, furthermore it is obviously coupled to the carbonate chemistry and the corresponding rate of precipitation. The uncertainty of the $\delta^{18}O_{DIC}$ values (Fig. 6.8) were propagated to the calculated fractionation factors. Almost all experiments show clearly decreasing isotope fractionation with decreasing precipitation rate, demonstrating the influence of precipitation rate on the corresponding isotope fractionation. This has also already been observed for the stable carbon isotopes in Part I of this study. These observations support the assumption of a disequilibrium (or 'kinetic') fractionation process. For the case of equilibrium a constant fractionation between HCO_3^- and $CaCO_3$ would be expected. This is only visible in two experiments (Fig. 6.8b; 5 mmol/l $CaCO_3$-solution at 20°C and 1000 ppmV CO_2 and Fig. 6.8d; 5 mmol/l $CaCO_3$-solution at 10 °C and 3000 ppmV CO_2). Note that these experiments also show very little dependence on the precipitation rate, which is not visible in Figures 6.8 and 6.9, due to scaling. Another obvious characteristic from Figure 6.9 is, that the highest precipitation rates correspond to the highest temperatures (30 °C in our experiments, e.g. Fig. 6.9 c and f) and also to the strongest effect of changing fractionation.

These results provide important information on disequilibrium fractionation processes for oxygen isotopes during precipitation of (speleothem) calcite. However, providing absolute numbers for the fractionation, $^{18}\varepsilon_{CaCO3/HCO3-}$, as a function of the experimental temperature remains difficult. This could be related to several minor uncertainties linked to the different experimental setups: (i) the DIC and the $CaCO_3$ experiments have slightly different flow velocities and, thus, also film thicknesses, caused by the fact that (ii) the experiments are conducted with slightly different setups (one glass plate vs two marble plates); (iii) the initial chemical and isotopic conditions of the solutions of individual experiments can be slightly different. For all solutions a SI of about 0 was adjusted by sparging the excess CO_2 with argon and carefully measuring the pH of the bulk solution (section 6.3). Establish the required pH values precisely is very difficult and small deviations from $SI = 0$ cannot be excluded. As a consequence, the $\delta^{18}O_{DIC}$ values might be influenced by $\delta^{18}O_{CO2}$ of small amounts of dissolved CO_2 which could be still in solution after equilibration, especially for the small distances of flow for at least some experiments.

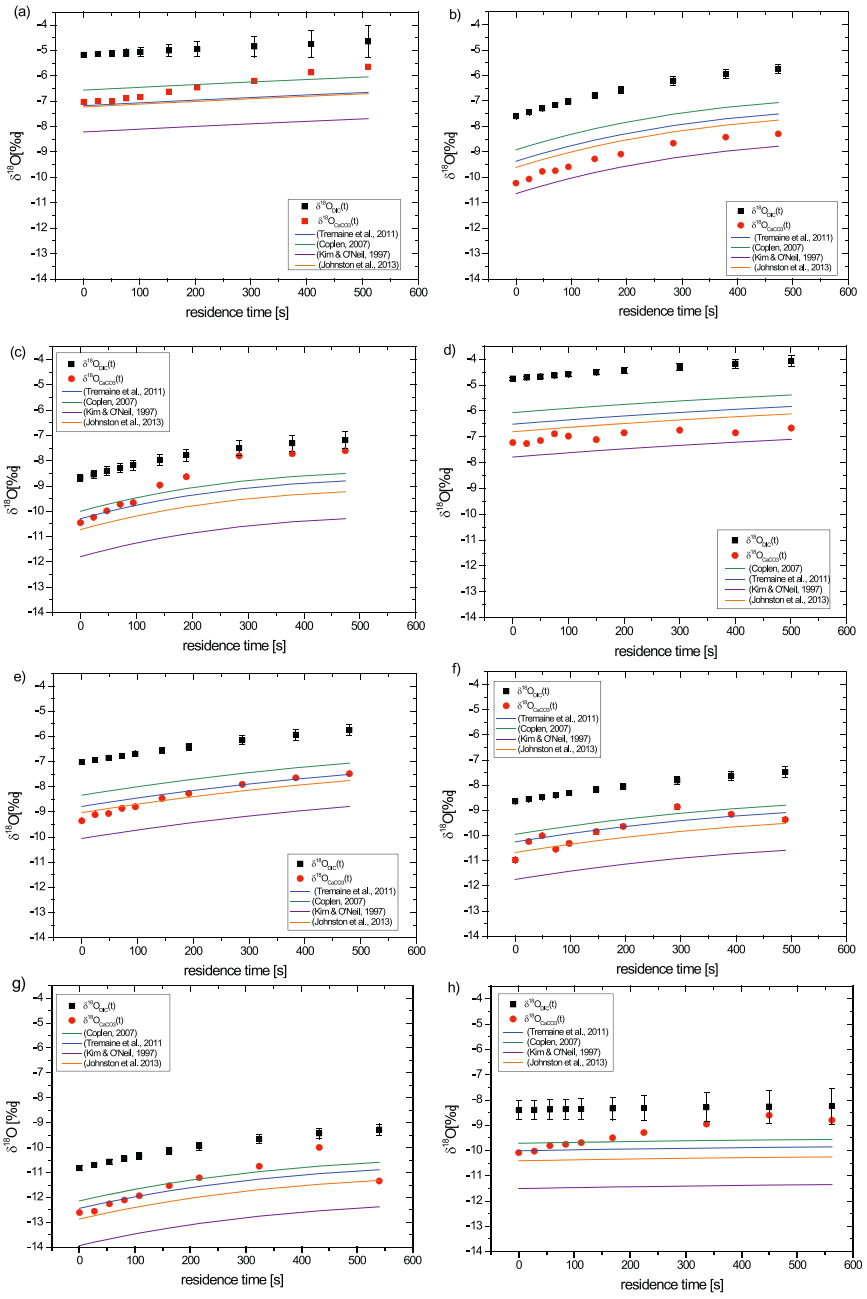

Fig. 6.8: Comparison of the $\delta^{18}O$ values of the DIC (black symbols) and the precipitated $CaCO_3$ (red symbols). Also shown are the $\delta^{18}O$ values expected for isotope equilibrium using different fractionation factors from the literature (green, blue, purple and orange straight lines). (a) 5 mmol/l $CaCO_3$-solution at 10°C and 1000 ppmV CO_2; (b) 5 mmol/l $CaCO_3$-solution at 20°C and 1000 ppmV CO_2; (c) 5 mmol/l $CaCO_3$-solution at 30°C and 1000 ppmV CO_2; (d) 5 mmol/l $CaCO_3$-solution at 10°C and 3000 ppmV CO_2; (e) 5 mmol/l $CaCO_3$-solution at 20°C and 3000 ppmV CO_2; (f) 5 mmol/l $CaCO_3$-solution at 30°C and 3000 ppmV CO_2; (g) 2 mmol/l $CaCO_3$-solution at 30°C and 1000 ppmV CO_2; (h) 3 mmol/l $CaCO_3$-solution at 20°C and 1000 ppmV CO_2.

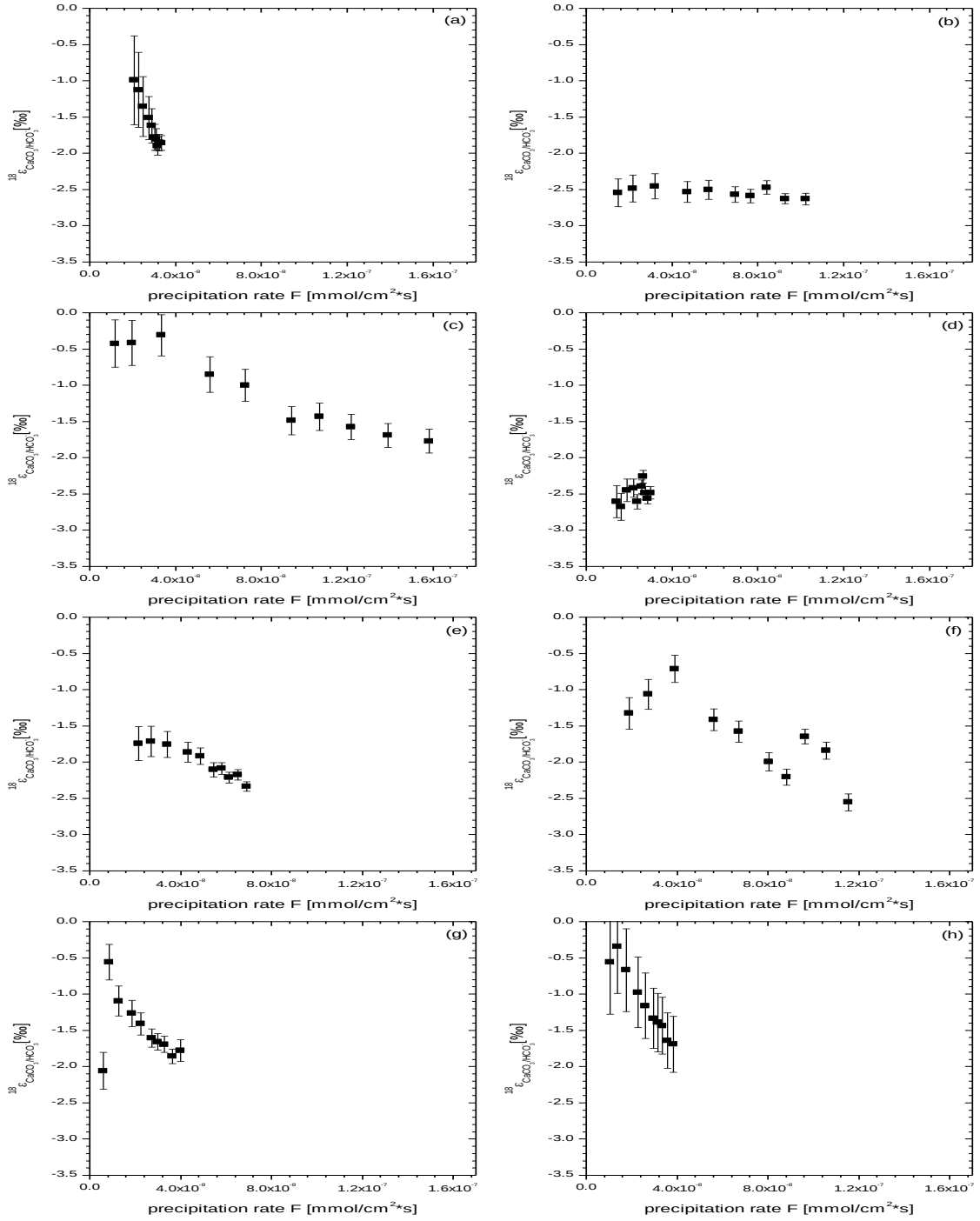

Fig. 6.9: Oxygen isotope fractionation between $CaCO_3$ and HCO_3^-, $^{18}\varepsilon_{CaCO3/HCO3-}$, plotted against the precipitation rate for all experiments. (a) 5 mmol/l $CaCO_3$-solution at 10°C and 1000 ppmV CO_2; (b) 5 mmol/l $CaCO_3$-solution at 20°C and 1000 ppmV CO_2; (c) 5 mmol/l $CaCO_3$-solution at 30°C and 1000 ppmV CO_2; (d) 5 mmol/l $CaCO_3$-solution at 10°C and 3000 ppmV CO_2; (e) 5 mmol/l $CaCO_3$-solution at 20°C and 3000 ppmV CO_2; (f) 5 mmol/l $CaCO_3$-solution at 30°C and 3000 ppmV CO_2; (g) 2 mmol/l $CaCO_3$-solution at 30°C and 1000 ppmV CO_2; (h) 3 mmol/l $CaCO_3$-solution at 20°C and 1000 ppmV CO_2.

5.3.2 Fractionation between DIC and H_2O– determination of $^{18}\varepsilon_{HCO3-/H2O}$

In the next step, the fractionation between the DIC (HCO_3^-) and the water of the solution can be determined for our experiments. The fractionation is, as for $CaCO_3/HCO_3^-$, simply given by the difference of $\delta^{18}O_{DIC}$ and $\delta^{18}O_{H2O}$:

$$^{18}\varepsilon_{HCO_3^-/H_2O}(t) = \delta^{18}O_{H_2O}(t) - \delta^{18}O_{HCO_3^-}(t), \quad (6.11)$$

In our experiments we frequently took water samples (see section 6.3). Only very small enrichments were observed, maybe linked to very small evaporation effects. Since the residence time of the solutions on the plates (about 600 s) are very small compared to the time needed for establishment of isotope equilibrium between DIC and H_2O (several hours for pH and temperatures of the experiments, Beck et al., 2005). The DIC is out of equilibrium as soon as the precipitation (and thus isotope fractionation) of $CaCO_3$ has started. Here we use the comparison of the water isotopes to the DIC values of our experiments in order to estimate whether the experimental solution has initially been in isotope equilibrium according to the fractionation factors provided by Beck et al. (2005). This can be done by calculating a mass balance for our experimental values, using the corresponding fractions of species as they can be determined by phreeqC (Parkhurst and Apello, 1999). Since the bulk solution is stored for several days inside the climate box at the experimental temperature it is reasonable to assume isotope equilibrium between all involved (contained) species. Water is by far the largest reservoir, thus, it is expected that all species establish an isotope equilibrium with the $\delta^{18}O$ value of the water. Considering all involved species in the system the mass balance for the expected $\delta^{18}O$ values for the DIC then reads:

$$\delta^{18}O_{DIC,eq} = x * \left(\frac{2}{3}\left(\delta^{18}O_{H_2O} + {}^{18}\varepsilon_{CO_2/H_2O}\right) + \frac{1}{3}\left(\delta^{18}O_{H_2O} + {}^{18}\varepsilon_{OH^-/H_2O}\right)\right) + (1-x) * \left(\delta^{18}O_{H_2O} + {}^{18}\varepsilon_{HCO_3^-/H_2O}\right), \quad (6.12)$$

where x denotes the portion of the dissolved CO_2, $^{18}\varepsilon$ the individual fractionation factors, and $\delta^{18}O_{H2O}$ the corresponding value of the water. Note that when dissolved CO_2 is precipitated, in our case as $SrCO_3$ by adding NaOH and $SrCl_2$ (see section 6.3), mass balance requires an additional O - atom which is then provided by one OH^-. Thus, 2/3 of the O isotopes are provided by the CO_2 and 1/3 is provided by the OH^- (see e.g., Beck et al., 2005).

To pick up the example from section 4.1.1 (Fig. 6.3), for a 5 mmol/l $CaCO_3$-solution at 20 °C and 1000 ppmV CO_2, the bulk solution had a $\delta^{18}O_{H2O}$, converted into VPDB (using Coplen et al., 1983), of - 39.52 ‰. The pH value was 6.7, this corresponds to a species distribution of about 34 % CO_2 and 66 % HCO_3^-. Using the fractionation between water and CO_2, OH^- and HCO_3^- by Beck

et al. (2005) one obtains an expected equilibrium value of about – 12.3 ‰. The corresponding experimentally measured $\delta^{18}O_{DIC}$ is – 12.6 ‰, which shows the very good agreement of predicted and measured values. After the equilibration plate the pH value is 8 and about 98 % of the DIC are then provided by HCO_3^-. Using the converted $\delta^{18}O_{H2O}$ measured at the end of the equilibration plate of – 39.38 ‰ the expected $\delta^{18}O_{DIC}$ is – 7.2 ‰, the corresponding experimentally observed value is – 7.6 ‰. This indicates that after chemical equilibration (i.e., the initial DIC value for the precipitation of $CaCO_3$) the $\delta^{18}O$ values of the DIC are still almost in isotope equilibrium with the water of the solution, documenting that most likely no $CaCO_3$ was precipitated on the upper (equilibration) plate. For this example the measured DIC value is about 0.4 ‰ more negative than expected for isotope equilibrium. This could be related to small amounts of dissolved, isotopically negative, CO_2. Note that within the experimental uncertainties of the precipitation method as $SrCO_3$ (which is about $\pm$0.5 ‰) the expected equilibrium and the observed values are in good agreement. For the water sampled at the end of the marble plate (after 100 and 40 cm distance of flow) the expected equilibrium values are clearly more negative than the experimentally observed ones. This is reasonable because, as stated above, the residence time on the plate is substantially lower than needed for establishing isotope equilibrium between DIC and H_2O (600 s vs. several hours, Beck et al., 2005).

In summary, fractionation factors provided by Beck et al. (2005) can be applied to calculate equilibrium state our experimental bulk solutions until $CaCO_3$ is precipitated. Thus, the time for establishing isotope equilibrium between all species in the bulk solutions was sufficiently long. The distance for chemical equilibration (i.e. degassing of dissolved CO_2 and establishment of supersaturation with respect to calcite) on the small upper marble plate can also be validated by the conformity of expected and observed $\delta^{18}O_{DIC}$ values. Once the precipitation of $CaCO_3$ started the fractionation between water and HCO_3^- is out of equilibrium, which is also in accordance with the expectations.

6.5.3.3 Fractionation between $CaCO_3$ and H_2O– determination of $^{18}\varepsilon_{CaCO3/H2O}$ and 1000 lnα

Analogously to the previous sections, the fractionation between calcite and water can be determined for our experimental data. The fractionation between $CaCO_3$ and water is often expressed as α, which can simply be calculated from our experimental data by:

$$^{18}\alpha_{CaCO_3/H_2O} = \frac{\delta^{18}O_{CaCO_3}+1000}{\delta^{18}O_{H_2O}+1000} \left(= \left(^{18}\varepsilon_{CaCO_3/H_2O} - 1\right) * 1000\right) \qquad (6.13)$$

In order to handle these numbers more easily they can also be expressed as $1000\ln^{18}\alpha$, which corresponds to the difference in (measured) $\delta^{18}O$ values of the calcite and of the water ($\Delta^{18}O_{CaCO3\text{-}H2O}$). As an example we apply this, as shown in section 6.2.3.2, to an experiment conducted with a 5 mmol/l $CaCO_3$-solution at 20 °C and 1000 ppmV CO_2. Figure 6.10a shows the $\delta^{18}O$ values of the $CaCO_3$ (black symbols) compared to those of the water (red symbols). Note that there is not a $\delta^{18}O_{H2O}$ available for every residence time of the $CaCO_3$. This is technically impossible, but we regularly sampled the solution for $\delta^{18}O$ analyses at the end of the glass plate (see section 6.3). The values differ by only about 0.2 ‰ between the impinging drip point of the glass plate and the exit of the glass plate. Thus evaporation only plays a minor role and the $\delta^{18}O_{CaCO3}$ can be compared to the average $\delta^{18}O_{H2O}$ at the end of the glass plate. As already described in section 4.2.1 (Fig. 6.5), with increasing distance of flow the $\delta^{18}O$ values of the $CaCO_3$ become more enriched of by + 1.9 ‰, whereas those of the water remain almost constant. This is analogous to the observations from section 6.5.3.2, the time required for maintaining isotope equilibrium between the water and the precipitated calcite is orders of magnitudes (about 98 times) larger than the time constant for precipitation of $CaCO_3$ in the experiment.

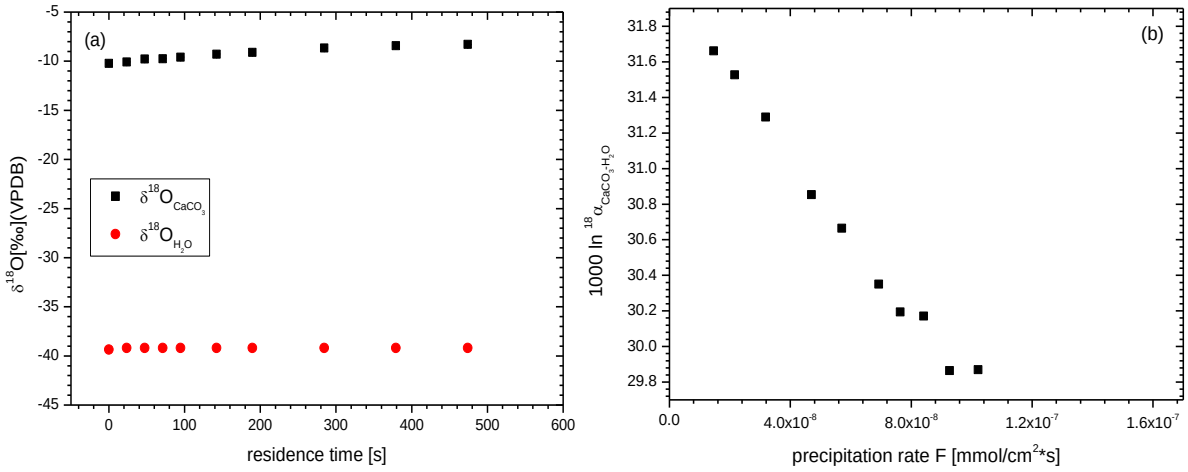

Fig. 6.10: Temporal evolution of $\delta^{18}O$ values of the precipitated $CaCO_3$ and the water for an experiment conducted with a 5 mmol/l $CaCO_3$-solution at 20°C and 1000 ppmV (a) and the corresponding fractionation $1000\ln^{18}\alpha$ plotted against the precipitation rate, F (b).

However, the difference between $CaCO_3$ and water, $\Delta^{18}O_{calcite\text{-}water}$, is relatively large and ranges for this example from + 29.9 to + 31.7 ‰. Figure 6.10b shows the fractionation, expressed as $1000\ln^{18}\alpha$, as a function of the precipitation rate. Contrary to the observations for $^{18}\varepsilon_{CaCO3/HCO3\text{-}}$ (section 6.5.3.1), the fractionation increases with decreasing precipitation rate. It is very important to note that this effect is linked to the disequilibrium caused by progressive removal of light isotopes from the DIC pool due to precipitation of $CaCO_3$ along the plate, whereas the water

values stay constant (see above). The increasing fractionation becomes also obvious from Figure 6.11 where the $1000\ln^{18}\alpha$ values of the same example are plotted against the residence time on the plate. Additionally shown are different $1000\ln^{18}\alpha$ values expected from the literature. We here compare our experimentally observed values to fractionation factors, which are frequently used in the speleothem literature. Some of them are determined in the laboratory by precipitating $CaCO_3$ from a bulk solution under controlled conditions (Kim and O'Neil, 1997; Watkins et al., 2013), others are observed from a natural (cave) system (Coplen, 2007; Johnston et al., 2013; Tremaine et al., 2011).

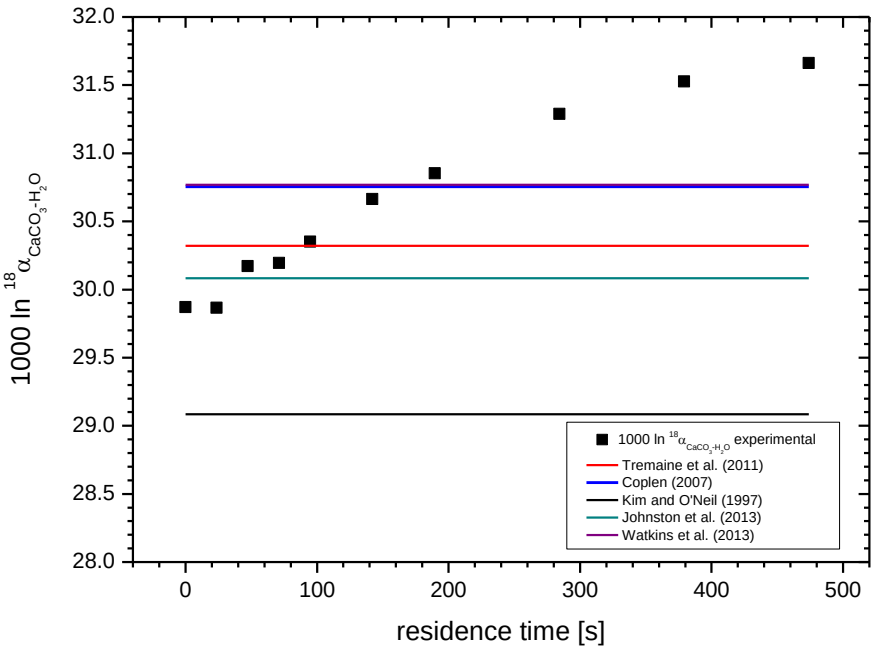

Fig. 6.11: $1000\ln^{18}\alpha$ for an experiment conducted with 5 mmol/l $CaCO_3$-solution at 20 °C and 1000 ppmV CO_2 plotted against the residence time on the plate. Additionally shown are the $1000\ln^{18}\alpha$ values predicted by different laboratory experiments and observations from natural (cave) systems. Note that the values calculated after Watkins et al. (2013) and Coplen (2007) plot directly on each other.

Our experimentally observed initial values (i.e., 0 – 80 s residence time) plot slightly below the $1000\ln^{18}\alpha$ values as predicted by Johnston et al. (2013) (up to - 0.2 ‰) and Tremaine et al. (2011) (up to - 0.4 ‰) but significantly higher than predicted by Kim and O'Neil (1997) (here about + 0.8 ‰). With increasing residence time and, thus, progressive precipitation of $CaCO_3$ the $1000\ln^{18}\alpha$ values increase and, however eventually cross the values of Johnston et al. (2013) and

Tremaine et al. (2011). Furthermore, they even cross the fractionation factors predicted by Coplen (2007) and Watkins et al. (2013) and reach a value of about 31.7 ‰. This is reasonable, since the solution seems to have an initial "equilibrium" state, which is then forced out of equilibrium due to progressive precipitation of calcite (see above). The initial values corresponds best to those of Johnston et al. (2013) and Tremaine et al. (2011), which are cave determined. This implies, (i) that our system closely resemble a natural cave system and (ii) our solution (similarly to the mass balance in section 6.5.3.2, Eq. 6.14) is initially in isotope equilibrium. In an ideal case the initial values (i.e. 0 cm of flow) corresponds to the apex of a stalagmite. These findings have also important implications for choosing samples for paleoclimate reconstruction and will be further discussed in section 6.5.4.

Similar observations are made for all experiments. Thus, the initial values for $1000\ln^{18}\alpha$ of all experiments appear to be best suited to be compared to each other and the corresponding literature values as a function of experimental temperature. Figure 6.12 shows the experimentally determined initial values of $1000\ln^{18}\alpha$ plotted against the experimental temperature (blue symbols). Unfortunately the initial water sample for the experiment conducted at 30° C with a 5 mmol/l $CaCO_3$-solution at 1000 ppmV CO_2 got lost during shipping. Thus, for 30 °C only the data point for the corresponding 3000 ppmV CO_2 experiment (blue open triangle, Fig. 6.12) is shown. However, since the water values during the $CaCO_3$ part of the experiment remained almost constant it is reasonable to estimate the initial value by inserting an average $\delta^{18}O_{H20}$ value. The result (not shown in Fig. 6.12) then plots very close to the value observed for the 3000 ppmV CO_2 experiment, the corresponding $1000\ln^{18}\alpha$ values are 28.55 ‰ for 3000 ppmV and ca. 28.78 ‰ for 1000 ppmV CO_2. Additionally shown are the fractionations from the literature (solid lines), as well as the experimental results from cave analogous experiments provided by Day and Henderson (2011)(orange symbols). All values for $1000\ln^{18}\alpha$ are compiled in Table 6.1.

As already stated for Figure 6.11, the experimentally determined initial values of this study correspond well to the predictions of Tremaine et al. (2011) and Johnston et al. (2013) supporting the assumption that the experiments of this study resembles a natural cave system. Another conspicuity in Figure 6.11 is, that the observed fractionations by Day and Henderson (2011) are also in the same range, but show a higher degree of scatter. This could be well related to the different setups such as dripping with splashing effects vs. laminarily flowing film of solution in this study. Furthermore, the conditions in this study had a more precise the control on the surrounding conditions, such as relative humidity (and minimizing evaporation effects), isotope composition of the CO_2 and more importantly the possibility to get water samples throughout the experiment. This was unfortunately not possible in the setup by Day and Henderson (2011).

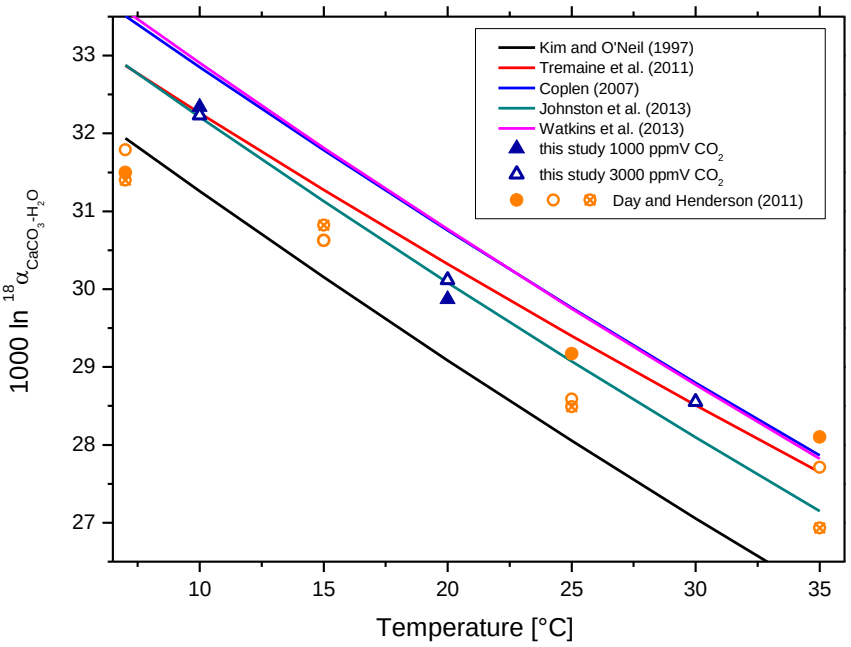

Fig. 6.12: 1000ln$^{18}\alpha$ values plotted as a function of the temperature, the different straight lines indicate the different fractionation factors suggested by different studies. The blue symbols denote the experimentally determined values of this study, whereas the orange symbols are the experimental observations provided by Day and Henderson (2011).

As obvious in Figure 6.12 there are several stable isotope fractionation factors available from the literature for the interface $CaCO_3/H_2O$. This is reasonable, because carbonates and especially the corresponding $\delta^{18}O$ values have been widely used for paleoclimate reconstruction such as temperature or (paleo-) precipitation patterns (e.g., Bar-Matthews et al., 2003; Cheng et al., 2016). However, for the interpretation of these paleoclimate records in terms of past precipitation and temperature signals from $\delta^{18}O$ values of (speleothem) calcite it is of utmost importance to know the corresponding fractionation factors. This has already been widely discussed by numerous studies (e.g., Coplen, 2007; Day and Henderson, 2011; Johnston et al., 2013; Kim and O'Neil, 1997; Tremaine et al., 2011). Especially the terms 'kinetic' and 'equilibrium' are frequently used and which of these factors is suited best or if 'disequilibrium' isotope fractionation needs to be taken into account is still an open question and an ongoing discussion for speleothem isotope records. Recently Watkins et al. (2014; 2013) carefully investigated the fractionation between water and calcite in dependence of reaction kinetics, such as temperature, precipitation rate and pH. They used a complex fractionation model which is additionally compared with experiments they conducted in the presence of carbonic anhydrase, which forces

the DIC into permanent isotope equilibrium with the water. Their findings suggest that almost all fractionation factors determined in the laboratory were out of equilibrium due to kinetic effects during precipitation. They conclude that the most likely case of equilibrium fractionation, if ever achieved, is in a natural system where calcite precipitates slowly under constant conditions from a bulk solution as for example in Devils Hole (Coplen, 2007). Comparing their results with our experimentally observed isotope fractionation as a function of the observed precipitation rates, for both the $CaCO_3$/DIC, as well as $CaCO_3/H_2O$, is in good agreement. The precipitation rates of Watkins et al. (2014; 2013) range between values of $\log_{10}R$ between - 5.73 and – 6.65, whereas our initial values range from - 6.98 to – 7.53. As already observed in Figure 6.12 the rates and fractionation observed in this study corresponds well to the observations from Tremaine et al. (2011).

Finally, it is possible to determine the temperature dependent fractionation between $CaCO_3$ and water by our experimental data. This is shown in Fig. 6.13, where the experimentally observed $1000\ln^{18}\alpha$ value are plotted against $10^3/T$, where T is the temperature in Kelvin. Applying a linear fit to these data, provides the temperature dependent fractionation:

$$1000ln^{18}\alpha = 16.516 \pm 1.267 * \frac{10^3}{T} - 26.141 \pm 4.356. \qquad (6.14)$$

As obvious from Eq. 6.14 the errors of the fit are relatively large. This is related to relatively low numbers of values. To establish a more reliable temperature equation it is necessary to conduct more experiments at a wider range of temperature to improve the precision of the temperature equation. However, another important point to note is that the rate dependence, and thus dependence on initial concentrations and saturation state of the solution need to be investigated in more detail in future experiments. This is crucial for paleoclimate interpretation from speleothem $\delta^{18}O$ records.

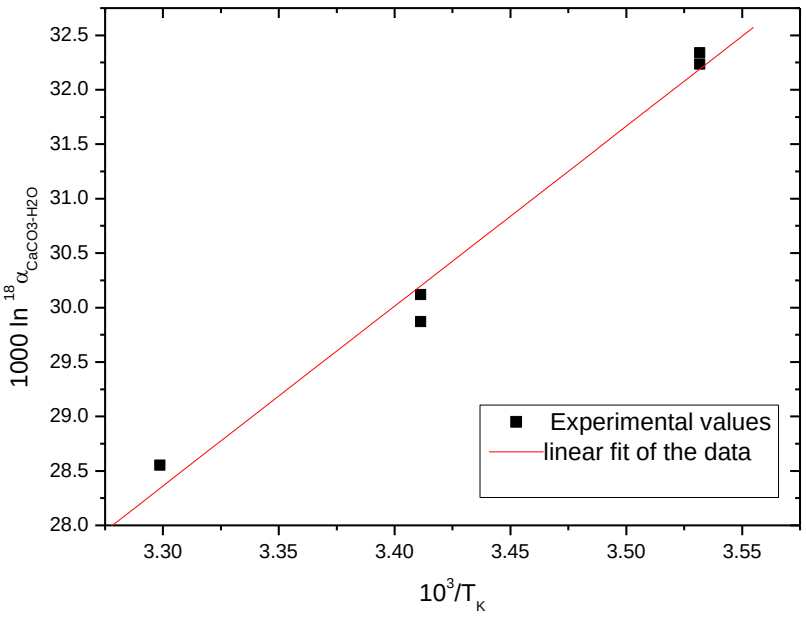

Fig. 6.13: Experimentally observed 1000ln$^{18}\alpha$ value plotted against 10^3/T. The red straight line denotes the linear fit of the experimental data.

6.5.4 Implications for interpretation of speleothem $\delta^{18}O$ records and limitations of the experiments

The results of this study suggest that a quantitative reconstruction of $\delta^{18}O$ of past precipitation and temperature remains very difficult, since the complex interplay of various parameters need to be taken into account (i.e., reaction kinetics, rate dependent fractionation and dynamic fractionation factors). The rate dependent fractionation could potentially lead to a systematic overestimation of $\delta^{18}O$ signals in speleothems. For instance, if the solution entering the cave precipitates $CaCO_3$ for only a few seconds prior to dripping down to the stalagmite (e.g. while flowing down a stalactite), the DIC is depleted in light isotopes and out of equilibrium with the water of the solution. As a result, the $\delta^{18}O$ signal that is incorporated into the stalagmite does not reflect the $\delta^{18}O$ value of the drip water, and can, thus, not be interpreted as precipitation signal (i.e., $\delta^{18}O$ value of originally infiltrating water). Drip (and stalagmite growth) sites that are not influenced by any PCP processes, which can be assessed by studying trace element signals (e.g., Treble et al., 2015), should be preferred. Additionally, it is half the battle to assess the present day conditions in the studied cave site by carefully conducted monitoring programs. Measuring the

present day temperature of the cave as well as $\delta^{18}O$ of the drip water and of in-situ precipitated calcite (e.g., Riechelmann et al., 2013; Riechelmann et al., 2011) is a valuable method to estimate the fractionation factors for the corresponding cave site. This could potentially provide very important information on the underlying mechanisms for the interpretation of paleoclimate records from the investigated cave.

Independently from the complexity of the processes that could affect the $\delta^{18}O$ signals in speleothems they still provide very important information on relative changes for example in temperature and source of meteoric precipitation. However, generating quantitative information remains challenging and need more carefully conducted experimental work.

The experimental results presented in this study can be well explained by a Rayleigh fractionation model as predicted by Scholz et al. (2009). However, a final validation of the Scholz et al. (2009) model or if the fractionation can be better described by the 'kinetic' model as proposed by Dreybrodt (2008) is not possible with the results of this study. This is related to the chemical resolution of our experiments, because the differences become relevant after about 75 % of the initial $[Ca^{2+}]$ have been precipitated (Fig 6.1). Prior to that, the temporal evolution of $\delta^{18}O$ in both models is very similar (Dreybrodt and Scholz, 2011; Scholz et al., 2009). During the experiments a maximum of 60 % of the initial $[Ca^{2+}]$ were precipitated, which is still off from approaching chemical equilibrium.

However, both models use a static fractionation factor, which only depends on the temperature during precipitation of $CaCO_3$. The results of our experiments, in contrast, suggest that the fractionation factor seems to be additionally coupled to the reaction kinetics, such as precipitation rate. In order to investigate whether the 'kinetic' model or the Rayleigh approach is more suitable or if a completely new model is necessary, further experimental work is needed, especially for lower concentrations closer to chemical equilibrium.

6.6 Conclusions

The experiments presented in this study, conducted under controlled, cave analogous conditions, allow for the first time to directly investigate oxygen isotope fractionation between precipitated $CaCO_3$ and all other involved species in the system (HCO_3^-, H_2O, CO_2) at the same time. The temporal evolution of $\delta^{18}O$ values for both, the precipitated $CaCO_3$ and the DIC, can be well explained by applying a Rayleigh fractionation model as proposed by Scholz et al. (2009). The total fractionation ${}^{18}\varepsilon_{tot}$ ranges between – 0.38 to – 3.3 ‰. All experiments show an initial fractionation between $CaCO_3$ and DIC, ${}^{18}\varepsilon_{CaCO3/HCO3-}$, which is in good agreement with combined

fractionation factors observed in natural cave systems (Johnston et al., 2013; Tremaine et al., 2011). With increasing residence time on the plate, and, thus, decreasing supersaturation and precipitation rate, the fractionation between DIC and $CaCO_3$ becomes smaller, approaching the predictions by Coplen (2007) and Watkins et al. (2014; 2013). The fractionation between DIC and water is initially (i.e. at 0 cm distance of flow) in isotope equilibrium as calculated using equilibrium fractionation factors, $^{18}\varepsilon_{HCO3-/H2O}$, by Beck et al. (2005). As soon as $CaCO_3$ is precipitated, the system is forced out of equilibrium, because the time required to re-equilibrate the DIC with the water is substantially longer than the residence time on the plates. As observed for the other species the initial fractionation between $CaCO_3$ and water are in good agreement to values observed in natural cave systems (Johnston et al., 2013; Tremaine et al., 2011) and provide a very similar temperature dependence. However, with progressive precipitation of $CaCO_3$, the fractionation $1000\ln^{18}\alpha$ increases, crossing the predictions by other (equilibrium) studies towards higher values. These findings suggest (i) that our system closely resembles a natural system because our observed values correspond best to those observed in natural cave systems; (ii) reaction kinetics have to be taken into account for interpretation of speleothem $\delta^{18}O$ records.

Analogously to Part I of this study ($\delta^{13}C$), the assumption of a static fractionation factor as proposed by different modeling studies (Dreybrodt, 2008; Dreybrodt and Scholz, 2011; Scholz et al., 2009) may not be completely applicable, since this study suggests that the fractionation seems to be coupled to chemical reaction kinetics. A final validation which fractionation model is more suitable to describe the incorporation of $\delta^{18}O$ values into a speleothem is not possible within this study. To resolve this issue it is mandatory to conduct experiments under even more constrained conditions and with a higher temporal resolution, as well as concentrations of $CaCO_3$ which are closer to chemical equilibrium.

Acknowledgements

M. Hansen and D. Scholz acknowledge funding by the Deutsche Forschungsgemeinschaft (DFG) through grants SCHO 1274/8-1 and SCHO 1274/9-1. We thank Marie Froeschmann for her credible support as student assistance during the experiments and preparation of samples for stable isotope analyses. Furthermore we are thankful to the workshop of the Institutes for Geosciences and Physics of the Atmosphere, University of Mainz, especially S. Klumb, for very helpful technical support during the experiments and to keep the climate box always running reliably.

6.7. References

Asmerom, Y., Polyak, V.J., Burns, S.J. (2010) Variable winter moisture in the southwestern United States linked to rapid glacial climate shifts. *Nature Geosci* **3**, 114-117.

Bar-Matthews, M., Ayalon, A., Gilmour, M., Matthews, A., Hawkesworth, C.J. (2003) Sea–land oxygen isotopic relationships from planktonic foraminifera and speleothems in the Eastern Mediterranean region and their implication for paleorainfall during interglacial intervals. *Geochimica et Cosmochimica Acta* **67**, 3181-3199.

Bar-Matthews, M., Ayalon, A., Matthews, A., Sass, E., Halicz, L. (1996) Carbon and oxygen isotope study of the active water-carbonate system in a karstic Mediterranean cave: Implications for paleoclimate research in semiarid regions. *Geochimica et Cosmochimica Acta* **60**, 337-347.

Beck, W.C., Grossman, E.L., Morse, J.W. (2005) Experimental studies of oxygen isotope fractionation in the carbonic acid system at 15°, 25°, and 40°C. *Geochimica et Cosmochimica Acta* **69**, 3493-3503.

Boch, R., Cheng, H., Spötl, C., Edwards, R., Wang, X., Häuselmann, P., 2011. NALPS: a precisely dated European climate record 120–60 ka, Clim. Past, 7, 1247–1259.

Buhmann, D., Dreybrodt, W. (1985) The kinetics of calcite dissolution and precipitation in geologically relevant situations of karst areas: 1. Open system. *Chemical Geology* **48**, 189-211.

Cheng, H., Edwards, R.L., Sinha, A., Spötl, C., Yi, L., Chen, S., Kelly, M., Kathayat, G., Wang, X., Li, X., Kong, X., Wang, Y., Ning, Y., Zhang, H. (2016) The Asian monsoon over the past 640,000 years and ice age terminations. *Nature* **534**, 640-646.

Coplen, T.B. (2007) Calibration of the calcite–water oxygen-isotope geothermometer at Devils Hole, Nevada, a natural laboratory. *Geochimica et Cosmochimica Acta* **71**, 3948-3957.

Coplen, T.B., Kendall, C., Hopple, J. (1983) Comparison of stable isotope reference samples. *Nature* **302**, 236-238.

Cruz, F.W., Burns, S.J., Karmann, I., Sharp, W.D., Vuille, M., Cardoso, A.O., Ferrari, J.A., Silva Dias, P.L., Viana, O. (2005) Insolation-driven changes in atmospheric circulation over the past 116,000 years in subtropical Brazil. *Nature* **434**, 63-66.

Day, C.C., Henderson, G.M. (2011) Oxygen isotopes in calcite grown under cave-analogue conditions. *Geochimica et Cosmochimica Acta* **75**, 3956-3972.

Deininger, M., Fohlmeister, J., Scholz, D., Mangini, A. (2012) Isotope disequilibrium effects: The influence of evaporation and ventilation effects on the carbon and oxygen isotope composition of speleothems – A model approach. *Geochimica et Cosmochimica Acta* **96**, 57-79.

Dietzel, M., Tang, J., Leis, A., Köhler, S.J. (2009) Oxygen isotopic fractionation during inorganic calcite precipitation — Effects of temperature, precipitation rate and pH. *Chemical Geology* **268**, 107-115.

Dorale, J.A., Liu, Z. (2009) Limitations of Hendy test criteria in judging the paleoclimatic suitability of speleothems and the need for replication. *Journal of Cave and Karst Studies* **71**, 73-80.

Dreybrodt, W. (1988) *Processes in Karst Systems*. Series in Physical Environment, Vol. **4**, Springer, Heidelberg.

Dreybrodt, W. (2008) Evolution of the isotopic composition of carbon and oxygen in a calcite precipitating $H_2O–CO_2–CaCO_3$ solution and the related isotopic composition of calcite in stalagmites. *Geochimica et Cosmochimica Acta* **72**, 4712-4724.

Dreybrodt, W. (2016) Problems in using the approach of Rayleigh distillation to interpret the ^{13}C and ^{18}O isotope compositions in stalagmite calcite. *Acta Carsologica* **45**.

Dreybrodt, W., Eisenlohr, L., Madry, B., Ringer, S. (1997) Precipitation kinetics of calcite in the system $CaCO_3$-H_2O-$C0_2$: The conversion to CO_2 by the slow process $H^+ + HCO_3^- \rightarrow CO_2 + H_2O$ as a rate limiting step. *Geochimica et Cosmochimica Acta* **61**, 3897-3904.

Dreybrodt, W., Hansen, M., Scholz, D. (2016) Processes affecting the stable isotope composition of calcite during precipitation on the surface of stalagmites: Laboratory experiments investigating the isotope exchange between DIC in the solution layer on top of a speleothem and the CO_2 of the cave atmosphere. *Geochimica et Cosmochimica Acta* **174**, 247-262.

Dreybrodt, W., Romanov, D. (2016) The evolution of ^{13}C and ^{18}O isotope composition of DIC in a calcite depositing film of water with isotope exchange between the DIC and a CO_2 containing atmosphere, and simultaneous evaporation of the water. Implication to climate proxies from stalagmites: A theoretical model. *Geochimica et Cosmochimica Acta* **195**, 323-338.

Dreybrodt, W., Scholz, D. (2011) Climatic dependence of stable carbon and oxygen isotope signals recorded in speleothems: From soil water to speleothem calcite. *Geochimica et Cosmochimica Acta* **75**, 734-752.

Fairchild, I.J., Baker, A. (2012) *Speleothem science: from process to past environments*. John Wiley & Sons.

Fantidis, J., Ehhalt, D.H. (1970) Variations of the carbon and oxygen isotopic composition in stalagmites and stalactites: Evidence of non-equilibrium isotopic fractionation. *Earth and Planetary Science Letters* **10**, 136-144.

Fleitmann, D., Burns, S.J., Neff, U., Mudelsee, M., Mangini, A., Matter, A. (2004) Palaeoclimatic interpretation of high-resolution oxygen isotope profiles derived from annually laminated speleothems from Southern Oman. *Quaternary Science Reviews* **23**, 935-945.

Fornaca-Rinaldi, G., Panichi, C., Tongiorgi, E. (1968) Some causes of the variation of the isotopic composition of carbon and oxygen in cave concretions. *Earth and Planetary Science Letters* **4**, 321-324.

Friedman, I., O'Neil, J.R., 1977. Data of geochemistry: Compilation of stable isotope fractionation factors of geochemical interest, Survey professional paper **440** KK. US Government Printing Office, Washington.

Hansen, M., Dreybrodt, W., Scholz, D. (2013) Chemical evolution of dissolved inorganic carbon species flowing in thin water films and its implications for (rapid) degassing of CO_2 during speleothem growth. *Geochimica et Cosmochimica Acta* **107**, 242-251.

Hansen, M., Scholz, D., Froeschmann, M.-L., Schöne, B.R., Spötl, C. (in press) Carbon isotope exchange between gaseous CO_2 and thin solution films: Artificial cave experiments and a complete diffusion-reaction model. *Geochimica et Cosmochimica Acta*.

Hendy, C.H. (1971) The isotopic geochemistry of speleothems—I. The calculation of the effects of different modes of formation on the isotopic composition of speleothems and their applicability as palaeoclimatic indicators. *Geochimica et Cosmochimica Acta* **35**, 801-824.

Hendy, C.H., Wilson, A.T. (1968) Palaeoclimatic Data from Speleothems. *Nature* **219**, 48-51.

Johnston, V.E., Borsato, A., Spötl, C., Frisia, S., Miorandi, R. (2013) Stable isotopes in caves over altitudinal gradients: fractionation behaviour and inferences for speleothem sensitivity to climate change. *Clim. Past* **9**, 99-118.

Kim, S.-T., O'Neil, J.R. (1997) Equilibrium and nonequilibrium oxygen isotope effects in synthetic carbonates. *Geochimica et Cosmochimica Acta* **61**, 3461-3475.

Mangini, A., Spötl, C., Verdes, P. (2005) Reconstruction of temperature in the Central Alps during the past 2000 yr from a $\delta^{18}O$ stalagmite record. *Earth and Planetary Science Letters* **235**, 741-751.

McCrea, J.M. (1950) On the isotopic chemistry of carbonates and a paleotemperature scale. *The Journal of Chemical Physics* **18**, 849-857.

McKinney, C.R., McCrea, J.M., Epstein, S., Allen, H.A., Urey, H.C. (1950) Improvements in Mass Spectrometers for the Measurement of Small Differences in Isotope Abundance Ratios. *Review of Scientific Instruments* **21**, 724-730.

Mickler, P.J., Banner, J.L., Stern, L., Asmerom, Y., Edwards, R.L., Ito, E. (2004) Stable isotope variations in modern tropical speleothems: Evaluating equilibrium vs. kinetic isotope effects 1. *Geochimica et Cosmochimica Acta* **68**, 4381-4393.

Mickler, P.J., Stern, L.A., Banner, J.L. (2006) Large kinetic isotope effects in modern speleothems. *Geological Society of America Bulletin* **118**, 65-81.

Mook, W.G., De Vries, J. (2000) Volume I: Introduction: Theory, Methods, Review. *Environmental Isotopes in the Hydrological Cycle—Principles and Applications, International Hydrological Programme (IHP-V), Technical Documents in Hydrology (IAEA/UNESCO) No* **39**, 75-76.

Mühlinghaus, C., Scholz, D., Mangini, A. (2007) Modelling stalagmite growth and $\delta^{13}C$ as a function of drip interval and temperature. *Geochimica et Cosmochimica Acta* **71**, 2780-2790.

Mühlinghaus, C., Scholz, D., Mangini, A. (2009) Modelling fractionation of stable isotopes in stalagmites. *Geochimica et Cosmochimica Acta* **73**, 7275-7289.

O'Neil, J.R., Clayton, R.N., Mayeda, T.K. (1969) Oxygen isotope fractionation in divalent metal carbonates. *The Journal of Chemical Physics* **51**, 5547-5558.

Parkhurst, D., Apello, C. (1999) User's Guide to PHREEQC (V2). *US Geol. Surv* **312**.

Plummer, L., Wigley, T., Parkhurst, D. (1978) The kinetics of calcite dissolution in CO_2-water systems at 5 degrees to 60 degrees C and 0.0 to 1.0 atm CO_2. *American Journal of Science* **278**, 179-216.

Polag, D., Scholz, D., Mühlinghaus, C., Spötl, C., Schröder-Ritzrau, A., Segl, M., Mangini, A. (2010) Stable isotope fractionation in speleothems: Laboratory experiments. *Chemical Geology* **279**, 31-39.

Richards, D.A., Dorale, J.A. (2003) Uranium-series chronology and environmental applications of speleothems. *Reviews in Mineralogy and Geochemistry* **52**, 407-460.

Riechelmann, D.F.C., Deininger, M., Scholz, D., Riechelmann, S., Schröder-Ritzrau, A., Spötl, C., Richter, D.K., Mangini, A., Immenhauser, A. (2013) Disequilibrium carbon and oxygen isotope fractionation in recent cave calcite: Comparison of cave precipitates and model data. *Geochimica et Cosmochimica Acta* **103**, 232-244.

Riechelmann, D.F.C., Schröder-Ritzrau, A., Scholz, D., Fohlmeister, J., Spötl, C., Richter, D.K., Mangini, A. (2011) Monitoring Bunker Cave (NW Germany): A prerequisite to interpret geochemical proxy data of speleothems from this site. *Journal of Hydrology* **409**, 682-695.

Romanov, D., Kaufmann, G., Dreybrodt, W. (2008a) Modeling stalagmite growth by first principles of chemistry and physics of calcite precipitation. *Geochimica et Cosmochimica Acta* **72**, 423-437.

Romanov, D., Kaufmann, G., Dreybrodt, W. (2008b) $\delta^{13}C$ profiles along growth layers of stalagmites: Comparing theoretical and experimental results. *Geochimica et Cosmochimica Acta* **72**, 438-448.

Scholz, D., Mühlinghaus, C., Mangini, A. (2009) Modelling $\delta^{13}C$ and $\delta^{18}O$ in the solution layer on stalagmite surfaces. *Geochimica et Cosmochimica Acta* **73**, 2592-2602.

Scholz, D., Hoffmann, D. (2008) $^{230}Th/U$-dating of fossil corals and speleothems. *Eiszeitalter und Gegenwart* **57**, 52-76.

Spötl, C. (2004) A simple method of soil gas stable carbon isotope analysis. *Rapid Communications in Mass Spectrometry* **18**, 1239-1242.

Spötl, C., Scholz, D., Mangini, A. (2008) A terrestrial U/Th-dated stable isotope record of the Penultimate Interglacial. *Earth and Planetary Science Letters* **276**, 283-292.

Treble, P.C., Fairchild, I.J., Griffiths, A., Baker, A., Meredith, K.T., Wood, A., McGuire, E. (2015) Impacts of cave air ventilation and in-cave prior calcite precipitation on Golgotha Cave dripwater chemistry, southwest Australia. *Quaternary Science Reviews* **127**, 61-72.

Tremaine, D.M., Froelich, P.N., Wang, Y. (2011) Speleothem calcite farmed in situ: Modern calibration of $\delta^{18}O$ and $\delta^{13}C$ paleoclimate proxies in a continuously-monitored natural cave system. *Geochimica et Cosmochimica Acta* **75**, 4929-4950.

Wassenburg, J.A., Dietrich, S., Fietzke, J., Fohlmeister, J., Jochum, K.P., Scholz, D., Richter, D.K., Sabaoui, A., Spotl, C., Lohmann, G., Andreae, M.O., Immenhauser, A. (2016) Reorganization of the North Atlantic Oscillation during early Holocene deglaciation. *Nature Geosci* **advance online publication**.

Watkins, J.M., Hunt, J.D., Ryerson, F.J., DePaolo, D.J. (2014) The influence of temperature, pH, and growth rate on the $\delta^{18}O$ composition of inorganically precipitated calcite. *Earth and Planetary Science Letters* **404**, 332-343.

Watkins, J.M., Nielsen, L.C., Ryerson, F.J., DePaolo, D.J. (2013) The influence of kinetics on the oxygen isotope composition of calcium carbonate. *Earth and Planetary Science Letters* **375**, 349-360.

Wiedner, E., Scholz, D., Mangini, A., Polag, D., Mühlinghaus, C., Segl, M. (2008) Investigation of the stable isotope fractionation in speleothems with laboratory experiments. *Quaternary International* **187**, 15-24.

Zeebe, R.E., Wolf-Gladrow, D.A., Jansen, H. (1999) On the time required to establish chemical and isotopic equilibrium in the carbon dioxide system in seawater. *Marine Chemistry* **65**, 135-153.

Zeebe, R.E., Wolf-Gladrow, D. (2001) *CO_2 in Seawater: Equilibrium, Kinetics, Isotopes*. Amsterdam: Elsevier Science, B.V. 346 pp.

6.8 Supplementary Information

Table S6.1 a: Experimental results for experiment #1, conducted using a 5 mmol/l $CaCO_3$ solution at 10° C and a pCO_2 of 1000 ppmV.

distance of flow [cm]	residence time DIC [s]	electrical conductivity σ [µS/cm]	pH	$\delta^{18}O_{DIC}$ [‰]	±	$\delta^{18}O_{H2O,DIC}$ [‰] VSMOW	±	residence time $CaCO_3$ [s]	$\delta^{18}O_{CaCO3}$ [‰]	±	$\delta^{18}O_{H2O,CaCO3}$ [‰] VSMOW	±
100	591	587	8.20	-4.66	0.02			510	-5.64	0.04	-9.11*	0.19*
80	473	614	8.21	-4.86	0.06	-8.77	0.10	408	-5.87	0.03		
60	355	652	8.10	-4.36	0.15			306	-6.20	0.07		
40	236	723	8.19	-5.07	0.62	-9.05	0.03	204	-6.46	0.05		
30	177	731	8.04	-4.90	0.10			153	-6.63	0.03		
20	118	753	8.14	-4.93	0.25			102	-6.84	0.04		
15	89	760	8.12	-5.09	0.01			76.5	-6.89	0.03		
10	59	780	7.89	-5.21	0.14			51	-7.01	0.04		
5	30	799	7.87	-5.30	0.10			25.5	-7.00	0.05		
0	0	817	7.79	-5.04	0.33	-9.29	0.06	0	-7.03	0.03	-9.26	0.08

*During the experiments three samples for this distance of flow were measured over the duration of the experiment after different times, the value shown here is the average of these values with the corresponding 1 σ sd.

Table S6.1 b: Experimental results for experiment #2, conducted using a 5 mmol/l $CaCO_3$ solution at 20° C and a pCO_2 of 1000 ppmV.

distance of flow [cm]	residence time DIC [s]	electrical conductivity σ [µS/cm]	pH	$\delta^{18}O_{DIC}$ [‰]	±	$\delta^{18}O_{H2O,DIC}$ [‰] VSMOW	±	residence time $CaCO_3$ [s]	$\delta^{18}O_{CaCO3}$ [‰]	±	$\delta^{18}O_{H2O,CaCO3}$ [‰] VSMOW	±
100	634	427	8.10	-5.63	0.15	-9.39	0.03	474	-8.29	0.01	-9.77*	0.12*
80	507	434	8.10	-5.90	0.06			379	-8.43	0.03		
60	380	486	8.10	-5.97	0.07			284	-8.66	0.04		
40	254	542	8.10	-6.41	0.05	-9.73	0.04	190	-9.09	0.03		
30	190	580	8.03	-6.60	0.01			142	-9.28	0.05		
20	127	629	8.05	-7.15	0.25			95	-9.59	0.04		
15	95	662	7.99	-7.10	0.20			71	-9.75	0.03		
10	63	671	8.02	-7.23	0.00			47	-9.77	0.05		
5	32	723	7.98	-7.39	0.05			24	-10.07	0.02		
0	0	768	7.81	-7.55	0.02	-10.04	0.03	0	-10.23	0.05	-10.02	0.10

*During the experiments three samples for this distance of flow were measured over the duration of the experiment after different times, the value shown here is the average of these values with the corresponding 1 σ sd.

Table S6.1 c: Experimental results for experiment #3, conducted using a 5 mmol/l $CaCO_3$ solution at 30° C and a pCO_2 of 1000 ppmV.

distance of flow [cm]	residence time DIC [s]	electrical conductivity σ [µS/cm]	pH	$\delta^{18}O_{DIC}$ [‰]	±	$\delta^{18}O_{H2O,DIC}$ [‰] VSMOW	±	residence time $CaCO_3$ [s]	$\delta^{18}O_{CaCO3}$ [‰]	±	$\delta^{18}O_{H2O,CaCO3}$ [‰] VSMOW	±
100	528	266	8.00	-7.00	0.16	-8.76	0.05	474	-7.61	0.04	-8.78*	0.46*
80	423	280	8.16	-6.86	0.05			379	-7.72	0.04		
60	317	321	8.16	-7.57	0.59			284	-7.81	0.04		
40	211	390	8.20	-8.28	0.38	-9.23	0.08	190	-8.63	0.03		
30	159	413	8.06	-7.85	0.28			142	-8.96	0.03		
20	106	470	8.06	-8.00	0.05			95	-9.66	0.02		
15	79	497	8.00	-7.98	0.26			71	-9.72	0.05		
10	53	533	8.02	-8.63	0.05			47	-9.99	0.03		
5	26	583	7.90	-8.29	0.02			24	-10.23	0.03		
0	0	660	8.09	-8.54	0.33	-9.47	0.10	0	-10.45	0.04	**	

* During the experiments three samples for this distance of flow were measured over the duration of the experiment after different times, the value shown here is the average of these values with the corresponding 1 σ sd.

** Sample got lost during shipping.

Table S6.1 d: Experimental results for experiment #4, conducted using a 5 mmol/l $CaCO_3$ solution at 10° C and a pCO_2 of 3000 ppmV.

distance of flow [cm]	residence time DIC [s]	electrical conductivity σ [µS/cm]	pH	$\delta^{18}O_{DIC}$ [‰]	±	$\delta^{18}O_{H2O,DIC}$ [‰] VSMOW	±	residence time $CaCO_3$ [s]	$\delta^{18}O_{CaCO3}$ [‰]	±	$\delta^{18}O_{H2O,CaCO3}$ [‰] VSMOW	±
100	589.69	590	7.94	-3.97	0.05	-8.54	0.04	501	-6.66	0.08	-9.16*	0.15*
80	471.75	602	7.98	-4.17	0.09			400	-6.85	0.05		
60	353.82	634	7.93	-4.21	0.12			300	-6.74	0.04		
40	235.88	673	7.87	-4.25	0.04	-8.86	0.04	200	-6.85	0.05		
30	176.91	692	7.87	-4.56	0.05			150	-7.11	0.02		
20	117.94	720	7.91	-4.59	0.00			100	-6.98	0.04		
15	88.45	730	7.88	-4.52	0.02			75	-6.88	0.04		
10	58.97	735	7.86	-4.60	0.05	-9.21	0.03	50	-7.15	0.06		
5	29.48	745	7.86	-4.80	0.05			25	-7.27	0.04		
0	0.00	762	7.82	-4.94	0.08	-9.29	0.06	0	-7.23	0.07	-9.36	0.03

* During the experiments three samples for this distance of flow were measured over the duration of the experiment after different times, the value shown here is the average of these values with the corresponding 1 σ sd.

Table S6.1 e: Experimental results for experiment #5, conducted using a 5 mmol/l $CaCO_3$ solution at 20° C and a pCO_2 of 3000 ppmV.

distance of flow [cm]	residence time DIC [s]	electrical conductivity σ [µS/cm]	pH	$\delta^{18}O_{DIC}$ [‰]	±	$\delta^{18}O_{H2O,DIC}$ [‰] VSMOW	±	residence time $CaCO_3$ [s]	$\delta^{18}O_{CaCO3}$ [‰]	±	$\delta^{18}O_{H2O,CaCO3}$ [‰] VSMOW	±
100	500	420	8.05	-5.71	0.04	-8.34	0.03	480	-7.49	0.03	-8.97*	0.25*
80	400	450	8.08	-5.77	0.01			384	-7.65	0.03		
60	300	485	8.03	-6.05	0.19			288	-7.91	0.04		
40	200	549	8.02	-6.46	0.08	-9.01	0.01	192	-8.27	0.02		
30	150	577	8.01	-6.57	0.13			144	-8.46	0.02		
20	100	612	7.98	-6.88	0.16			96	-8.80	0.04		
15	75	625	7.97	-6.69	0.02			72	-8.86	0.02		
10	50	644	7.94	-6.89	0.08			48	-9.07	0.03		
5	25	665	7.93	-6.77	0.03			24	-9.11	0.03		
0	0	700	7.95	-6.89	0.03	-9.23	0.05	0	-9.36	0.03	-9.38	0.07

* During the experiments three samples for this distance of flow were measured over the duration of the experiment after different times, the value shown here is the average of these values with the corresponding 1 σ sd.

Table S6.1 f: Experimental results for experiment #6, conducted using a 5 mmol/l $CaCO_3$ solution at 30° C and a pCO_2 of 3000 ppmV.

distance of flow [cm]	residence time DIC [s]	electrical conductivity σ [µS/cm]	pH	$\delta^{18}O_{DIC}$ [‰]	±	$\delta^{18}O_{H2O,DIC}$ [‰] VSMOW	±	residence time $CaCO_3$ [s]	$\delta^{18}O_{CaCO3}$ [‰]	±	$\delta^{18}O_{H2O,CaCO3}$ [‰] VSMOW	±
100	591	255	7.88	-21.98	0.77	-8.68	0.02	489	-9.37	0.07	-8.90*	0.38*
80	473	295	7.89	-20.38	1.08			392	-9.16	0.08		
60	355	328	7.93	-20.99	2.08			294	-8.87	0.10		
40	236	392	7.98	-20.99	0.25	-9.15	0.05	196	-9.64	0.07		
30	177	433	7.87	-22.89	1.25			147	-9.85	0.10		
20	118	480	7.88	-23.85	0.52			98	-10.31	0.08		
15	89	533	7.81	-24.59	0.46			73	-10.55	0.06		
10	59	559	7.81	-23.96	0.54			49	-10.02	0.06		
5	30	602	7.80	-25.35	0.40			24	-10.24	0.09		
0	0	650	7.79	-26.18	0.19	-9.38	0.06	0	-10.98	0.09	-9.46	0.06

* During the experiments three samples for this distance of flow were measured over the duration of the experiment after different times, the value shown here is the average of these values with the corresponding 1 σ sd.

Table S6.1 g: Experimental results for experiment #9, conducted using a 2 mmol/l $CaCO_3$ solution at 30° C and a pCO_2 of 1000 ppmV.

distance of flow [cm]	residence time DIC [s]	electrical conductivity σ [µS/cm]	pH	$\delta^{18}O_{DIC}$ [‰]	±	$\delta^{18}O_{H2O,DIC}$ [‰] VSMOW	±	residence time $CaCO_3$ [s]	$\delta^{18}O_{CaCO3}$ [‰]	±	$\delta^{18}O_{H2O,CaCO3}$ [‰] VSMOW	±
100	655	202	8.21	-9.31	0.01	***		540	-11.34	0.12	***	
80	524	216	8.20	-9.20	0.03			432	-10.00	0.12		
60	393	238	8.15	-9.52	0.04			324	-10.75	0.06		
40	262	252	8.18	-9.81	0.03			216	-11.21	0.07		
30	197	267	8.17	-10.08	0.02			162	-11.53	0.04		
20	131	282	8.18	-9.93	0.05			108	-11.94	0.02		
15	98	299	8.15	-10.15	0.07			81	-12.11	0.02		
10	66	316	8.15	-10.56	0.02			54	-12.26	0.04		
5	33	327	8.15	-10.64	0.06			27	-12.55	0.03		
0	0	348	8.04	-11.07	0.05	***		0	-12.61	0.12	***	

*** Water values have not been measured.

Table S6.1 h: Experimental results for experiment #10, conducted using a 3 mmol/l $CaCO_3$ solution at 20° C and a pCO_2 of 1000 ppmV.

distance of flow [cm]	residence time DIC [s]	electrical conductivity σ [µS/cm]	pH	$\delta^{18}O_{DIC}$ [‰]	±	$\delta^{18}O_{H2O,DIC}$ [‰] VSMOW	±	residence time $CaCO_3$ [s]	$\delta^{18}O_{CaCO3}$ [‰]	±	$\delta^{18}O_{H2O,CaCO3}$ [‰] VSMOW	±
100	693	308	8.18	-7.62	0.00	***		562	-8.80	0.03	***	
80	555	327	8.18	-8.03	0.01			450	-8.61	0.05		
60	416	356	8.17	-8.60	0.09			337	-8.96	0.02		
40	277	382	8.17	-9.99	0.02			225	-9.29	0.03		
30	208	404	8.16	-8.13	0.07			169	-9.50	0.02		
20	139	433	8.14	-7.94	0.02			112	-9.69	0.02		
15	104	444	8.23	-7.75	0.05			84	-9.76	0.03		
10	69	454	8.20	-8.25	0.04			56	-9.81	0.04		
5	35	469	8.20	-8.40	0.06			28	-10.03	0.03		
0	0	498	7.96	-8.52	0.00	***		0	-10.09	0.03	***	

*** Water values have not been measured.

Chapter 7: Conclusions

The experiments presented within this thesis provide important information and significantly increase the knowledge on the various processes potentially influencing the isotope signal until speleothem calcite is precipitated. For the *first time* it is possible to *directly* investigate the temporal evolution of stable isotopes and the inorganic carbon chemistry in thin solution films as they occur on the surface of speleothems.

Two different approaches are introduced to quantify the isotope exchange between the gaseous CO_2 of the (cave) atmosphere and the DIC of a thin solution film. The theory and the experiments presented in Chapter 3, which were performed mainly at high pCO_2 (12,500 and 25,000 ppmV) with a 5 and 10 mmol/l $NaHCO_3$ solution and film thicknesses between 0.13 and 2 mm at 20 °C, are in good agreement. The derived exchange times allow to estimate the impact of isotope exchange for speleothems, which might be an important issue for the selection of suitable samples for paleoclimate reconstruction. In Chapter 4, an alternative approach, a complete diffusion-reaction model for the carbon isotope exchange between gaseous CO_2 and the DIC in a thin solution film (ca 0.1 mm) is presented. Further experiments were performed totest the model at conditions closer to a natural system (wider range of temperatures and concentrations as well as significantly lower pCO_2 of 1000 and 3000 ppmV). The results show, that isotope exchange might get significant at an earlier stage than suggested by the model in Chapter 3 and could have an influence on speleothems, which grow at low precipitation rates and long drip intervals.

The cave analogue experiments, in which calcite is precipitated (Chapter 5 and 6) onto a marble or borosilicate glass plate from thin solution films as they occur on top of speleothems, provide new insights into stable isotope fractionation and the basic physical and chemical controls during precipitation of speleothem calcite. Precipitation rates, the time constants for precipitation of $CaCO_3$, as well as the observed pH values are in good agreement to previously published theoretical studies and show the expected dependence on temperature (e.g., Baker et al., 1998; Buhmann and Dreybrodt, 1985b; Dreybrodt et al., 1997). The temporal evolution of stable isotopes ($\delta^{13}C$ and $\delta^{18}O$) for the DIC and the $CaCO_3$ can be well described using a Rayleigh distillation model as previously suggested by Scholz et al. (2009). The total fractionation for the stable carbon isotopes, $^{13}\varepsilon_{tot}$, is much larger than expected from typical isotope equilibrium values. The fractionation between $CaCO_3$ and DIC is large and negative, becoming smaller with increasing residence time on the plates and is, thus, also dependent on the precipitation rate. With decreasing supersaturation with respect to calcite and decreasing precipitation rate, the fractionation becomes progressively smaller and approaches values in the range of equilibrium fractionation. The initial fractionation (i.e. 0 cm distance of flow, corresponding to the impinging point of a drip to the tip of a stalagmite) for the stable oxygen isotopes ($\delta^{18}O$), are in good agreement to previously reported values from natural cave systems (e.g., Johnston

et al., 2013; Tremaine et al., 2011) and show a similar dependence on temperature. This indicates, that the experimental setup closely resembles a natural system. The same is observed for the initial fractionation between DIC and water, which corresponds well to previously reported equilibrium fractionation factors ($^{18}\varepsilon_{HCO3-/H2O}$) by Beck et al. (2005). With progressive precipitation of $CaCO_3$, the fractionation between the carbon species and the water is forced out of equilibrium because the residence time on the plates is too short to re-equilibrate with the water. The fractionation between DIC and $CaCO_3$ initially corresponds to the combination of the fractionations of Johnston et al. (2013) or Tremaine et al. (2011) with those of Beck et al. (2005). With increasing residence time on the plate, and, thus, decreasing supersaturation and precipitation rate, the fractionation between DIC and $CaCO_3$ becomes smaller, approaching the predictions by Coplen (2007) and Watkins et al. (2014; 2013). As observed for the carbon isotopes, the reaction kinetics must also be taken into account for the interpretation of speleothem $\delta^{18}O$ records.

These findings show that previous assumptions of a constant fractionation factor, as used in all modeling studies (e.g., Dreybrodt, 2008; Dreybrodt and Scholz, 2011; Scholz et al., 2009), may not be correct, since the results of this thesis suggest that the fractionation additionally seems to be coupled to chemical reaction kinetics (e.g., growth rate). This might be of great importance for the interpretation of speleothem stable isotope record, because "kinetic", negative or even rate dependent fractionation factors might lead to a systematic over (or under) estimation of past environmental or climatic signals. Thus, the interpretation of these records should always be handled with care. Thoroughly conducted cave monitoring studies testing the present-day-conditions of fractionation processes inside the individual cave system might be a valuable tool to access the most suitable fractionation factors for interpretation of the corresponding speleothem records.

7.1 Limitations of the Experiments and future research perspectives

The results presented in the framework of this thesis significantly improve the insights on the controls of stable isotope fractionation factors for speleothem calcite. However, a final validation which fractionation model (i.e., Dreybrodt, 2008; vs.Scholz et al., 2009) describes the fractionation of stable isotopes more realistically is not possible within the (temporal) resolution of the presented experiments. To solve this issue, future experimental work should be conducted with longer residence times on the plates, which probably provides information on the temporal evolution after 75 % of the equilibrium concentration have been reached. This could also be accessed by using $CaCO_3$-concentrations closer to chemical equilibrium. However, then further isotope exchange models taking isotope exchange for $\delta^{18}O$ and $\delta^{13}C$ during precipitation of calcite would be needed. For future studies, there are several points which should be addressed to provide further information on the controls how climate signals are imprinted into speleothems:

(i) The samples from the $CaCO_3$ and DIC experiments are currently analyzed for their clumped isotope thermometry. The clumped isotopes of $CaCO_3$-minerals are suggested to directly provide quantitative information on their formation temperature, independently of the isotope composition of the solution from which the calcite is precipitated from (e.g., Ghosh et al., 2006). However, the strong disequilibrium and rate dependent fractionation processes observed for the stable isotopes in this thesis renders this assumption highly questionable. Furthermore, this supports previous assumptions that the "clumped isotope paleo thermometer" for speleothems might only be applicable after thorough corrections for "kinetic" processes (e.g., Affek et al., 2008; Kluge and Affek, 2012). The results from measuring samples from this thesis will, for the first time, provide the possibility to directly and quantitatively compare the clumped isotopes values of the DIC to those of the $CaCO_3$ under speleothem analogue conditions (i.e. precipitation of $CaCO_3$ from thin films of solution).

(ii) Another important point, which future experiments should consider, is the comparability between the individual experiments. The data of the individual experiment are consistent, and all experiments show similar dependences on fractionation rate, temperature and pCO_2. The initial conditions, however, are slightly different for the individual experiments, mainly due to the problematic adjustment of a saturation index of approximately 0 of the bulk solution, which is discussed in detail in Chapter 3.3.5. To enable a better comparability and to provide absolute fractionation factors (e.g. in dependence of concentration, temperature, supersaturation with respect to calcite), all solutions need to be isotopically identical. This issue could be solved by using more precise probes for measuring the pCO_2 and Ca^{2+} concentration of the bulk solution.

(iii) The precision of the isotope measurements of the DIC samples, which are precipitated as $SrCO_3$, needs to be improved. The precipitation method is the only way to investigate the temporal evolution of $\delta^{18}O$ values of the DIC, but these values scatter sometimes up to $\pm$ 0.5 ‰ within one filter (corresponding to one residence time). Therefore, the method needs to be refined in terms of the reproducibility.

(iv) In an ideal setting, the DIC, the water and the water vapor as well as the CO_2 of the atmosphere would be measured in situ. This would substantially increase the control in the surrounding conditions and provide a more detailed insight into the direct fractionation processes (e.g. between DIC and gaseous CO_2).

(v) Of great interest would be the investigation of trace element incorporation into speleothem calcite under well constrained conditions. Trace elements, or more precisely, the distribution coefficients of the different trace elements could potentially provide important information for example on environmental changes or prior calcite precipitation. Changes in the distribution coefficients for example in Mg/Ca and Sr/Ca

ratios are interpreted as trigger for the solution composition and the calcite which is removed from it (e.g., Fairchild and Treble, 2009). As a consequence, changes in the trace element composition will also affect the pH value, supersaturation with respect to calcite and the precipitation rate. This, in turn, could also have implications for the controls on the stable isotope signals since the results of this thesis show that stable isotope fractionation is maybe linked to the precipitation kinetics. Conducting such experiments with the presented experimental setup would significantly improve the knowledge on trace element incorporation, because the setup would enable to directly investigate the solution and the precipitated substrate at the same time.

In summary, the presented experiments and the corresponding setup in the climate box should ultimately be used and extended in future studies because they provide the possibility to generate very detailed insights into various processes, which could not be investigated (not experimentally nor in a natural system) at this resolution so far.

References

Affek, H.P. (2013) Clumped isotopic equilibrium and the rate of isotope exchange between CO_2 and water. *American Journal of Science* **313**, 309-325.

Affek, H.P., Bar-Matthews, M., Ayalon, A., Matthews, A., Eiler, J.M. (2008) Glacial/interglacial temperature variations in Soreq cave speleothems as recorded by 'clumped isotope' thermometry. *Geochimica et Cosmochimica Acta* **72**, 5351-5360.

Appelo, C.A.J., Postma, D. (2004) *Geochemistry, groundwater and pollution*. CRC press.

Asmerom, Y., Polyak, V.J., Burns, S.J. (2010) Variable winter moisture in the southwestern United States linked to rapid glacial climate shifts. *Nature Geosci* **3**, 114-117.

Baker, A., Genty, D., Dreybrodt, W., Barnes, W.L., Mockler, N.J., Grapes, J. (1998) Testing theoretically predicted stalagmite growth rate with recent annually laminated samples: Implications for past stalagmite deposition. *Geochimica et Cosmochimica Acta* **62**, 393-404.

Baldini, J.U.L., McDermott, F., Hoffmann, D.L., Richards, D.A., Clipson, N. (2008) Very high-frequency and seasonal cave atmosphere PCO_2 variability: Implications for stalagmite growth and oxygen isotope-based paleoclimate records. *Earth and Planetary Science Letters* **272**, 118-129.

Bar-Matthews, M., Ayalon, A., Gilmour, M., Matthews, A., Hawkesworth, C.J. (2003) Sea–land oxygen isotopic relationships from planktonic foraminifera and speleothems in the Eastern Mediterranean region and their implication for paleorainfall during interglacial intervals. *Geochimica et Cosmochimica Acta* **67**, 3181-3199.

Bar-Matthews, M., Ayalon, A., Matthews, A., Sass, E., Halicz, L. (1996) Carbon and oxygen isotope study of the active water-carbonate system in a karstic Mediterranean cave: Implications for paleoclimate research in semiarid regions. *Geochimica et Cosmochimica Acta* **60**, 337-347.

Baskaran, M., Krishnamurthy, R.V. (1993) Speleothems as proxy for the carbon isotope composition of atmospheric CO_2. *Geophysical Research Letters* **20**, 2905-2908.

Beck, W.C., Grossman, E.L., Morse, J.W. (2005) Experimental studies of oxygen isotope fractionation in the carbonic acid system at 15°, 25°, and 40°C. *Geochimica et Cosmochimica Acta* **69**, 3493-3503.

Boch, R., Cheng, H., Spötl, C., Edwards, R., Wang, X., Häuselmann, P., 2011. NALPS: a precisely dated European climate record 120–60 ka, Clim. Past, 7, 1247–1259.

Breecker, D.O. (2017) Atmospheric pCO_2 control on speleothem stable carbon isotope compositions. *Earth and Planetary Science Letters* **458**, 58-68.

Breitenbach, S.F.M., Lechleitner, F.A., Meyer, H., Diengdoh, G., Mattey, D., Marwan, N. (2015) Cave ventilation and rainfall signals in dripwater in a monsoonal setting – a monitoring study from NE India. *Chemical Geology* **402**, 111-124.

Buhmann, D., Dreybrodt, W. (1985a) The kinetics of calcite dissolution and precipitation in geologically relevant situations of karst areas: 1. Open system. *Chemical Geology* **48**, 189-211.

Buhmann, D., Dreybrodt, W. (1985b) The kinetics of calcite dissolution and precipitation in geologically relevant situations of karst areas: 2. Closed system. *Chemical Geology* **53**, 109-124.

Cerling, T.E. (1984) The stable isotopic composition of modern soil carbonate and its relationship to climate. *Earth and Planetary Science Letters* **71**, 229-240.

Cheng, H., Edwards, R.L., Sinha, A., Spötl, C., Yi, L., Chen, S., Kelly, M., Kathayat, G., Wang, X., Li, X., Kong, X., Wang, Y., Ning, Y., Zhang, H. (2016) The Asian monsoon over the past 640,000 years and ice age terminations. *Nature* **534**, 640-646.

Coplen, T.B. (2007) Calibration of the calcite–water oxygen-isotope geothermometer at Devils Hole, Nevada, a natural laboratory. *Geochimica et Cosmochimica Acta* **71**, 3948-3957.

Coplen, T.B., Kendall, C., Hopple, J. (1983) Comparison of stable isotope reference samples. *Nature* **302**, 236-238.

Cowan, B.D., Osborne, M.C., Banner, J.L. (2013) Temporal variability of cave-air CO_2 in central Texas. *Journal of Cave and Karst Studies* **75**, 38-50.

Crank, J. (1979) *The mathematics of diffusion*. Oxford university press.

Cruz, F.W., Burns, S.J., Karmann, I., Sharp, W.D., Vuille, M., Cardoso, A.O., Ferrari, J.A., Silva Dias, P.L., Viana, O. (2005) Insolation-driven changes in atmospheric circulation over the past 116,000 years in subtropical Brazil. *Nature* **434**, 63-66.

Curl, R.L. (1973) Minimum diameter stalagmites. *Bulletin National Speleological Society of America (Nat. Speleol. Soc. Bull)* **35**, 1-9.

Dandurand, J.L., Gout, R., Hoefs, J., Menschel, G., Schott, J., Usdowski, E. (1982) Kinetically controlled variations of major components and carbon and oxygen isotopes in a calcite-precipitating spring. *Chemical Geology* **36**, 299-315.

Day, C.C., Henderson, G.M. (2011) Oxygen isotopes in calcite grown under cave-analogue conditions. *Geochimica et Cosmochimica Acta* **75**, 3956-3972.

Day, C.C., Henderson, G.M. (2013) Controls on trace-element partitioning in cave-analogue calcite. *Geochimica et Cosmochimica Acta* **120**, 612-627.

Deininger, M., Fohlmeister, J., Scholz, D., Mangini, A. (2012) Isotope disequilibrium effects: The influence of evaporation and ventilation effects on the carbon and oxygen isotope composition of speleothems – A model approach. *Geochimica et Cosmochimica Acta* **96**, 57-79.

Dietzel, M., Tang, J., Leis, A., Köhler, S.J. (2009) Oxygen isotopic fractionation during inorganic calcite precipitation — Effects of temperature, precipitation rate and pH. *Chemical Geology* **268**, 107-115.

Dorale, J.A., Edwards, R.L., Ito, E., González, L.A. (1998) Climate and Vegetation History of the Midcontinent from 75 to 25 ka: A Speleothem Record from Crevice Cave, Missouri, USA. *Science* **282**, 1871-1874.

Dorale, J.A., Liu, Z. (2009) Limitations of Hendy test criteria in judging the paleoclimatic suitability of speleothems and the need for replication. *Journal of Cave and Karst Studies* **71**, 73-80.

Dreybrodt, W. (1988) *Processes in Karst Systems*. Series in Physical Environment, Vol. **4**, Springer, Heidelberg.

Dreybrodt, W. (2008) Evolution of the isotopic composition of carbon and oxygen in a calcite precipitating H_2O–CO_2–$CaCO_3$ solution and the related isotopic composition of calcite in stalagmites. *Geochimica et Cosmochimica Acta* **72**, 4712-4724.

Dreybrodt, W. (2009) Physik von Stalagmiten. Physik Journal **8** Nr. 2, 25-30.

Dreybrodt, W. (2011) Comments on processes contributing to the isotope composition of ^{13}C and ^{18}O in calcite deposited to speleothems. *Acta Carsologica* **40**, 233-238.

Dreybrodt, W. (2012) Comment on "Oxygen isotopes in calcite grown under cave-analogue conditions" by C.C. Day and G.M. Henderson. *Geochimica et Cosmochimica Acta* **85**, 383-387.

Dreybrodt, W. (2016) Problems in using the approach of Rayleigh distillation to interpret the ^{13}C and ^{18}O isotope compositions in stalagmite calcite. *Acta Carsologica* **45**.

Dreybrodt, W., Deininger, M. (2014) The impact of evaporation to the isotope composition of DIC in calcite precipitating water films in equilibrium and kinetic fractionation models. *Geochimica et Cosmochimica Acta* **125**, 433-439.

Dreybrodt, W., Eisenlohr, L., Madry, B., Ringer, S. (1997) Precipitation kinetics of calcite in the system $CaCO_3$-H_2O-$C0_2$: The conversion to CO_2 by the slow process $H^+ + HCO_3^- \rightarrow CO_2 + H_2O$ as a rate limiting step. *Geochimica et Cosmochimica Acta* **61**, 3897-3904.

Dreybrodt, W., Hansen, M., Scholz, D. (2016) Processes affecting the stable isotope composition of calcite during precipitation on the surface of stalagmites: Laboratory experiments

investigating the isotope exchange between DIC in the solution layer on top of a speleothem and the CO_2 of the cave atmosphere. *Geochimica et Cosmochimica Acta* **174**, 247-262.

Dreybrodt, W., Romanov, D. (2016) The evolution of ^{13}C and ^{18}O isotope composition of DIC in a calcite depositing film of water with isotope exchange between the DIC and a CO_2 containing atmosphere, and simultaneous evaporation of the water. Implication to climate proxies from stalagmites: A theoretical model. *Geochimica et Cosmochimica Acta* **195**, 323-338.

Dreybrodt, W., Scholz, D. (2011) Climatic dependence of stable carbon and oxygen isotope signals recorded in speleothems: From soil water to speleothem calcite. *Geochimica et Cosmochimica Acta* **75**, 734-752.

Eigen, M. (1964) Proton Transfer, Acid-Base Catalysis, and Enzymatic Hydrolysis. Part I: ELEMENTARY PROCESSES. *Angewandte Chemie International Edition in English* **3**, 1-19.

Emrich, K., Ehhalt, D.H., Vogel, J.C. (1970) Carbon isotope fractionation during the precipitation of calcium carbonate. *Earth and Planetary Science Letters* **8**, 363-371.

Fairchild, I.J., Baker, A. (2012) *Speleothem science: from process to past environments*. John Wiley & Sons.

Fairchild, I.J., Treble, P.C. (2009) Trace elements in speleothems as recorders of environmental change. *Quaternary Science Reviews* **28**, 449-468.

Fantidis, J., Ehhalt, D.H. (1970) Variations of the carbon and oxygen isotopic composition in stalagmites and stalactites: Evidence of non-equilibrium isotopic fractionation. *Earth and Planetary Science Letters* **10**, 136-144.

Fleitmann, D., Burns, S.J., Neff, U., Mudelsee, M., Mangini, A., Matter, A. (2004) Palaeoclimatic interpretation of high-resolution oxygen isotope profiles derived from annually laminated speleothems from Southern Oman. *Quaternary Science Reviews* **23**, 935-945.

Fohlmeister, J., Scholz, D., Kromer, B., Mangini, A. (2011) Modelling carbon isotopes of carbonates in cave drip water. *Geochimica et Cosmochimica Acta* **75**, 5219-5228.

Fornaca-Rinaldi, G., Panichi, C., Tongiorgi, E. (1968) Some causes of the variation of the isotopic composition of carbon and oxygen in cave concretions. *Earth and Planetary Science Letters* **4**, 321-324.

Friedman, I., O'Neil, J.R., 1977. Data of geochemistry: Compilation of stable isotope fractionation factors of geochemical interest, Survey professional paper **440** KK. US Government Printing Office, Washington.

Frisia, S., Borsato, A., SpÖTl, C., Villa, I.M., Cucchi, F. (2005) Climate variability in the SE Alps of Italy over the past 17 000 years reconstructed from a stalagmite record. *Boreas* **34**, 445-455.

Frisia, S., Fairchild, I.J., Fohlmeister, J., Miorandi, R., Spötl, C., Borsato, A. (2011) Carbon mass-balance modelling and carbon isotope exchange processes in dynamic caves. *Geochimica et Cosmochimica Acta* **75**, 380-400.

Gázquez, F., Quindós-Poncela, L., Sainz-Fernández, C., Fernández-Villar, A., Fuente-Merino, I., Celaya-Gonzalez, S. (2016) Spatiotemporal distribution of $\delta^{13}C_{CO2}$ in a shallow cave and its

potential use as indicator of anthropic pressure. *Journal of Environmental Management* **180**, 421-432.

Genty, D., Blamart, D., Ouahdi, R., Gilmour, M., Baker, A., Jouzel, J., Van-Exter, S. (2003) Precise dating of Dansgaard-Oeschger climate oscillations in western Europe from stalagmite data. *Nature* **421**, 833-837.

Ghosh, P., Adkins, J., Affek, H., Balta, B., Guo, W., Schauble, E.A., Schrag, D., Eiler, J.M. (2006) ^{13}C–^{18}O bonds in carbonate minerals: A new kind of paleothermometer. *Geochimica et Cosmochimica Acta* **70**, 1439-1456.

Green, M., Taube, H. (1963) ISOTOPIC FRACTIONATION IN THE OH^--H_2O EXCHANGE REACTION. *The Journal of Physical Chemistry* **67**, 1565-1566.

Hansen, M., Dreybrodt, W., Scholz, D. (2013) Chemical evolution of dissolved inorganic carbon species flowing in thin water films and its implications for (rapid) degassing of CO_2 during speleothem growth. *Geochimica et Cosmochimica Acta* **107**, 242-251.

Hansen, M., Scholz, D., Froeschmann, M.-L., Schöne, B.R., Spötl, C. (in press) Carbon isotope exchange between gaseous CO_2 and thin solution films: Artificial cave experiments and a complete diffusion-reaction model. *Geochimica et Cosmochimica Acta*.

Hellstrom, J., McCulloch, M., Stone, J. (1998) A Detailed 31,000-Year Record of Climate and Vegetation Change, from the Isotope Geochemistry of Two New Zealand Speleothems. *Quaternary Research* **50**, 167-178.

Hellstrom, J.C., McCulloch, M.T. (2000) Multi-proxy constraints on the climatic significance of trace element records from a New Zealand speleothem. *Earth and Planetary Science Letters* **179**, 287-297.

Hendy, C.H. (1971) The isotopic geochemistry of speleothems—I. The calculation of the effects of different modes of formation on the isotopic composition of speleothems and their applicability as palaeoclimatic indicators. *Geochimica et Cosmochimica Acta* **35**, 801-824.

Hendy, C.H., Wilson, A.T. (1968) Palaeoclimatic Data from Speleothems. *Nature* **219**, 48-51.

Hofmann, M.E.G., Horváth, B., Pack, A. (2012) Triple oxygen isotope equilibrium fractionation between carbon dioxide and water. *Earth and Planetary Science Letters* **319–320**, 159-164.

Jähne, B., Heinz, G., Dietrich, W. (1987) Measurement of the diffusion coefficients of sparingly soluble gases in water. *Journal of Geophysical Research: Oceans* **92**, 10767-10776.

Johnson, K.R., Lynn Ingram, B., Sharp, W.D., Zhang, P. (2006) East Asian summer monsoon variability during Marine Isotope Stage 5 based on speleothem $\delta^{18}O$ records from Wanxiang Cave, central China. *Palaeogeography, Palaeoclimatology, Palaeoecology* **236**, 5-19.

Johnson, K.S. (1982) Carbon dioxide hydration and dehydration kinetics in seawater. *Limnol. Oceanogr* **27**, 849-855.

Johnston, V.E., Borsato, A., Spötl, C., Frisia, S., Miorandi, R. (2013) Stable isotopes in caves over altitudinal gradients: fractionation behaviour and inferences for speleothem sensitivity to climate change. *Clim. Past* **9**, 99-118.

Keeling, C.D.P., S. C.; Bacastow, R. B.; Wahlen, M.; Whorf, T. P.; Heimann, M.; Meijer, H. A., 2005. Atmospheric CO_2 and $^{13}CO_2$ exchange with the terrestrial biosphere and oceans from 1978 to 2000: observations and carbon cycle implications A history of Atmospheric CO_2 and its effects on Plants Animals and Ecosystems. Springer Verlag, New York, pp. 83 - 113.

Kim, S.-T., Coplen, T.B., Horita, J. (2015) Normalization of stable isotope data for carbonate minerals: Implementation of IUPAC guidelines. *Geochimica et Cosmochimica Acta* **158**, 276-289.

Kim, S.-T., O'Neil, J.R. (1997) Equilibrium and nonequilibrium oxygen isotope effects in synthetic carbonates. *Geochimica et Cosmochimica Acta* **61**, 3461-3475.

Kluge, T., Affek, H.P. (2012) Quantifying kinetic fractionation in Bunker Cave speleothems using D47. *Quaternary Science Reviews* **49**, 82-94.

Kowalczk, A.J., Froelich, P.N. (2010) Cave air ventilation and CO_2 outgassing by radon-222 modeling: How fast do caves breathe? *Earth and Planetary Science Letters* **289**, 209-219.

Li, Y.-H., Gregory, S. (1974) Diffusion of ions in sea water and in deep-sea sediments. *Geochimica et Cosmochimica Acta* **38**, 703-714.

Mandić, M., Mihevc, A., Leis, A., Bronić, I.K. (2013) Concentration and stable carbon isotopic composition of CO_2 in cave air of Postojnska jama, Slovenia. *International Journal of Speleology* **42**, 279-287.

Mangini, A., Spötl, C., Verdes, P. (2005) Reconstruction of temperature in the Central Alps during the past 2000 yr from a $\delta^{18}O$ stalagmite record. *Earth and Planetary Science Letters* **235**, 741-751.

Mattey, D., Lowry, D., Duffet, J., Fisher, R., Hodge, E., Frisia, S. (2008) A 53 year seasonally resolved oxygen and carbon isotope record from a modern Gibraltar speleothem: Reconstructed drip water and relationship to local precipitation. *Earth and Planetary Science Letters* **269**, 80-95.

Mattey, D.P., Fairchild, I.J., Atkinson, T.C., Latin, J.-P., Ainsworth, M., Durell, R. (2010) Seasonal microclimate control of calcite fabrics, stable isotopes and trace elements in modern speleothem from St Michaels Cave, Gibraltar. *Geological Society, London, Special Publications* **336**, 323-344.

McCrea, J.M. (1950) On the isotopic chemistry of carbonates and a paleotemperature scale. *The Journal of Chemical Physics* **18**, 849-857.

McDermott, F. (2004) Palaeo-climate reconstruction from stable isotope variations in speleothems: a review. *Quaternary Science Reviews* **23**, 901-918.

McKinney, C.R., McCrea, J.M., Epstein, S., Allen, H.A., Urey, H.C. (1950) Improvements in Mass Spectrometers for the Measurement of Small Differences in Isotope Abundance Ratios. *Review of Scientific Instruments* **21**, 724-730.

Meyer, K.W., Feng, W., Breecker, D.O., Banner, J.L., Guilfoyle, A. (2014) Interpretation of speleothem calcite $\delta^{13}C$ variations: Evidence from monitoring soil CO_2, drip water, and modern speleothem calcite in central Texas. *Geochimica et Cosmochimica Acta* **142**, 281-298.

Mickler, P.J., Banner, J.L., Stern, L., Asmerom, Y., Edwards, R.L., Ito, E. (2004) Stable isotope variations in modern tropical speleothems: Evaluating equilibrium vs. kinetic isotope effects 1. *Geochimica et Cosmochimica Acta* **68**, 4381-4393.

Mickler, P.J., Stern, L.A., Banner, J.L. (2006) Large kinetic isotope effects in modern speleothems. *Geological Society of America Bulletin* **118**, 65-81.

Millo, C., Dupraz, S., Ader, M., Guyot, F., Thaler, C., Foy, E., Ménez, B. (2012) Carbon isotope fractionation during calcium carbonate precipitation induced by ureolytic bacteria. *Geochimica et Cosmochimica Acta* **98**, 107-124.

Mischel, S.A., Scholz, D., Spötl, C., Jochum, K.P., Schröder-Ritzrau, A., Fiedler, S. (2016) Holocene climate variability in Central Germany and a potential link to the polar North Atlantic: A replicated record from three coeval speleothems. *The Holocene*.

Mook, W.G., Bommerson, J.C., Staverman, W.H. (1974) Carbon isotope fractionation between dissolved bicarbonate and gaseous carbon dioxide. *Earth and Planetary Science Letters* **22**, 169-176.

Mook, W.G., De Vries, J. (2000) Volume I: Introduction: Theory, Methods, Review. *Environmental Isotopes in the Hydrological Cycle—Principles and Applications, International Hydrological Programme (IHP-V), Technical Documents in Hydrology (IAEA/UNESCO) No* **39**, 75-76.

Moreno, A., Stoll, H., Jiménez-Sánchez, M., Cacho, I., Valero-Garcés, B., Ito, E., Edwards, R.L. (2010) A speleothem record of glacial (25–11.6 kyr BP) rapid climatic changes from northern Iberian Peninsula. *Global and Planetary Change* **71**, 218-231.

Mühlinghaus, C., Scholz, D., Mangini, A. (2007) Modelling stalagmite growth and $\delta^{13}C$ as a function of drip interval and temperature. *Geochimica et Cosmochimica Acta* **71**, 2780-2790.

Mühlinghaus, C., Scholz, D., Mangini, A. (2009) Modelling fractionation of stable isotopes in stalagmites. *Geochimica et Cosmochimica Acta* **73**, 7275-7289.

Murray, C.N., Riley, J.P. (1971) The solubility of gases in distilled water and sea water—IV. Carbon dioxide. *Deep Sea Research and Oceanographic Abstracts* **18**, 533-541.

Nordstrom, D.K., Plummer, L.N., Langmuir, D., Busenberg, E., May, H.M., Jones, B.F., Parkhurst, D.L., 1990. Revised chemical equilibrium data for major water-mineral reactions and their limitations, ACS symposium series. Oxford University Press, pp. 398-413.

O'Leary, M.H., Madhavan, S., Paneth, P. (1992) Physical and chemical basis of carbon isotope fractionation in plants. *Plant, Cell & Environment* **15**, 1099-1104.

O'Neil, J.R., Clayton, R.N., Mayeda, T.K. (1969) Oxygen isotope fractionation in divalent metal carbonates. *The Journal of Chemical Physics* **51**, 5547-5558.

Parkhurst, D., Apello, C. (1999) User's Guide to PHREEQC (V2). *US Geol. Surv* **312**.

Plummer, L., Wigley, T., Parkhurst, D. (1978) The kinetics of calcite dissolution in CO_2-water systems at 5 degrees to 60 degrees C and 0.0 to 1.0 atm CO_2. *American Journal of Science* **278**, 179-216.

Polag, D., Scholz, D., Mühlinghaus, C., Spötl, C., Schröder-Ritzrau, A., Segl, M., Mangini, A. (2010) Stable isotope fractionation in speleothems: Laboratory experiments. *Chemical Geology* **279**, 31-39.

R Core Team, 2016. R: A Language and Environment for Statistical Computing. R Foundation for Statistical Computing, Vienna, Austria.

Richards, D.A., Dorale, J.A. (2003) Uranium-series chronology and environmental applications of speleothems. *Reviews in Mineralogy and Geochemistry* **52**, 407-460.

Ridley, H.E., Asmerom, Y., Baldini, J.U.L., Breitenbach, S.F.M., Aquino, V.V., Prufer, K.M., Culleton, B.J., Polyak, V., Lechleitner, F.A., Kennett, D.J., Zhang, M., Marwan, N., Macpherson, C.G., Baldini, L.M., Xiao, T., Peterkin, J.L., Awe, J., Haug, G.H. (2015) Aerosol forcing of the position of the intertropical convergence zone since ad 1550. *Nature Geosci* **8**, 195-200.

Riechelmann, D.F.C., Deininger, M., Scholz, D., Riechelmann, S., Schröder-Ritzrau, A., Spötl, C., Richter, D.K., Mangini, A., Immenhauser, A. (2013) Disequilibrium carbon and oxygen isotope fractionation in recent cave calcite: Comparison of cave precipitates and model data. *Geochimica et Cosmochimica Acta* **103**, 232-244.

Riechelmann, D.F.C., Schröder-Ritzrau, A., Scholz, D., Fohlmeister, J., Spötl, C., Richter, D.K., Mangini, A. (2011) Monitoring Bunker Cave (NW Germany): A prerequisite to interpret geochemical proxy data of speleothems from this site. *Journal of Hydrology* **409**, 682-695.

Romanek, C.S., Grossman, E.L., Morse, J.W. (1992) Carbon isotopic fractionation in synthetic aragonite and calcite: Effects of temperature and precipitation rate. *Geochimica et Cosmochimica Acta* **56**, 419-430.

Romanov, D., Kaufmann, G., Dreybrodt, W. (2008a) Modeling stalagmite growth by first principles of chemistry and physics of calcite precipitation. *Geochimica et Cosmochimica Acta* **72**, 423-437.

Romanov, D., Kaufmann, G., Dreybrodt, W. (2008b) $\delta^{13}C$ profiles along growth layers of stalagmites: Comparing theoretical and experimental results. *Geochimica et Cosmochimica Acta* **72**, 438-448.

Rudzka, D., McDermott, F., Baldini, L.M., Fleitmann, D., Moreno, A., Stoll, H. (2011) The coupled $\delta^{13}C$-radiocarbon systematics of three Late Glacial/early Holocene speleothems; insights into soil and cave processes at climatic transitions. *Geochimica et Cosmochimica Acta* **75**, 4321-4339.

Salomons, W., Mook, W. (1986) Isotope geochemistry of carbonates in the weathering zone. *Handbook of environmental isotope geochemistry* **2**, 239-269.

Scholz, D., Frisia, S., Borsato, A., Spötl, C., Fohlmeister, J., Mudelsee, M., Miorandi, R., Mangini, A. (2012) Holocene climate variability in north-eastern Italy: potential influence of the NAO and solar activity recorded by speleothem data. *Clim. Past* **8**, 1367-1383.

Scholz, D., Hoffmann, D. (2008) $^{230}Th/U$-dating of fossil reef corals and speleothems. *E&G Quaternary Science Journal* **57**, 52-77.

Scholz, D., Mühlinghaus, C., Mangini, A. (2009) Modelling $\delta^{13}C$ and $\delta^{18}O$ in the solution layer on stalagmite surfaces. *Geochimica et Cosmochimica Acta* **73**, 2592-2602.

Schulz, K.G., Riebesell, U., Rost, B., Thoms, S., Zeebe, R.E. (2006) Determination of the rate constants for the carbon dioxide to bicarbonate inter-conversion in pH-buffered seawater systems. *Marine Chemistry* **100**, 53-65.

Sharp, Z. (2007) *Principles of stable isotope geochemistry*. Pearson Education Upper Saddle River, NJ.

Soetaert, K., Cash, J., Mazzia, F. (2012) *Solving differential equations in R*. Springer Science & Business Media.

Soetaert, K., Meysman, F. (2012) Reactive transport in aquatic ecosystems: Rapid model prototyping in the open source software R. *Environmental Modelling & Software* **32**, 49-60.

Soetaert, K.E.R., Petzoldt, T., Setzer, R.W. (2010) Solving differential equations in R: package deSolve. *Journal of Statistical Software* **33**.

Spötl, C. (2004) A simple method of soil gas stable carbon isotope analysis. *Rapid Communications in Mass Spectrometry* **18**, 1239-1242.

Spötl, C. (2005) A robust and fast method of sampling and analysis of $\delta^{13}C$ of dissolved inorganic carbon in ground waters. *Isotopes in Environmental and Health Studies* **41**, 217-221.

Spötl, C., Fairchild, I.J., Tooth, A.F. (2005) Cave air control on dripwater geochemistry, Obir Caves (Austria): Implications for speleothem deposition in dynamically ventilated caves. *Geochimica et Cosmochimica Acta* **69**, 2451-2468.

Spötl, C., Scholz, D., Mangini, A. (2008) A terrestrial U/Th-dated stable isotope record of the Penultimate Interglacial. *Earth and Planetary Science Letters* **276**, 283-292.

Spötl, C., Vennemann, T.W. (2003) Continuous-flow isotope ratio mass spectrometric analysis of carbonate minerals. *Rapid Communications in Mass Spectrometry* **17**, 1004-1006.

Stockmann, G.J., Wolff-Boenisch, D., Bovet, N., Gislason, S.R., Oelkers, E.H. (2014) The role of silicate surfaces on calcite precipitation kinetics. *Geochimica et Cosmochimica Acta* **135**, 231-250.

Thode, H.G., Shima, M., Rees, C.E., Krishnamurty, K.V. (1965) CARBON-13 ISOTOPE EFFECTS IN SYSTEMS CONTAINING CARBON DIOXIDE, BICARBONATE, CARBONATE, AND METAL IONS. *Canadian Journal of Chemistry* **43**, 582-595.

Thornton, E.R. (1962) Solvent Isotope Effects in H_2O^{16} and H_2O^{18}. *Journal of the American Chemical Society* **84**, 2474-2475.

Treble, P.C., Fairchild, I.J., Griffiths, A., Baker, A., Meredith, K.T., Wood, A., McGuire, E. (2015) Impacts of cave air ventilation and in-cave prior calcite precipitation on Golgotha Cave dripwater chemistry, southwest Australia. *Quaternary Science Reviews* **127**, 61-72.

Tremaine, D.M., Froelich, P.N., Wang, Y. (2011) Speleothem calcite farmed in situ: Modern calibration of $\delta^{18}O$ and $\delta^{13}C$ paleoclimate proxies in a continuously-monitored natural cave system. *Geochimica et Cosmochimica Acta* **75**, 4929-4950.

Usdowski, E., Hoefs, J., Menschel, G. (1979) Relationship between^{13}C and^{18}O fractionation and changes in major element composition in a recent calcite-depositing spring — A model of chemical variations with inorganic $CaCO_3$ precipitation. *Earth and Planetary Science Letters* **42**, 267-276.

Usdowski, E., Michaelis, J., Bottcher, M., Hoefs, J. (1991) Factors for the oxygen isotope equilibrium fractionation between aqueous and gaseous CO_2, carbonic-acid, bicarbonate, carbonate, and water (19-degrees-C). *ZEITSCHRIFT FUR PHYSIKALISCHE CHEMIE-INTERNATIONAL JOURNAL OF RESEARCH IN PHYSICAL CHEMISTRY & CHEMICAL PHYSICS* **170**, 237-249.

Verheyden, S., Genty, D., Deflandre, G., Quinif, Y., Keppens, E. (2008) Monitoring climatological, hydrological and geochemical parameters in the Père Noël cave (Belgium): implication for the interpretation of speleothem isotopic and geochemical time-series. *International Journal of Speleology* **37**, 221-234.

Vogel, J.C., Grootes, P.M., Mook, W.G. (1970) Isotopic fractionation between gaseous and dissolved carbon dioxide. *Zeitschrift für Physik* **230**, 225-238.

Wackerbarth, A., Langebroek, P.M., Werner, M., Lohmann, G., Riechelmann, S., Borsato, A., Mangini, A. (2012) Simulated oxygen isotopes in cave drip water and speleothem calcite in European caves. *Clim. Past* **8**, 1781-1799.

Wassenburg, J.A., Dietrich, S., Fietzke, J., Fohlmeister, J., Jochum, K.P., Scholz, D., Richter, D.K., Sabaoui, A., Spotl, C., Lohmann, G., Andreae, M.O., Immenhauser, A. (2016) Reorganization of the North Atlantic Oscillation during early Holocene deglaciation. *Nature Geosci* **advance online publication**.

Watkins, J.M., Hunt, J.D., Ryerson, F.J., DePaolo, D.J. (2014) The influence of temperature, pH, and growth rate on the $\delta^{18}O$ composition of inorganically precipitated calcite. *Earth and Planetary Science Letters* **404**, 332-343.

Watkins, J.M., Nielsen, L.C., Ryerson, F.J., DePaolo, D.J. (2013) The influence of kinetics on the oxygen isotope composition of calcium carbonate. *Earth and Planetary Science Letters* **375**, 349-360.

Wiedner, E., Scholz, D., Mangini, A., Polag, D., Mühlinghaus, C., Segl, M. (2008) Investigation of the stable isotope fractionation in speleothems with laboratory experiments. *Quaternary International* **187**, 15-24.

Williams, P.W., King, D.N.T., Zhao, J.X., Collerson, K.D. (2005) Late Pleistocene to Holocene composite speleothem ^{18}O and ^{13}C chronologies from South Island, New Zealand—did a global Younger Dryas really exist? *Earth and Planetary Science Letters* **230**, 301-317.

Wong, C.I., Banner, J.L., Musgrove, M. (2011) Seasonal dripwater Mg/Ca and Sr/Ca variations driven by cave ventilation: Implications for and modeling of speleothem paleoclimate records. *Geochimica et Cosmochimica Acta* **75**, 3514-3529.

Wong, C.I., Banner, J.L., Musgrove, M. (2015) Holocene climate variability in Texas, USA: An integration of existing paleoclimate data and modeling with a new, high-resolution speleothem record. *Quaternary Science Reviews* **127**, 155-173.

Zeebe, R.E. (2011) On the molecular diffusion coefficients of dissolved CO_2, HCO_3^-, and CO_3^{2-} and and their dependence on isotopic mass. *Geochimica et Cosmochimica Acta* **75**, 2483-2498.

Zeebe, R.E., Bijma, J., Wolf-Gladrow, D.A. (1999a) A diffusion-reaction model of carbon isotope fractionation in foraminifera. *Marine Chemistry* **64**, 199-227.

Zeebe, R.E., Wolf-Gladrow, D.A., Jansen, H. (1999b) On the time required to establish chemical and isotopical equilibrium in the carbon dioxide system in seawater. *Marine Chemistry* **65**, 135-153.

Zeebe, R.E., Wolf-Gladrow, D. (2001) *CO_2 in Seawater: Equilibrium, Kinetics, Isotopes*. Amsterdam: Elsevier Science, B.V. 346 pp.

Appendix

Curriculum Vitae

[redacted]

[redacted]

[redacted]